ASPECTS OF COSMIC ACCELERATION

Proefschrift

ter verkrijging van
de graad van Doctor aan de Universiteit Leiden,
op gezag van Rector Magnificus prof. mr. C.J.J.M. Stolker,
volgens besluit van het College voor Promoties
te verdedigen op woensdag 18 September 2019
klokke 10:00 uur

door

Valeri Vardanyan

geboren te Jerevan (Armenië) in 1992

Promotor:	Prof. Dr. Ana Achúcarro
Co-promotor:	Dr. Alessandra Silvestri
Promotiecommissie:	Prof. Dr. L. Amendola (ITP, University of Heidelberg, Germany)
	Prof. Dr. A.-C. Davis (DAMTP, University of Cambridge, UK)
	Prof. Dr. E. R. Eliel
	Prof. Dr. H. Hoekstra

The cover shows a Λ-shaped sketch of W. de Sitter. The Dutch text around the balloon translates into "Who is really blowing up the balloon? What makes the universe expand, or swell up? This is done by Lambda. Another answer cannot be given". The original version of the sketch first appeared accompanying an interview with De Sitter in Algemeen Handelsblad, published in 1930. The large scale structure image is taken from the website of The Millennium Simulation Project. The author of this thesis thanks Tsovinar Martirosyan for realizing the idea.

Casimir PhD series, Delft-Leiden 2019-31

ISBN 978-90-8593-414-1

An electronic version of this thesis can be found at `https://openaccess.leidenuniv.nl`

This work is supported by a Leiden De Sitter fellowship that is funded by the Netherlands Organisation for Scientific Research (NWO).

CONTENTS

1

INTRODUCTION

Cosmological research is about the global, large-scale properties of the universe. It is one of the most actively developing fields of modern physics. This rapid flourishing of the field is partly motivated by the Nobel Prize winning discovery of cosmic acceleration in 1998 [1, 2], and partly by the fact that cosmology can serve as a uniquely fascinating laboratory for testing various aspects of fundamental theories of physics. Indeed, it is already widely acknowledged that the cosmological observations suggest tests at regimes which are by far not accessible at the laboratory setups.

All the wealth of cosmological observations are consistently explained by a phenomenological model referred to as the *cosmological standard model*. This model assumes, first of all, that the universe is homogeneous and isotropic at the largest scales. Additionally, it is now well measured that the biggest share in the energy budget of the universe, about 68%, belongs to the *cosmological constant*, Λ - a constant energy density component with a negative pressure. Such a component causes the universe to expand with increasing rate, a phenomenon known as *cosmic acceleration*. In addition to this, about 27% of the universe is composed of a non-relativistic, pressureless gas called *cold dark matter*, which interacts gravitationally, but does not interact electromagnetically, and hence can be observed only through its gravitational effects. The conventional baryonic matter and radiation together make only about 5% of the universe's energy budget. This matter

content, together with a hypothesized short period of very rapid expansion of spacetime in the very early universe, known as *cosmic inflation*, provides a beautifully simple interpretation of practically all the currently available cosmological observations in the context of *General Theory of Relativity (GR)*. This cosmological model is often referred to as the Λ-Cold Dark Matter (ΛCDM) model.

The rough timeline of the universe is that it experienced a rapid (inflationary) expansion during its earliest stages. This expansion caused most of the inhomogeneity and anisotropies in spacetime to reduce, and the spatial curvature to flatten out (see later in this chapter). After the inflationary stage the universe *reheats*, i.e it becomes dominated by a relativistic plasma. As universe expands, the energy density of this relativistic plasma decreases and the universe enters the epoch dominated by non-relativistic particles - baryons and dark matter. At some point the energy of collisions in cosmic plasma decreases so much that neutral atoms are formed, and the residual photons, unable to Compton-scatter on free electrons anymore, freestream through the entire universe. Later on, as the universe becomes dominated by dark matter, the small fluctuations in density start to grow, eventually leading to formation of galaxies and galaxy clusters. The matter dominated epoch then is followed by an accelerated expansion caused by yet unknown mechanism. Phenomenologically the simplest candidate for this unknown mechanism is the cosmological constant mentioned above.

Even though phenomenologically extremely successful, the cosmological standard model is in fact very difficult to incorporate into fundamental physics. The 95% of the universe's energy budget, namely the cosmological constant and the dark matter sectors are still waiting for their theoretical explanations. A completely satisfactory model for cosmic inflation is also still a subject of active research. In this thesis our primary interest will be the phenomenon of comic acceleration, and the nature of dark matter, while also very important and interesting, is beyond the scope of this thesis.

It is a very curious fact that the standard framework of quantum field theory already leads to accelerated expansion of the universe. Indeed, quantum mechanically we expect a non-zero vacuum energy, which behaves exactly like a cosmological constant. If the theoretically estimated value of the vacuum energy density would agree with the cosmological observations, this would have been one of the most elegant predictions in theoretical physics. Unfortunately the reality is by far not as simple as that. The trouble is that the theoretical expectation for the value of this vacuum energy is at least tens of orders of magnitude larger than the value inferred from cosmological observations (see [3] for a pedagogical treatment of the topic). Besides the quantum mechanical contribution, there is also a classical contribution to the vacuum energy density originating, e.g., from the minima of scalar field potentials. The huge value of the quantum mechanical vacuum energy can in principle be cancelled against the classical contributions. This cancellation between two huge values, however, is highly unsatisfactory as we would need a very precise, finely-tuned cancellation.

In the last decades this problem has motivated a substantial effort in exploring possible modifications to the standard model of cosmology. This effort can be overall split into two main categories. One category is dubbed as *dynamical dark energy scenario*. In this scenario the cosmological constant sector is replaced by a field which evolves during cosmic history and is responsible for late-time cosmic acceleration. Another category goes under the name of *modified gravity*, where one constructs gravitational theories which posses so-called self-accelerating solutions, i.e. they can explain the accelerated expansion without the need of cosmological constant. Both of these possibilities, of course, do not provide an explanation for the abovementioned difficulty with the quantum-field theoretical vacuum energy. The typical attitude is to assume that there is a yet unknown symmetry or mechanism which makes the vacuum energy exactly zero, and instead achieve the cosmic acceleration via either the dynamical dark energy or the appropriate modifications of General Relativity.

The line of research of exploring the alternatives to the cosmological standard model, while originating from the need of explaining the accelerated expansion, has now to some extent diverged from its origins. Indeed, now a big part of research in this direction is devoted to using cosmological observations for testing various theoretical models, without necessarily requiring these models to give cosmic acceleration in absence of cosmological constant.

The theme of this dissertation is largely motivated by the phenomenon of cosmic acceleration and is devoted to understanding various properties of the fundamental laws of nature by exploiting the cosmological phenomena. Before moving to the main chapters of this thesis, let us quickly review the main ideas in modern cosmology.

1.1 THE COSMOLOGICAL STANDARD MODEL IN A NUTSHELL

Homogeneous and isotropic universe

In order to understand the basic dynamical properties of the universe, we should note that the most relevant interaction at such large scales is the gravity. Our current picture of the latter is dominated by the fact that spacetime is a dynamical object described by the metric tensor $g_{\mu\nu}$ (we use Greek indices for denoting the 4-dimensional spacetime coordinates). In this thesis we will employ the $(-,+,+,+)$ sign convention for the metric.

Cosmological observations suggest that on very large scales (larger than $\mathcal{O}(100)$ megaparsecs) the universe is described by a spatially homogeneous and isotropic manifold, first presented by Friedmann [4, 5]. The most general metric compatible with spatial homogeneity and isotropy is known as Friedmann-Lemaître-Robertson-Walker (FLRW) metric and can be written as

$$\mathrm{d}s^2 = -N(t)^2\mathrm{d}t^2 + a(t)^2\left(\frac{\mathrm{d}r^2}{1-\kappa r^2} + r^2\mathrm{d}^2\Omega\right), \tag{1.1}$$

where t is the time coordinate, r is a radial coordinate on the spatial hypersurfaces, $\mathrm{d}^2\Omega$ is the metric of a two-sphere and κ is introduced for accounting for the spatial curvature of the metric. As we see, we need to introduce two functions of time, $N(t)$ and $a(t)$ known as the *lapse function* and the *scale factor* of the universe. The former is related to the time-reparametrization invariance of the metric, and can be safely fixed to any functional form. This reparametrization invariance originates from the symmetries of General Theory of Relativity to be discussed below. Two important choices for $N(t)$ are the so-called cosmic time, corresponding to $N(t) = t$ and the conformal time, corresponding to $N(t) = a(t)$. The scale factor keeps track of how length intervals on spatial slices of spacetime shrink or expand over cosmic time t. For example, the ratio of physical distances between two galaxies at times t_1 and t_2 is simply given by $a(t_1)/a(t_2)$. This change between the distances is an inherent feature of an FLRW metric and should not be confused with the change caused by the peculiar motion of galaxies, which can be, for example, due to the gravitational force exerted on the considered galaxies by their neighbouring mass. An additional comment on terminology is appropriate here. The radial coordinate r in FLRW metric is typically referred to as a *comoving coordinate.* This reflects the fact that the distance r between two point does not change during the cosmic evolution. The physical distance between two points, $r_{\mathrm{phys}} = a(t)r$, however, of course changes as the universe expands or contracts.

It is worth noting that the metric given in Eq. (1.1) is left invariant under the following rescalings

$$a(t) \to \sigma a(t), \quad r \to r/\sigma, \quad k \to \sigma^2 \kappa, \tag{1.2}$$

where σ is a constant. This property, rather conveniently, allows us to rescale the radial coordinate in such a way that the scale factor at present time is equal to unity, i.e. $a_0 = 1$.

Observationally it is well-known that $a(t)$ is in fact an increasing function of time, i.e. the observable universe is expanding. This fact is established

by noticing that the spectra of distant galaxies are redshifted, i.e. a spectral line with a restframe wavelength λ_{rest} is observed to have $\lambda_{\text{observed}} > \lambda_{\text{rest}}$. This is expected in an expanding universe, as the electromagnetic waves are stretched alongside with cosmic evolution. An important relation between the redshift factor z and the cosmic scale factor a is given by

$$z \equiv \frac{\lambda_{\text{observed}}}{\lambda_{\text{rest}}} - 1 = \frac{a_0}{a(t_\star)} - 1, \tag{1.3}$$

where a_0 is the present-time scale factor and $a(t_\star)$ is the value of the scale factor when the wave has been emitted.

The redshift of galaxy spectra can be interpreted as a result of *Doppler effect*. When the considered galaxy moves much slower than the speed of light, then the corresponding Doppler redshift of spectral lines would be given by $z \approx v/c$, where c is the speed of light in vacuum and v is the speed of the galaxy with respect to the observer.

As discussed above, in an expanding FLRW universe the physical distances between two points at fixed comoving distance r is given by $r_{\text{phys}} = a(t)r$. This then leads to the recession speed of a galaxy at the distance r_{phys} from the observer to be

$$v = H r_{\text{phys}} \approx H_0 r_{\text{phys}}, \tag{1.4}$$

where $H \equiv \dot{a}/a$, with a dot denoting a derivative with respect to cosmic time t, is known as the *Hubble function*. In the last part of this equation we have assumed the galaxy to have a small redshift, so that the Hubble function can be assumed to be approximately constant and equal to its present-day value of H_0. This result is the celebrated Hubble's law of cosmic expansion discovered in 1920's. We recommend Ref. [6] for an interesting summary of the story behind the discovery of this law.

Dynamics of the FLRW universe

In the context of Einstein's theory of General Relativity [7], the dynamics of the metric tensor field can be derived from the Einstein-Hilbert action, given by

$$S = \frac{M_{\rm Pl}^2}{2} \int \mathrm{d}^4x \sqrt{-g} R + S_{\rm m}(g_{\mu\nu}, \Psi_i), \tag{1.5}$$

where g is the determinant of the metric tensor, $R \equiv g^{\mu\nu} R_{\mu\nu}$ is the Ricci scalar constructed from the metric tensor $g_{\mu\nu}$ and the corresponding Ricci tensor $R_{\mu\nu}$. $S_{\rm m}$ is the action describing the dynamics of matter fields, collectively denoted by Ψ_i. Additionally, we have introduced the reduced Planck mass, defined by $M_{\rm Pl} \equiv \sqrt{\frac{\hbar c}{8\pi G_{\rm N}}}$, with $\hbar$ being the reduced Planck constant and $G_{\rm N}$ - the Newton's constant. It should be noted that the central property of GR is that all the matter species Ψ_i are universally coupled to the metric. This coupling is proportional to the Newtonian gravitational constant $G_{\rm N}$.

An additional observation at this point is that the symmetries of the action (1.5), namely, the invariance under general coordinate transformations, or, the diffeomorphism invariance, allow us to add a constant term in the Einstein-Hilbert action. This term, known as the cosmological constant discussed earlier, is an essential piece for constructing the phenomenologically simplest cosmological model which is compatible with all the currently known experimental and observational evidence, namely the ΛCDM model.

We are going to assume that the matter content of the universe is described by a perfect fluid with an energy density $\rho(a)$ and pressure $p(a)$. Our next step is to derive the equations of motion which govern the dynamics of this metric. For that purpose we can plug our FLRW metric ansatz Eq. (1.1) into the Einstein-Hilbert action (including the cosmological constant term -2Λ and the matter energy density $\rho(a)$) and obtain the so-called *minisuperspace* action. Varying the action with respect to the lapse

function $N(t)$ yields the energy constraint equation, which is the celebrated *first Friedmann equation*

$$3M_{\rm Pl}^2 H^2 = M_{\rm Pl}^2 \Lambda + \rho(a) - 3M_{\rm Pl}^2 \frac{\kappa}{a^2}. \tag{1.6}$$

Additionally, the variation of the action with respect to the scale factor $a(t)$ gives

$$\dot{H} + H^2 = -\frac{1}{6M_{\rm Pl}^2}\left(\rho(a) + 3p(a)\right) + \frac{\Lambda}{3}. \tag{1.7}$$

where we have set $N(t) = 1$ and defined the pressure as

$$p(a) = -\rho(a) - \frac{1}{3} a \frac{\delta\rho(a)}{\delta a}. \tag{1.8}$$

An important consequence of the diffeomorphism invariance is the automatic conservation of the energy-momentum tensor, given the Einstein field equations are satisfied. This conservation is given by $\nabla^\mu T_{\mu\nu} = 0$, where ∇^μ is the covariant derivative compatible with the metric $g_{\mu\nu}$. For the perfect fluids considered here this equation takes the form $\dot{\rho} + 3H\rho(1+w) = 0$, where $w \equiv p/\rho$ is the equation of state of the considered fluid. From this simple relation it follows that the energy densities of dark matter with $w = 0$, radiation with $w = 1/3$ and cosmological constant with $w = -1$ (which are assumed to be non-interacting, hence are conserved separately) are evolving as

$$\rho_{\rm r} = \rho_{\rm r}(a_0) a^{-4}, \tag{1.9}$$

$$\rho_{\rm m} = \rho_{\rm m}(a_0) a^{-3}, \tag{1.10}$$

$$\rho_\Lambda = \rho_\Lambda(a_0), \tag{1.11}$$

where a_0 is the present-day value of the scale factor.

Let us note that radiation dilutes away faster than non-relativistic matter, which means that no matter how subdominant the latter is initially, it will

dominate over radiation at some later stage. Additionally, both radiation and non-relativistic matter will eventually become subdominant compared to cosmological constant. This shows that in the ΛCDM model the universe asymptotically approaches an epoch described by a constant Hubble function. This spacetime metric at this epoch is known as the *de Sitter metric*.

It is also useful to introduce the dimensionless density parameters as

$$\Omega_{\rm r}(a) \equiv \rho_{\rm r}(a)/3H^2M_{\rm Pl}^2, \tag{1.12}$$
$$\Omega_{\rm m}(a) \equiv \rho_{\rm m}(a)/3H^2M_{\rm Pl}^2, \tag{1.13}$$
$$\Omega_{\Lambda}(a) \equiv \Lambda/3H^2, \tag{1.14}$$
$$\Omega_{\kappa}(a) \equiv -\kappa/H^2a^2. \tag{1.15}$$

In terms of these dimensionless parameters the first Friedmann equation can be rewritten as

$$\Omega_{\rm m}(a) + \Omega_{\rm r}(a) + \Omega_{\Lambda}(a) + \Omega_{\kappa}(a) = 1. \tag{1.16}$$

Let us mention that the cosmological observations tightly constrain the spatial curvature κ to be tiny [8]. In this thesis we will mainly assume it being exactly zero.

Perturbing the FLRW universe

As we mentioned above, the FLRW metric provides a valid description of the universe on scales larger than $\mathcal{O}(100)$ megaparsecs. On smaller scales, however, the universe is no longer homogeneous and isotropic. Various observational surveys have particularly seen a web of clustered matter, known as the *cosmic web* or cosmic large scale structure (LSS) of the universe. This means that after specifying *the cosmological background*, the next important step is to consider perturbations around it. Of course, in complete generality one would aim at solving the full Einstein's equations, which are, in general, are highly non-linear partial differential equations.

However, it is a fortunate property of the universe that at large enough scales the perturbations of the relevant fields are small enough, so we can make use of the perturbation theory. The starting point for this perturbative approach is to specify the form of the perturbed metric. Naively, one would start perturbing all the components of the metric tensor, which would lead to extremely complicated calculations. However, as we mentioned earlier, one of the central properties of GR is its invariance under general coordinate transformations. For a given calculation in the framework of GR we can choose a particularly suitable coordinate system, where the given problem is solved the easiest. This coordinate freedom is known as the *gauge freedom* of GR, and the particular coordinate choice is often called a gauge choice for the metric.

In the previous subsection, when deriving the Firedmann equations, we did not make direct use of the Einstein's field equations. For deriving the equations of motion for the perturbed quantities we can proceed similarly and first derive the action which would then directly lead to the equations of motion for the desired perturbation variables. For example, if we are interested in the linear order perturbations, then we would need to expand the Einstein-Hilbert action to second order in these perturbations. Such a second order action then would lead to linear equations of motion. Alternatively, we could derive the full equations of motion and perturb them to the desired order. In the bulk of this thesis we have used both of these approaches. Here, in order to demonstrate the main features of the standard cosmological model at perturbative level, let us make use of the latter approach.

The starting point are the Einstein's field equations, derived from Eq. (1.5) by varying with respect to the metric tensor. They read as

$$G_{\mu\nu} \equiv R_{\mu\nu} - \frac{1}{2} g_{\mu\nu} R = \frac{1}{M_{\rm Pl}^2} T_{\mu\nu}, \tag{1.17}$$

where $T_{\mu\nu}$ is the energy-momentum tensor of the matter fields defined as

$$T_{\mu\nu} \equiv -\frac{2}{\sqrt{-g}}\frac{\delta S_{\rm m}}{\delta g^{\mu\nu}}. \tag{1.18}$$

The first step of our perturbative treatment is to write the metric as

$$g_{\mu\nu} = \bar{g}_{\mu\nu} + \delta g_{\mu\nu}, \tag{1.19}$$

where $\bar{g}_{\mu\nu}$ is the FLRW background metric and $\delta g_{\mu\nu}$ is a perturbation around it. We will then plug it in the left hand side of Eq. (1.17) and keep only the terms up to first order in $\delta g_{\mu\nu}$. Such a background-perturbation splitting is an arbitrary choice, but is perhaps the most intuitive one from the point of view of a generic observer in a Hubble flow. The most general form of the metric is

$$\mathrm{d}s^2 = -(1+2\phi)\mathrm{d}t^2 + 2aB_i\mathrm{d}t\mathrm{d}x^i + a^2\left(\delta_{ij} - h_{ij}\right)\mathrm{d}x^i\mathrm{d}x^j, \tag{1.20}$$

where one can show that ϕ, B_i and h_{ij} are, respectively, 3−scalar, vector and tensor. It turns out that the perturbative calculations simplify significantly if we decompose these perturbations into scalar, vector and tensor degrees of freedom. For the vectors this decompositions is well known from general physics. Namely, any 3−vector can be written as

$$B_i = \partial_i B + S_i, \tag{1.21}$$

where B transforms as a 3−scalar, while S_i is a divergence-free 3−vector. Similar decomposition is possible for higher-rank objects, namely for h_{ij}:

$$h_{ij} = 2\psi\delta_{ij} + 2E_{,ij} + F_{i,j} + F_{j,i} + \tilde{h}_{ij}, \tag{1.22}$$

where ψ and E are two additional 3−scalars, F_i is a devergence-free 3−vector and the 3−tensor $\tilde{h}_{ij}$ is such that

$$\tilde{h}^i_i = 0 = \partial_i\tilde{h}^i_j. \tag{1.23}$$

As such, we have decomposed the 10 independent components of the symmetric 4×4 metric $\delta g_{\mu\nu}$ into 4 scalar functions (namely, ϕ, ψ, B, E), 4 vector modes (encoded in the 6 components of B_i and F_i and the corresponding divergence-free conditions), and 2 tensor degrees of freedom (encoded in the 6 components of $\tilde{h}_{ij}$ and the corresponding conditions given in Eq. (1.23)).

The significant advantage of such a decomposition is that it turns out that the linearized Einstein's equations lead to decoupled dynamics of these scalar, vector and tensor sectors. The formation of the large scale structure of the universe is largely given by the scalar sector of the metric, and now we will be considering only this sector. Let us mention, however, that the dynamics of the tensor sector characterizes the propagation of gravitational waves, and hence, even though not relevant for the large scale structure formation, contains valuable information by its own.

The most general way to write the scalar-perturbed metric is as follows

$$\mathrm{d}s^2 = -(1+2\phi)\mathrm{d}t^2 + 2a\partial_i B \mathrm{d}t\mathrm{d}x^i + a^2\left[(1-2\psi)\delta_{ij} + 2\partial_i\partial_j E\right]\mathrm{d}x^i\mathrm{d}x^j. \quad (1.24)$$

A widely used gauge choice is the Newtonian gauge, specified by $E = 0 = B$.

Our next step is to include the perturbed energy-momentum tensor $T_{\mu\nu}$. The latter for a generic perfect fluid can be written as

$$T_{\mu\nu} = (\rho + P)u_\mu u_\nu + p g_{\mu\nu}, \quad (1.25)$$

where, u_μ is the four-velocity of the fluid element as seen by a comoving observer, ρ is its energy density, p - its pressure. Here we will assume any deviations from the perfect fluid approximation to be exactly zero. The perturbed sector of the energy-momentum tensor is given by

$$\delta T^0{}_0 = -\delta\rho, \quad (1.26)$$

$$\delta T^0{}_i = -\delta T^i{}_0 = (1+w)\bar{\rho}v_i, \quad (1.27)$$

$$\delta T^1{}_1 = \delta T^2{}_2 = \delta T^3{}_3 = c_s^2\delta\rho. \quad (1.28)$$

Here we have denoted the spatially averaged energy density as $\bar{\rho}$, and the perturbations around this background are denoted by $\delta\rho \equiv \rho(x) - \bar{\rho}(t)$. Additionally, v^i are the components of the three-velocity and $c_s^2 \equiv \delta p/\delta\rho$ denotes the square of the sound speed of the considered fluid.

The linearly perturbed Einstein equations have the following form (see e.g. Ref. [9])

$$6H^2\phi - \frac{2}{a^2}\partial^i\partial_i\psi + 6H\dot{\psi} = \frac{1}{M_{\rm Pl}^2}\delta T^0_0, \tag{1.29}$$

$$-2\partial_i\left(\dot{\psi} + H\phi\right) = \frac{1}{M_{\rm Pl}^2}\delta T^0_i, \tag{1.30}$$

$$\ddot{\psi} + 3H\dot{\psi} + H\dot{\phi} + (3H^2 + 2\dot{H})\phi + \frac{1}{3a^2}\partial^i\partial_i\left(\phi - \psi\right) = \frac{1}{6M_{\rm Pl}^2}\delta T^i_i, \tag{1.31}$$

$$\frac{1}{a^2}\partial^i\partial_j\left(\psi - \phi\right) = \frac{1}{M_{\rm Pl}^2}\delta T^i_j, \quad i \neq j. \tag{1.32}$$

These equations are more conveniently studied in the spatial Fourier space, i.e. using the spatial Fourier components of the corresponding variables. Our convention for Fourier decomposition for a field $\varphi(x)$ is

$$\varphi(x) = \int \mathrm{d}^3k\varphi_{\mathbf{k}}e^{i\mathbf{k}\cdot\mathbf{r}}, \tag{1.33}$$

where $\mathbf{k}$ is the spatial Fourier wavenumber and $\mathbf{r}$ is the spatial real-space coordinate.

Now, going to Fourier space and combining Eqs. (1.29) and (1.30) we obtain the Poisson equation

$$\frac{k^2}{a^2}\psi = \frac{1}{2M_{\rm Pl}^2}\left(3H(1+w)\bar{\rho}v - \delta\rho\right), \tag{1.34}$$

where v is the scalar sector of the matter velocity, i.e. $v^i \equiv \partial^i v$.

Additionally, for matter sources which have $\delta T^i_j = 0$ we have an important relation

$$\phi = \psi. \tag{1.35}$$

For simplicity in our analysis we will consider only the modes which are very deep inside the Hubble horizon, i.e. $k^2/a^2 \gg H^2$. Additionally, we will be considering the so-called *quasistatic regime*, where one assumes that the cosmological variables can change only at the time scales close to the order of the Hubble rate, i.e $H^2\delta\varphi \sim H\dot{\delta\varphi} \sim \ddot{\delta\varphi}$. In this approximation we have

$$\frac{2k^2}{a^2}\psi = -\frac{1}{M_{\rm Pl}^2}\delta\rho \tag{1.36}$$

Besides the Einstein equations an extra information is contained in the perturbed conservation equations. The $\nu = 0$ and $\nu = i$ components of the continuity equation $\nabla_\mu T^\mu_{\ \nu} = 0$ in sub-horizon limit, during dark matter domination, yield

$$\delta' + \theta = 0, \tag{1.37}$$

$$\theta' + \mathcal{H}\theta - k^2\left(\phi + c_{\rm s}^2\delta\right) = 0, \tag{1.38}$$

where we have now started to use the conformal time, related to the cosmic time through $a{\rm d}t = {\rm d}\tau$, and primes denote derivatives with respect to conformal time. Additionally, we have defined $\theta \equiv \partial_i v^i$ and $\delta \equiv (\rho(x) - \bar{\rho}(t))/\bar{\rho}(t)$. From these two equations we then obtain the master equation for linear structure formation

$$\delta'' + \mathcal{H}\delta' + \left(c_{\rm s}^2k^2 - \frac{3}{2}\mathcal{H}^2\right)\delta = 0. \tag{1.39}$$

The perturbations will experience a growing force by gravity, but the growth will be slowed down by the non-zero sound speed (i.e. by pressure). For cold dark matter the sound speed is negligible, $c_{\rm s}^2k^2 \ll \mathcal{H}^2$, and the perturbations δ will grow as $\sim t^{2/3}$.

1.2 OBSERVATIONS

In the past decades several types of observations have become sufficiently robust and now serve as the basis for our current understanding of the cosmological standard model. Let us here briefly discuss the main of these cosmological observables (see, e.g., [10]). Before doing that, however, it is important to mention that various distance definitions are used for interpreting different cosmological observations. Distances between two points in FLRW spacetime are in fact not uniquely defined, so let us start by defining various useful distances and give the relationships among them.

- **Comoving distance.** The *comoving distance* from us to an object at a given redshift z is given by

$$D_{\rm com} \equiv \frac{c}{a_0 H_0} \int_0^z \frac{\mathrm{d}\tilde{z}}{E(\tilde{z})}, \tag{1.40}$$

  where H_0 is the value of the Hubble rate at present time, and $E(z) \equiv H(z)/H_0$.

- **Luminosity distance.** For a source with an absolute luminosity $\mathcal{L}$, observed to have a flux $\mathcal{F}$ on our detectors, we can define the so-called *luminosity distance* to the source

$$D_{\rm lum}^2 \equiv \frac{\mathcal{L}}{4\pi\mathcal{F}}. \tag{1.41}$$

- **Angular diameter distance.** For an object of proper size (in the direction perpendicular to the line of observation) $\Delta\ell$, observed to subtend an angle $\Delta\theta$, we can define the so called *angular diameter distance* to the object as

$$D_{\rm ang} \equiv \frac{\Delta\ell}{\Delta\theta}. \tag{1.42}$$

For a spatially flat universe the luminosity distance is related to the comoving cosmic distance by $D_{\rm lum} = (1+z)D_{\rm com}$. This expression is rather generic and holds for almost any cosmology. It should, however, be kept in mind that it will be violated in a theory where the photon number is not conserved, for example, due to mixing of photons with some hidden sector. Additionally, the luminosity distance is related to the angular diameter distance by $D_{\rm lum} = (1+z)^2 D_{\rm ang}$.

After this prelude we can start discussing the main cosmological observations.

Supernovae Type Ia. Perhaps the best-known cosmological constraints are from *Supernovae.* The luminosities (or the absolute magnitudes) of these objects are known to be highly correlated with the widths of their light-curves. This fact allows for an accurate determination of the absolute magnitude, given the light-curve observation of a supernova. A key relation for cosmological purposes is the relation between the *distance modulus* μ (the difference between the apparent and absolute magnitudes) and the luminosity distance

$$\mu = 5 \log D_{\rm lum}/10{\rm pc}, \tag{1.43}$$

Having the distance modulus measurements of supernovae, one then can measure the luminosity distance, and hence constrain a particular cosmological model.

Cosmic Microwave Background. The Cosmic Microwave Background (CMB) is one of the major sources of information in cosmology. As we mentioned earlier, after inflation the universe was filled with a hot photon-baryon plasma. The baryons tend to cluster through gravitational attraction, but the photonic pressure stops this clustering. As a result the cosmic plasma experiences acoustic oscillations. When the universe cools down sufficiently the photons decouple from baryons and start to free-stream through the universe. This decoupling happens at redshift $z_{\rm dec} \approx 1090$ and is known as the *decoupling* or *recombination* era. The free-streaming photons

make up the CMB sky. The fluctuations of the photon temperature are sensitive to the density perturbations of the relevant energy components at the decoupling era, their velocities and the gravitational potentials. These fluctuations, measured as a function of direction $\hat{n}$, can be decomposed in spherical harmonics as

$$\frac{\delta T(\hat{n})}{T} = \sum_{\ell} \sum_{m} a_{\ell m} Y_{\ell m}(\hat{n}), \tag{1.44}$$

where T is the average temperature of the CMB, $a_{\ell m}$'s are the corresponding angular modes and $Y_{\ell m}(\hat{n})$'s denote the spherical harmonics.

For each mode ℓ, the variance of the $a_{\ell m}$ modes is known as the angular power spectrum, given by

$$C_{\ell} = \frac{1}{2\ell + 1} \sum_{m} \langle |a_{\ell m}|^2 \rangle \tag{1.45}$$

A relatively simple information in the CMB angular power spectrum is encoded in the scale of acoustic oscillations. The effective sound speed of the photon-baryon fluid $c_{\rm s}$ determines this scale through

$$r_{\rm s}(z_{\rm dec}) = \int_{z_{\rm dec}}^{\infty} {\rm d}\tilde{z} \frac{c_{\rm s}(\tilde{z})}{H(\tilde{z})}. \tag{1.46}$$

The associated angular scale $\theta_{\rm ang}(z_{\rm dec})$ and the angular diameter distance to the acoustic scale $D_{\rm ang}(z_{\rm dec})$ are related with each other by

$$(1 + z_{\rm dec}) D_{\rm ang}(z_{\rm dec}) = \frac{r_{\rm s}(z_{\rm dec})}{\theta_{\rm ang}(z_{\rm dec})}. \tag{1.47}$$

Baryon Acoustic Oscillations (BAO). The acoustic oscillations mentioned in the context of CMB affect not only photons but also baryons. Similarly to the acoustic scale in Eq. (1.46), there is a similar scale for baryons, imprinted during the so-called drag epoch, taking place at $z_{\rm drag} \approx 1020$, when baryons are decoupled from photons.

One expects an enhanced galaxy population at the scales of cosmic structure separated by $r_s(z_{drag})$. The corresponding angular scale at a particular redshift z then serves as a useful probe for the cosmic background. The relevant geometric expression is similar to (1.47) and is given by

$$(1+z)\theta_s(z) = \frac{r_s(z_{drag})}{D_{ang}(z)}. \tag{1.48}$$

Growth of structure An instrumental quantity often employed in LSS studies is the growth rate f, defined as

$$f \equiv \frac{d\ln\delta}{d\ln a}. \tag{1.49}$$

There is a useful fitting formula for this quantity, given by $f = \Omega_m^\gamma$, where the power is constant in ΛCDM and is approximately equal to $\gamma \sim 0.55$. An observed deviation from this value will be a smoking gun evidence for beyond ΛCDM physics.

Weak lensing. One of the striking predictions of any modern theory of gravity is the light deflection by massive sources. Cosmologists have come up with a beautiful idea which exploits the gravitational lensing for measuring the properties of the large scale structure. When a light from a galaxy is travelling trough the LSS, it gets slightly distorted. The distortions of this light can be characterized by the gradient $\partial\theta^i_{source}/\partial\theta^j$, where θ^j is the angle under which we observe the given light ray, while θ^i_{source} is the unaltered (unlensed) angle, and the indices (i,j) label two directions on the sky. In a theory of gravity (not necessarily GR) this gradient is given by

$$\frac{\partial\theta^i_{source}}{\partial\theta^j} - \delta_{ij} \equiv \int_0^{r_{source}} d\tilde{r}\left(1 - \frac{\tilde{r}}{r_{source}}\right)\tilde{r}(\phi-\psi)_{,ij}, \tag{1.50}$$

where r_{source} denotes the comoving distance to the considered galaxy.

This matrix is conventionally written as

$$\frac{\partial\theta^i_s}{\partial\theta^j} - \delta_{ij} \equiv \begin{pmatrix} -\kappa_{wl}-\gamma_1 & -\gamma_2 \\ -\gamma_2 & -\kappa_{wl}+\gamma_1 \end{pmatrix}. \tag{1.51}$$

It can be shown that the so-called *convergence* $\kappa_{\rm wl}$ describes the overall magnification of the sources, while the components of the *shear* γ_1 and γ_2 describe its distortions. The measurements of these quantities and their cross-correlations provide valuable cosmological information.

1.3 THE INFLATIONARY PARADIGM

In the previous sections of this introduction we have presented the main ideas of the cosmological standard model. In that discussion we have taken the observed large-scale homogeneity and isotropy of the universe, as well as the small value of the spatial curvature, as granted. They are, however, rather unnatural in the standard FLRW universe with a sequence of radiation and matter dominated epochs. This has motivated the birth of the inflationary paradigm.

Let us start our discussion from the so-called *flatness problem*. In a decelerating universe[1] the absolute value of the curvature contribution in Eq. (1.16) increases, because its denominator $aH = \dot{a}$ decreases, unless the curvature of the universe is exactly zero. The observed spatial flatness then suggests that in the past the universe has experienced a phase of accelerated expansion, known as *cosmic inflation* (see e.g. [10] for a pedagogical introduction to inflation).

Another striking issue with the standard cosmological picture is the overall homogeneity of CMB. It can be estimated that the CMB patches of more than ~ 1 degree apart never would have time to communicate with each other starting from the time of infinitely small universe (the *Big Bang*)

1 Notice that both radiation- and matter-dominated epochs are necessarily decelerating because the second Friedmann equation Eq. (1.7) shows that $\ddot{a} < 0$ for any equation of state satisfying $1 + 3w > 0$.

to the time of recombination [10][2]. While the CMB photons were, in fact, in causal contact after the last scattering, the entire idea of CMB suggests that they shouldn't interact, hence they cannot thermalize after decoupling.

The crucial quantity for our discussion here is the *comoving particle horizon*, defined as

$$d_{\rm H,com} \equiv \int_0^a \frac{{\rm d}\tilde{a}}{\tilde{a}} \frac{1}{\tilde{a}H(\tilde{a})}, \tag{1.52}$$

which measures the maximum distance the light could have travelled in FLRW spacetime between times characterized by scale factors 0 and a. It is instructive to rewrite $d_{\rm H,com}$ in terms of the *comoving Hubble radius* $(aH)^{-1}$ as

$$d_{\rm H,com} = \int_1^{\ln a} \frac{{\rm d}\ln\tilde{a}}{\tilde{a}H(\tilde{a})}. \tag{1.53}$$

The last expression suggests a solution to the horizon problem. If we could have en epoch during which $(aH)^{-1}$ is increasing towards the past, then $d_{\rm H,com}$ could be made larger. What we are seeking for is a mechanism which would make $d_{\rm H,com}$ much larger than $(aH)^{-1}$ during the standard expansion. This is precisely the idea of inflation; make the comoving Hubble radius larger in the past, so that the entire observable CMB would have been in causal contact at some point in the past.

It is easy to notice that achieving such a regime does not only resolve the issue with the horizon, but also resolves the flatness problem. Indeed, the condition ${\rm d}(aH)^{-1}/{\rm d}t < 0$ implies that $\ddot{a} > 0$ and hence, using the second Friedmann equation, that $w < -1/3$, which is exactly the condition for the flat universe to be an attractor under cosmic evolution.

The most common dynamical realization of inflation is through a canonically normalized scalar field φ with a potential $V(\varphi)$. The homogeneous

2 There is, however, a substantial assumption here. In such arguments we assume that the classical picture of spacetime holds till the very Big Bang. From quantum gravity perspective this might be seen as an oversimplification.

and isotropic equation of motion (i.e. taking $\varphi(x)$ to be a function of time only) of such a field is given by

$$\ddot{\varphi} + 3H\dot{\varphi} + V(\varphi)_{,\varphi} = 0, \tag{1.54}$$

where $V(\varphi)_{,\varphi} \equiv \partial V(\varphi)/\partial\varphi$.

Additionally, the energy and momentum of the scalar field can be shown to be

$$\rho_\varphi = \frac{1}{2}\dot{\varphi}^2 + V(\varphi), \tag{1.55}$$

$$p_\varphi = \frac{1}{2}\dot{\varphi}^2 - V(\varphi), \tag{1.56}$$

respectively.

In order this field to be able to successfully drive the inflationary dynamics, we need the equation of state of the scalar field to be close enough to -1, which is the case of the shallow potentials. Additionally, in order to have long enough inflation, we need the above condition to be satisfied for long enough period. These two conditions are formally written as $\epsilon \equiv -\dot{H}/H^2 \ll 1$ and $\eta \equiv \dot{\epsilon}/H\epsilon \ll 1$. The inflationary stage should be followed by the stage of hot FLRW expansion, which means that the inflationary stage must end eventually. This additionally means that inflation cannot be realized via a cosmological constant, because in that case the universe would have no physical clock specifying when the inflation should end.

While the primary goal of inflationary scenario was to solve the abovementioned horizon and flatness problems, it turned out that it can do much more than that. In fact, inflation is a beautiful mechanism which transfers the quantum fluctuations of the inflationary scalar field and the spacetime metric to the classical seeds of the large scale structure. Particularly, inflation predicts that the power of primordial fluctuations in matter density, which later seeds the LSS formation, should be nearly scale

invariant, with a slight tilt characterized by a slope of $n_s - 1$, where n_s is typically referred to as *scalar spectral index*. Additionally, inflation also predicts presence of primordial gravitational waves, again from the initial quantum fluctuations of the metric. The amount of produced primordial gravitational waves are typically characterized by the ratio of powers in tensor and scalar fluctuations, referred to as the *tensor to scalar ratio*, and denoted by r.

The idea of inflation is summarized in Fig. 1.1. The decreasing comoving Hubble radius $(Ha)^{-1}$ makes the particle horizon at the epoch of CMB formation larger compared to the value in the standard, non-inflationary scenario. This additionally resolves the flatness problem. Moreover, and perhaps more importantly, inflation is an elegant mechanism for generating the observed large scale structure from the primordial quantum fluctuations of the inflaton field and the spacetime metric.

1.4 BEYOND THE STANDARD MODEL: DYNAMICAL DARK ENERGY AND MODIFIED GRAVITY

Dynamical dark energy Similarly to inflation, one might naturally think that the present-day accelerated expansion of the universe is not caused by a cosmological constant but rather by a slowly rolling scalar field. Such a scenario is known as dynamical dark energy (also referred to as *quintessence*) scenario [11, 12]. Unlike the inflationary epoch, the late-universe acceleration does not need to end, hence the cosmological constant explanation is a completely viable one from this point of view. However, one might argue that a dynamical scenario is a more elegant explanation for the accelerated expansion, and it is one of the motivations to study such models in detail. There is, of course, also a strong theoretical motivation to do this. It turns out that the low-energy, effective descriptions of the potentially fundamental theories contain scalar degrees of freedom. This means that if the future probes detect a deviation from the ΛCDM scenario, we can potentially

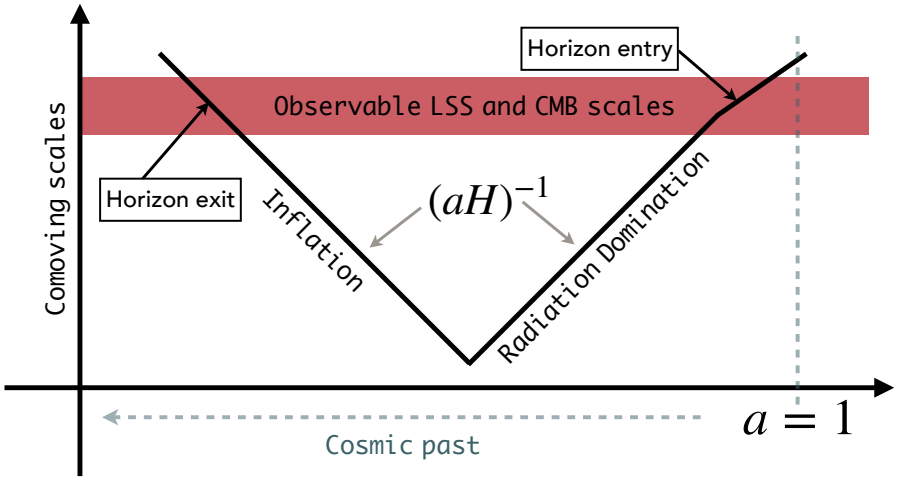

Figure 1.1: The idea of inflation is to modify the expansion history of the universe in such a way that the comoving Hubble radius is decreasing before the standard expansion regime starts.

learn about the fundamental theories. In practice this argument, of course, is more complicated, as the observational consequences of, for example, string theory so far are rather ambiguous. An interesting development in this direction was suggested in [13]. The authors have *conjectured* that the scalar field potential for all consistent theories should satisfy the constraint

$$\frac{|\nabla_\phi V|}{V} \geq c\,, \qquad c \sim 1\,. \tag{1.57}$$

This conjecture is in contrast to the string theory landscape scenario [14–19] (see Ref. [20] for a brief review of related ideas), where it is considered that string theory describes an enormous number of metastable de-Sitter vacua.

There is no consensus about the theoretical validity of Eq. (1.57) in the string theory community (see [21] for a review). Moreover, the use of the conjecture in its current shape for cosmological phenomenology is still rather ambiguous. Indeed, as the conjecture does not specify the value of the constant c, it is difficult to confront it with phenomenological studies. The way forward in this situation is to study the phenomenological implications of the models presented in [13] which have been served as the primary support for the conjecture. These models are given in terms of concrete potentials and therefore their precise phenomenologies can be worked out. The main result of such an investigation in [22] is that all these considered models are incompatible with cosmological data. This, perhaps, is difficult to interpret as a very strong observational challenge for Eq. (1.57) because, again, in the latter the imprecise nature of c makes it impossible to draw decisive, quantitative conclusions.

Even if not making the connection to any fundamental theory, the dynamical dark energy scenario is still very interesting to study. One of the interesting motivations to study such alternatives is the so-called *coincidence problem*, which is based on the question of why is the universe starting to accelerate exactly at the present time, and not, say, much later in the future. In this context let us discuss a particularly appealing feature, namely the presence of the so called *scaling fixed points* in the phase space of quintessence models. The model that we will study has a simple exponential potential of the form $V(\phi) = V_0 e^{\lambda\phi}$. For $\lambda^2 > 3(w_B + 1)$, with w_B being the equation of state for the background fluid (e.g. dark matter or radiation), the universe enters a scaling regime where the scalar field mimics the evolution of the background fluid, with $w_{DE} = w_B$; the dark energy density parameter takes the form $\Omega_{DE} = 3(w_B + 1)/\lambda^2$ (see [23] for a review). This scaling property is illustrated in the left panel of Fig. 1.2 for a sufficiently large value of λ

(chosen to be $\sqrt{750}$ in this example), where we have shown the evolution of the quintessence energy density compared to that of dark matter. The figure shows that the scalar field, after some oscillations, quickly follows the background and one can achieve a scaling solution during matter domination in this example. Te horizontal axis here is $N \equiv \ln a$, with $N = 0$ corresponding to the present time. Such scaling solutions may indeed provide a solution to the coincidence problem. Even though these are very interesting features, the obvious problem, of course, is that a single-exponential potential has a constant slope, and therefore, once the scaling regime is switched on it never ends, so there is no dark energy domination.

A particular extension of the considered model is the following two-exponential potential

$$V(\phi) = V_1 e^{\lambda_1 \phi} + V_2 e^{\lambda_2 \phi} \,. \tag{1.58}$$

The phenomenological merit of this double exponential model is that under certain conditions the scaling solution can gracefully exit to the desired accelerating phase at late times. This transition can be obtained if $\lambda_1^2 > 3(w_B + 1)$ and $\lambda_2^2 < 3(w_B + 1)$ in the potential (1.58). At early times, the potential is dominated by the $e^{\lambda_1 \phi}$ term, for which the scalar field follows the equation of state of radiation and/or matter, hence scaling solutions. Later in the evolution of the universe, the $e^{\lambda_2 \phi}$ term dominates, for which the evolution is not of the scaling form and the late-time attractor is the scalar field dominated solution (with $\Omega_{DE} = 1$). In this scenario, the asymptotic value of the dark energy equation of state is $w_{DE} = -1 + \lambda_2^2/3$, providing viable cosmologies, just as for the single exponential with $\lambda^2 < 3(w_B + 1)$. The right panel of Fig. 1.2 shows an example of this so-called *scaling freezing* scenario with the double-exponential potential, where the transition from the scaling evolution to the scalar field dominated evolution has been depicted.

Modifications of gravity. The *dynamical dark energy scenario* mentioned above is one interesting way to go beyond the standard ΛCDM scenario.

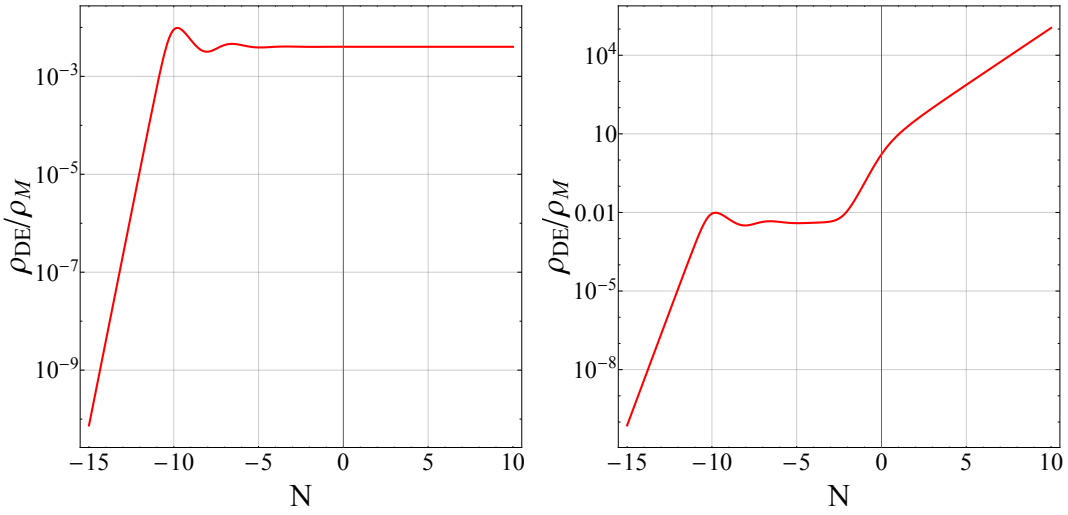

Figure 1.2: The ratio of the dark energy density ρ_{DE} to that of matter ρ_M as a function of N. *The left panel* demonstrates the scaling solutions of a single-exponential model $V(\phi) = V_0 e^{\lambda\phi}$ with $\lambda^2 > 3(w_B + 1)$, while *the right panel* is for $V(\phi) = V_1 e^{\lambda_1\phi} + V_2 e^{\lambda_2\phi}$ with $\lambda_1^2 > 3(w_B + 1)$ and $\lambda_2^2 < 3(w_B + 1)$.

There is, however, another exciting prospect. As we mentioned earlier, gravity is the most relevant interaction at the cosmological scales. This means that cosmology is an ideal playground for testing the underlying theory of gravity. In order to effectively study the limitations of GR at cosmological scales, one needs to consider its viable modifications.

GR, in fact, is the *unique* theory of interacting, massless, spin-2 field (see [24] for a proof). This immediately suggests that in order to construct an alternative to GR one can either consider a massive extension of the latter, or add extra dynamical degrees of freedom, such as additional scalar field(s).

In the second class of modifications a particularly well-studied and understood class is the scalar-tensor gravity, where the dynamics of GR is extended with a scalar field. It turns out, however, that many a-priori valid modifications should be actually discarded based on theoretical arguments.

A particular problem for a given theory is the presence of unstable solutions. Commonly discussed types of instabilities are the so-called *ghost* and *gradient instabilities*.

Let us start by discussing the gradient instability. It basically originates from a wrong sign gradient term in the Lagrangian of the theory. For the simplest possible example let us consider a scalar field theory in Minkowski spacetime which has a wrong sign spatial gradient term. The equation of motion for the scalar field φ of such a theory in Fourier space is simply given by

$$\ddot{\varphi}_k - k^2\varphi = 0, \tag{1.59}$$

where k is the absolute value of the spatial Fourier wavenumber. Note that in a healthy theory the second term would have been with an opposite sign. The solutions of this equation scale as $\varphi_k(t) \sim e^{\pm kt}$, the growing part of which leads to a *gradient instability*. The characteristic timescale of the instability scales with the wavenumber as $1/k$.

Another widely encountered type of pathology is the ghost instability. To understand ghosts it is enough to consider the following, non-gravitational toy example for two scalar fields χ and φ

$$\mathcal{L} = \frac{1}{2}\partial^\mu\chi\partial_\mu\chi - \frac{1}{2}\partial^\mu\varphi\partial_\mu\varphi + V(\chi,\varphi), \tag{1.60}$$

where the potential $V(\chi,\varphi)$ is given by

$$V(\chi,\varphi) = -\frac{1}{2}m_\chi^2\chi^2 - \frac{1}{2}m_\varphi^2\varphi^2 + \lambda\chi^2\varphi^2, \tag{1.61}$$

with m_χ and m_φ being the masses of the fields and λ a positive constant.

Note, in particularly, that the two fields have opposite sign kinetic terms. This is precisely what we mean by a ghost degree of freedom - a field with a wrong sign kinetic term. As the χ field has a negative energy, the vacuum state can decay into χ and φ particles and the rate of this decay is in fact

infinite [25, 26] (assuming the considered theory is valid up to arbitrarily high energies). This means that the presence of ghosts makes the theory highly undesirable. Ghost fields are typically present in theories whose equations of motion contain higher than second order time derivatives [27, 28]. This fact is one of the main locomotives for constructing alternatives to GR. One of the most well studied class of theories is in fact the Horndeski theory - the theory of a single scalar field coupled to gravity in such a way that the resulting equations of motion are second order in time [29, 30]. This last requirement ensures the absence of ghosts.

Horndeski theory is a generalization of *scalar-tensor* theories known since a long time ago. One of the first examples is the *Brans-Dicke theory* [31], the main idea of which is to promote the gravitational constant to a dynamical field. In the so called *Jordan frame* (which means that the matter fields are minimally coupled to the metric $g_{\mu\nu}$), the Brans-Dicke theory has the following action

$$S = \frac{M_{\rm Pl}^2}{2}\int \mathrm{d}^4x\sqrt{-g}\left[\frac{1}{2}\varphi R - \frac{\omega_{\rm BD}}{2\varphi}\nabla^\mu\varphi\nabla_\mu\varphi - V(\varphi)\right] + S_{\rm m}(g_{\mu\nu},\Psi_i), \quad (1.62)$$

where $\omega_{\rm BD}$ is a constant. The GR limit of this theory is recovered in the limit of infinitely large Brans-Dicke parameter $\omega_{\rm BD}$.

From the point of view of cosmology this theory is an interesting example of modified gravity because we can clearly see the effects of the additional scalar degree of freedom on large scale structure. Particularly, the Poisson equation (which in GR is given by Eq. (1.34)) in this theory, in the quasistatic limit, is given by

$$\frac{k^2}{a^2}\phi = -4\pi G\mu(a,k)\rho_{\rm m}\delta, \quad (1.63)$$

where

$$\mu(a,k) \equiv \frac{M_{\rm Pl}}{\bar{\varphi}}\frac{2(2+\omega_{\rm BD}) + (\bar{\varphi}/M_{\rm Pl})m^2a^2/k^2}{3+2\omega_{\rm BD} + (\bar{\varphi}/M_{\rm Pl})m^2a^2/k^2}, \quad (1.64)$$

with $\bar{\varphi}$ being the homogeneous background sector of the scalar field φ, and m being the mass of the scalar field. As we see, contrary to GR, here the gravitational strength, which controls the effectiveness of dark matter clustering, is a function of scale and time.

Additionally, the relation between the two gravitational potentials (which in GR is given by the simple identity Eq. (1.35)) in the quasistatic limit is given by:

$$\eta(a,k) \equiv \frac{\phi}{\psi} = \frac{2(1+\omega_{\rm BD}) + m^2\bar{\varphi}a^2/k^2}{2(2+\omega_{\rm BD}) + m^2\bar{\varphi}a^2/k^2}. \tag{1.65}$$

Interestingly, the functional forms of these two new fucntions $\mu(a,k)$ and $\eta(a,k)$ are generic for the entire class of Horndeski gravity [32]. Particularly, these can be written as

$$\mu(a,k) = h_1(a)\frac{1+k^2h_5(a)}{1+k^2h_3(a)} \tag{1.66}$$

$$\eta(a,k) = h_2(a)\frac{1+k^2h_4(a)}{1+k^2h_5(a)}, \tag{1.67}$$

where h_i are functions of background only, and their form is model-specific.

Horndeski gravity is expected to be constrained by several high-precision large-scale structure surveys. However, the recent detection of the gravitational waves originating from a pair of merging neutron stars and the simultaneous detection of their electromagnetic counterpart, the LIGO event GW170817 [33] and its counterpart GRB 170817A [34], have already cut a large portion out from the Horndeski Lagrangian. This has been achieved through the strong bounds imposed on the speed of gravitational waves (which is constrained to be very close to the speed of light in vacuum); see [35] for a recent review on the topic. Note, however, that the mentioned bound on the speed of gravitational waves is strictly valid only at the scales of LIGO events, which is $k \sim \mathcal{O}(10-100)$ Hz. Horndeski gravity, on the other hand, in the cosmological context is typically used at the scale of

present-time cosmic expansion rate, H_0, which is about 20 orders of magnitude smaller than the LIGO scale. This means that for interpreting the LIGO bounds one might need to include corrections to the considered theories, which can then naturally bring the speed of gravitational waves in these theories to be very close to the speed of light.

Let us conclude this section by mentioning that while the Horndeski-type general approach to Modified Gravity is very fruitful, it still misses some important classes of theories. Among these modifications to gravity, the bimetric theory of ghost-free, massive gravity is of particular interest. It stands out especially because of the strong theoretical restrictions on the possibilities for constructing a healthy theory of this type. Indeed, historically it has proven to be difficult to invent a healthy theory of massive, spin-two field beyond the linear regime. The linearised theory has been known for a long time [36], while at the fully nonlinear level the theory has been discovered only recently by constructing the ghost-free theory of massive gravity [37–46]. This development has also naturally led to the healthy theory of interacting, spin-2 fields, i.e. the theory of ghost-free, massive bigravity [47]; see Refs. [48–50] for reviews.

Over the past decade, there has been a substantial effort directed towards understanding the cosmological behaviour of bimetric models, both theoretically and observationally. Particularly, it has been shown that bigravity admits FLRW cosmologies which perfectly agree with cosmological observations at the background level (see Ref. [51, 52] for reviews). At the level of linear perturbations the cosmological solutions have been shown to suffer from either ghost or gradient instabilities, although the latter can be pushed back to arbitrarily early times by imposing a hierarchy between the parameters of the theory [53]. It is also conjectured [54] that the gradient instability might be cured at the nonlinear level due to the presence of the Vainshtein screening mechanism (see later in this chapter) in the theory.

The version of the bimetric theory studied in all these works is the so-called singly-coupled scenario, where the matter sector is assumed to

couple to only one of the two metrics (spin-2 fields). The metric directly coupled to matter is called physical metric, and the other spin-2 field, called reference metric, affects the matter sector only indirectly and through its interaction with the physical metric.

1.5 SCREENING MECHANISMS IN MODIFIED GRAVITY

One of the most well-understood properties of modified gravity theories is that there is an extra (often referred to as a "fifth") force in addition to the standard Newtonian force. To understand this effect let us study the following, quite generic coupling of the matter fields to the scalar field sector:

$$S = \int \mathrm{d}^4x\sqrt{-g}\left[\frac{M_{\rm Pl}^2}{2}R - \frac{1}{2}\nabla^\mu\varphi\nabla_\mu\varphi - V(\varphi)\right] + S_{\rm m}(\tilde{g}_{\mu\nu}, \Psi_i), \quad (1.68)$$

where

$$\tilde{g}_{\mu\nu} \equiv A(\varphi)g_{\mu\nu}. \quad (1.69)$$

A central equation here is the geodesic equation for a non-relativistic test particle in the Newtonian limit:

$$\ddot{x}^i + \Gamma^i_{00} = -\frac{\mathrm{d}\ln A}{\mathrm{d}\varphi}\nabla^i\varphi, \quad (1.70)$$

where Γ denotes the Christoffel symbol, and x^i are the spatial coordinates of the considered test particle. This equation motivates us to interpret the right hand side as a fifth force.

This then leads to a problem – gravity is very well tested at small scales, for example in Solar System, and no fifth forces have been detected [55]. The obvious question then is how to reconcile the modifications of gravity with the local tests. There are several interesting proposals which allow

for the fifth force to be *screened* in an environment-dependent manner. For demonstrating the main idea behind the common screening mechanisms let us consider the field equation of motion of the theory given in Eq. (1.68)

$$\Box\varphi = V(\varphi)_{,\varphi} - \frac{\mathrm{d}\ln A}{\mathrm{d}\varphi}\mathrm{Tr}\left[T^{\mu\nu}\right], \tag{1.71}$$

where $T^{\mu\nu}$ is the Einstein frame metric, $\Box \equiv \nabla^{\mu}\nabla_{\mu}$ is the d'Alambert operator, and the trace is taken with $g_{\mu\nu}$. For a non-relativistic matter sector, such as cold dark matter, $\mathrm{Tr}\left[T^{\mu\nu}\right] = -\rho$, with ρ being the matter density.

This motivates us to define $V^{\mathrm{eff}}(\varphi;\rho) \equiv V(\varphi) + \rho\ln A(\varphi)$; an effective potential which reacts to the matter density of the ambient space. Let us discuss two qualitatively different choices for the $A(\varphi)$ function and the potential $V(\varphi)$:

- $V(\varphi) = \frac{\Lambda^{n+4}}{\varphi^n}$, $A(\varphi) = e^{\varphi/M_{\mathrm{c}}}$,
- $V(\varphi) = -\frac{1}{2}\mu^2\varphi^2 + \frac{\lambda}{4}\varphi^4$, $A(\varphi) = 1 + \frac{\varphi^2}{2M_{\mathrm{s}}^2}$,

where Λ (not to be confused with the cosmological constant), μ, λ, M_{c} and M_{s} are constants.

The first of these choices is in the class of *Chameleon screening mechanisms* [56], the idea of which is to enhance the effective mass of the scalar field, hence rendering the corresponding fifth force to be a short-range one; see the left panel of Fig. 1.3. The second choice corresponds to the *Symmetron mechanism*, [57] the idea of which is to suppress the coupling of the scalar field to the matter; see the right panel of Fig. 1.3.

Another important mechanism is the Vainshtein mechanism [58, 59], which relies on the non-linearities of the scalar field induced due to higher order derivative self-couplings, such us $\mathcal{L} \supset\sim \partial_{\mu}\varphi\partial^{\mu}\varphi\Box\varphi$. Vainshtein mechanism is central for several interesting theories, including massive gravity/bigravity discussed above.

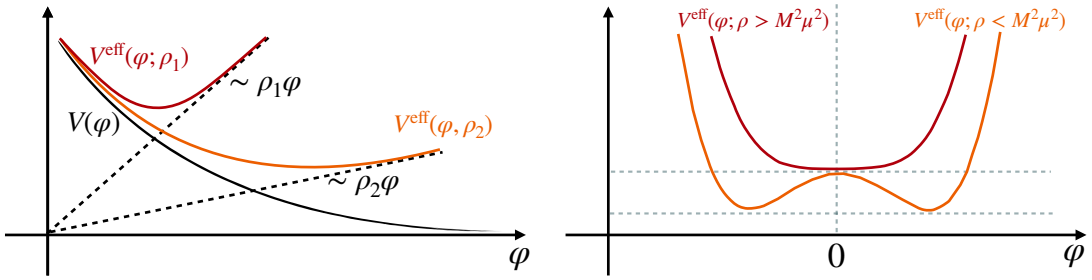

Figure 1.3: *Left panel:* Demonstration of the Chameleon screening mechanism *Right panel:* Demonstration of the Symmetron screening mechanism. See the text for details.

1.6 THE ERA OF PRECISION COSMOLOGY

Before summarizing the content of this thesis let us present a comment on how fast the presion of cosmological observations grows. The quality of modern cosmological datasets posits very high standards in front of cosmological model building initiatives. As a striking demonstration of this let us examine Fig. 1.4, which shows the current observational constraints on inflationary models by the CMB data given by the Planck collaboration [60] alongside with the same constraints from a decade-old WMAP collaboration [61]. We see that many interesting models, e.g. the polynomial inflationary models with potential ϕ^k with $k = 2, 4/3, 1, 2/3$, are now disfavored or ruled out by date. All these models were inside the 95% sweet spot of the data in 2009 provided by the WMAP collaboration, as one can see in Fig. 1.4, while they are now either outside or close to the boundary of the 95% confidence region of the Planck 2018 data.

This demonstrates that in the theoretical analysis of the data, it is no longer possible to perform a *parametric, order of magnitude analysis* as it was

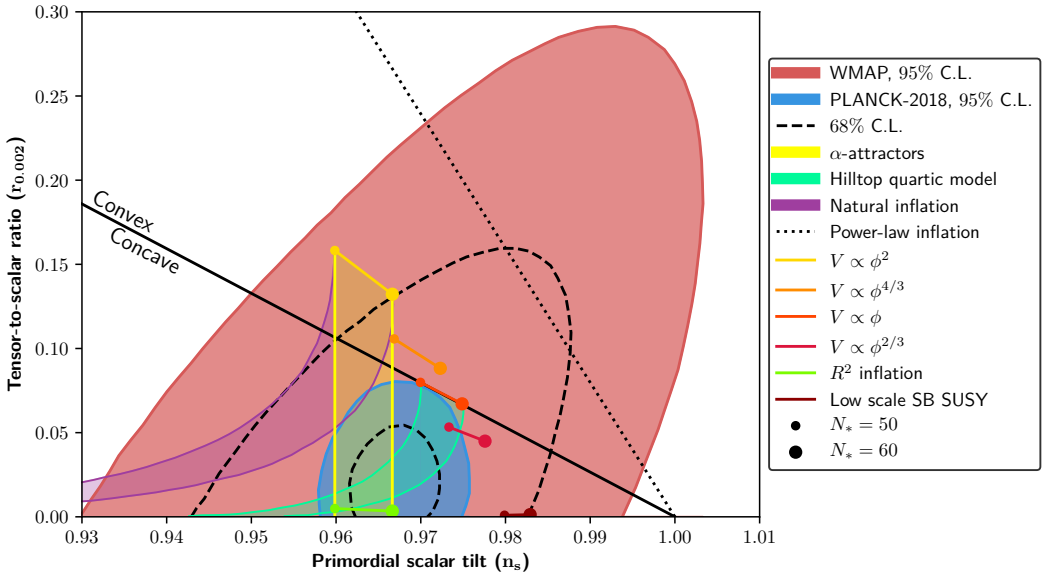

Figure 1.4: Evolution of precision in inflationary parameters over a decade, from WMAP [61] to Planck [60]. The reconstructed Planck constraints correspond to the combination TT,TE,EE+lensing+BK14+BAO provided in [60]. One can look, for example, at the area between $n_s = 0.95$ and $n_s = 0.98$. Although both of these values were inside the 68% contour back in 2009, they are now strongly disfavored with more than 95% confidence.

normal in the past, especially in string theory phenomenology. The same concerns such expressions as "parametrically small", or "parametrically large". We can see examples in Fig. 1.4 showing that reducing the bound on r from ~ 0.08 to ~ 0.04 has made various theoretical ideas either supported or ruled out by the precision data in cosmology.

Similarly, the constraints on dark energy become more and more precise. For example, 15 years ago the constraints on the parameter λ in the exponential potential $e^{\pm\lambda\phi}$ for quintessence, allowed $\lambda = 1.6$ [62, 63]. Meanwhile, in the discussion of the quintessence models supporting the recent swampland conjecture [13] it was necessary to pay full attention to a small

difference between numbers such as $\lambda < 1$ and $\lambda < 1.4$. Indeed, models with $\lambda > 1$ are ruled out by cosmological observations with more than 99.7% confidence, whereas the condition $\lambda < 1$ is not satisfied by the string theory models of [13].

1.7 THIS THESIS

- Chapter 2 is dedicated to a study of a new class of inflationary models known as cosmological *α-attractors*. We promote these models towards a unified framework describing both inflation and dark energy. We construct and study several phenomenologically rich models which are compatible with current observations. In the simplest models, with vanishing cosmological constant Λ, one has the tensor to scalar ratio $r = \frac{12\alpha}{N^2}$, with N being the number of e-folds till the end of inflation, and the asymptotic equation of state of dark energy $w = -1 + \frac{2}{9\alpha}$. For example, for a theoretically interesting model given by $\alpha = 7/3$ one finds $r \sim 10^{-2}$ and the asymptotic equation of state is $w \sim -0.9$. Future observations, including large-scale structure surveys as well as Cosmic Microwave Background B-mode polarization experiments will test these, as well as more general models presented here. We also discuss the gravitational reheating in models of quintessential inflation and argue that its investigation may be interesting from the point of view of inflationary cosmology. Such models require a much greater number of *e*-folds, and therefore predict a spectral index n_s that can exceed the value in more conventional models of inflationary α-attractors by about 0.006. This suggests a way to distinguish the conventional inflationary models from the models of quintessential inflation, even if the latter predict $w = -1$. This chapter is based on Ref. [64].

- The topic of Chapter 3 is the theory of massive bigravity, where one has two dynamical tensor degrees of freedom. We consider an interesting extension where both of the metrics are coupled to the matter sector, which is known as the *doubly-coupled bigravity*. The main aim of this chapter is the study of gravitational-wave propagation in this theory. We demonstrate that the bounds on the speed of gravitational waves imposed by the recent detection of gravitational waves emitted by a pair of merging neutron stars and their electromagnetic counterpart, events GW170817 and GRB170817A, strongly limit the viable solution space of the doubly-coupled models. We have shown that these bounds either force the two metrics to be proportional at the background level or the models to become singly-coupled (i.e. only one of the metrics to be coupled to the matter sector). The mentioned proportional background solutions are particularly interesting. Indeed, it is shown that they provide stable cosmological solutions with phenomenologies equivalent to that of ΛCDM at the background level and at the level of linear perturbations. The nonlinearities, on the other hand, are expected to show deviations from ΛCDM. This chapter is based on Ref. [65].

- In Chapter 4 we study the first cosmological implications of a novel massive gravity theory, recently proposed by Chamseddine and Mukhanov, known as the *mimetic theory of massive gravity*. This is a theory of ghost-free massive gravity, which additionally contains a so-called *mimetic dark matter* component. In an echo of other modified gravity theories, there are self-accelerating solutions which contain a ghost instability. In the ghost-free region of parameter space, the effect of the graviton mass on the cosmic expansion history amounts to an effective negative cosmological constant, a radiation component, and a negative curvature term. This allows us to place constraints on the model parameters—particularly the graviton mass—by insisting that

the effective radiation and curvature terms be within observational bounds. The late-time acceleration must be accounted for by a separate positive cosmological constant or other dark energy sector. We impose further constraints at the level of perturbations by demanding linear stability. We comment on the possibility of distinguishing this theory from ΛCDM with current and future large-scale structure surveys. This chapter is based on Ref. [66].

- The final Chapter 5 is dedicated to the study of the effects of screening mechanisms in modified gravity on the dynamics of the spherical collapse of dark matter. In particular, we investigate the splashback scale in *Symmetron modified gravity.* The splashback radius $r_{\rm sp}$ has been identified in cosmological N-body simulations as an important scale associated with gravitational collapse and the phase-space distribution of recently accreted material. We employ a semi-analytical approach, namely the self-similar spherical collapse framework, to study the spherical collapse of dark matter halos in Symmetron gravity. We provide, for the first time, insights into how the phenomenology of splashback is affected by modified gravity. The Symmetron is a scalar-tensor theory which exhibits a screening mechanism whereby higher-density regions are screened from the effects of a fifth force. In this model, we find that, as over-densities grow over cosmic time, the inner region becomes heavily screened. In particular, we identify a sector of the parameter space for which material currently sitting at the splashback radius $r_{\rm sp}$, during its collapse has followed the formation of this screened region. As a result, we find that for this part of the parameter space the splashback radius is maximally affected by the Symmetron force and we predict changes in $r_{\rm sp}$ up to around 10% compared to its General Relativity value. Because this margin is within the precision of present splashback experiments, we expect

this feature to soon provide constraints for Symmetron gravity on previously unexplored scales. This chapter is based on Ref. [67].

Other papers of the author include Refs. [22, 68–75].

Part I

COSMIC ACCELERATION IN SUPERGRAVITY

2

DARK ENERGY, α-ATTRACTORS, AND LARGE-SCALE STRUCTURE SURVEYS

This chapter is dedicated to a study of a new class of inflationary models known as cosmological *α-attractors*. We promote these models towards a unified framework describing both inflation and dark energy. We construct and study several phenomenologically rich models which are compatible with current observations. In the simplest models, with vanishing cosmological constant Λ, one has the tensor to scalar ratio $r = \frac{12\alpha}{N^2}$, with N being the number of e-folds till the end of inflation, and the asymptotic equation of state of dark energy $w = -1 + \frac{2}{9\alpha}$. For example, for a theoretically interesting model given by $\alpha = 7/3$ one finds $r \sim 10^{-2}$ and the asymptotic equation of state is $w \sim -0.9$. Future observations, including large-scale structure surveys as well as Cosmic Microwave Background B-mode polarization experiments will test these, as well as more general models presented here. We also discuss the gravitational reheating in models of quintessential inflation and argue that its investigation may be interesting from the point of view of inflationary cosmology. Such models require a much greater number of *e*-folds, and therefore predict a spectral index n_s that can exceed the value in more conventional models of inflationary α-attractors by about 0.006. This suggests a way to distinguish the conventional inflationary models from the models of quintessential inflation, even if the latter predict $w = -1$.

This chapter is based on: Y. Akrami, R. Kallosh, A. Linde, V. Vardanyan, *Dark energy, α-attractors, and large-scale structure surveys*, JCAP **1806** (2018) 041, arXiv:1712.09693.

2.1 INTRODUCTION

In this chapter we are going to construct viable dynamical dark energy models in the context of recent progress achived in cosmological applications of *supergravity*. We particularly will be using some novel ideas which have been discovered in inflationary cosmology. More concretely, recent investigations have found a broad class of theories, known as cosmological α-attractors, which are based on models where the kinetic term of a scalar field has a pole [76–81]. In such theories, the potential has a plateau shape, exponentially rapidly approaching a constant at large values of the inflaton field φ. These models, to be described in section 2.2 of this chapter, are favored by the recent inflation-related cosmological observations [82].

Because of the extreme flatness of the potential in α-attractors, these models can be suitable not only for describing inflation but also to describe dark energy, see e.g. Refs. [83–88]. Moreover, it may also be possible to find α-attractor models which can simultaneously describe inflation and dark energy [84, 87, 88] in the context of the *quintessential inflation* [89].

In this chapter, we extend the investigation of the quintessential inflation models based on α-attractors. We study models with arbitrary Λ, relax some of the assumptions made in Refs. [84, 87, 88], and consider a much more general class of theories. In particular, we describe the α-attractor version of the simplest linear dark energy model, a model with exponential potential with two shoulders proposed in Ref. [90], and a generalized version of the model studied in Refs. [84, 88].

The asymptotic value w_∞ of the parameter w in the equation of state $p = w\rho$ for quintessential inflation depends on the limiting value of the quintessence potential. If this value is negative, the universe eventually collapses, but under certain conditions it may pass through a temporary but long stage of acceleration. Here we call w_∞ the asymptotic value of w for dark energy, to distinguish it from the time-dependent dark energy

equation of state $w_{\rm DE}$ and the observable "all-inclusive" effective equation of state $w_{\rm eff}$.

If the potential V of the quintessential inflation models asymptotically vanishes (i.e. if the cosmological constant is zero), the value of w_∞ in the simplest models is given by

$$w_\infty = -1 + \frac{2}{9\alpha}\,. \tag{2.1}$$

Interestingly, the difference between w_∞ and the equation of state $w = -1$ for the cosmological constant is inversely proportional to α, whereas the tensor to scalar ratio is directly proportional to it,

$$r = \frac{12\alpha}{N^2}\,, \tag{2.2}$$

where N corresponds to the remaining number of e-folds from the end of inflation at the moment of generation of perturbations studied by WMAP and Planck. This may help us either to rule out, or to confirm theories of that type by a combination of searches for B-modes and investigation of dark energy.

Note that this result is valid only if the cosmological constant is zero, which provides us with an intriguing possibility to test this hypothesis. Meanwhile in the theories with a negative cosmological constant, the universe eventually collapses. However, in some cases one may have a prolonged state of accelerated expansion, just as in the model proposed in Ref. [91].

If the asymptotic value of the potential is positive (i.e. if the cosmological constant is positive), and the quintessence field slowly rolls towards infinity, the universe asymptotically approaches a de Sitter regime with

$$w_\infty = -1\,. \tag{2.3}$$

This is the most general regime that is relatively easy to achieve in the supergravity constructions discussed here. Of course, if these models correctly describe our world, the observations looking for deviations of quintessence from the cosmological constant will not bring us anything exciting. But there may be a silver lining here.

Indeed, the process of reheating in the models of quintessential inflation is non-standard, and it can be very inefficient. In that case, the inflaton field after the end of inflation may enter a long stage when its energy density is dominated by the kinetic energy with $w = +1$. This simple fact affects the number of e-folds N [84]. Indeed, as we will show, the number of e-folds in the α-attractor models of quintessential inflation with gravitational reheating can be greater than the corresponding number in the conventional (non-quintessential) versions of α-attractors and in the Starobinsky model by $\Delta N \sim 10$. This is a significant difference, which may have important observational consequences.

In particular, the general prediction of α attractors for n_s is

$$n_s = 1 - \frac{2}{N}\,. \tag{2.4}$$

One can easily check that the difference between n_s for conventional α-attractors with $N \sim 50$ and α-attractor models of quintessential inflation with $N \sim 60$ is about 0.006, which coincides with 1σ error bar in the Planck 2015 results [82]. This increase in the value of n_s and N is not very easy to achieve otherwise, see e.g. Refs. [92, 93].

This suggests that future observations may be able to differentiate between the regular versions of inflationary α-attractors and their quintessential generalizations. More generally, we might be able to differentiate, though somewhat indirectly, the cosmological constant and quintessence without relying on extreme accuracy in measuring w. This is a rather intriguing byproduct of the present investigation.

In this chapter we will also describe the models which involve two different fields with α-attractor potentials. The first of these two fields (or

the combination of the two) will be responsible for inflation, and the second field will be responsible for quintessence. The resulting models are very flexible; they are close in spirit to the models of multi-field cascade inflation proposed in Ref. [94].

In addition to the current cosmic microwave background (CMB) experiments, such as WMAP [95], Planck [96], ACTPol [97] and SPT-Pol [98], as well as the Stage III CMB experiments like AdvACT [99] and SPT-3G [100], and the future CMB Stage IV ground [101] and space based experiments such as LiteBIRD [102, 103], aiming at more precise measurements of the CMB B-modes, arguably the next leading cosmological probes are the large-scale structure surveys, measuring baryon acoustic oscillations (BAO) and the growth of structure through redshift-space distortions (RSD), as well as weak gravitational lensing. There is a classification of the LSS surveys similar to that of the CMB experiments. This includes Stage III experiments currently taking data and continuing to do so for the next two or three years, as well as Stage IV experiments that are currently being designed and constructed to provide a large amount of high quality data in the next five to ten years. The Stage III experiments include, for example, the Canada-France Hawaii Telescope Lensing Survey (CFHTLenS) [104, 105], the Kilo Degree Survey (KiDS) [106, 107], the Extended Baryon Oscillation Spectroscopic Survey (eBOSS) [108], and the Dark Energy Survey (DES) [109–111]. We however expect an exciting time to come when the Stage IV LSS surveys start to deliver data. These include several ground based experiments such as the Dark Energy Spectroscopic Instrument (DESI) [112, 113], the Large Synoptic Survey Telescope (LSST) [114, 115], and the Square Kilometre Array (SKA) [116–121], as well as the space based experiments Euclid [122, 123] and the Wide Field InfraRed Survey Telescope (WFIRST) [124, 125]. A synergy of all these various probes of both early- and late-time observables will provide invaluable information about the models of inflation and dark energy.

In this chapter, we perform an analysis of our α-attractor models of dark energy in view of their implications for the current and future large-scale structure surveys. We do not intend here to perform a comprehensive comparison of our models to the current data or a detailed forecast analysis of the models for the future LSS experiments (such a study is currently ongoing). For some models, we base our discussions solely on simple numerical computations of cosmic histories as well as dark energy and effective equations of state, without going through a detailed comparison to observations, to see whether these models can potentially provide viable cosmologies. For some others, though, we perform a statistical analysis and compare their predictions to geometrical constraints on the cosmic history using a combination of current observational data, which we believe can provide a sufficiently good understanding of our models and their viability. We also discuss the implications of our findings for future cosmological surveys and in particular ask the question of whether the more precise measurements of dark energy properties will enable us to test our models against ΛCDM. Here we similarly do not perform a detailed forecast analysis of the models and are interested only in a rough estimate of the testability of the models using future data.

2.2 ASYMMETRIC COSMOLOGICAL α-ATTRACTORS

There are several different ways to introduce the theory of α-attractors, see Refs. [76–81]. On a purely phenomenological level, the main features of all of these models can be represented in terms of a single-field model with the Lagrangian [80, 81]

$$\frac{1}{\sqrt{-g}}\mathcal{L} = \frac{R}{2} - \frac{(\partial_\mu \phi)^2}{2\left(1-\frac{\phi^2}{6\alpha}\right)^2} - V(\phi)\,. \tag{2.5}$$

Here $\phi(x)$ is the scalar field, and we use units where $M_{\rm Pl} = 1$. The origin of the pole in the kinetic term can be explained in the context of hyperbolic geometry of the field-space manifold. These geometries are natural in extended supergravity, although they may also describe cosmological models unrelated to supergravity. The parameter α can take any positive value in the minimal $\mathcal{N} = 1$ supergravity, but recent developments based on extended supergravity, M-theory, and string theory favor 7 particular choices: $3\alpha = 1, 2, 3, ..., 7$ [94, 126, 127].

In the limit $\alpha \to \infty$ this model coincides with the standard chaotic inflation with a canonically normalized field ϕ and the inflaton potential $V(\phi)$ [128]. However, for any finite value of α, the field ϕ in (2.5) is not canonically normalized, and must satisfy the condition $\phi^2 < 6\alpha$.

Instead of the variable ϕ, one can use a canonically normalized field φ by solving the equation $\frac{\partial\phi}{1-\frac{\phi^2}{6\alpha}} = \partial\varphi$, which yields

$$\phi = \sqrt{6\alpha}\,\tanh\frac{\varphi}{\sqrt{6\alpha}}\,. \tag{2.6}$$

The full theory, in terms of the canonical variables, becomes

$$\frac{1}{\sqrt{-g}}\mathcal{L} = \frac{R}{2} - \frac{(\partial_\mu\varphi)^2}{2} - V\big(\sqrt{6\alpha}\,\tanh\frac{\varphi}{\sqrt{6\alpha}}\big)\,. \tag{2.7}$$

Note that in the limit $\phi \to 0$ the variables ϕ and φ coincide; the main difference appears in the limit $\phi^2 \to 6\alpha$: In terms of the new variables, a tiny vicinity of the boundary of the moduli space at $\phi^2 = 6\alpha$ stretches and extends to infinitely large $|\varphi|$. We will assume that the potential $V(\phi)$ and its derivatives are non-singular for $\phi^2 \leq 6\alpha$. In that case, generic potentials $V(\phi) = V(\sqrt{6\alpha}\,\tanh\frac{\varphi}{\sqrt{6\alpha}})$ at large $|\varphi|$ approach two infinitely long plateaus with the heights corresponding to the values of $V(\phi)$ at the two boundaries,

$$V_\pm \equiv V(\phi)|_{\phi=\pm\sqrt{6\alpha}}\,. \tag{2.8}$$

The simplest example of such a theory is given by the model with $V(\phi) = m^2\phi^2/2$. In terms of the canonically normalized field φ, the potential is given by

$$V(\varphi) = 3\alpha m^2 \tanh^2 \frac{\varphi}{\sqrt{6\alpha}}\,. \tag{2.9}$$

This is the simplest representative of the so-called T-models, with the T-shaped potential shown in Fig. 2.1.

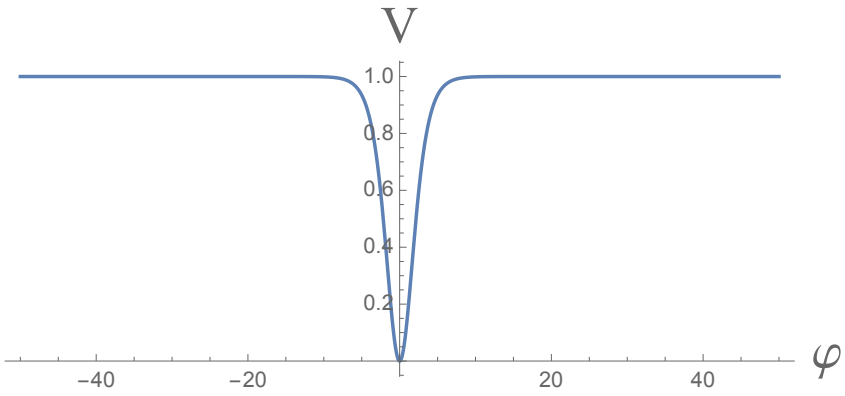

Figure 2.1: The potential $V(\varphi) = 3\alpha m^2 \tanh^2 \frac{\varphi}{\sqrt{6\alpha}}$ for $\alpha = 1$, shown in units of $3m^2$, with φ in Planck units. For $1/3 < \alpha < 10$ one has $n_s \sim 0.965$ and the tensor to scalar ratio r is in the range from 3×10^{-2} to 10^{-3}, providing a good match to the Planck data.

For any values of $\alpha \lesssim 10$, the amplitude of the inflationary perturbations, the prediction for the spectral index n_s, and the tensor to scalar ratio r match observational data under a single condition [129]

$$\frac{V_\pm}{\alpha} \sim 3m^2 \sim 10^{-10}\,. \tag{2.10}$$

To understand what is going on in this class of theories for general potentials $V(\phi)$, let us consider, for definiteness, positive values of ϕ and study a small

vicinity of the point $\phi = \sqrt{6\alpha}$, which becomes stretched to infinitely large values of the canonical field φ upon the change of variables $\phi \to \varphi$. If the potential $V(\phi)$ is non-singular at the boundary $\phi = \sqrt{6\alpha}$, we can expand it in series with respect to the distance from the boundary,

$$V(\phi) = V_+ + (\phi - \sqrt{6\alpha})\, V'_+ + \mathcal{O}\left((\phi - \sqrt{6\alpha})^2\right), \tag{2.11}$$

where we have introduced $V'_+ \equiv \partial_\phi V|_{\phi=+\sqrt{6\alpha}}$.

In the vicinity of the boundary $\phi = \sqrt{6\alpha}$, the relation (2.6) between the original field variable ϕ and the canonically normalized inflaton field φ is given by

$$\phi = \sqrt{6\alpha}\, \left(1 - 2e^{-\sqrt{\frac{2}{3\alpha}}\varphi}\right), \tag{2.12}$$

up to the higher order terms $\mathcal{O}\left(e^{-2\sqrt{\frac{2}{3\alpha}}\varphi}\right)$. At $\varphi \gg \sqrt{6\alpha}$, these terms are exponentially small as compared to the terms $\sim e^{-\sqrt{\frac{2}{3\alpha}}\varphi}$, and the potential acquires the following asymptotic form

$$V(\varphi) = V_+ - 2\sqrt{6\alpha}\, V'_+\, e^{-\sqrt{\frac{2}{3\alpha}}\varphi}. \tag{2.13}$$

The constant $2\sqrt{6\alpha}\, V'_+$ in this expression can be absorbed into a redefinition of the field φ. This is the reason of the universal inflationary predictions, given the inflation takes places at large $\varphi \gg \sqrt{\alpha}$.

In particular, the parameters n_s and r describing the spectrum of inflationary perturbations are given by

$$r = \frac{12\alpha}{N^2}, \qquad n_s = 1 - \frac{2}{N}. \tag{2.14}$$

These results depend only on α and the number of e-folds N remaining to the end of inflation since the moment when quantum fluctuations were generated. Meanwhile, the amplitude of scalar perturbations for α-attractors generated at the upper plateau of the potential (2.13) is given by

$$\mathcal{P}_{\mathcal{R}}(k) = \frac{N^2}{18\pi^2}\,\frac{V_+}{\alpha}\,. \tag{2.15}$$

Thus the COBE/Planck normalization constrains the ratio V_+/α [129]. Taking the value $(2.208 \pm 0.075) \times 10^{-9}$ [130, 131] for $\mathcal{P}_{\mathcal{R}}$ and $N \sim 60$ e-folds for inflation, we find the constraint on the height of the inflationary plateau,

$$\frac{V_+}{\alpha} \sim 10^{-10}\,. \tag{2.16}$$

These results were explained in Refs. [76, 78] and formulated in a particularly general way in Ref. [80]; the kinetic term in this class of models has a pole at the boundary of the moduli space. If inflation occurs in a vicinity of such a pole, and the potential near the pole has a finite first derivative, all other details of the potential $V(\phi)$ and of the kinetic term far away from the pole are not important for making cosmological predictions. That is why these models are called cosmological attractors.

The simplest model $V(\phi) = m^2\phi^2/2$ considered above is symmetric with respect to the change $\phi \to -\phi$. However, this is not a universal property. Consider, for example, its generalization [90] with the potential

$$V = \frac{m^2}{2(1+c)^2}(\phi + c\sqrt{6\alpha})^2\,. \tag{2.17}$$

In terms of the canonically normalized field φ, the potential becomes

$$V = \frac{3\alpha m^2}{(1+c)^2}\left(\tanh\frac{\varphi}{\sqrt{6\alpha}} + c\right)^2\,. \tag{2.18}$$

The coefficient $(1+c)^{-2}$ is introduced to preserve the height of the inflationary plateau at $\varphi \to \infty$.

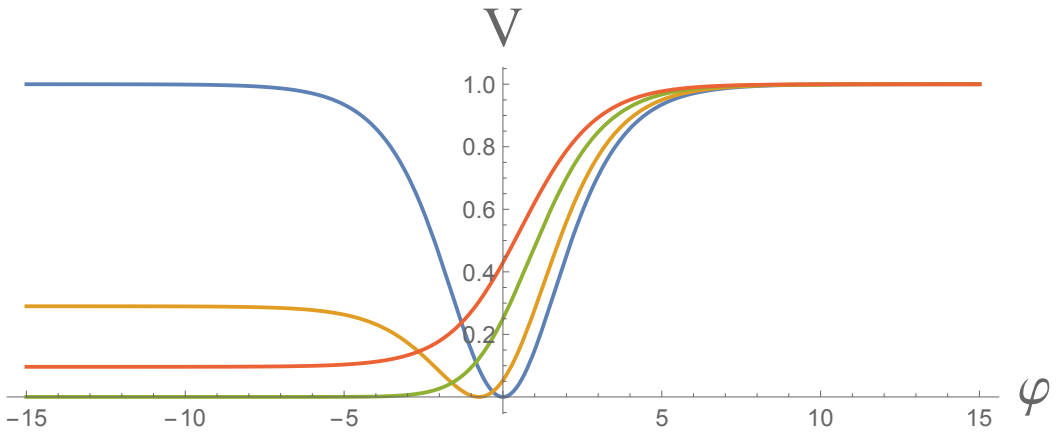

Figure 2.2: The potential (2.17) shown in units of αm^2 for $\alpha = 1$, and $c = 0$ (blue), 0.3 (orange), 1 (red), and 1.9 (green).

For $|c| < 1$ this potential has a minimum and two asymptotically flat shoulders of different heights, as shown by the orange curve in Fig. 2.2. For $c = 1$ the minimum of the potential disappears and the left shoulder describes a potential which exponentially decreases to zero at large, negative values of φ. Finally, for $c < -1$, the potential at large, negative φ approaches a constant value of $V_- = 3\alpha m^2(c-1)^2/(c+1)^2$. One can further modify the potential by adding to it a constant of any sign, which is absolutely legitimate from the point of view of the string theory landscape.

Historically, the first versions of α-attractor models have been developed in Refs. [76–81] in the supergravity context, where the potentials could be represented as $f^2(\phi)$, where $f(\phi)$ is a real holomorphic function of the argument. That is why we started the discussion of α-attractors with presenting models with a quadratic potential $V(\phi)$. However, recently a more general approach to α-attractors in supergravity has been developed [94, 132], which allows us to describe models with arbitrary potentials

$V(\phi)$, including the simplest linear dark energy potential $V(\phi) = \gamma\phi + \Lambda$ proposed as early as in Ref. [91].

In this chapter, we study $V(\varphi)$ at very large, negative φ. Therefore we will often identify Λ not with $V(0)$, but with V_-, the height of the potential in this limit of large, negative φ. This can be achieved by representing the linear potential as $V(\phi) = \gamma\phi + \gamma\sqrt{6\alpha} + \Lambda$. In terms of the canonically normalized field φ, this potential is given by

$$V(\varphi) = \gamma\sqrt{6\alpha}(\tanh\frac{\varphi}{\sqrt{6\alpha}} + 1) + \Lambda\,, \tag{2.19}$$

where $\Lambda = V_-$ is now the asymptotic value of the potential at $\varphi \to -\infty$.

We illustrate the shape of this potential for various values of its parameters in Fig. 2.3.

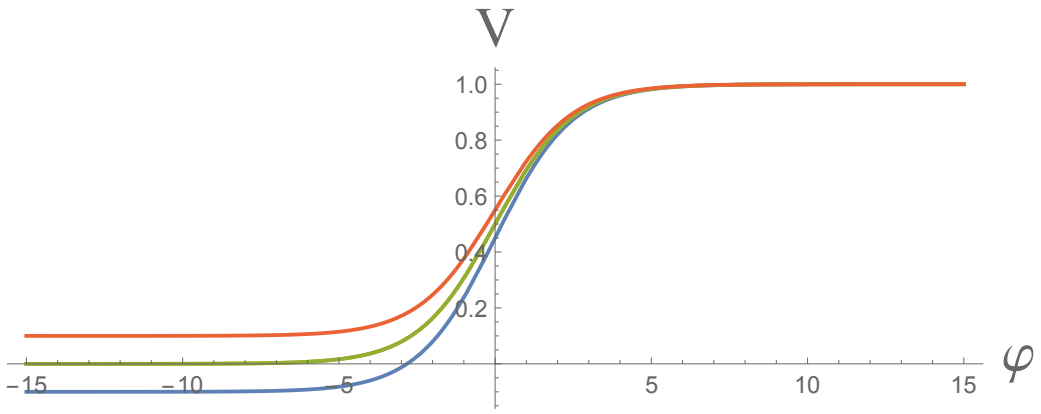

Figure 2.3: The potential (2.19) has two plateaus, with $V = V_\pm$. We illustrate its values for $V_+ = 1$ and $V_- = \Lambda = -0.1$ (blue), 0 (green), and $+0.1$ (red).

At $\varphi \gg \sqrt{6\alpha}$ the potential is given by

$$V = V_+ - 2\gamma\sqrt{6\alpha}\, e^{-\sqrt{\frac{2}{3\alpha}}\varphi}\,, \tag{2.20}$$

whereas at $\varphi \ll -\sqrt{6\alpha}$ one has

$$V = V_- + 2\gamma\sqrt{6\alpha}\, e^{\sqrt{\frac{2}{3\alpha}}\varphi}\,. \tag{2.21}$$

In general, the asymptotic behavior of asymmetric potentials $V(\varphi)$ at large, negative values of the field, $\varphi \ll -\sqrt{6\alpha}$, is given by an expression similar to (2.13),

$$V(\varphi) = V_- + 2\sqrt{6\alpha}\, V'_-\, e^{\sqrt{\frac{2}{3\alpha}}\varphi}\,, \tag{2.22}$$

where $V'_- \equiv \partial_\phi V|_{\phi=-\sqrt{6\alpha}}$. Thus, as long as V'_- is non-singular and does not vanish,[1] all such potentials have the same universal asymptotic behavior at large, negative φ: up to a shift $\varphi \to \varphi - \sqrt{\frac{3\alpha}{2}}\log(2\sqrt{6\alpha}\, V'_-)$ and a redefinition $\sqrt{\frac{2}{3\alpha}} \to \lambda$, they can be represented in a more familiar way,

$$V(\varphi) = \Lambda + e^{\lambda\varphi}\,. \tag{2.23}$$

This general asymptotic expression will be very helpful in evaluation of α-attractors as dark energy candidates.

To explain the basic idea, let us first consider the simplest case of $\Lambda = 0$. Then we will have an exponential potential [2]

$$V(\varphi) = e^{\lambda\varphi}\,, \tag{2.24}$$

1 If one fine-tunes the potential $V(\phi)$ to have a minimum, or maximum, at one of the boundaries $\phi = \pm\sqrt{6\alpha}$, the first derivative V'_- in (2.22), or V'_+ in (2.13), vanishes. This affects the asymptotic behavior of the potential. For example, in the theory with the quadratic potential (2.17) with $c = 1$, the asymptotic behavior at $\varphi \to -\infty$ is governed by the higher exponent $e^{2\sqrt{\frac{2}{3\alpha}}\varphi}$, which is equivalent to making α four times smaller.

2 The related effective models of accelerated expansion in string theory were proposed in Ref. [133], and they lead to $w_{\rm DE} < -1/3$.

where

$$\lambda = \sqrt{\frac{2}{3\alpha}}\,. \tag{2.25}$$

This potential vanishes in the limit $\varphi \to -\infty$. For $\lambda \ll 1$, the potential is flat, the energy density of normal matter decreases faster than V, and the system eventually enters the asymptotic regime of power-law inflation with (see for example the review [134])

$$w_\infty = -1 + \frac{\lambda^2}{3} = -1 + \frac{2}{9\alpha}\,. \tag{2.26}$$

It is interesting to compare this result with the inflationary predictions of α-attractors (2.14): $n_s = 1 - \frac{2}{N}$, $r = \frac{12\alpha}{N^2}$. Thus, in this scenario, inflationary predictions, as well as the value of w_∞, are determined by the parameter α. In particular, for $\Lambda = 0$, and $\alpha = 7/3$ (i.e. $\lambda \sim 0.53$), which is one of the values advocated in Refs. [94, 126, 127], the asymptotic equation of state of dark energy is given by

$$w_\infty = -0.905\,. \tag{2.27}$$

Note, however, that in the derivation of (2.26) we assumed that $\Lambda = 0$. This assumption, which simplifies the investigation, is very hard to justify in the supergravity framework. For any positive Λ one has

$$w_\infty = -1\,, \tag{2.28}$$

but for large α the transition from $w = -1 + \frac{2}{9\alpha}$ to $w = -1$ may take a long time. On the other hand, while in the models with $\Lambda < 0$, the universe eventually collapses, if $\lambda \ll 1$ and $|\Lambda| \ll 10^{-120}$, there is a very long interval, potentially longer than the present age of the universe, during

which w is very close to -1 [135]. Also, our universe may be very far from the asymptotic regime discussed above. Therefore, one should keep the estimate (2.26) in mind, but perform a more detailed analysis of different dark energy models, as we will do in this chapter.

2.3 α-ATTRACTORS AND SUPERGRAVITY

2.3.1 *General formulation, geometry, and special values of* α

One of the nice features of all cosmological α-attractor models which we will study here is that they can be easily embedded into the string theory motivated supergravity where the scalar fields are complex. The most advanced version of these models [94] is based on anti-D3-brane induced geometric models — here we review these models in the simple case where a bosonic model has a single inflaton-quintessence field.

There is one complex scalar Z, a coordinate of the Poincaré disk with the following geometry

$$ds^2 = 3\alpha \frac{dZ d\bar{Z}}{(1 - Z\bar{Z})^2}\,. \tag{2.29}$$

Advanced formulations of α-attractors in supergravity also contain a nilpotent superfield S such that $S(x,\theta)^2 = 0$, whose Kähler geometry represents the interaction between the anti-D3-brane and the background fields, including the inflaton-quintessence field Z. The scalar component of it, $S(x)$, vanishes on the inflationary trajectory, since in this Volkov-Akulov multiplet the scalar is not independent but is a bilinear of fermions. It is convenient to use the geometric Kähler function formalism [94], where

$$\mathcal{G} \equiv K + \log W + \log \overline{W}\,, \qquad \mathbf{V} = e^{\mathcal{G}}(\mathcal{G}^{\alpha\bar{\beta}}\mathcal{G}_{\alpha}\mathcal{G}_{\bar{\beta}} - 3)\,, \tag{2.30}$$

$$\mathcal{G} = \ln W_0^2 - \frac{3\alpha}{2}\log\frac{(1-Z\bar{Z})^2}{(1-Z^2)(1-\bar{Z}^2)} + S + \bar{S} + \frac{W_0^2}{|F_S|^2 + f(Z,\bar{Z})}S\bar{S}\,, \quad (2.31)$$

and $f(Z,\bar{Z})$ is an arbitrary, real function of Z and $\bar{Z}$. This employs the Kähler frame that has a manifest inflaton shift symmetry [136]. The potential has a stable minimum at $Z = \bar{Z}$. Its value along the inflaton direction $Z = \bar{Z} = \tanh\frac{\varphi}{\sqrt{6\alpha}}$ is given by

$$\mathbf{V}|_{Z=\bar{Z}} = f(Z,\bar{Z})|_{Z=\bar{Z}} + \Lambda = f(\tanh\frac{\varphi}{\sqrt{6\alpha}}) + \Lambda\,. \quad (2.32)$$

Here, the cosmological constant Λ can take arbitrary values determined by the choice of F_S and W_0:

$$\Lambda = F_S^2 - 3W_0^2\,. \quad (2.33)$$

The choice of the Kähler potential for Z was made in Ref. [94] such that

$$K(Z,\bar{Z})|_{Z=\bar{Z}} = -\frac{3\alpha}{2}\log\frac{(1-Z\bar{Z})^2}{(1-Z^2)(1-\bar{Z}^2)}|_{Z=\bar{Z}} = 0\,, \qquad K_Z(Z,\bar{Z})|_{Z=\bar{Z}} = 0\,. \quad (2.34)$$

This Kähler frame leads to a simple relation between the inflaton potential (2.32) and the S-field geometry $g_{S\bar{S}} = \frac{W_0^2}{|F_S|^2+f(Z,\bar{Z})}$. It also provides stabilization of the sinflaton field $Z - \bar{Z}$ at $Z - \bar{Z} = 0$.

In the disk geometry (2.29) $3\alpha = \mathcal{R}^2$ is a geometric parameter defining the radius square of the Poincaré disk of the hyperbolic geometry of the α-

attractor models, since by change of variables $Z' = Z\sqrt{3\alpha}$ one can represent the metric in the form

$$ds^2 = \frac{dZ' d\bar{Z}'}{\left(1 - \frac{Z'\bar{Z}'}{3\alpha}\right)^2}\,, \qquad |Z'|^2 < 3\alpha\,. \tag{2.35}$$

The parameter α also defines a curvature of the corresponding Kähler manifold, $\mathbf{R}_K = -\frac{2}{3\alpha}$. Finally, one can return to the variables used in the previous section by representing the real part of Z' as $\frac{\phi}{\sqrt{2}} = \sqrt{3\alpha}\,\tanh\frac{\varphi}{\sqrt{6\alpha}}$.

The asymptotic freedom of the interactions of the field φ with all other fields protects the asymptotic flatness of the potential for any α. Thus, in general quantum field theory models, as well as in $\mathcal{N} = 1$ supergravity, there are no constraints on α, it can take any value $\alpha > 0$[3].

From the point of view of maximal supergravity, string theory, and M-theory, the most interesting values of α are [94, 126, 127]

$$3\alpha = 1, 2, 3, 4, 5, 6, 7\,. \tag{2.36}$$

An interpretation of this family of models is rather interesting. These models describe 7 unit size Poincaré disks with $3\alpha = 1$ for seven different fields Z_i. The basic choice of $\alpha = 1/3$ corresponds to a single unit size disk model with $Z_1\bar{Z}_1 < 1$. If all other fields are stabilized and cannot move, one has a

3 One should distinguish the general theoretical constraints on α and the model-dependent cosmological constraints. In Ref. [84], the authors assumed $0.03 < \alpha < 1/3$. In a subsequent paper [88], they noted that these conditions did not lead to a satisfactory dark energy model in their scenario, and instead picked the range $1.5 < \alpha < 4.2$. However, they admitted that the constraint $\alpha < 4.2$ is not firmly motivated because of the asymptotic freedom of the field φ in α-attractors [137]. Meanwhile, we find that the condition $\alpha > 1.5$ is excessive, and it completely disappears in the models with a positive cosmological constant, see section 2.5.3.2. In particular, in section 2.5.1 we will present a model with a positive cosmological constant where one can have quintessential inflation for $\alpha \lesssim 10^{-2}$.

single attractor with $\alpha = 1/3$, where the corresponding field ϕ_1 can change from $-\sqrt{2}$ to $+\sqrt{2}$. If all seven of them interact and are forced dynamically to move together [94, 127], then each of them also moves from $-\sqrt{2}$ to $+\sqrt{2}$, but the combination of these fields changes from $-\sqrt{14}$ to $+\sqrt{14}$, along the diagonal of a 7-dimensional cube.

The choice of $\alpha = 1$ describes α-attractor formulations of the Starobinsky model and Higgs inflation. The fibre inflation model, which is based on the large volume compactification in string theory, corresponds to $\alpha = 2$ [138, 139]. The choice of $\alpha = 7/3$, which we will sometimes use in various examples, corresponds to the maximally symmetric realization of the 7-disk M-theory model [94, 126, 127].

2.3.2 *Suppressing the fifth force*

There is a well known issue with quintessence regarding the fifth force problem. This problem appears if the masses of particles in the standard model depend on the quintessence field ϕ.

Consider first an unrealistic example and assume that the electron mass m_e receives a contribution $\Delta m_e = g\phi$. Then (in addition to electromagnetic interactions) electrons would attract each other through the gravitational force $\sim \frac{(m_e+g\phi)^2}{r^2}$, as well as through an additional fifth force $F_5 \sim \frac{g^2}{r^2}$ due to the interactions via the nearly massless quintessence field ϕ. This force will have the same dependence on r as the gravitational attraction, but it will not be proportional to m_e^2, which would violate the equivalence principle.

An obvious way to avoid this problem is to suppress the interaction of the standard model fields with quintessence. For example, as was already observed in Ref. [88], the asymptotic freedom of the field φ in α-attractors [137] allows to exponentially suppress this coupling even if it were present. However, the suppression of the fifth force should be extremely strong, which may require very large values of φ. In the α-attractor models to be discussed in this paper, this may not be a problem since we do not introduce

any direct coupling between ϕ and electrons or quarks, which would lead to the force $F_5 \sim \frac{g^2}{r^2}$ discussed above.

However, one may wonder whether this coupling may appear in supergravity even if the field φ belongs to the hidden sector, without a direct coupling to the standard model fields. Fortunately, there is a specific feature of our underlying supergravity models which helps to avoid the fifth force issues. The coupling of the inflationary sector to matter in these models has been studied in Ref. [140]. The inflaton-quintessence field is Z, and there is also a nilpotent superfield S, as explained above. It has been found how to construct the interaction between matter and the inflationary sector so that the presence of the matter fields does not affect a successful inflationary evolution and that there are no tachyons in the matter sector during and after inflation.

One of the most important features of this class of models is the requirement of the flatness of the Kähler potential for the inflaton-quintessence field Z, shown in Eq. (2.34). In particular, since the field $Z - \bar{Z}$ orthogonal to the inflaton direction is heavy and is stabilized at the inflaton-quintessence trajectory $Z = \bar{Z}$, one finds that

$$e^{K(Z=\bar{Z})} = 1 \,, \tag{2.37}$$

and there is no dependence of the mass of the matter fields on the inflaton field via the Kähler potential since

$$K_Z(Z = \bar{Z}) = 0 \,. \tag{2.38}$$

These features of the Kähler potential have been discussed in Ref. [141] as the reason for the fifth force problem to be alleviated in supergravity. Our models, which were constructed with the purpose of stabilization of the sinflaton field $Z - \bar{Z}$ during the cosmological evolution, just satisfy the properties required from the Kähler potentials in Ref. [141].

Moreover, according to Ref. [140] one can construct satisfactory cosmological models where the mass of the matter field U does not depend on the inflaton-quintessence field Z. Examples of such models in Ref. [140] include the following Kähler potential and superpotential:

$$K(Z,\bar{Z}) = -\frac{3\alpha}{2}\log\frac{(1-Z\bar{Z})^2}{(1-Z^2)(1-\bar{Z}^2)} + S\bar{S} + U\bar{U}\ , \tag{2.39}$$

$$W = g(Z) + Sf(Z) + \frac{m}{2}U^2. \tag{2.40}$$

For our purposes, we need to assume that $g(Z)$ has a negligible dependence on Z or is completely Z-independent, and the same for the parameter m in the superpotential. The mass eigenvalues of the scalar field U are

$$\mu^2 = V + |g|^2 \pm |g|m + m^2\ . \tag{2.41}$$

The value of the potential V during the quintessence stage is negligible, $V \sim 10^{-120}$. The rest of the mass formula is Z-independent by the choice of the parameters in the superpotential. The situation with fermions is similar, their masses are Z-independent (see Ref. [140] for more details). This means that with a proper embedding of the standard model in our theory, matter fields decouple from quintessence. Such models do not suffer from the fifth force problem.

2.4 SINGLE-FIELD QUINTESSENTIAL INFLATION MODELS

2.4.1 *Inflationary dynamics, late-time evolution, and cosmic acceleration*

In this section, we focus on several interesting models where a single scalar field ϕ is responsible for both inflation and dark energy. The action for

these single-field, α-attractor, quintessential inflation models has the general structure

$$S = \frac{1}{2}\int \mathrm{d}^4x\sqrt{-g}R - \int \mathrm{d}^4x\sqrt{-g}\left(\frac{\partial_\mu\phi\partial^\mu\phi}{2\left(1-\frac{\phi^2}{6\alpha}\right)^2} + V(\phi)\right) + S_{\rm matter}[g_{\mu\nu},\Psi] \tag{2.42}$$

where the scalar field ϕ has a potential $V(\phi)$. Here $S_{\rm matter}$ is the matter action where matter fields are denoted collectively by Ψ. Note that we have absorbed any cosmological constant term Λ into the potential. This action can be rewritten in terms of the canonical field φ, as discussed earlier.

Before we discuss specific models, defined by assuming specific forms for the potential $V(\phi)$, we briefly review the general dynamical equations and some important quantities for the studies of cosmic histories, during inflation and after that.

During inflation, matter and radiation are both negligible, and the dynamics of our system is given by

$$3H^2 = \frac{1}{2}\dot{\varphi}^2 + V(\varphi)\,, \tag{2.43}$$

$$\ddot{\varphi} + 3H\dot{\varphi} + \frac{\mathrm{d}}{\mathrm{d}\varphi}V(\varphi) = 0\,, \tag{2.44}$$

where $H \equiv \frac{\dot{a}}{a}$ is the Hubble parameter, and a dot denotes derivatives with respect to cosmic time. It is useful to work with the number of e-folds $N \equiv \ln a$ as a time coordinate. Denoting a derivative with respect to N by a prime, we have $\frac{\mathrm{d}\varphi}{\mathrm{d}t} = \varphi' H$. Introducing slow-roll parameter as

$$\epsilon \equiv -\frac{H'}{H}\,, \tag{2.45}$$

we will have

$$H^2 = \frac{V(\varphi)}{3 - \frac{1}{2}\varphi'^2}\,, \tag{2.46}$$

$$\varphi'' + (3 - \epsilon)\varphi' + \frac{1}{H^2}\frac{\mathrm{d}}{\mathrm{d}\varphi}V(\varphi) = 0\,, \tag{2.47}$$

$$\epsilon = \frac{1}{2}\varphi'^2\,. \tag{2.48}$$

Note that here we have not made any slow-roll approximation for ϵ, and all the expressions are exact. The second slow-roll parameter η has the form,[4]

$$\eta \equiv \frac{\epsilon'}{\epsilon}\,. \tag{2.50}$$

One can solve Eqs. (2.46)-(2.48) numerically to obtain the evolution of φ, H, ϵ, and η during inflation, as we will do for our quintessential inflation models in this chapter. In addition, given ϵ and η, we can compute two other important inflationary quantities, namely the *spectral index* for scalar perturbations n_s and the *tensor-to-scalar ratio* r — assuming the approximate relations between these quantities we have

4 Note that here we have adopted the definition of η from e.g. Ref [142]. There exists another definition for this second slow-roll parameter, namely [143]

$$\tilde{\eta} \equiv -\frac{\ddot{\varphi}}{H\dot{\varphi}} = -\frac{\mathrm{d}\ln|H_{,\varphi}|}{\mathrm{d}N} = 2\frac{H_{,\varphi\varphi}}{H} = \frac{\mathrm{d}\ln|\dot{\varphi}|}{\mathrm{d}N}\,, \tag{2.49}$$

where $H_{,\varphi} \equiv \frac{\mathrm{d}}{\mathrm{d}\varphi}H$ and $H_{,\varphi\varphi} \equiv \frac{\mathrm{d}}{\mathrm{d}\varphi}H_{,\varphi}$. $\tilde{\eta}$ is related to our η by $\tilde{\eta} = \epsilon - \frac{1}{2}\eta$. The spectral index n_s now has the form $n_s \approx 1 + 2\tilde{\eta} - 4\epsilon$, and since $\epsilon \approx \epsilon_{\rm v}$ and $\tilde{\eta} \approx \tilde{\eta}_{\rm v} - \epsilon_{\rm v}$, where $\epsilon_{\rm v}$ and $\tilde{\eta}_{\rm v}$ are the slow-roll approximations to ϵ and $\tilde{\eta}$, respectively, we have that $n_s \approx 1 + 2\tilde{\eta}_{\rm v} - 6\epsilon_{\rm v}$.

$$n_s \approx 1 - 2\epsilon - \eta\,, \tag{2.51}$$

$$r \approx 16\epsilon\,. \tag{2.52}$$

Later in this paper, we will discuss several observational constraints on the parameters of the quintessential inflation models that we consider in this work, and for that we will scan over the parameters of the models and compare their theoretical predictions to the data. It is therefore important to have an idea for theoretical priors on the values of the parameters in the potential, for a given model, which can provide viable inflation. This can be achieved by applying the approximate constraint placed on the inflationary potentials from the requirement that the power spectrum of curvature fluctuations after inflation should match the COBE/Planck normalization, as discussed in section 2.2. Assuming a slow-roll regime for inflation, i.e. neglecting the terms including φ' and φ'' in Eqs. (2.46) and (2.47), respectively, the equations simplify to

$$H^2 = \frac{1}{3}V(\varphi)\,, \tag{2.53}$$

$$3\varphi' + \frac{1}{H^2}\frac{\mathrm{d}}{\mathrm{d}\varphi}V(\varphi) = 0\,. \tag{2.54}$$

In this slow-roll regime, the potential is related to the power spectrum of primordial curvature perturbations $\mathcal{P}_{\mathcal{R}}(k)$ through the COBE/Planck normalization equation,

$$\frac{V(\varphi)^3}{(\mathrm{d}V(\varphi)/\mathrm{d}\varphi)^2} = 12\pi^2\mathcal{P}_{\mathcal{R}}(k)\,, \tag{2.55}$$

see e.g. Ref. [144]. By solving these equations in the slow-roll approximation, one finds that in the large N approximation the results for n_s, r, and the

amplitude of perturbations for α attractors are given by Eqs. (2.14), (2.15) and (2.16).

In order to see whether a model of quintessential inflation is able to describe the dynamics of the universe after inflation, we need to add matter and radiation to the system of equations (2.46)-(2.48). In this case, the equations are modified as

$$H^2 = \frac{V(\varphi) + \rho_{\rm M} + \rho_{\rm R}}{3 - \frac{1}{2}\varphi'^2}\,, \tag{2.56}$$

$$\varphi'' + (3 - \epsilon)\varphi' + \frac{1}{H^2}\frac{\mathrm{d}}{\mathrm{d}\varphi}V(\varphi) = 0\,, \tag{2.57}$$

$$\epsilon = \frac{1}{2}\left(\varphi'^2 - \frac{\rho'_{\rm M} + \rho'_{\rm R}}{3H^2}\right), \tag{2.58}$$

where $\rho_{\rm M}$ and $\rho_{\rm R}$ are the energy densities of matter and radiation, respectively. They can be written as

$$\rho_{\rm M} = 3H_0^2\Omega_{\rm M}e^{-3N}\,, \tag{2.59}$$

$$\rho_{\rm R} = 3H_0^2\Omega_{\rm R}e^{-4N}\,, \tag{2.60}$$

with $\Omega_{\rm M}$ and $\Omega_{\rm R}$ being the present values of density parameters for matter and radiation, respectively, and H_0 is the present value of the Hubble parameter. We can solve the set of Eqs. (2.56)-(2.60) numerically and obtain the cosmic evolution in terms of H for a specific model and for a set of parameters. This can then be compared to the cosmological measurements of H and therefore constrain the model. We should however note that one important ingredient in solving the evolution equations is the initial conditions for the field φ. This is set by the reheating mechanism after inflation, as we will discuss in section 2.4.2 below.

At this stage it is useful to remember about two quantities. The first one is the equation of state $w_{\rm DE}$ of the scalar field:

$$w_{\rm DE} \equiv \frac{p_{\rm DE}}{\rho_{\rm DE}} = \frac{\frac{1}{2}\varphi'^2 H^2 - V(\varphi)}{\frac{1}{2}\varphi'^2 H^2 + V(\varphi)}\,, \tag{2.61}$$

where $\rho_{\rm DE}$ and $p_{\rm DE}$ are the dark energy density and pressure, respectively, and $V(\varphi)$ is again the dark energy potential (which, as we discussed, can in principle contain a piece from the cosmological constant Λ). $w_{\rm DE}$ for a pure Λ is -1.

Similarly to the slow-roll quantity ϵ for inflation, a useful quantity for late-time evolution of the universe is the so-called *effective equation of state* $w_{\rm eff}$, defined as

$$w_{\rm eff} \equiv -1 - \frac{2}{3}\frac{\dot{H}}{H^2} = -1 + \frac{2}{3}\epsilon\,. \tag{2.62}$$

During radiation and matter domination epochs, $w_{\rm eff}$ becomes $1/3$ and 0, corresponding to $\epsilon = 2$ and $3/2$, respectively. In ΛCDM, the dark energy domination epoch corresponds to $w_{\rm eff} = -1$ ($\epsilon = 0$).

We can study in more detail the behavior of dark energy in a given model by parameterizing the dark energy equation of state $w_{\rm DE}$ in terms of the two so-called Chevallier-Polarski-Linder (CPL) [145, 146] parameters w_0 and w_a through

$$w_{\rm DE}(z) = w_0 + w_a z/(1+z), \tag{2.63}$$

where z is the redshift. This parameterization is however valid only near the present time (i.e. in the range $-1 \lesssim N \lesssim 0$, with $N = 0$ corresponding to today). However, even though Eq. (2.63) cannot be used to fit the equation of state at early times or in the future, it gives a rough idea of how much the models deviate from ΛCDM at present time. w_0 and w_a are also the

parameters used in the definition of the *figure of merit* for the upcoming Stage IV large-scale structure surveys to quantify how well they can distinguish dark energy and modified gravity models from ΛCDM. We will therefore compute also w_0 and w_a for our models below.

It is important to note that it is $w_{\rm eff}$ (and not $w_{\rm DE}$) which is used in direct comparison of the dynamics of the universe in a given model to the cosmological data, and one cannot directly constrain $w_{\rm DE}$ without parametrizing it. Even though parametrizations of $w_{\rm DE}$ are helpful in comparison of a model to the data, a detailed statistical analysis is always required in order to test and constrain the model.

2.4.2 *Gravitational reheating versus instant preheating*

The conventional mechanism of reheating after inflation is associated with a period of oscillations of the inflaton field at the minimum of its potential. In quintessential inflation, where the inflaton field does not oscillate, this mechanism does not work, and is replaced by gravitational reheating [89, 147, 148], which occurs due to particle production in changing gravitational background [149–151], and instant preheating [152–154]. Out of these two mechanisms, the gravitational reheating is the least efficient but the most general one, so we start with describing it here, limiting ourselves to simple estimates.

Inflationary quantum fluctuations of a light scalar field produced during inflation have the energy density of $\rho \sim \frac{3H^4}{8\pi^2}$ [155]. When inflation stops, some of this energy converts to the energy of scalar particles. This is an oversimplified way to describe the effect of particle production during inflation, but it shows a special role of the light scalar particles in this process. For example, massless vector particles are not produced, massless fermions are not produced, massive particles with masses much greater than H are not produced. Following Refs. [89, 147], and ignoring factors of

$\mathcal{O}(1)$, one can estimate the energy of the produced particles at the end of inflation as

$$\rho_{\rm gr} \sim 10^{-2} H_{\rm end}^4 \sim 10^{-3} \rho_{\rm end}^2 \sim 10^{-2} V_{\rm end}^2 \,. \tag{2.64}$$

Here $H_{\rm end}^4$ and $\rho_{\rm end} \sim 2V_{\rm end}$ are, respectively, the Hubble constant and the inflaton energy at the end of inflation, which happens at some field φ end when the kinetic energy of the field approaches $V_{\rm end}$ and the universe stops accelerating.

The energy density $\rho_{\rm gr}$ subsequently decreases as a^{-4} due to the expansion of the universe, as long as the produced particles have masses much smaller than H, which is the case for the flat quintessence potentials.

If the potential after inflation is very steep, as is the case in the single-field models to be considered below, soon after inflation the scalar field falls down and almost all of its energy proportional to V becomes converted to its kinetic energy $\rho_{\rm kin} = \frac{1}{2}\dot\varphi^2$. Thus in the first approximation $\rho_{\rm kin} \sim V$. This kinetic energy corresponds to the equation of state $w = +1$, and decreases as a^{-6}.

Thus, shortly after inflation the universe enters the regime of kinetic energy domination, which is sometimes called *kination*, but this regime ends when $\rho_{\rm kin} \sim \rho_{\rm end} a^{-6}$ becomes smaller than $\rho_{\rm gr} \sim 10^{-3}\rho_{\rm end}^2 a^{-4}$. This happens at $a^2 \sim 10^3 \rho_{\rm end}^{-1}$, when the energy density of radiation produced by reheating was $\rho_{\rm reh} \sim 10^{-9}\,\rho_{\rm end}^4$. The energy density scale $\rho_{\rm end}$ at the end of inflation in α-attractors is typically in the range close to $\rho_{\rm end} \sim 10^{-10}$ in the Planck density units. In that case one finds $\rho_{\rm reh} \sim 10^{-49}$ in Planck density units, or, equivalently $\rho_{\rm reh} \sim (10^6 {\rm GeV})^4$.

After that, the field φ continues rolling towards its large negative values until it freezes at some value $\varphi_{\rm F}$ due to the famous Hubble friction term $3H\dot\varphi$ in its equation of motion. Eventually, after the densities of radiation and cold dark matter become sufficiently small, the field φ starts rolling down again. The final results of the investigation of the equation of state of

all matter in the universe depend on the value of φ_F. This value has been estimated in Ref. [84], with the final result that in realistic models with gravitational preheating one may expect

$$|\Delta\varphi| = |\varphi_F - \varphi_{end}| \sim 43 \,. \tag{2.65}$$

Note that this does not necessarily mean $|\varphi_F| \sim 43$ as stated in Ref. [84], where the authors have considered the case with $\alpha \ll 1$ rendering φ_{end} negligible. Meanwhile for $\alpha = 7/3$ the end of inflation in the model studied in Ref. [84] occurs not at $\varphi_{end} \sim 0$, but at $\varphi_{end} \sim 8$, which implies $\varphi_F \sim -35$.

The value of $|\varphi_F|$ may become much smaller if one takes into account the possibility of instant preheating [152–154]. This effect occurs if we consider interactions of the field φ with some other fields.

For example, one may add to the original theory (2.5) a massless field σ interacting with ϕ as $\frac{g^2}{2}\phi^2\sigma^2$. When the field ϕ moves through the point $\phi = 0$ with velocity $\dot{\phi}_0$, it creates particles σ in the small vicinity of the point $\phi = 0$, with the width $|\Delta\phi| \sim \sqrt{\dot{\phi}_0/g}$. The value of $\dot{\phi}_0$ in our problem is always smaller than $\sqrt{\rho_{end}} \lesssim 10^{-5}$. Therefore, for sufficiently large g one has $\sqrt{\dot{\phi}_0/g} < \sqrt{6\alpha}$. In that case, particle production occurs in a small region where $\phi \approx \varphi$, and the old results of Refs. [152–154] derived for the canonical field φ apply. These results show that the density of massless particles σ, created when the field φ passes through the point $\varphi = 0$ is given by

$$n_\sigma = \frac{(g\dot{\phi}_0)^{3/2}}{8\pi^3} \,. \tag{2.66}$$

Then the field ϕ continues rolling further, giving each particle σ a mass $g|\phi|$. This creates a gas of particles σ with the energy density

$$\rho_\sigma = \frac{(g\dot{\phi}_0)^{3/2}}{8\pi^3}\, g|\phi| \,. \tag{2.67}$$

This potential grows in both directions away from $\phi = 0$. For sufficiently large g, this may lead to a temporary trapping of the field ϕ near $\phi = 0$ [154]. The field continues oscillating near this point until it loses some energy, particle production becomes inefficient, and the previously produced particles become diluted either by cosmic expansion or through their decay. Then the field ϕ resumes its rolling downhill. If instead of a single interaction term considered above one considers a more general interaction $\sum \frac{g_i^2}{2}(\phi - \phi_i)^2\sigma^2$ with $|\phi_i| \ll \sqrt{6\alpha}$, one may have a chain of particle production events at each point $\phi = \phi_i$ [154, 156].

It is not our goal here to study all the regimes that are possible due to instant preheating; see Refs. [88, 152–154, 156] for a discussion of other possibilities. The efficiency of this process is controlled not only by the values of the couplings g_i, but also by the possibility of the decay of particles σ. This suggests that by a proper tuning of this scenario one may achieve freezing of the field φ much earlier than in the gravitational reheating scenario. Therefore, in our subsequent analysis we will examine a broad range of possible values of φ_F.

2.4.3 *Spectral index: Comparison with the non-quintessence scenario*

The calculation of the inflationary parameters n_s and r in quintessential inflation have some distinguishing features. As we will show shortly, extending the results of Refs. [84, 88, 157], predictions for n_s and r in quintessential inflation may differ rather significantly from the ones in the more traditional versions of α-attractors, which do not have a stage of kination where the energy density of the universe is for a long time dominated by the kinetic energy of the inflaton field. This may give us a novel possibility to test quintessential inflation with gravitational reheating and a long stage of kination.

Let us remember that the values of n_s and r for α-attractors are given by

$$n_s = 1 - \frac{2}{N}\,, \qquad r = \frac{12\alpha}{N^2}\,, \tag{2.68}$$

where N is the number of e-folds corresponding to the moment of production of the perturbations with momentum k_* generated when the potential was equal to $V_* = V(\varphi_*)$.

We use the standard equation for the required number of e-folds, see Eq. (47) and a description of the notations in Ref. [82]:

$$N \approx 67 - \ln\left(\frac{k_*}{a_0 H_0}\right) + \frac{1}{4}\ln\left(\frac{V_*}{M_{\rm Pl}^4}\right) + \frac{1}{4}\ln\left(\frac{V_*^2}{\rho_{\rm end}}\right) \tag{2.69}$$

$$+ \frac{1-3w_{\rm int}}{12(1+w_{\rm int})}\ln\left(\frac{\rho_{\rm reh}}{\rho_{\rm end}}\right) - \frac{1}{12}\ln(g_{\rm th})\,. \tag{2.70}$$

Using this equation, one can calculate the required number of e-folds N for any model based on α-attractors. Unless one studies models with extremely large or extremely small α, one has $\rho_{\rm end} \sim V_* = \mathcal{O}(10^{-10})$, with some variations which typically do not affect too much the value of the term $\frac{1}{4}\ln\left(\frac{V_*^2}{\rho_{\rm end}}\right)$. The main difference between N for different α-attractors can be attributed to the term $\Delta N = \frac{1-3w_{\rm int}}{12(1+w_{\rm int})}\ln\left(\frac{\rho_{\rm reh}}{\rho_{\rm end}}\right)$.

In the simplest α-attractor models, as well as in the Starobinsky model, which can be represented as an α-attractor with $\alpha = 1$, after inflation one typically has $w_{\rm int} = 0$, i.e. $\Delta N = \frac{1}{12}\ln\left(\frac{\rho_{\rm reh}}{\rho_{\rm end}}\right)$. In supergravity-based α-attractors and in the simplest versions of the Starobinsky model one often encounters an inefficient reheating with the reheating temperature $T_{\rm reh} \sim 10^9 - 10^{11}$ GeV. For $T_{\rm reh} \sim 10^{10}$ GeV and assuming $\mathcal{O}(100)$ different types of particles in thermal equilibrium after reheating, one finds $\Delta N \sim -4$.

Meanwhile, in the quintessential α-attractors with gravitational reheating and a long stage of kinetic energy domination, one has $\Delta N = -\frac{1}{12}\ln\left(\frac{\rho_{\rm reh}}{\rho_{\rm end}}\right)$.

Notice the important sign change. Using the numerical estimates made in section 2.4.2, one finds $\Delta N = +7.5$. This particular number is rather sensitive to various assumptions on the energy scale of gravitational reheating, but let us take it at its face value. It shows that the required number of e-folds N in the quintessential α-attractor models can be greater than the one in the more conventional α-attractors or in the Starobinsky model by $\Delta N \sim 10$.

As a result, the value of n_s in quintessential α-attractors with gravitational reheating is typically greater than in more traditional models by about 0.006. This number coincides with one standard deviation in the Planck results [82]. Thus, by a more precise determination of n_s, which can be achieved in the future, we may be able to distinguish quintessential α-attractors with gravitational reheating from other models with more efficient reheating and without a long stage of kinetic energy domination. This result may become quite interesting for development of inflationary models if more precise observations shift n_s towards greater values as compared to the Planck 2015 results [82]. Moreover, further improvement of the accuracy of the measurement of n_s may help us to distinguish the conventional inflationary models with the cosmological constant from the models of quintessential inflation, even if the equation of state of dark energy almost exactly coincides with $w = -1$.

2.5 EXAMPLES OF SINGLE-FIELD MODELS OF QUINTESSENTIAL INFLATION

2.5.1 *Linear potential*

We begin with the α-attractor version of the simplest linear dark energy potential [91]

$$V(\phi) = \gamma\phi + \Lambda\,. \tag{2.71}$$

In terms of the canonically normalized field φ, this potential is given by

$$V(\varphi) = \gamma\sqrt{6\alpha}(\tanh\frac{\varphi}{\sqrt{6\alpha}} + 1) + \Lambda\,. \tag{2.72}$$

At $\varphi \gg +\sqrt{6\alpha}$ and $\Lambda \ll \gamma\sqrt{6\alpha}$ the potential is given by

$$V(\varphi) = 2\gamma\sqrt{6\alpha}(1 - e^{-\sqrt{\frac{2}{3\alpha}}\varphi})\,, \tag{2.73}$$

whereas at $\varphi \ll -\sqrt{6\alpha}$ one has

$$V(\varphi) = \Lambda + 2\gamma\sqrt{6\alpha}\; e^{\sqrt{\frac{2}{3\alpha}}\varphi}\,. \tag{2.74}$$

From the COBE/Planck normalization (2.16), we find a constraint

$$\frac{\gamma}{\sqrt{\alpha}} \sim 2\times 10^{-11}\,. \tag{2.75}$$

One could expect that the simplest linear model (2.71) with $\Lambda = 0$ can be used as a model of quintessential inflation if one takes $\alpha \gtrsim 1$; see e.g.

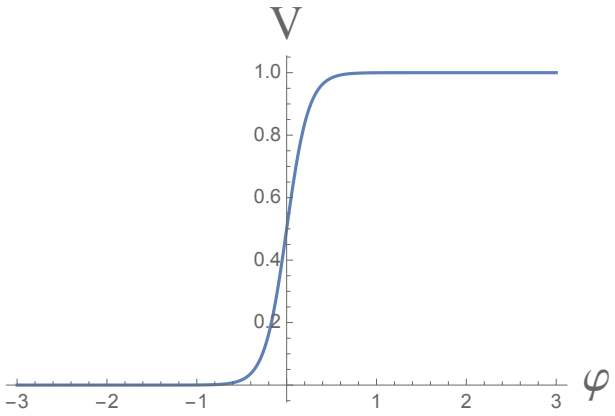

Figure 2.4: Linear potential $V = \frac{1}{2\sqrt{6\alpha}}(\sqrt{6\alpha}+\phi) + \Lambda = \frac{1}{2}(1+\tanh\frac{\varphi}{\sqrt{6\alpha}}) + \Lambda$ for $\alpha = 10^{-2}$ and $\Lambda \sim 10^{-120}$. The tiny cosmological constant Λ is crucial for the validity of our scenario, but Λ is so small that it is invisible in this figure.

(2.26) and (2.27) for $\alpha = 7/3$. However, one can check that in this model with $\alpha > 1/3$ the inflationary slow-roll parameter ϵ always remains smaller than 1 and inflation never ends.

This problem can be solved by using $\alpha \ll 1$, for example $\alpha = \mathcal{O}(10^{-2})$, and adding a small cosmological constant $\Lambda \sim 10^{-120}$, see Fig. 2.4. In that case, inflation does end in a vicinity of $\varphi = 0$, at $\varphi_{\rm end} \approx \sqrt{\frac{3\alpha}{8}}\ln\frac{1}{3\alpha} \sim 0.2$. Then the field φ rolls down until it freezes at some value $\varphi = \varphi_{\rm F}$ depending on the efficiency of reheating, see section 2.4.2. If $|\varphi_{\rm F}| > \sqrt{\frac{3\alpha}{2}}\ln\frac{\Lambda}{2\gamma\sqrt{6\alpha}}$, then the potential (2.72) is dominated by the positive cosmological constant Λ. In that case, at the moment when the field starts moving again, the universe gradually enters the stage of expansion dominated by the cosmological constant Λ with the equation of state $w_{\rm DE} = -1$.

To go beyond the simple estimates given above and in order to determine the range of possible values of $\varphi_{\rm F}$ required in this scenario, we performed a numerical analysis for two different values of $\alpha = O(10^{-2})$. Figs. 2.5 and 2.6

show the effective equation of state $w_{\rm eff}$ (thick, blue curves), as well as the equation of state of dark energy $w_{\rm DE}$ (thick, orange curves) for this linear potential and for two illustrative choices of $\alpha = 0.02$ and $\alpha = 0.005$, and for different choices of $\varphi_{\rm F}$. In both cases, Λ has been set to $0.7\rho_{\rm c}$, with $\rho_{\rm c} \equiv 3H_0^2$ being the present value of the critical density, providing a total dark energy density today in agreement with observational data. The value of $\gamma\sqrt{6\alpha}$ has been set to 2.57×10^{-12} and 6.4×10^{-13} for $\alpha = 0.02$ and $\alpha = 0.005$, respectively, in order to obtain a correct inflationary scale; see (2.15) and (2.75). In addition, we have presented $w_{\rm eff}$ for ΛCDM in each case (thin, black curves) for comparison.

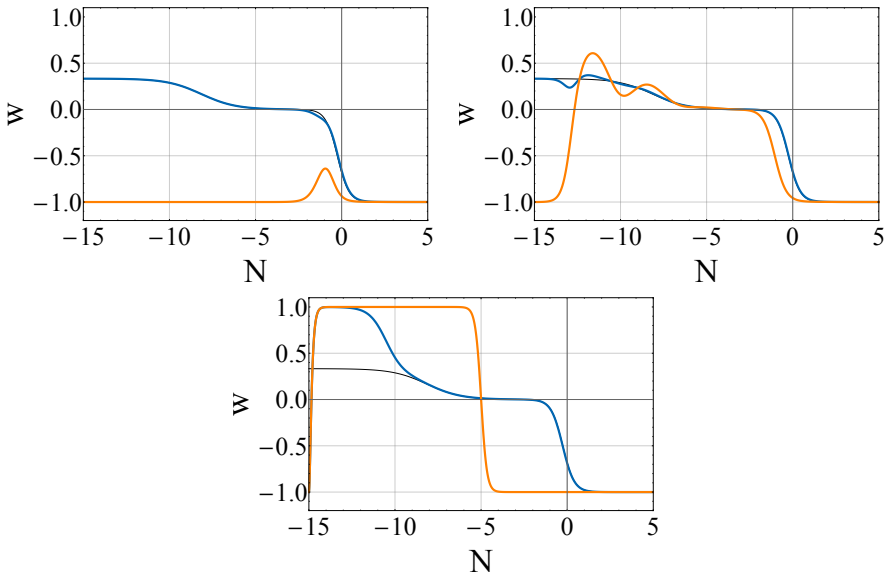

Figure 2.5: Evolution of the equation of state as a function of the number of e-folds N after reheating for the linear potential $\gamma\sqrt{6\alpha}(\tanh\frac{\varphi}{\sqrt{6\alpha}}+1)+\Lambda$ with $\Lambda = 0.7\rho_{\rm c}$ and α set to 0.02. The panels in the clockwise direction, starting from the top left, correspond to $\varphi_{\rm F} = -43$, $\varphi_{\rm F} = -36$, and $\varphi_{\rm F} = -33$, respectively. The blue and orange curves in each case correspond to $w_{\rm eff}$ and $w_{\rm DE}$, respectively, and we have also shown $w_{\rm eff}$ for ΛCDM with a thin, black curve for comparison. $N = 0$ corresponds to the present time.

For $\alpha = 0.02$, we have plotted three cases with $\varphi_F = -43$ (top left panel), $\varphi_F = -36$ (top right panel), and $\varphi_F = -33$ (bottom panel). Looking first at $w_{\rm eff}$ for $\varphi_F = -43$ we see that the desired cosmic history has been recovered although the evolution of $w_{\rm eff}$ shows a small difference from the ΛCDM model at around $N = -2$. $w_{\rm DE}$ in this scenario, however, shows a significant difference compared to the standard model — $w_{\rm DE}$ is not -1 always, contrary to a pure Λ, and has a bump at late times. For $\varphi_F = -36$, we see that although the late-time behavior of $w_{\rm eff}$ is almost identical to that of ΛCDM, it shows a difference at early times ($N \lesssim -10$), and $w_{\rm DE}$ is drastically different from a pure Λ dark energy. By increasing φ_F to -33, we now see that the times earlier than $N \sim -8$ (corresponding to the matter-radiation equality in ΛCDM) are strongly affected by the dynamics of the scalar field. We no longer recover a radiation domination epoch as in ΛCDM, and $w_{\rm eff}$ goes all the way to $+1$ back in time rather than $1/3$ for radiation. This can be understood by looking at how $w_{\rm DE}$ behaves at early times. The inflaton is in a kination phase at $N \lesssim -5$, and is dominant over matter and radiation at $N \lesssim -8$, hence the effective equation of state follows mainly the contribution from the inflaton and takes the value of $\sim +1$ at early times. Note that in this case the model does not give an early dark energy as $w_{\rm DE}$ is $\sim +1$ and not ~ -1.

Having this observation, let us systematically study different scenarios depending on the value of φ_F. Our numerical investigation of the model with $\alpha = 0.02$ reveals three different possibilities:

- $-43 \leqslant \varphi_F \lesssim -34$: $\varphi_F \approx -43$ is the lowest value that φ_F is allowed to take due to the reheating constraints, see section 2.4.2. For the entire range of $[-43, -34]$ we obtain a dark energy which, while provides viable cosmologies over the entire history, it predicts deviations from a pure Λ that are detectable by future observations. For example, for the two ends of the range, $\varphi_F = -43$ and $\varphi_F = -34$, we obtain $w_0 \sim -0.936$ and $w_a \sim 0.192$, and $w_0 = -0.956$ and $w_a = 0.119$, respectively, which both should be detectable by the future Stage IV

large-scale structure surveys, see section 2.5.3.2. In addition, for this range we recover radiation and matter domination epochs which are very similar to those of ΛCDM, with some small distortions due to the fact that the scalar field is not completely subdominant at early times; the larger the value of φ_F, the larger the distortions. $w_{\rm eff}$ and $w_{\rm DE}$ for another example of φ_F in this range are presented in Fig. 2.5 (top right panel) for $\varphi_F = -36$ with $w_0 \sim -0.956$ and $w_a \sim 0.119$. Note that in this case we are dealing with a tracking solution, with $w_{\rm DE}$ mimicking the equation of state of the dominating background fluid.

- $-34 \lesssim \varphi_F \lesssim -32$: In this case, the model is viable from the point of view of late-time cosmology, with a Λ-like dark energy at late times ($w_0 \sim -1$ and $w_a \sim 0$), the reason being that the Λ term is dominant over the scalar field during this period. The very early times ($N \lesssim -8$) in this range are however strongly affected by the scalar field, and behave significantly differently from that of ΛCDM, i.e. we do not get radiation domination at early times, but a domination by the inflaton in a kination phase. The model therefore gives viable cosmologies from the point of view of late-time observations, but we obtain no radiation domination epoch at early times. An example of this case has been presented in Fig. 2.5 (bottom panel) for $\varphi_F = -33$.

- $-32 \lesssim \varphi_F$: By increasing φ_F to values larger than ~ -32 the scalar field stays in the kination phase for a longer period of time, and is also dominant over matter and radiation for a longer period, resulting in an extended epoch of $w_{\rm eff} = +1$ at early times. Increasing φ_F to -30.5 already extends the domination of the scalar field with $w_{\rm DE} = +1$ all the way to $N \approx -5$, which is the beginning of matter domination. The more we increase φ_F, the longer the period of dark energy domination (with $w_{\rm DE} = +1$), so that the model will give predictions that are in clear contradiction with observations. Of course, for any values of φ_F

the energy density of dark energy will eventually be dominated by the cosmological constant with $w = -1$, but our numerical studies show that this happens later and later in time when φ_F increases, and the Λ domination eventually happens only in the future.

In summary, our analysis shows that the linear model with $\alpha = 0.02$ provides viable cosmologies as long as φ_F remains in the relatively broad range of $\sim [-43, -34]$, while predicting detectable deviations from ΛCDM that are sufficiently large for the model to be tested against ΛCDM. One should note that larger values of φ_F all the way to about -32 can also provide viable late-time cosmologies and only affect the epoch of radiation domination in the early universe.

Let us now decrease α to 0.005. Fig. 2.6 shows the evolution of w_{DE} and w_{eff} for this scenario, but for three choices of $\varphi_F = -22.5$ (top left panel), $\varphi_F = -18$ (top right panel), and $\varphi_F = -16$ (bottom panel). We see that for $\varphi_F = -22.5$, the model already behaves almost identically to ΛCDM, with w_{DE} being -1 for the entire history. Clearly, for $\varphi_F < -22.5$ all the way to our lower bound of -43, the model will remain like ΛCDM. Let us now increase φ_F from -22.5 to -21.5 (not shown in Fig. 2.6). Our numerical analysis gives $w_0 \sim -0.983$ and $w_a \sim 0.050$ in this case. This shows that the deviations from a pure Λ increases by increasing φ_F. Increasing φ_F further to ~ -16 still gives viable cosmologies, while the values larger than ~ -16 will make the early times ($N \lesssim -8$) completely affected by the kination domination of the inflaton over radiation, and radiation domination will be lost; the model, however, behaves like a pure cosmological constant at late times, i.e. with $w_0 \sim -1$ and $w_a \sim 0$. An example of how w_{eff} and w_{DE} behaves for the range $[-21.5, -16]$ is presented for $\varphi_F = -18$ (with $w_0 \sim -0.989$ and $w_a \sim 0.030$) in Fig. 2.6 (top right panel), while the behavior of w_{eff} and w_{DE} for $\varphi_F = -16$ is given in the bottom panel of the figure. We see that dark energy for $\varphi_F = -18$ shows an evolution similar to the previous case of $\alpha = 0.02$ with $\varphi_F = -36$. For values of φ_F larger than -16 we see a behavior similar to the case of $-32 \lesssim \varphi_F$ for $\alpha = 0.02$, i.e

the epoch of dark energy domination in the kination phase gets extended to later times, making the model more and more unviable by increasing φ_F. We therefore conclude that the linear model with $\alpha = 0.005$ provides viable cosmologies for $\varphi_F \in [\sim -21.5, \sim -16]$ with w_0 and w_a showing deviations from ΛCDM, and for $\varphi_F \lesssim -21$ with dark energy behaving almost identically to a pure Λ. The deviations for the range $[-21.5, -16]$ are not as large as the ones we obtained for $\alpha = 0.02$, but *might* still be detectable by the Stage IV LSS surveys.

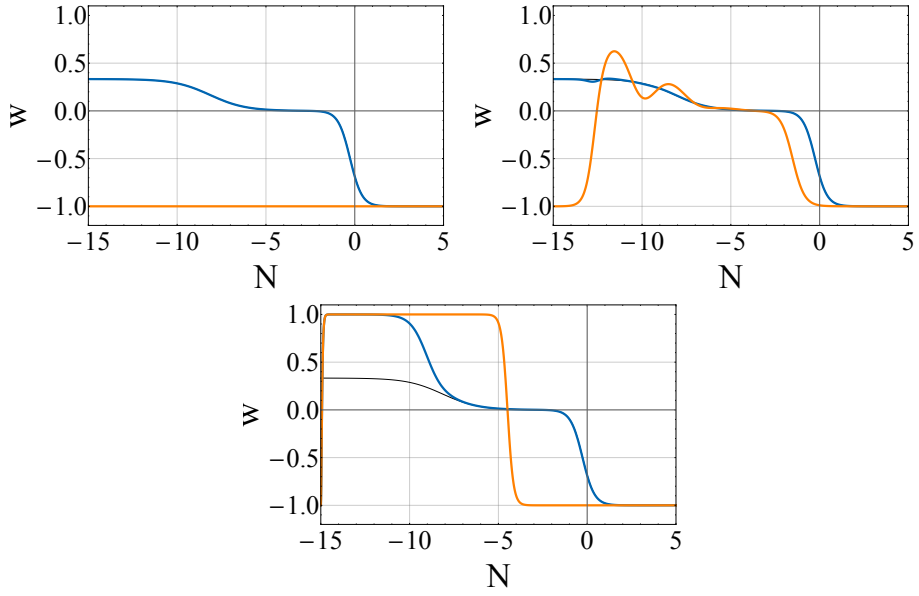

Figure 2.6: The same as in Fig. 2.5 but for $\alpha = 0.005$. The panels in the clockwise direction, starting from the top left, now correspond to $\varphi_F = -22.5$, $\varphi_F = -18$, and $\varphi_F = -16$, respectively.

In conclusion, we have found a realistic model of quintessential inflation based on the α-attractor model with a linear potential. This model requires $\frac{\gamma}{\sqrt{\alpha}} \sim 2 \times 10^{-11}$, $\alpha \lesssim 0.02$, and a cosmological constant in the anthropically allowed range of $\Lambda \sim 10^{-120}$. The smaller the value of α, the larger the

range of φ_F for which viable cosmic histories exist, although deviations from ΛCDM are expected to become less and less likely in the limit $\alpha \ll 0.01$.

This is the simplest model of quintessential inflation based on α-attractors, so let us pause here a little, before turning to other, more complicated models. The linear potential $V(\phi) = \gamma\phi + \Lambda$ is the simplest potential ever, and yet it was never used in inflationary theory until now, for a good reason: This potential is unbounded from below, so unless γ is extraordinarily small, it leads to a rapid instability and a collapse of the universe. A linear potential was used in Ref. [91] for describing dark energy and solving the cosmological constant problem, but it required an extremely small constant $\gamma \lesssim 10^{-120}$ to avoid the collapse of the universe within 14 billion years.

In our new model described in this section, we have $\frac{\gamma}{\sqrt{\alpha}} \sim 2 \times 10^{-11}$ (2.75), which is the standard inflationary requirement for the COBE/Planck normalization. Thus γ can be 110 orders of magnitude greater than in the quintessence model of Ref. [91]. And nevertheless, we do not have any vacuum instability, because in the context of α-attractors the potential is defined only in the finite range $|\phi| < \sqrt{6\alpha}$. The lower part of the potential in this range becomes an infinite, exponentially flat plateau in canonical variables.

By modifying the value of α and the strength of interaction of the field φ with matter, one can control the parameter w. One may also increase the value of the inflationary spectral index n_s by about one standard deviation of the Planck 2015 results for n_s. The only additional fine-tuning required in this model, as compared to the more conventional models of inflationary α-attractors, is the condition $\alpha \lesssim 0.02$. It would be nice to find consistent versions of such models with $\alpha = O(1)$, and especially with $\alpha = 1/3, ..., 7/3$, which are better motivated in extended supergravity, M-theory, and string theory [94, 126, 127]. However, $N = 1$ supergravity does not impose any constraints on α. From a purely phenomenological point of view, the requirement $\alpha \lesssim 0.02$ is not an unreasonable price to pay for a simple, unified description of inflation and dark energy.

2.5.2 *Two-shoulder model with exponential potential*

The next example to consider is the exponential two-shoulder potential introduced in Ref. [90],

$$V(\phi) = M^2 e^{-2\gamma}\left(e^{\frac{\gamma\phi}{\sqrt{6\alpha}}} - 1\right)^2 . \tag{2.76}$$

In the canonical variables, one finds

$$V(\varphi) = M^2 e^{-2\gamma}\left(e^{\gamma \tanh\frac{\varphi}{\sqrt{6\alpha}}} - 1\right)^2 . \tag{2.77}$$

The potential has a minimum at $\varphi = 0$. The general shape of such potentials is illustrated by Fig. 2.7 for a toy model with $M = 1$, $\alpha = 1/3$, and $\gamma = 2$. In realistic models, we need to take $\gamma \gg 1$. In this limit, the right shoulder has the height $V_+ = M^2$, and the left shoulder has the height $V_- = M^2 e^{-\gamma}$.

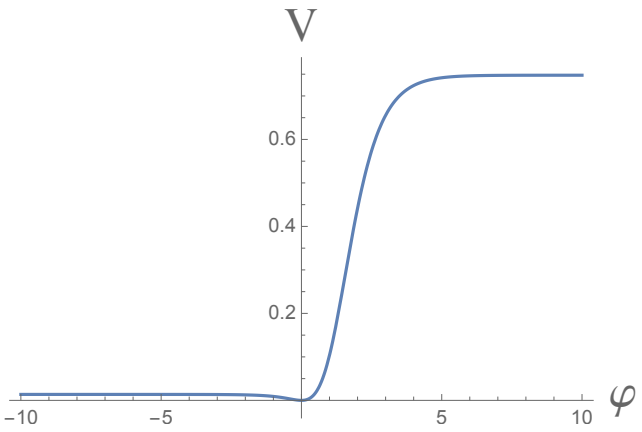

Figure 2.7: The potential (2.77) shown for a toy model with $M = 1$, $\gamma = 4$, and $\alpha = 1/3$. It illustrates the main feature of the models of this class: two shoulders with an exponentially large difference in their heights.

An advantage of this model is that it can easily incorporate the exponentially large hierarchy $e^{2\gamma}$ between the inflationary energy scale $V_+ = M^2 \sim 10^{-10}$ and the dark energy scale $V_- = M^2 e^{-2\gamma} \sim 10^{-120}$. For $\alpha = \mathcal{O}(1)$, $M \sim 10^{-5}$, and $\gamma \sim 126$, this model fits all the inflationary data, and describes the present stage of acceleration driven by the effective cosmological constant $V_- \sim 10^{-120}$. It is difficult to show the right and the left plateaus in one figure, because the height of the right shoulder is 110 orders of magnitude greater than the height of the left one. Therefore, we show only the left shoulder of the potential and a small vicinity of its minimum in Fig. 2.8.

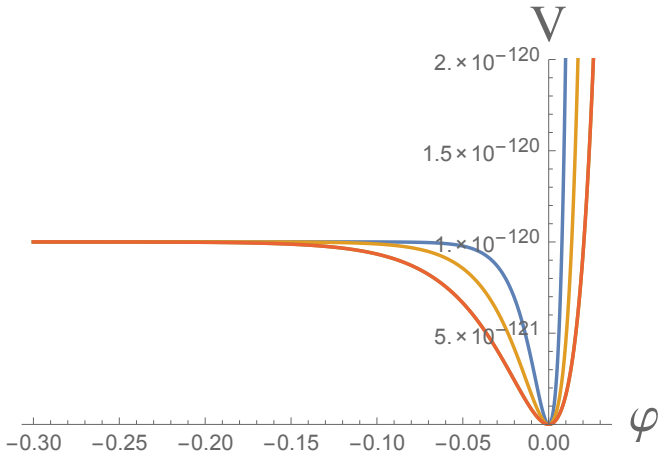

Figure 2.8: The potential (2.77) shown in Planck energy density units for $M \sim 10^{-5}$, $\gamma \sim 126$, $\alpha = 1/3$ (blue curve), 1 (yellow curve), and $7/3$ (red curve). Inflation begins at the right shoulder of this potential, which is not shown here because it is 110 orders of magnitude higher. After that, the field rolls to the left plateau, which almost immediately becomes flat. That is why it is practically indistinguishable from the cosmological constant.

The shape of the left plateau shown in Fig. 2.8 is determined by the following asymptotic expression for $V(\varphi)$ at large negative φ:

$$V = M^2 e^{-2\gamma}\left(1 - 4\gamma e^{-\gamma} e^{\sqrt{\frac{2}{3\alpha}}\varphi}\right) . \tag{2.78}$$

The potential approaches $V_- = M^2 e^{-2\gamma} \sim 10^{-120}$, and the asymptotic deviation from this value at large, negative φ is suppressed not only by the factor $e^{\sqrt{\frac{2}{3\alpha}}\varphi}$, but also by an extra factor $e^{-\gamma} \sim 10^{-55}$. This means that the potential is extremely flat everywhere outside a small vicinity near $\varphi = 0$. One can check, for example, that the slow-roll parameter ϵ_V in this model is smaller than 10^{-25} for $\varphi < 1$. The simplest way to understand it is to note that even the potential (2.76) in terms of the original variable ϕ is exponentially flat at the boundary of the moduli space $\phi = \sqrt{6\alpha}$ for $\gamma \gg 1$, and the transition to the canonical variables leads to an additional flattening. As a result, a generic prediction for dark energy in this model is $w = -1$.

In general, one may add an arbitrary constant Λ to the potential (2.77). By adding a negative constant one may decrease the required value of the parameter γ. As one can see from Fig. 2.9, one can easily tune the asymptotic value of the potential to be $\Lambda = V_- \sim 10^{-120}$ in accordance with anthropic considerations.

Since we generically obtain $w = -1$ in this model, one may wonder whether it has any merit over the simple ΛCDM. In fact, the model presented here demonstrates that one can easily construct a family of inflationary models in which inflation ends without any need to stabilize the inflaton field at the minimum of its potential. Even in the models where the potential has an anti-de Sitter minimum with a negative cosmological constant at $\varphi = 0$, as in Fig. 2.9, one can safely live in a de Sitter-like state on an exponentially flat low plateau. The flatness of the potential in this model, just as in all other models considered in this paper, is protected by the geometric origin of α-attractors.

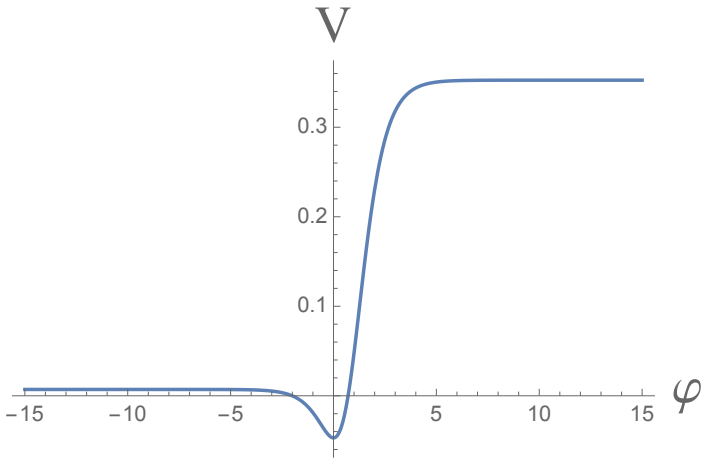

Figure 2.9: In the asymmetric potential with a minimum at $V < 0$ one can achieve exponential hierarchy of the heights V_+ and V_- with smaller values of γ. For illustration, in this figure we used $M = 1$, $\gamma = 1$, $\alpha = 1/3$, and added a constant $V_0 = -0.047$. By taking a slightly smaller value of V_0, one can easily make the asymptotic value of the potential $\Lambda = V_- \sim 10^{-120}$, as required by anthropic considerations.

As we have already mentioned, further improvement of the accuracy of the measurement of n_s may help to distinguish this model and other models of quintessential inflation from the more conventional α-attractors, even if the equation of state of dark energy in quintessential inflation almost exactly coincides with $w = -1$, see section 2.4.3. The possibility of having a somewhat larger value of n_s due to the long stage of kination in this scenario may become very welcome in the future, depending on the observational data.

2.5.3 *Exponential potential*

Let us now assume a simple exponential form for the non-canonical potential $V(\phi)$ where a free cosmological constant term Λ is also (implicitly)

included. We will later fix Λ to specific values in order to construct two specific working models with this potential.

The total potentials of our single-field, quintessential inflation models have the structure

$$V(\phi) = M^2 e^{\gamma(\frac{\phi}{\sqrt{6\alpha}}-1)} + V_0\,, \tag{2.79}$$

which, again with $\phi = \sqrt{6\alpha}\,\tanh\frac{\varphi}{\sqrt{6\alpha}}$, gives

$$V(\varphi) = M^2 e^{\gamma\,(\tanh\frac{\varphi}{\sqrt{6\alpha}}-1)} + V_0\,. \tag{2.80}$$

At large, positive φ this potential tends to the inflationary plateau with $V_+ = M^2 + V_0$, and at large, negative φ it tends to the cosmological constant $\Lambda = V_- = M^2 e^{-2\gamma} + V_0$. Instead of making a general investigation for arbitrary V_0 (or Λ), we concentrate here on two particular cases, which we call Exp-model I and Exp-model II:

- **Exp-model I**: The constant V_0 is set to zero. In this case the potential for dark energy is solely the exponential one,

  $$V = M^2 e^{\gamma\left(\tanh\frac{\varphi}{\sqrt{6\alpha}}-1\right)}. \tag{2.81}$$

  At large, positive φ this potential tends to $V_+ = M^2$. Its asymptotic value at large, negative φ is given by the cosmological constant $\Lambda = V_- = M^2 e^{-2\gamma}$.

- **Exp-model II**: The constant V_0 is set to $-M^2 e^{-2\gamma}$ [84]. In this case the potential for dark energy is

  $$V = M^2 e^{-2\gamma}\left(e^{\gamma\left(\tanh\frac{\varphi}{\sqrt{6\alpha}}+1\right)} - 1\right). \tag{2.82}$$

At large, positive φ in the large γ limit it reaches M^2, as before, up to an exponentially small correction $-M^2 e^{-2\gamma}$. It vanishes asymptotically for large, negative φ, i.e. $\Lambda = V_- = 0$.

The ratio of V_- to V_+ in Exp-model I is given by

$$\frac{V_-}{V_+} = e^{-2\gamma} \approx 10^{-110} \approx e^{-252}\,. \tag{2.83}$$

An analogous relation should be valid for Exp-model II, but instead of V_- one should have the present value of dark energy $V_{\rm today} \sim 10^{-120}$. One can view this property of our quintessential inflation models as a drawback, since our potentials have a huge number built in. This is however the price to pay for having one plateau of the model for the early universe at about 10^{-10} in Planck density units, and another one for the current and future acceleration at about 10^{-120}. In the context of a phenomenological model, however, we may view this as a parameter which is determined observationally,

$$\gamma \approx \ln \frac{H_{\rm infl}}{H_{\rm DE}}\,. \tag{2.84}$$

In such a case, we still have to find the working models which show a consistent deviation from the cosmological constant dynamically.

Clearly, scenarios with other choices of V_0 (and the resulting cosmological constant Λ) are also possible in general, but as we will discuss later, our Exp-models I and II are of particular interest, and capture all the interesting features of the exponential potential. The two potentials for our Exp-models I and II are shown in Fig. 2.10. Exp-model I (orange curve) has a constant, nonzero asymptotic value for large, negative φ, while Exp-model II (blue curve) decreases to zero when $\varphi \to -\infty$.

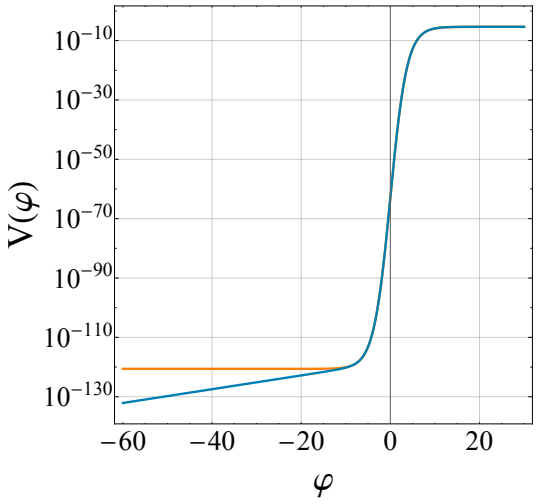

Figure 2.10: The two quintessential inflation models with an exponential potential studied in this work: Exp-model I (orange curve) with the form $M^2 e^{\gamma(\tanh\frac{\varphi}{\sqrt{6\alpha}}-1)}$, and a constant, nonzero asymptotic value for $\varphi \to -\infty$, and Exp-model II (blue curve) with the form $M^2 e^{-2\gamma}\left(e^{\gamma\left(\tanh\frac{\varphi}{\sqrt{6\alpha}}+1\right)}-1\right)$ and a vanishing asymptotic value.

2.5.3.1 *Inflationary and late-time dynamics*

Fig. 2.11 shows an example of the evolution of the inflationary quantities ϵ and η, introduced in section 2.4.1, for Exp-model II and for a typical set of parameters with viable cosmologies. The parameters chosen for the plots are the best-fit ones found through the comparison of the model to the current late-time cosmological observations as described in section 2.5.3.2 below. In particular, α has been set to $7/3$. The results for Exp-model I are very similar and we do not present them here.

In each panel, the red, vertical line shows the end of inflation (i.e. when ϵ becomes unity), and N is the number of e-folds before that, such that the end of inflation is at $N = 0$. Both ϵ and η have very small values during the inflationary period. $N \approx 63$ corresponds to the moment at which the cosmological scales observed by the CMB experiments had left the horizon.

Fig. 2.11 shows that ϵ at the beginning of the last 63 e-folds has a value very close to zero, and stays almost vanishing for a long period (which is a necessary condition for slow-roll inflation), and then suddenly increases and becomes of $\mathcal{O}(1)$; this ends inflation. The transition of ϵ from almost zero to 3 corresponds to a transition from slow roll (where the potential dominates) to a kination period (where the kinetic energy dominates over the potential). This transition is required for inflation to end, and in order to enter a reheating phase. The second slow-roll parameter, η, is also small during inflation and becomes of $\mathcal{O}(1)$ at the end of inflation. For both ϵ and η we have computed their exact values over time, i.e. Eqs. (2.45) and (2.50), whereas the *slow-roll* values for these two quantities, which can be written in terms of the potential and its derivatives, are valid only during the inflationary period and not in general. The values of ϵ and η measured by the CMB are the ones at $N \sim 63$.

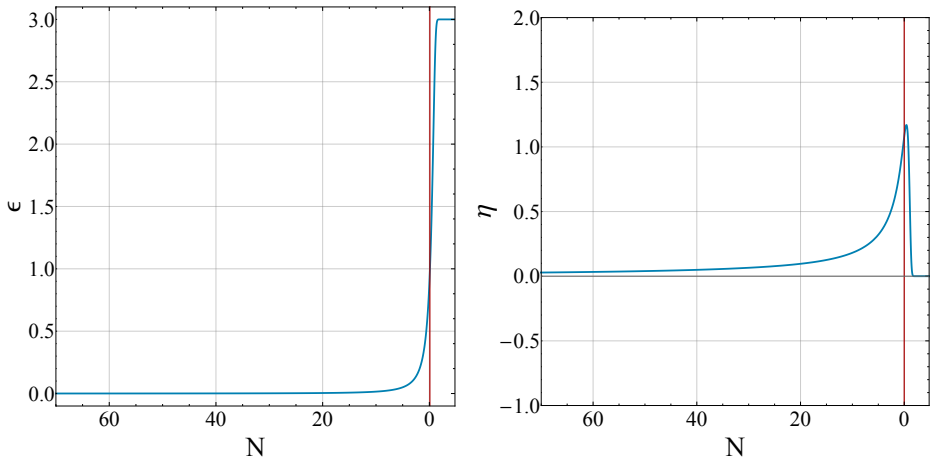

Figure 2.11: Evolution of the slow-roll parameters ϵ and η as functions of the number of e-folds N before the end of inflation for Exp-model II and for a typical set of parameters which give viable late-time cosmological histories. In each panel, the red, vertical line depicts the end of inflation (i.e. when ϵ becomes of $\mathcal{O}(1)$), and $N = 63$ corresponds to the moment at which the cosmological scales observed by the CMB experiments had left the horizon.

We can also solve the set of Eqs. (2.56)-(2.60) numerically and obtain the cosmic evolution in terms of H for a given set of the free parameters $\Omega_{\rm M}$, $\Omega_{\rm R}$, M^2, and γ. This can then be compared to the cosmological measurements of H and therefore constrain the models. We should however note that one important ingredient in solving the evolution equations is the initial conditions for the field φ. The initial value of φ is the freezing value $\varphi_{\rm F}$ set by the reheating mechanism after inflation, see section 2.4.2.

Let us recap the story. As discussed in section 2.4.2, the field takes positive values during inflation, and rolls down the potential with its value reducing with time and approaching zero. Around this time, and when $\varphi \sim +8$, reheating takes place and matter particles are produced. In case the only reheating at work is gravitational particle production, which is not a very efficient mechanism, the field continues rolling down to values around -35 and then freezes. In case other reheating mechanisms, such as instant preheating [152–154], are at work in addition to gravitational particle production, reheating will be more efficient and the field will freeze earlier, to values that can be much larger than -35; we call this value of the field after reheating $\varphi_{\rm F}$, at which φ is frozen. The field remains frozen at $\varphi_{\rm F}$ for some time after reheating until the Hubble friction becomes so low that the field starts rolling down its potential again. The evolution of the field after reheating and starting from the value $\varphi_{\rm F}$ determines the evolution of the universe and cosmic histories at late times, i.e. from radiation domination all the way to the present time.

Fig. 2.12 depicts an example of the evolution of the scalar field φ as a function of the number of e-folds N for the entire history of the universe from inflation to late times, for both Exp-models I (left panel) and II (right panel). These have been computed for the same set of parameters as the ones used for computing the inflationary quantities of Fig. 2.11, providing viable late-time cosmological histories. We have set the value of $\varphi_{\rm F}$ to -10 in both cases.

The vertical, red bands depict the period after the end of inflation and before the time at which the scalar field freezes, separating the inflationary and late-time periods. Note that this period starts with a kination phase, followed by radiation domination, after the occurrence of reheating. Since the exact behavior of the field depends on the details of reheating, we have shown this period of kination plus the start of the radiation domination by a red band. The details of this period are not important for our numerical and statistical analysis later, as long as we have the required information on the initial conditions of the field for our late-time investigation. This boils down to the values of $\varphi_{\rm F}$ used in our analysis, which we have ensured to be achievable through our reheating mechanisms. The red bands should therefore be considered only as a sketch for illustrative purposes, while the inflationary evolution and the late-time dynamics shown in Fig. 2.12 are the results of precise numerical computations. Note how the field behaves differently in the future ($N > 0$) for the two models.

The evolutions of the effective equation of state $w_{\rm eff}$ as well as the equation of state of dark energy $w_{\rm DE}$ as functions of the number of e-folds N are presented in Fig. 2.13 for both Exp-models I (upper panel) and II (lower panel). The set of parameters used are the same as in Figs. 2.11 and 2.12 with viable late-time cosmological histories. The blue and green curves depict, respectively, $w_{\rm eff}$ and $w_{\rm DE}$, and for comparison we have also shown the effective equation of state for the ΛCDM cosmology (orange curve). $N = 0$ corresponds to the present time. For computing these quantities, and for both models, we have again set φ to -10 and φ' to 0 initially. These initial values have been set at $N = -15$, i.e. well inside the radiation domination epoch.

First of all, the figures show that the evolutions of $w_{\rm eff}$ for both Exp-models I and II closely follow the one for ΛCDM in the past, while there are deviations in the future ($N > 0$). $w_{\rm eff}$ for Exp-model I approaches -1 asymptotically (when $N \to +\infty$), just as in ΛCDM, while its asymptotic

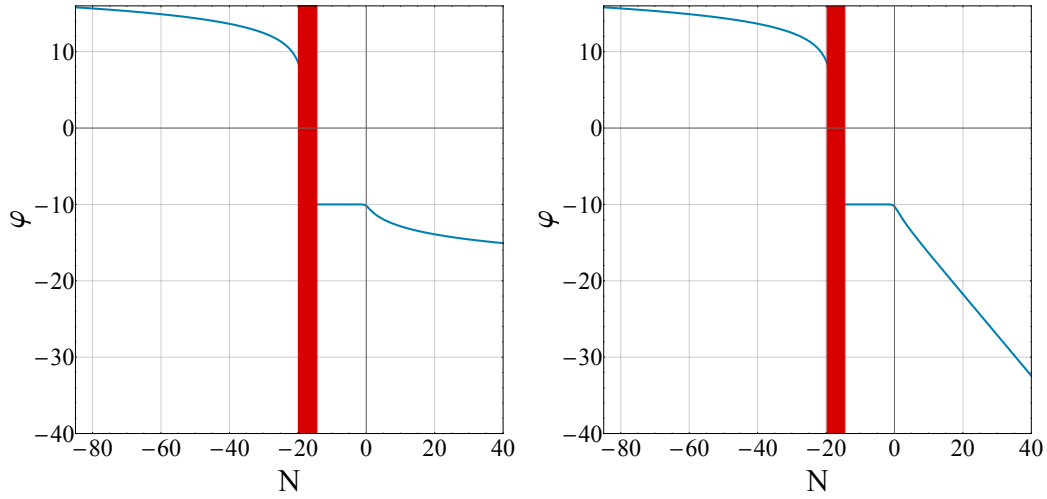

Figure 2.12: *Left panel:* Evolution of the scalar field φ as a function of the number of e-folds N over the entire history of the universe for Exp-model I and for the same set of parameters used for computing the inflationary variables shown in Fig. 2.11 with a viable late-time cosmological history. The vertical, red bands depict the period after the end of inflation and before the time at which the scalar field freezes, separating the inflationary and late-time periods. This period includes kination and reheating. Note that the field rolls down during inflation and kination (not shown), and then freezes after reheating (to -10 in this example), for almost the entire history until very recently when it unfreezes again and starts rolling its potential; this is the onset of dark energy domination. $N = 0$ corresponds to the present time. *Right panel:* The same as in the left panel, but for Exp-model II. Note the different dynamics for φ compared to Exp-model I in the future ($N > 0$).

value in Exp-model II differs from -1. This asymptotic value w_∞ for Exp-model II is

$$w_\infty = -1 + \frac{2}{3}\frac{1}{3\alpha}\,, \tag{2.85}$$

which is a universal result that does not depend on the values of M^2 and γ; it depends only on the value of α. It is this interesting situation, already mentioned earlier in this chapter, where one geometric parameter α defines

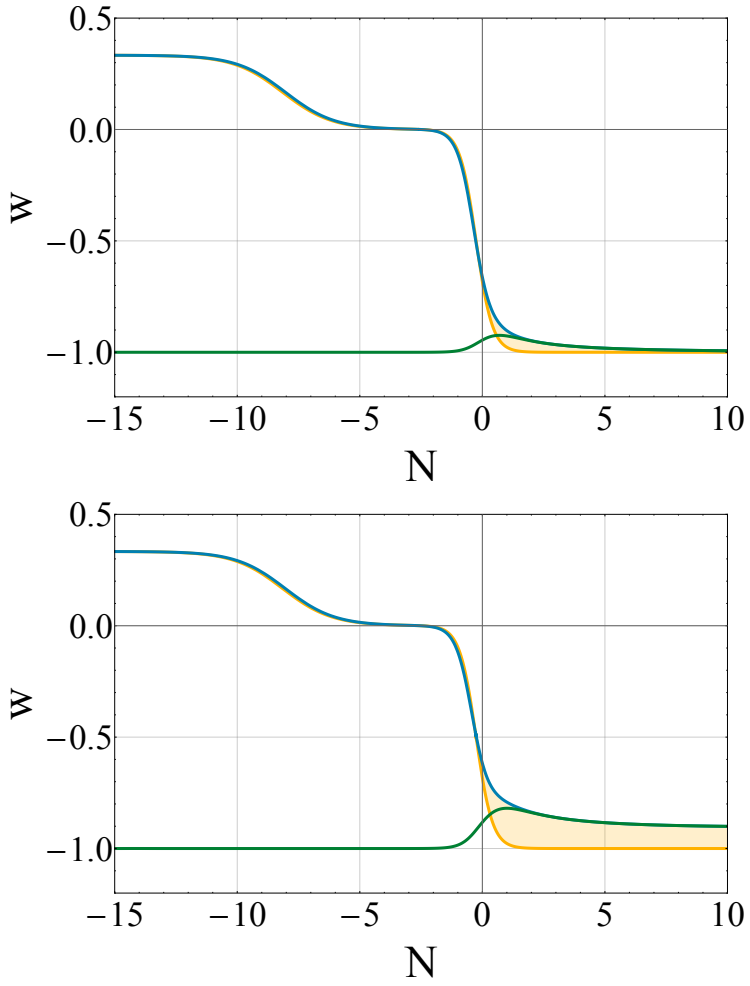

Figure 2.13: *Upper panel:* Evolution of the equation of state as a function of the number of e-folds N after reheating for Exp-model I and for the same set of parameters used in Figs. 2.11 and 2.12 with a viable late-time cosmological history. The blue and green curves show, respectively, the effective equation of state $w_{\rm eff}$ and the equation of state of dark energy $w_{\rm DE}$. For comparison, the effective equation of state for ΛCDM is also presented as an orange curve. $N = 0$ corresponds to the present time. *Lower panel:* The same as in the left panel, but for Exp-model II.

the deviation of w_∞ from -1, as well as the level of primordial gravity waves from inflation, see Eqs. (2.1) and (2.2).

Another interesting observation in Fig. 2.13 is the behavior of the dark energy equation of state $w_{\rm DE}$, shown by green curves for both models. Clearly, in both cases, $w_{\rm DE}$ today deviates from the equation of state for Λ, and is also different from its asymptotic value w_∞ in the case of Exp-model II. We will discuss this in more detail in the next section.

2.5.3.2 *Comparison to observations, and constraints on parameters*

We perform a statistical MCMC analysis of Exp-models I and II in order to understand whether the models are cosmologically viable, how much their parameters are constrained by cosmological observations, and to which extent we expect deviations from the standard model. This will also tell us whether the models can be distinguished from ΛCDM using the current and upcoming cosmological surveys. For that, as mentioned in section 2.1, we consider geometrical constraints on the cosmic history at the background level using a combination of the redshift-luminosity relation of supernovae [158], the observed angular scales of the CMB anisotropies [130], measurements of the baryon acoustic oscillations (BAO) [159–163], and the local measurements of the Hubble constant H_0 [164].

Our aim in the present work is not an exhaustive and detailed comparison of the models to observations, and the primary goal is to reach a qualitative understanding of the models, their cosmological viability, and their differences in terms of the observational implications. Additionally, contrary to models of modified gravity for cosmic acceleration, minimally coupled quintessence models (including ours) affect observations only through their impacts on the background dynamics, and they do not directly affect clustering and growth of structure as well as other LSS observables such as weak lensing. For these reasons we believe that the geometrical measurements of the cosmic history on their own should provide sufficiently good con-

straints on our models; we leave an extensive and detailed analysis of the models using all the available cosmological observations, including those involving the constraints from the full CMB temperature and polarization power spectra, as well as galaxy clustering and weak lensing, for future work where a perturbative analysis of the models will be performed and the models will be implemented in a numerical Boltzmann code. Additionally, here we do not perform detailed forecasts for future galaxy surveys using for example a Fisher matrix approach.

Here, therefore, we use only a simple and rough criterion for a model to be testable against ΛCDM: We assume a point in the parameter space of the model to be distinguishable from ΛCDM if the corresponding w_0 and w_a are different from the ΛCDM values of -1 and 0 by more than $\sim 2\%$ and $\sim 4\%$, respectively. These numbers are clearly only rough estimates, and can be different depending on the specific experiments and probes that are being considered. However, we believe that they are good (and perhaps optimistic) estimates of what one will be able to reach using the combination of various probes from the upcoming Stage IV large-scale structure surveys and CMB experiments; see e.g. Ref. [122] for the values that are targets of one of these experiments. In addition, the situation is more subtle than using only the separate errors on w_0 and w_a, for example because of possible correlations between the two parameters — in fact a more proper way of using these errors is through the 2-dimensional confidence contours for w_0 and w_a. However, since we do not intend to perform a detailed statistical analysis in this chapter, and are concerned more with a qualitative analysis of the models, we leave these subtle issues to be addressed in future work.

Before we present and discuss the results of our statistical analysis based on the cosmological data described above, let us use the expression (2.55) for the COBE/Planck normalization discussed in section 2.4.1 and see which constraints we can obtain on the values of the parameters in our potentials solely from early-time (inflationary) physics. We will shortly see that the

COBE/Planck normalization indeed provides us with an approximate but a quite strong constraint on the two potentials $M^2 e^{\gamma(\tanh\frac{\varphi}{\sqrt{6\alpha}}-1)}$ and $M^2 e^{-2\gamma}\left(e^{\gamma\left(\tanh\frac{\varphi}{\sqrt{6\alpha}}+1\right)}-1\right)$, for Exp-models I and II.

We should first note that on the tails of the potentials for large and positive φ, where we assume inflation to take place, the form of the effective potential is approximated by the expression

$$V(\varphi) = M^2(1-2\gamma e^{-\frac{2\varphi}{\sqrt{6\alpha}}}) + V_0 + \mathcal{O}(e^{-\frac{4\varphi}{\sqrt{6\alpha}}})\,, \tag{2.86}$$

where we have left the cosmological constant undetermined. Note that even for Exp-model II with a nonvanishing V_0, its contribution $M^2 e^{-2\gamma}$ to the potential (2.86) is exponentially small compared to the leading term M^2, by a factor of $e^{-2\gamma}$. We will see later that we need γ to be ~ 125 in order to obtain viable cosmic histories for both models, and therefore the contribution from V_0 to the inflationary potential (2.86) is negligible and we can ignore it.

Integrating the slow-roll equations of motion over an arbitrary interval $[N_1, N_2]$ during the inflationary epoch we will get

$$\int_{\varphi_1}^{\varphi_2} \frac{V(\varphi)}{V_\varphi(\varphi)}\mathrm{d}\varphi = -\int_{N_1}^{N_2}\mathrm{d}N\,, \tag{2.87}$$

where φ_1 and φ_2 are the values of the field at N_1 and N_2, respectively. Assuming that both φ_1 and φ_2 are sufficiently large, we can use the approximate expression (2.86) and arrive at

$$\frac{\sqrt{6\alpha}}{4\gamma}\left(\frac{\sqrt{6\alpha}}{2}\left(e^{\frac{2\varphi_2}{\sqrt{6\alpha}}}-e^{\frac{2\varphi_1}{\sqrt{6\alpha}}}\right)-2\gamma(\varphi_2-\varphi_1)\right) = N_1 - N_2\,. \tag{2.88}$$

Now, choosing N_1 to be the moment of horizon crossing $N_{\rm crossing}$ for the observable modes and N_2 to correspond to the end of inflation $N_{\rm end}$ we arrive at the approximate expression

$$e^{\frac{2\varphi_*}{\sqrt{6\alpha}}} = \frac{4}{3\alpha}\gamma N\,, \tag{2.89}$$

where φ_* is the value of the field at the horizon crossing, and $N \equiv N_{\rm end} - N_{\rm crossing}$ is the number of e-folds corresponding to the duration of inflation since the moment at which the observable perturbations left the horizon until the end of inflation. In order to obtain Eq. (2.89) we have assumed that the field has travelled at least a few Planck units between the horizon crossing and the end of inflation, and therefore the term proportional to $e^{\frac{2\varphi_1}{\sqrt{6\alpha}}}$ on the left-hand side of Eq. (2.88) is the dominant one; we ignore all the other terms. For $\gamma \sim 125$, and assuming $N \approx 63$, Eq. (2.89) gives $\varphi_* \sim 15.74$ for $\alpha = 7/3$, which is in full agreement with our numerical analysis; note that $\varphi_{\rm end} \sim +8$.

Let us now plug the asymptotic expression for our potential (2.86) into the COBE/Planck normalization equation (2.55). Using Eq. (2.89) we arrive at

$$M^2 = \frac{144\pi^2\alpha N}{(2N-3\alpha)^3}\,\mathcal{P}_{\mathcal{R}}(k)\,. \tag{2.90}$$

Taking into account that $V_+ \approx M^2$ and considering the limit $N \gg \alpha$, we see that this equation reproduces the previously mentioned general α-attractor result (2.15).

Thus the COBE/Planck normalization constrains the ratio M^2/α [129]. Assuming $N \approx 63$, using (2.90), and applying the measured value of $\mathcal{P}_{\mathcal{R}}$, we find that

$$\frac{M^2}{\alpha} \sim 10^{-10}\,. \tag{2.91}$$

This means that this early-universe condition does not constrain M^2 and/or α separately, and the two parameters are degenerate as far as the COBE/-Planck normalization is concerned. We will see later that this degeneracy will be broken when the late-time cosmological data are used.

Let us first focus on $\alpha = 7/3$, which is an interesting case. In that case $M^2 \sim 3 \times 10^{-10}$. We will later discuss the dependence of our results on α, as well as the constraints on α itself. We first scan over all the free parameters of Exp-models I and II, i.e. M^2, γ, $\Omega_{\rm M}$, and $\Omega_{\rm R}$, as well as the initial value of the field, $\varphi_{\rm F}$, comparing the models to the (late-time) cosmological observations described above. Note that although we do not impose the COBE/Planck constraint in our numerical scans, we scan over a range of $\log M^2$ around the value given by the COBE/Planck normalization (2.91). Additionally, as we argued before, we expect $\varphi_{\rm F}$ for this potential to be in the range $[-35, +8]$, depending on the reheating mechanism — this is the range we choose for our numerical analysis. We will see, however, that because of the steepness of the potential for large values of $\varphi_{\rm F}$, the effective, viable range for $\varphi_{\rm F}$ will be $\sim [-35, -5]$. With all these, we scan over the parameters and compare the cosmic histories with observations. Fig. 2.14 shows the obtained MCMC samples of $\log M^2$ and γ (upper panels), as well as of the two CPL parameters w_0 and w_a (lower panels) introduced in Eq. (2.63). The color assigned to each point corresponds to the value of $\varphi_{\rm F}$ and w_a for the upper and lower panels, respectively, and the vertical, red lines depict the value of $\log M^2$ given by the COBE/Planck constraint. The figure shows that the constraints on γ are quite tight for Exp-model I (left) compared to Exp-model II (right).

We first focus on Exp-model II, which gives a wider region for γ. The color clearly shows that lower values of γ correspond to larger $|\varphi_{\rm F}|$. The cut from below comes therefore from the fact that we imposed an upper bound of 35 on $|\varphi_{\rm F}|$ in our scans, i.e. we did not allow $\varphi_{\rm F}$ to become smaller than -35 due to gravitational reheating. (This means that in principle there would be no lower bound on γ if $|\varphi_{\rm F}|$ were allowed to take arbitrarily large values.) The upper bound on γ, on the other hand, comes from the fact that if the field does not sufficiently roll down its potential after inflation and before freezing, the model will not provide a viable cosmic history.

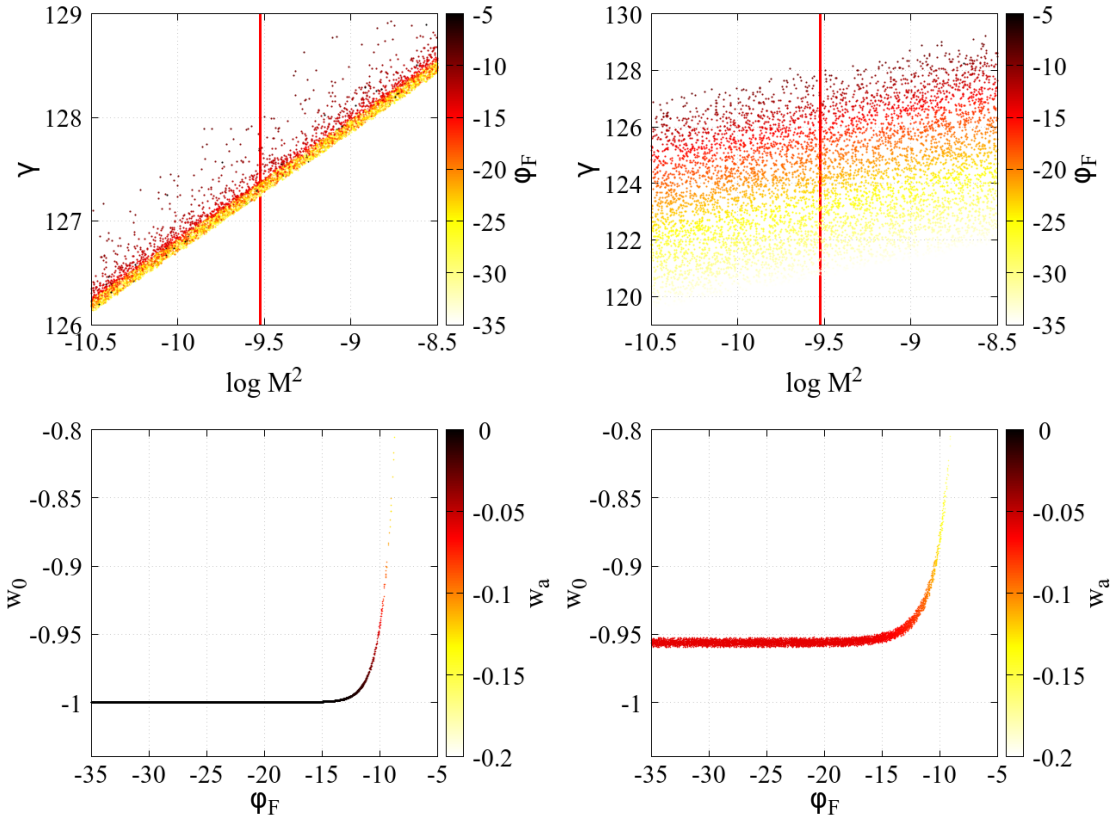

Figure 2.14: *Upper panels:* Cosmological MCMC samples of $\log M^2$ and γ for Exp-model I (left panel) and Exp-model II (right panel) in term of $\varphi_{\rm F}$, when it is allowed to vary between -35 and $+8$. $\log M^2$ has been scanned over only in a range around the COBE/Planck normalization value depicted by the vertical, red lines. *Lower panels:* CPL parameters w_0 and w_a for the dark energy equation of state, for Exp-models I (left panel) and II (right panel) as functions of $\varphi_{\rm F}$. The points cluster around $w_0 = -1$ (model I) and $w_0 \sim -0.96$ (model II) for large, negative values of $\varphi_{\rm F}$.

Focusing now on the left, upper panel in Fig. 2.14 for Exp-model I, we see that the lower bound on γ, for a given value of $\log M^2$, seems to be highly strict and even increasing $|\varphi_{\rm F}|$ will not decrease γ. This can be understood if we remember again that Exp-model I possesses a cosmological constant

limit. Increasing $|\varphi_F|$ moves the field more and more on the tail of the potential, and the model becomes more and more like ΛCDM. There is however no possibility of decreasing the total potential energy of the field further, as the scalar field only contributes with a positive energy on top of the cosmological constant. Note that the $\gamma - \log M^2$ degeneracy in these plots can be understood by looking at the $\varphi \to -\infty$ limit of the models:

$$\text{Exp} - \text{modelI}: \qquad V(\varphi) = M^2 e^{-2\gamma}(1 + 2\gamma e^{2\frac{\varphi}{\sqrt{6\alpha}}}), \tag{2.92}$$

$$\text{Exp} - \text{modelII}: \qquad V(\varphi) = M^2 e^{-2\gamma}\gamma e^{2\frac{\varphi}{\sqrt{6\alpha}}}. \tag{2.93}$$

The lower panels of Fig. 2.14 show how the CPL parameters w_0 and w_a vary with φ_F in both models. First note that the viability regions are quite thin, and already tight as far as the constraints from the cosmological data are concerned. We have checked that by imposing the full COBE/Planck constraint (2.91) these regions become only slightly thiner, which means that the late-time data are quite constraining on their own, independently of the strong constraint on the model imposed by the COBE/Planck normalization. Second, we can clearly see that the models deviate more and more from ΛCDM by increasing φ_F to less and less negative values, as illustrated by the deviations in w_0 and w_a from -1 and 0, respectively. Note that all the points shown in Fig. 2.14 are cosmologically viable, and therefore, by having a sufficiently efficient reheating to stop the field from rolling too much after inflation, we can expect a relatively large deviation from ΛCDM, detectable by future cosmological surveys. The deviations are already quite large around $\varphi_F = -8$ so that we do not obtain viable cosmologies for larger values of φ_F. In addition, it is important to note that for Exp-model II, the model does not predict the asymptotic value of $w_\infty = -1 + \frac{2}{9\alpha}$ (~ -0.9 in this case for $\alpha = 7/3$) for the present value of the dark energy equation of state. The closest value to w_∞ it can reach is ~ -0.96 for large, negative φ_F, and deviates more and more from it when φ_F increases.

Let us now restrict ourselves to specific values of φ_F to see how much deviation from ΛCDM we can expect for Exp-models I and II by decreasing $|\varphi_F|$. This is interesting because specific, observed deviations from $w_0 = -1$ and $w_a = 0$ may constrain the initial value of the field after reheating, and therefore in turn constrain the reheating mechanism itself within the framework of these models.

The upper panel of Fig. 2.15 shows the results of our scans of Exp-model I when φ_F has been fixed to three values -10 (red contours), -10.5 (blue contours), and -11 (green contours). Each set of contours shows 1σ, 2σ, and 3σ confidence regions. The shaded, grey regions indicate the planned sensitivity of the upcoming Stage IV large-scale structure surveys in combination with the CMB measurements, which are expected to detect deviations of up to $\sim 2\%$ and $\sim 4\%$ in w_0 and w_a, respectively, from the ΛCDM values; see the discussion earlier in this section.

We first notice that the three sets of contours are extremely tight and w_0 and w_a are strongly constrained, even though M^2 in these numerical scans is not set to the exact COBE/Planck normalization value, and the range is relatively large. The constraints are already quite strong that even though constraining M^2 to the COBE/Planck-normalization value makes the contours even smaller, it will not affect the results significantly. Our results show that $|\varphi_F|$ of around 10 or smaller will be detectable by future LSS experiments. It is also interesting to note that the changes in w_0 and w_a are highly sensitive to the value of φ_F; we do not expect to detect any deviations from ΛCDM for $|\varphi_F|$ larger than ~ 10.5 in Exp-model I using the next generation of the LSS surveys. Our analysis also shows that for values smaller than ~ 10, on the other hand, it becomes difficult to obtain viable late-time cosmologies.

The upper panel of Fig. 2.15 shows the same as the lower panel, but for Exp-model II, where red, blue, green, and orange contours correspond to -10, -10.5, -11, and -12 for φ_F, respectively. The deviations from ΛCDM in this model are generically larger compared to Exp-model I, and are

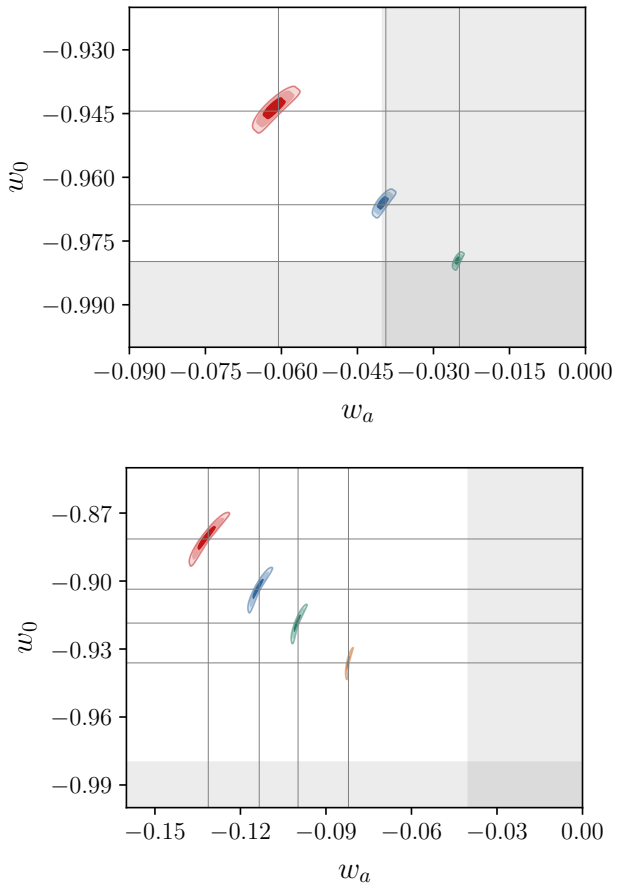

Figure 2.15: *Upper panel:* Constraints on w_0 and w_a for Exp-model I, and for three cases of $\varphi_F = -10$ (red contours), $\varphi_F = -10.5$ (blue contours), and $\varphi_F = -11$ (green contours). The shaded, grey regions indicate a rough estimate of the target sensitivity for Stage IV large-scale structure surveys in combination with CMB experiments, expected to detect deviations of up to $\sim 2\%$ and $\sim 4\%$ in w_0 and w_a, respectively, from the ΛCDM values. *Lower panel:* The same as in the left panel, but for Exp-model II. Here, red, blue, green, and orange contours correspond to $\varphi_F = -10$, $\varphi_F = -10.5$, $\varphi_F = -11$, and $\varphi_F = -12$, respectively. Note that all these cases for Exp-model II show detectable deviations from ΛCDM.

therefore more easily detectable by upcoming surveys; note how all four contours are located outside the shaded, grey regions.

It is interesting to see what happens with Fig. 2.15 when the inflationary constraints on M^2 are relaxed. Fig. 2.16 shows the results of our scans for Exp-model I when $\varphi_{\rm F}$ is fixed to the same three values of -10 (red contours), -10.5 (blue contours), and -11 (green contours) as before. First of all, the figure shows that the deviations can be as large as about 10% for both w_0 and w_a if $|\varphi_{\rm F}|$ is allowed to take values as low as about 10. More importantly, since here we have not imposed any inflationary constraints on M^2, the contours are continuously connected to the ΛCDM values $w_0 = -1$ and $w_a = 0$. We find similar results for Exp-model II, with the only main difference that in that case the contours are no longer connected to the ΛCDM point, as expected; we do not show them here for brevity.

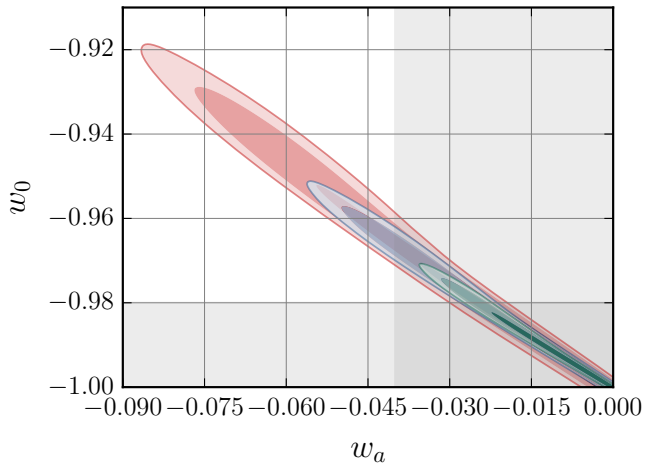

Figure 2.16: The same as in Fig. 2.15, but by fully relaxing the power spectrum normalization.

Finally, we study the effects of varying α in our two exponential models I and II, by leaving it as a free parameter. We have chosen a representative value for $\varphi_{\rm F}$ and have fixed it to -10. The results are presented in Fig. 2.17;

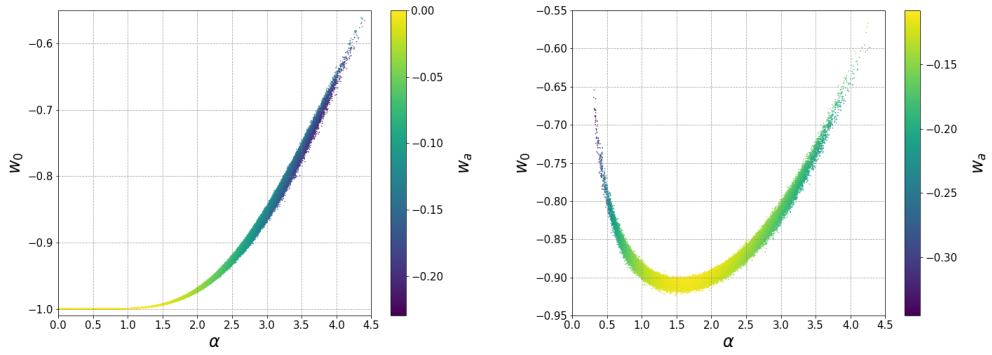

Figure 2.17: The dependence of w_0 and w_a on α for Exp-model I (left panel) and Exp-model II (right panel). Here the inflationary power spectrum normalization has been imposed as $M^2 \approx 10^{-10}\alpha$ and $\varphi_{\rm F}$ has been fixed to -10.

the left panel corresponds to Exp-model I, and the right panel corresponds to Exp-model II. For Exp-model I, we now see that there is an upper bound of ~ 4 on α in order for the model to provide cosmic histories consistent with current data; α can however take any values smaller than this bound. Exp-model II, on the other hand, now allows only values of α in the approximate range of $[0.5, 3.5]$ when $\varphi_{\rm F}$ is fixed to -10. In addition, it is interesting to see that both w_0 and w_a show different behavior in terms of α for the two models. The left panel of Fig. 2.17 shows that increasing α enhances the deviation from ΛCDM in Exp-model I, while the right panel shows that for Exp-model II both w_0 and w_a are extremized around some intermediate values of $\alpha \sim 1.5$, below and above which the deviations from ΛCDM are larger.

2.6 2-FIELD QUINTESSENTIAL INFLATION MODELS

2.6.1 *Dark energy and exponential potentials*

As we discussed in section 2.2, the asymptotic expression for the α-attractor potential at large negative φ, Eq. (2.22), after a change of variables and a redefinition $\sqrt{\frac{2}{3\alpha}} \to \lambda$ can be represented in a more familiar way $V(\varphi) = \Lambda + e^{\lambda\varphi}$. These models with a vanishing cosmological constant $\Lambda = 0$ were among the first candidates for the role of dark energy, see e.g. Refs. [165, 166]. However, unlike the dark energy model with the linear potential, which was proposed a year earlier [91], the original models with exponential potentials discussed in Refs. [165, 166] did not provide a solution to the cosmological constant problem. Some progress in this direction was achieved only much later, in the models with the potential (2.23) and $\Lambda < 0$ [135]. Even though the models considered in Ref. [135] described single field exponential potentials, the context of this theory was similar to the linear model of Refs. [91, 167], which presumed the prior stage of inflation driven by another field. Therefore, before discussing dark energy in the context of two-field α-attractors, we describe and generalize the results of Ref. [135], in the light of the string theory landscape developments.

Let us first consider the simplest case of $\Lambda = 0$. For $\lambda \ll 1$ ($\alpha \gg 1/3$), the potential is flat, the energy density of normal matter decreases faster than V, and the system eventually enters the asymptotic regime of power-law inflation with

$$w_\infty = -1 + \frac{\lambda^2}{3} = -1 + \frac{2}{9\alpha}\ . \tag{2.94}$$

Meanwhile in the models with a dS plateau, $\Lambda > 0$, the asymptotic value of w is -1, but for large α the transition from $w = -1 + \frac{2}{9\alpha}$ to $w = -1$ may take a long time. In the models with $\Lambda < 0$, the universe eventually collapses,

but if $\lambda \ll 1$ and $|\Lambda| \ll 10^{-120}$, there is a very long interval, longer than the present age of the universe, when life as we know it can exist, and w is very close to -1 [135]. Thus, one could argue that exponential potentials, as well as α-attractors, can easily provide us with viable dark energy models with w very close to -1, but still noticeably different from it. However, a more detailed investigation shows that the situation is much more nuanced.

First of all, models with exponential potentials cannot simultaneously describe inflation *and* quintessence. They support inflation for $\lambda \ll 1$, but then inflation never ends. A way around it is to assume, along the lines of Ref. [91], that the potential of the dark energy field φ is given by $V(\varphi) \sim e^{\lambda\varphi} + \Lambda$, but inflation is driven by some other field. Then, because of inflationary fluctuations of the ultra-light field φ, after inflation the universe becomes divided into exponentially many exponentially large parts where φ takes different values, so that its potential energy $V(\varphi)$ takes all possible values of Λ, including values many orders of magnitude higher than 10^{-120}. In each of these parts, the field φ is locally very homogeneous. Thus, just as in the linear model of Ref. [91], the universe becomes divided into many parts with different values of the effective cosmological constant $\Lambda + e^{\lambda\varphi}$. Therefore all values of the field φ with $\Lambda + e^{\lambda\varphi} \gg 10^{-120}$ are anthropically forbidden.

Indeed, in the parts of the post-inflationary universe models with $\lambda \ll 1$ and $|\Lambda| \ll 10^{-120}$, the scalar field starts moving (very slowly, because $V' \sim \lambda V \ll V$) when the density of cold (and hot) matter of the universe, which rapidly decreases during its expansion, becomes smaller than $V(\varphi)$. If the field was frozen and starts moving at $V(\varphi) \gg 10^{-120}$, the universe enters the regime of quasi-exponential expansion too early, which disrupts galaxy formation.

If Λ is negative, but the initial value of $V(\varphi) \sim e^{\lambda\varphi} + \Lambda$ was positive, the universe in these models may enter the stage of accelerated expansion which may continue for a few billion years after that, until the universe collapses [135]. However, this regime is possible only for $\lambda \lesssim 1$, and only in

some finite (λ-dependent) range of $\Lambda < 0$ and post-inflationary values of the field φ [135].

On the other hand, if Λ is small but positive, $\Lambda \sim +10^{-120}$, the universe may enter the stage consistent with the presently available data for *any* value of λ, and for an infinitely large range of post-inflationary values of the field φ such that $e^{\lambda\varphi} \lesssim 10^{-120}$. Only in a finite part of this range of φ does one have $e^{\lambda\varphi} \sim \Lambda$ and w close to -1 but distinctly different from it. Meanwhile in the infinitely large range of φ, all the way down to $-\infty$, one has $e^{\lambda\varphi} \ll \Lambda$. Therefore, for any given λ, the anthropically viable "phase space" of Λ and φ is dominated by positive $\Lambda \sim +10^{-120}$ and by indefinitely large negative φ, where dark energy is indistinguishable from the cosmological constant, and the equation of state is given by $w = -1$ with an exponentially good accuracy. A similar conclusion was reached in Ref. [168] for a broad class of dark energy models, though some exceptions from this rule are possible, see e.g. Refs. [169, 170].

2.6.2 *Non-interacting α-attractors*

A similar conclusion can be reached in many models of two-field α-attractors, if one assumes, as we did before, that the potential of the field ϕ responsible for dark energy is very small, and inflation is driven by some other field χ, not interacting with the field ϕ. To illustrate this possibility, we consider here a toy model of two non-interacting fields.

Let us consider an extended version of the α-attractor model, adding to it a scalar field σ with a non-canonical kinetic term:

$$\frac{1}{\sqrt{-g}}\mathcal{L} = \frac{R}{2} - \frac{(\partial_\mu\phi)^2}{2(1-\frac{\phi^2}{6\alpha})^2} - \frac{(\partial_\mu\sigma)^2}{2(1-\frac{\sigma^2}{6\beta})^2} - \frac{m^2}{2}\sigma^2 - \gamma\phi - V_0\,. \qquad (2.95)$$

As before, one can represent this theory in terms of two canonically normalized fields,

$$\phi = \sqrt{6\alpha}\,\tanh\frac{\varphi}{\sqrt{6\alpha}}, \quad \sigma = \sqrt{6\beta}\,\tanh\frac{\chi}{\sqrt{6\beta}}\,. \tag{2.96}$$

The inflaton potential in terms of the canonically normalized fields φ and χ becomes

$$V(\varphi,\chi) = 3\beta m^2\,\tanh^2\frac{\chi}{\sqrt{6\beta}} + \gamma\sqrt{6\alpha}\,\tanh\frac{\varphi}{\sqrt{6\alpha}} + V_0\,. \tag{2.97}$$

We illustrate the general structure of this potential for $\alpha = \beta = 1$ and some particular (non-realistic) values of parameters such that $3\beta m^2 \gg \gamma\sqrt{6\alpha}$, and $V_0 \approx \gamma\sqrt{6\alpha}$, see Fig. 2.18. In that case the term $3\beta m^2\,\tanh^2\frac{\varphi}{\sqrt{6\beta}}$ is responsible for inflation in this model, the dark energy potential $\gamma\sqrt{6\alpha}\,\tanh\frac{\varphi}{\sqrt{6\alpha}} + V_0$ is very shallow, and it approaches a small cosmological constant $V_- = V_0 - \gamma\sqrt{6\alpha}$ in the limit $\varphi \to -\infty$, and $V_+ = V_0 + \gamma\sqrt{6\alpha}$ in the limit $\varphi \to \infty$.

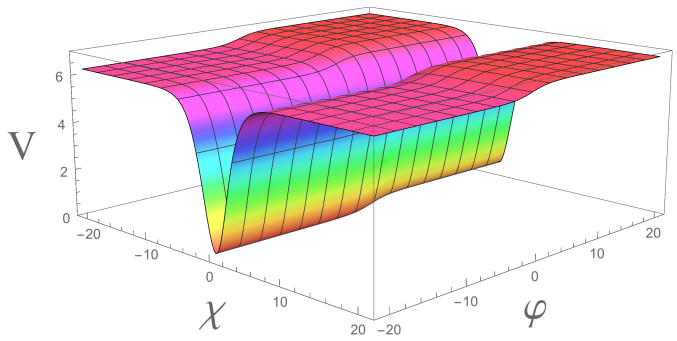

Figure 2.18: The shape of the potential $V(\varphi,\chi)$ (2.97) for $\alpha = \beta = 1$, $3\beta m^2 \gg \gamma\sqrt{6\alpha}$, and $V_0 \approx \gamma\sqrt{6\alpha}$.

Inflation begins at the plateau with $V(\varphi,\chi) = 3\beta m^2 \gg V_+$. This plateau is almost exactly flat, so inflation may begin with an equally large probability at any point of the plateau with $\chi \gg \sqrt{6\beta}$ [171]. It ends when the field χ falls down to the dark energy valley with $\chi = 0$. Since the field φ at the beginning of inflation can take any value with (almost exactly) equal probability because of a (nearly exact) shift symmetry of the potential in the φ direction, all values of the field φ after inflation will be equally probable as well.

In that case, one can use the same argument as the one we used for the theory with exponential potential: After inflation, the fields roll down either to the right plateau, or to the left plateau, but it is most probable that it will end up extremely far from $\varphi = 0$. By a proper choice of parameters, including adjustment of the parameter V_0, one can easily have the regime of acceleration at the time $t \sim 10^{10}$ years. However, with an overwhelmingly large probability the absolute value of the field φ after inflation will be extremely large, and therefore this stage will be indistinguishable from the pure cosmological constant with $w = -1$.

The same conclusion is valid for most of the dark energy models based on the α-attractors with $V(\varphi)$ much smaller than the energy density of the inflaton field χ during inflation. Indeed, for most of such models the asymptotic behavior of the potential $V(\varphi)$ in the limit $|\varphi| \to \infty$ is given by one of the two asymptotic expressions (2.13) or (2.22). The asymptotic values of the cosmological constant Λ along the two shoulders of the potential is given either by V_- or by V_+. By adding a constant to the potential, one can adjust at least one of these parameters to belong to the anthropic range $|\Lambda| \lesssim 10^{-120}$. Then all arguments given above apply.

Thus we see that one can easily obtain a viable dark energy model in any model of α-attractors, with a very broad range of parameters and potentials, as long as the value of dark energy potential $V(\varphi)$ is sufficiently small. But the observational consequences of these models for the most general class of initial conditions are practically indistinguishable from the predictions

of the simplest cosmological constant models. This is good news from the point of view of generality of the predictions, but perhaps not very good news from the point of view of observers.

However, these conclusions were obtained under the conditions some of which can be relaxed. For example, consider the same model as before, but instead of the regime with $3\beta m^2 \gg \gamma\sqrt{6\alpha}$ we may investigate an opposite regime $3\beta m^2 \ll \gamma\sqrt{6\alpha}$. The potential in this case is shown in Fig. 2.19.

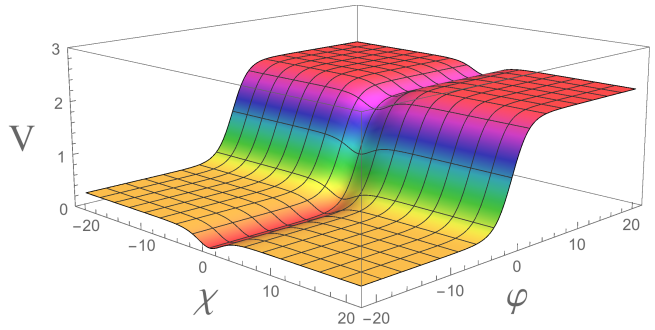

Figure 2.19: The shape of the potential $V(\varphi,\chi)$ (2.97) for $\alpha = \beta = 1$, $3\beta m^2 \ll \gamma\sqrt{6\alpha}$, and $V_0 \approx \gamma\sqrt{6\alpha}$.

In this model, the potential at the first stage of inflation is dominated by the quintessence potential $V(\varphi) = \gamma\sqrt{6\alpha}\tanh\frac{\varphi}{\sqrt{6\alpha}} + V_0$, falling from the high (red) plateau. Depending on initial conditions, inflationary scenario can be realized in two distinct ways. In the first scenario, the initial value of the field χ is extremely large, and its potential is very flat. In that case, the fields will first roll in the φ direction and fall from the cliff to the yellow plateau determined by the term $3\beta m^2 \tanh^2\frac{\chi}{\sqrt{6\beta}}$. Then there will be a second stage of inflation driven by the field χ, which ends at $\chi = 0$. We call this scenario "cascade inflation" [94]. The value of the field φ at the end of inflation will be determined by the initial conditions, and by the two stages of cascade inflation, including (for some initial conditions) a stage of eternal inflation.

On the other hand, if the initial value of the field χ is relatively small, and the field φ is very large, then in the beginning of inflation, the field χ rolls down the valley with $\chi = 0$, and the subsequent stage of inflation and quintessential evolution will be determined by the single field evolution of the field φ.

In the next section we will briefly describe a simple model of two interacting attractors; as we will see taking into account interactions may open many other possibilities.

2.6.3 *Interacting α-attractors*

Now we add an interaction term $g^2\phi^2\sigma^2$ to the potential of the model (2.95),

$$\frac{1}{\sqrt{-g}}\mathcal{L} = \frac{R}{2} - \frac{(\partial_\mu\phi)^2}{2(1-\frac{\phi^2}{6\alpha})^2} - \frac{(\partial_\mu\sigma)^2}{2(1-\frac{\sigma^2}{6\beta})^2} - \frac{m^2}{2}\sigma^2 - g^2\phi^2\sigma^2 - \gamma\phi - V_0. \quad (2.98)$$

The inflaton potential in terms of the canonically normalized fields φ and χ becomes

$$V(\varphi,\chi) = 36\alpha\beta g^2 \tanh^2\frac{\varphi}{\sqrt{6\alpha}}\,\tanh^2\frac{\chi}{\sqrt{6\beta}} + 3\beta m^2\,\tanh^2\frac{\chi}{\sqrt{6\beta}} + \gamma\sqrt{6\alpha}\tanh\frac{\varphi}{\sqrt{6\alpha}} + V_0. \quad (2.99)$$

We will take the parameters such that $36\alpha\beta g^2 \gg 3\beta m^2 \gg \gamma\sqrt{6\alpha}, V_0$. In that case, the potential can be illustrated (not to scale) by Fig. 2.20. Inflation begins at one of the high red plateaus of the height approximately given by $36\alpha\beta g^2$. The blue valley describes the α-attractor inflationary potential $V(\chi) = 3\beta m^2\,\tanh^2\frac{\chi}{\sqrt{6\beta}} + V_0$. The green valley corresponds to the dark energy potential $\gamma\sqrt{6\alpha}\tanh\frac{\varphi}{\sqrt{6\alpha}} + V_0$.

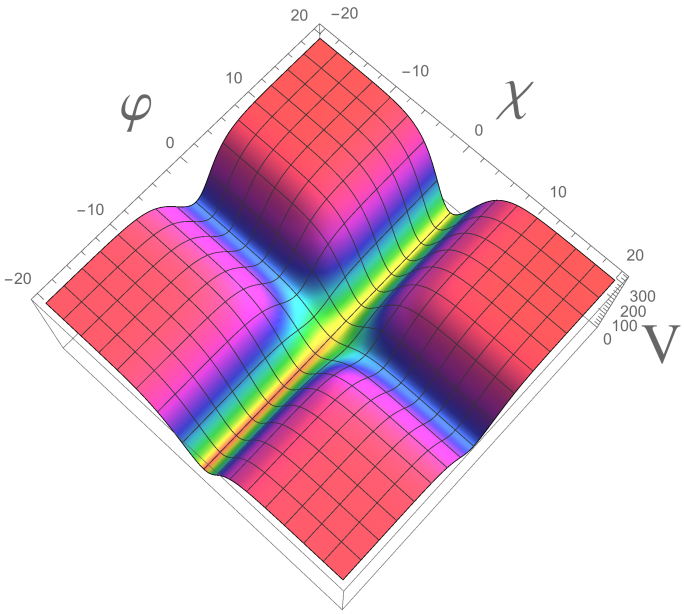

Figure 2.20: The shape of the potential $V(\varphi, \chi)$ (2.99) for $\alpha = \beta = 1$ and $36\alpha\beta g^2 \gg 3\beta m^2 \gg \gamma\sqrt{6\alpha}, V_0$. The green valley corresponds to quintessence with the linear potential $V = \gamma\phi + V_0 = \gamma\sqrt{6\alpha}\tanh\frac{\varphi}{\sqrt{6\alpha}} + V_0$.

One can show that about half of all inflationary trajectories starting at the red plateau describe the fields falling directly to the dark energy valley. We assume that $3\beta m^2 \sim 10^{-10}$ and $36\alpha\beta g^2$ is much greater, possibly even as large as $\mathcal{O}(1)$ in Planck units, then the inflationary trajectories falling directly to the dark energy valley produce parts of the universe with too large perturbations of density, which make such parts of the universe anthropically disfavored.

Another half of all inflationary trajectories starting at the red plateau describe the fields falling towards the blue inflationary valley. Then the inflaton field χ rolls along this valley, which generates perturbations of the proper magnitude in accordance with the α-attractor scenario. The process of reheating occurs due to oscillations of the field χ near the point $\varphi = \chi = 0$. At this point, the potential has a tiny slope which pushes the

dark energy field φ towards its large negative values, but this field does not start rolling until the density of particles produced by reheating drops down substantially. When this happens, the field φ starts moving towards $\varphi \to -\infty$.

Consider the simplest case of $V_0 = \gamma\sqrt{6\alpha} \sim 10^{-120}$. Then the dark energy potential $\gamma\sqrt{6\alpha}\tanh\frac{\varphi}{\sqrt{6\alpha}} + V_0$ is given by $V_0 \sim 10^{-120}$ at $\varphi = 0$, and vanishes in the limit $\varphi \to -\infty$. To give a particular example, one may consider $\alpha = 7/3$. Then, just like in the theory with exponential potential, the asymptotic value of w for dark energy will be about 0.905, but its initial value at the moment when the field φ starts moving down will be given (almost) exactly by -1. By taking V_0 slightly greater than $\gamma\sqrt{6\alpha}$, one can make w much closer to -1. This model represents a simple α-attractor version of the dark energy model with the linear potential proposed in Ref. [91].

2.6.4 *Quintessence with a linear potential*

Inspired by our discussions in the previous section, let us now consider a concrete example of the 2-field, interacting, α-attractor scenario where the simplest linear potential for the quintessence field ϕ has the form given in Eq. (2.19), i.e.

$$V(\varphi) = \gamma\sqrt{6\alpha}(\tanh\frac{\varphi}{\sqrt{6\alpha}} + 1) + \Lambda\,, \tag{2.100}$$

in terms of the canonical field φ, with Λ being a constant. We additionally assume $36\alpha\beta g^2 \gg 3\beta m^2 \gg \gamma\sqrt{6\alpha}, \Lambda$. As discussed in the previous section, we further assume that the inflationary trajectory starts at the red plateau of Fig. 2.20 at large values of the field χ, and then the fields φ and χ fall towards the blue inflationary valley at $\varphi = 0$. The inflaton field χ then rolls along the valley, and reheating occurs through the oscillations of χ near the

point $\phi = \chi = 0$. At this point, the tiny slope in the dark energy potential pushes the quintessence field φ towards its negative values. As stated before, in this scenario inflation is *not* driven by φ, and it only sets the value of φ to something around 0 as the initial value of the dark energy field for the late-time evolution of the universe, contrary to the quintessential inflation models, studied in section 2.4, which could accommodate a wide range of initial conditions for the quintessence field φ that was also responsible for inflation.

Now we consider the case with both $\gamma\sqrt{6\alpha}$ and Λ being of $\mathcal{O}(10^{-120})$. Note that the potential approaches a cosmological constant $V_- = \Lambda$ for large, negative φ, and therefore $\Lambda = 0$ corresponds to a potential with a vanishing asymptotic value in the limit $\varphi \to -\infty$. The potential has been shown in Fig. 2.21 for $\Lambda = 0$ (left panel) and $\Lambda = \gamma\sqrt{6\alpha}$ (right panel); we have set $\alpha = 7/3$ for both cases. The figure shows that the potential monotonically decreases for $\Lambda = 0$ and takes an asymptotic, constant value for $\Lambda = \gamma\sqrt{6\alpha}$ at large, negative φ. The value of γ has been chosen such that the asymptotic value of the potential gives 10^{-120}.

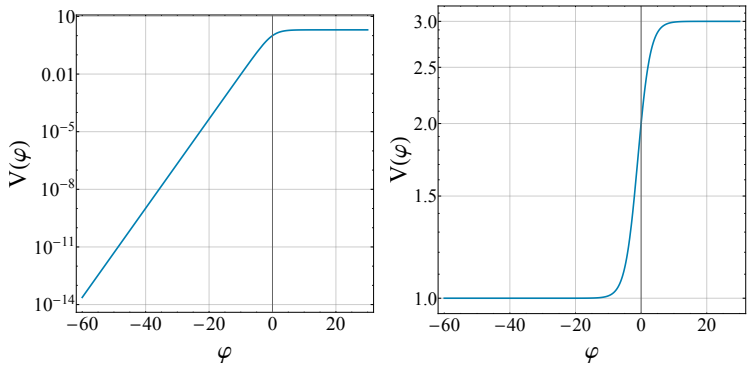

Figure 2.21: The shape of the potential $V(\varphi) = \gamma\sqrt{6\alpha}(\tanh\frac{\varphi}{\sqrt{6\alpha}} + 1) + \Lambda$ for $\Lambda = 0$ (left panel) and $\Lambda = \gamma\sqrt{6\alpha}$ (right panel). Here we have set $\gamma\sqrt{6\alpha}$ to 10^{-120} and α to $7/3$. The values of the potentials on the y-axes are normalized to 10^{-120}.

The asymptotic value for the equation of state of dark energy, $w_{\rm DE}$, in this model can be obtained by assuming a slow-roll approximation. As we discussed before, this asymptotic value for $\Lambda = 0$ is

$$w_\infty = -1 + \frac{2}{9\alpha} \,, \tag{2.101}$$

which depends only on α. The asymptotic value for $\Lambda \neq 0$ is -1.

Let us now study the time evolution of $w_{\rm eff}$ as well as $w_{\rm DE}$ for a few values of Λ and for $\alpha = 7/3$. The results have been presented in Fig. 2.22 for $\Lambda = 0$, $10^{-2} \times \gamma\sqrt{6\alpha}$, and $10^{-1} \times \gamma\sqrt{6\alpha}$. Note that $w_{\rm eff}$ is almost identical in the past ($N < 0$) for all the cases (blue curve), and shows different behavior for the future ($N > 0$). Note also that $w_{\rm eff}$ is different from $w_{\rm DE}$ in the past, and becomes identical to it in the future, when the field φ dominates. In addition, as expected, the figure shows that the deviation from ΛCDM is maximal when $\Lambda = 0$, and decreases when Λ increases. For the specific case of $\Lambda = 0$, w has an asymptotic value of ~ -0.905, in full agreement with our analytical expression (2.101), while for any other values of Λ the asymptotic value is -1.

2.6.5 *Comparison to observations, and constraints on parameters*

With the qualitative discussions of the previous section, let us now study our 2-field, interacting, α-attractor model in a rigorous way and through the comparison of the late-time predictions of the model to the observations. The potential is of the form given in Eq. (2.100). We scan over the parameters of the model, i.e. γ, α, and Λ, and compare the evolution of the background cosmological observables to the data. We set $\varphi_{\rm F}$ to 0 in all our scans.

The upper panels of Fig. 2.23 present our results for γ versus α (left panel) and Λ (right panel). Note that the values of γ and Λ are given in units of the critical density today. For the left panel, where α is kept free, the value

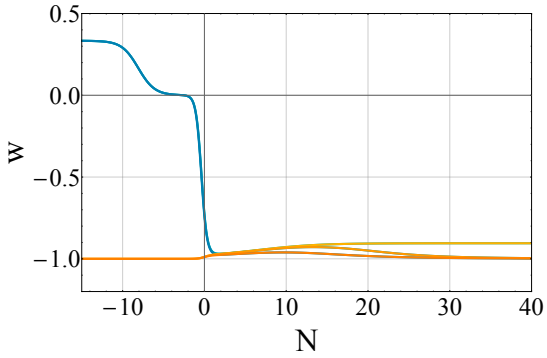

Figure 2.22: Evolution of the equation of state as a function of the number of e-folds N after reheating for the linear potential $V(\varphi) = \gamma\sqrt{6\alpha}(\tanh\frac{\varphi}{\sqrt{6\alpha}} + 1) + \Lambda$ in the framework of the interacting, 2-field α-attractors. The three yellow-to-orange curves show the dark energy equation of state $w_{\rm DE}$ for $\Lambda = 0$, $10^{-2} \times \gamma\sqrt{6\alpha}$, and $10^{-1} \times \gamma\sqrt{6\alpha}$, respectively. The effective equation of state $w_{\rm eff}$ is almost identical for all values of Λ in the past (shown collectively by a blue curve), is different from $w_{\rm DE}$ in the past, and becomes identical to it in the future when the field φ becomes dominant. $N = 0$ corresponds to the present time, $\gamma\sqrt{6\alpha}$ has been set to 10^{-120}, and α has been set to $7/3$ for all the cases.

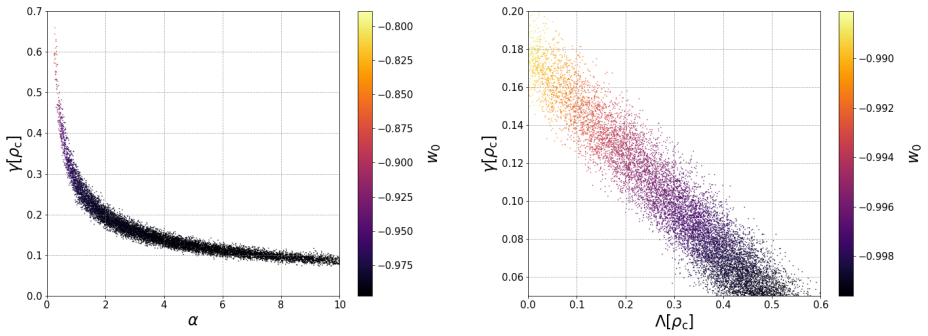

Figure 2.23: Constraints on γ, α and Λ for the linear, interacting, α-attractor model with the linear potential $V(\varphi) = \gamma\sqrt{6\alpha}(\tanh\frac{\varphi}{\sqrt{6\alpha}} + 1) + \Lambda$, when Λ is fixed to 0 (left) and when α is fixed to $7/3$ (right). Note that both γ and Λ are presented in units of the critical density today. The samples are color-coded with the value of w_0.

of Λ has been set to 0, while for the right panel, with Λ being scanned over, α has been fixed to 7/3. The value of γ is correlated with both α and Λ. In order to see this correlation clearly, let us first focus on the left panel with Λ being fixed to 0, i.e. when the potential is $V(\varphi) = \gamma\sqrt{6\alpha}(\tanh\frac{\varphi}{\sqrt{6\alpha}} + 1)$. The figure shows that γ increases by decreasing α. When α becomes very small, we know that the potential rapidly decreases and the $\tanh\frac{\varphi}{\sqrt{6\alpha}}$ piece in the potential drops quickly to ~ -1. This will be largely cancelled by the constant piece $\gamma\sqrt{6\alpha}$, and one therefore would need an enormous value of γ to compensate for that and to obtain the required amount of dark energy given by observations. This may mean that we should in principle be able to obtain good fits to the data for very small α with very large γ. However, the figure tells us that even though γ indeed seems to be increasing at small α, very small α ($\lesssim 0.3$) are disfavored by our analysis. This can be understood by looking at the color-code of the left panel of the figure, which shows the values of w_0. This shows that reducing α corresponds to larger deviations form ΛCDM. This illustrates why α cannot be smaller than ~ 0.3 for this $\Lambda = 0$ case, as the model predicts an equation of state for dark energy with present values that deviate too much from the observed values, and the number of viable points is therefore almost vanishing for very small α. Therefore, even though the required *amount* of dark energy can be provided by the model for small α, it does not produce the correct behavior for the dark energy *equation of state*. Clearly, by increasing Λ to nonzero values, which is equivalent to adding a cosmological constant to the potential, small α can also provide viable models of dark energy.

Let us now investigate the effect of changing Λ on the predictions of the model, by focusing on the right panel of Fig. 2.23, where α has been fixed to 7/3 and Λ has been allowed to vary. The figure shows that the larger the value of Λ, the smaller the value of γ. This behavior is easily understood, as the total dark energy in our model is a combination of the φ-dependent piece and the cosmological constant Λ, and by increasing Λ the contribution from the φ-dependent piece should reduce in order for

the model to produce the correct, total amount of dark energy consistent with observations, i.e. to provide $\Omega_{\rm DE} \approx 0.7$. $\Omega_{\rm DE}$ in general includes two pieces, one from the dynamics of the scalar field (i.e. the field-dependent part of the potential plus the kinetic energy of the field), and one from the cosmological constant Λ. Here therefore, by increasing the contribution from the cosmological constant the contribution from the field needs to drop in order to have the total amount of $\Omega_{\rm DE} \approx 0.7$. Decreasing γ to zero in the right panel of Fig. 2.23 will make Λ take a value of ≈ 0.7 in units of ρ_c, which is what we expect. Note also that, as expected, increasing Λ makes w_0 closer to its ΛCDM value, which is consistent with our illustration in Fig. 2.22.

Our conclusion, based on these results, is that this class of 2-field, interacting models, can provide interesting cosmological evolutions perfectly consistent with the current data. The deviations from the ΛCDM model depend however on the value of α. For relatively large α, such as $7/3$, the deviations are not large enough to be detected by the next generation of the LSS experiments, as w_0 and w_a are not sufficiently different from the ΛCDM values, but (depending on the value of Λ) decreasing α can make the deviations larger and potentially detectable. This class of models, therefore, has predictions that in some cases can be tested, verified, or ruled out by the future cosmological surveys.

2.7 CONCLUSIONS

In this chapter we constructed several viable models of dark energy based on the theory of α-attractors, using the flexibility of choosing the cosmological constant provided by the string theory landscape. We studied a broad variety of the models, such as the models of quintessential inflation, where a single field φ plays the double role of the inflaton and the quintessence. The simplest of these models is the α-attractor version of the theory with a linear potential described in section 2.5.1. We also performed a detailed

investigation of the models with exponential potential in sections 2.5.2 and 2.5.3.

The asymptotic flatness of the plateau potential in α-attractors and the possibility to avoid the fifth force problem, see section 2.3.2, make these models particularly suitable candidates for the role of dark energy. In several different models with the asymptotically vanishing height of the potential $V_- = \Lambda = 0$, we have a universal α-dependent prediction relating to each other the tensor-to-scalar ratio r and the asymptotic value of the equation of state w_∞:

$$r = \frac{12\alpha}{N^2}, \qquad w_\infty = -1 + \frac{2}{9\alpha}\,; \tag{2.102}$$

see Eqs. (2.1) and (2.2). This is a rather interesting correlation between r and w_∞, which may seem to be suggesting a possible way to test these models using a combination of the upcoming Stage IV cosmological experiments aiming at measuring both the B-mode polarization of the CMB and the growth and evolution of large-scale structure in the universe. One should however note that, as we have shown in this paper for various models of quintessential inflation, w_∞ is only the ultimate value of the dark energy equation of state parameter and not its present value. This means that w_∞ cannot be used directly to test the models, and one needs a detailed analysis in order to compare the predictions of the models to the cosmological observations.

Moreover, if one accepts the simplest interpretation of the predictions of the string theory landscape, one is free to add to the potential any constant that keeps the effective value of Λ within the anthropically allowed range of $|\Lambda| \lesssim 10^{-120}$. If, for example, one adds a positive cosmological constant $\Lambda \lesssim 10^{-120}$, the last prediction in (2.102) changes to $w_\infty = -1$, without altering the prediction for r and the spectral index n_s. In other words, by combining quintessential inflation with the string theory landscape, we

have a possibility to describe a broad range of outcomes for w without altering the inflationary predictions of the models.

We also studied α-attractor models where inflaton and quintessence are described by two different fields. From the point of view of model building, these models described in section 2.6 can be quite simple, but they allow much greater flexibility, which deserves a more detailed investigation.

An interesting byproduct of our investigation of α-attractors is the realization that their universal prediction $n_s = 1 - 2/N$ may give distinctly different numerical results for the quintessential α-attractors as compared to the usual α-attractors with a conventional reheating mechanism. We noticed that for some of the quintessential α-attractors with gravitational reheating, the required number of inflationary e-folds N can be greater than the required number of e-folds in more conventional models by $\Delta N \sim 10$, which increases the value of n_s by about 0.006. This increase coincides with the Planck 1σ error bar for n_s [82]. Therefore with the future improvement in the accuracy of CMB observations we might be able to distinguish the conventional inflationary models where the field after inflation oscillates and relaxes at the minimum of its potential, from the simplest models of quintessential inflation, even if these models predict $w = -1$.

Acknowledgments We thank A. Achúcarro, P. Bull, P. Creminelli, R. Flauger, G. Hinshaw, E. Komatsu, E. Linder, M. Martinelli, L. Senatore, E. Silverstein, A. Silvestri, D.-G. Wang, and Y. Yamada for their interest in this work and for helpful discussions and comments.

Part II

MODIFICATIONS OF GRAVITY

3

NEUTRON STAR MERGER GW170817 STRONGLY CONSTRAINS DOUBLY-COUPLED BIGRAVITY

The topic of this chapter is the theory of massive bigravity, where one has two dynamical tensor degrees of freedom. We consider an interesting extension where both of the metrics are coupled to the matter sector, which is known as the *doubly-coupled bigravity*. The main aim of this chapter is the study of gravitational-wave propagation in this theory. We demonstrate that the bounds on the speed of gravitational waves imposed by the recent detection of gravitational waves emitted by a pair of merging neutron stars and their electromagnetic counterpart, events GW170817 and GRB170817A, strongly limit the viable solution space of the doubly-coupled models. We have shown that these bounds either force the two metrics to be proportional at the background level or the models to become singly-coupled (i.e. only one of the metrics to be coupled to the matter sector). The mentioned proportional background solutions are particularly interesting. Indeed, it is shown that they provide stable cosmological solutions with phenomenologies equivalent to that of ΛCDM at the background level and at the level of linear perturbations.

This chapter is based on: Y. Akrami, Ph. Brax, A.-C. Davis, V. Vardanyan, *Neutron star merger GW170817 strongly constrains doubly-coupled bigravity*, Phys. Rev. D **97** (2018) 124010, arXiv:1803.09726.

3.1 INTRODUCTION

In the introduction of this thesis we have briefly discussed the theories of massive gravity and their natural extension to bimetric gravity. We particularly had discussed the so-called singly-coupled regime of the theory, where only one of the metrics is coupled to the matter sector.

However, in the absence of any theoretical mechanism that forbids the coupling of the matter fields directly to the reference metric, it is natural to go beyond the singly-coupled scenarios and study *doubly-coupled* models, where the two metrics couple to matter either directly or through a composite metric constructed out of the two spin-2 fields. This generalisation might look even more natural since the gravity sector of ghost-free bigravity is fully symmetric in terms of the two metrics, and it might feel unnatural to impose the matter sector to break this symmetry by coupling only to one metric.[1] Theories of doubly-coupled massive gravity and bigravity, and in particular their cosmologies, have also been extensively studied [172–194]. It has been shown, particularly, that the dangerous Boulware-Deser (BD) ghost [195] re-emerges almost always if the same matter fields couple to both metrics. One interesting exception has been proposed in Ref. [177], where an acceptable doubly-coupled theory of bimetric gravity has been constructed with matter coupled to a composite metric of the form

$$g^{\rm eff}_{\mu\nu} = \alpha^2 g_{\mu\nu} + 2\alpha\beta g_{\mu\gamma}(\sqrt{g^{-1}f})^{\gamma}{}_{\nu} + \beta^2 f_{\mu\nu}\,, \tag{3.1}$$

with $g_{\mu\nu}$ and $f_{\mu\nu}$ being the two metrics of the theory, and α and β being two arbitrary constants. Clearly, setting β to zero (α to zero) turns the doubly-coupled theory into a singly-coupled one with $g_{\mu\nu}$ ($f_{\mu\nu}$) being the

1 Note also that such theories do not necessarily violate the equivalence principle, and if they do, this may not be an issue. For discussions on the violation of the equivalence principle in theories with both metrics minimally coupled to matter, see Refs. [172, 173]. For theories with a composite metric coupled to matter the (weak) equivalence principle is not violated, as all particles move along the geodesics of the composite metric.

physical metric. Even though in this case the BD ghost is not completely removed from the theory, it is effective only at high energies, above the cutoff scale of the theory,[2] making it a valid effective field theory at low energies.

This doubly-coupled theory has been shown to provide viable and interesting cosmological solutions at the background level [179, 189], with linear perturbations that are stable at least around specific cosmological backgrounds [196] (see also Refs. [185, 192–194]). In particular, in contrast to the singly-coupled theory, this double coupling admits combinations of proportional metrics at the background level, and interestingly, the effective metric always corresponds to the massless fluctuations around such backgrounds, i.e. it satisfies the linearized Einstein equations. This means that around proportional backgrounds the theory is equivalent to general relativity at the background level as well as for linear perturbations, and differences from general relativity are expected only at the nonlinear level, at least in the sector coupled to matter. The immediate implication of this feature is that doubly-coupled bigravity admits viable and stable cosmologies at least for proportional metrics, which are potentially distinguishable from standard cosmology in the nonlinear regime.[3] As we show in this

2 This cut-off scale for massive gravity, corresponding to the strong-coupling scale, is $\Lambda_3 \equiv (m^2 M_{\rm Pl})^{1/3}$, where m is the graviton mass and $M_{\rm Pl}$ is the Planck mass. The cut-off scale can be higher for bigravity [53].

3 The linear cosmological perturbations for doubly-coupled bigravity around proportional, FLRW backgrounds separate into two decoupled sectors. The first (visible) sector coupled to matter is equivalent to general relativity. The second (hidden) sector is decoupled from matter and is not free from some instabilities. The most dangerous one [192, 196] occurs for vectors, which have a gradient instability in the radiation era. This may jeopardise the perturbativity of the models very early on in the Universe. On the other hand, however, the doubly-coupled models with a mass $m \sim H_0$ are expected to have an ultraviolet (UV) cut-off scale of order $\Lambda_3 = (H_0^2 M_{\rm Pl})^{1/3}$, which is low and prevents any reliable description of the physics of bigravity when the horizon scale becomes smaller than Λ_3^{-1}. Strictly speaking, for bimetric theories Λ_3 is the cut-off scale in the decoupling limit, and the cut-off scale for the full theory can be higher, contrary to massive gravity. However, since the decoupling

chapter, proportional metrics are extremely interesting also from the point of view of gravitational waves (GWs), as they are the only cases that survive after the recent measurements of the speed of gravity in addition to the singly-coupled models. This provides us with a unique class of bimetric models that are healthy and compatible with all cosmological observations as well as gravitational wave constraints.

GWs in bigravity have been studied in Refs. [193, 197–205], although they have been investigated for the doubly-coupled models only in Ref. [193]. In the literature, bigravity models are often considered to be on the safe side with respect to the bounds placed by current observations of GWs. While this holds for singly-coupled models, we show in this chapter that the bounds on the speed of GWs severely constrain the parameter space of the doubly-coupled scenarios. We particularly show that the models which survive the bounds from current gravitational wave observations are the ones for which the two background metrics are proportional, or for the choices of the parameters of the model that render it singly-coupled.

We first derive, analytically, the conditions under which bimetric models are safe in terms of the gravitational wave measurements. We then perform a Markov Chain Monte Carlo (MCMC) analysis of the parameter space of doubly-coupled bigravity by imposing the constraints from geometrical measurements of cosmic history, now taking into account also the constraints from gravitational wave observations. We illustrate that this numerical analysis confirms our analytical arguments.

The chapter is organised as follows: In section 3.2 we summarise the basics of doubly-coupled bigravity and its cosmology, and present the equations necessary for studying the background cosmological evolution.

---

limit is not well defined above Λ_3, we expect the entire theory to need modifications. The Λ_3 scale happens at a redshift of order 10^{12} which is just before Big Bang Nucleosynthesis. The unknown UV completion of doubly-coupled bigravity would certainly affect the early-Universe instability. In the late Universe as we consider here, no instability is present and the decoupled sector can be safely ignored for proportional backgrounds.

Section 3.3 discusses the evolution equations and the speed of GWs in the theory and presents the cosmological conditions that result in the speed equal to the speed of light. Section 3.4 provides the results of our MCMC scans, and our conclusions are given in section 3.5. Finally, in Appendix 3.6 we derive the cosmological evolution equations for tensor modes in detail, at the level of the field equations as well as the action.

3.2 COSMOLOGY OF DOUBLY-COUPLED BIGRAVITY

The theory of doubly-coupled bigravity can be formulated in terms of an action of the form [177, 179]

$$S = -\frac{M_{\rm eff}^2}{2}\int \mathrm{d}^4x\sqrt{-g}R_g - \frac{M_{\rm eff}^2}{2}\int \mathrm{d}^4x\sqrt{-f}R_f + m^2M_{\rm eff}^2\int \mathrm{d}^4x\sqrt{-g}\sum_{n=0}^{4}\beta_n e_n(\sqrt{g^{-1}f}) + S_{\rm matter}[g_{\mu\nu}^{\rm eff},\Psi]\,, \qquad (3.2)$$

where $g_{\mu\nu}$ and $f_{\mu\nu}$ are the two metrics of the theory with determinants g and f, respectively, and standard Einstein-Hilbert kinetic terms. $M_{\rm eff}$ plays the role of the Planck mass,[4] e_n are the elementary symmetric polynomials of the matrix $\sqrt{g^{-1}f}$ (see Ref. [47] for their detailed definitions), and the quantities β_n $(n = 0, ..., 4)$ are five free parameters determining the strength of the possible interaction terms. The parameter m sets the mass scale of the interactions and is not an independent parameter of the theory as it can be absorbed into the β_n parameters; m needs to be of the order of H_0, the present value of the Hubble parameter H, in order for the theory to provide

4 It should be noted that the theory can be formulated in terms of two separate Planck masses M_g and M_f corresponding to the g and f sectors, respectively. As has been shown in Ref. [179], the effective metric in this case will not include any free parameters and will have the fixed form $g_{\mu\nu} + 2g_{\mu\gamma}(\sqrt{g^{-1}f})^{\gamma}{}_{\nu} + f_{\mu\nu}$. We have chosen the formulation in terms of $M_{\rm eff}$ with α and β being present explicitly since it shows the singly-coupled limits of the theory more clearly.

self-accelerating solutions consistent with observational data. Matter fields have been shown collectively by Ψ, which couple to the effective metric $g^{\rm eff}_{\mu\nu}$ defined in Eq. (3.1) in terms of $g_{\mu\nu}$ and $f_{\mu\nu}$ and the two coupling parameters α and β.

In order to study the cosmological implications of the theory, we assume the background metrics $g_{\mu\nu}$ and $f_{\mu\nu}$ to have the FLRW forms

$$\mathrm{d}s_g^2 = -N_g^2\mathrm{d}t^2 + a_g^2\mathrm{d}x_i\mathrm{d}x^i\,, \tag{3.3}$$
$$\mathrm{d}s_f^2 = -N_f^2\mathrm{d}t^2 + a_f^2\mathrm{d}x_i\mathrm{d}x^i\,, \tag{3.4}$$

where t is the cosmic time, N_g and N_f are the lapse functions for $g_{\mu\nu}$ and $f_{\mu\nu}$, respectively, and a_g and a_f are the corresponding scale factors, all functions of t only.

Using the forms (3.3) and (3.4) for the background metrics $g_{\mu\nu}$ and $f_{\mu\nu}$, Eq. (3.1) fixes the form of the effective metric $g^{\rm eff}_{\mu\nu}$ to

$$\mathrm{d}s^2_{\rm eff} = -N^2\mathrm{d}t^2 + a^2\mathrm{d}x_i\mathrm{d}x^i\,, \tag{3.5}$$

where [179]

$$N \equiv \alpha N_g + \beta N_f\,, \tag{3.6}$$
$$a \equiv \alpha a_g + \beta a_f\,, \tag{3.7}$$

are the lapse and the scale factor of the effective metric, respectively. The dynamics of $g_{\mu\nu}$ and $f_{\mu\nu}$ are governed by their Friedmann equations, which take the forms

$$3H_g^2 = \frac{\alpha}{M_{\rm eff}^2}\rho\frac{a^3}{a_g^3} + H_0^2(\beta_0 + 3\beta_1 r + 3\beta_2 r^2 + \beta_3 r^3)\,, \tag{3.8}$$

$$3H_f^2 = \frac{\beta}{M_{\rm eff}^2}\rho\frac{a^3}{a_f^3} + H_0^2(\frac{\beta_1}{r^3} + 3\frac{\beta_2}{r^2} + 3\frac{\beta_3}{r} + \beta_4)\,, \tag{3.9}$$

where

$$H_g \equiv \frac{\dot{a}_g}{N_g a_g}\,, \qquad H_f \equiv \frac{\dot{a}_f}{N_f a_f}\,, \tag{3.10}$$

are the Hubble parameters for $g_{\mu\nu}$ and $f_{\mu\nu}$, respectively, ρ is the energy density of matter and radiation, the dot denotes a derivative with respect to t, and

$$r \equiv \frac{a_f}{a_g} \tag{3.11}$$

is the ratio of the two scale factors a_f and a_g. We have also fixed m to H_0 in the two Friedmann equations, as we are interested in self-accelerating solutions for which $m \sim H_0$.

In addition to the two Friedmann equations (3.8) and (3.9), the consistency of the theory requires the Bianchi constraint [179]

$$\frac{N_f}{N_g} = \frac{\dot{a}_f}{\dot{a}_g} \to H_g = rH_f \tag{3.12}$$

to be satisfied.[5] Having introduced the effective lapse and scale factor N and a, one can naturally introduce an effective Hubble parameter associated with the effective metric $g^{\rm eff}_{\mu\nu}$,

$$H \equiv \frac{\dot{a}}{Na}\,, \tag{3.13}$$

which satisfies its own effective Friedmann equation [179],

$$H^2 = \frac{\rho}{6M^2_{\rm eff}}(\alpha+\beta r)(\alpha+\frac{\beta}{r}) + H_0^2\frac{B_0+r^2B_1}{6(\alpha+\beta r)^2}\,, \tag{3.14}$$

where we have also introduced

$$B_0 \equiv \beta_0 + 3\beta_1 r + 3\beta_2 r^2 + \beta_3 r^3\,, \tag{3.15}$$

$$B_1 \equiv \frac{\beta_1}{r^3} + 3\frac{\beta_2}{r^2} + 3\frac{\beta_3}{r} + \beta_4\,. \tag{3.16}$$

Eq. (3.14) is obtained by adding the two Friedman equations (3.8) and (3.9), and applying the Bianchi constraint (3.12). The effective Hubble parameter H can be written in terms of H_g or H_f as

$$H = \frac{H_g}{\alpha+\beta r} = \frac{rH_f}{\alpha+\beta r}\,. \tag{3.17}$$

In addition to the Friedmann equation for H, by again using the Bianchi constraint (3.12) and now subtracting the two Friedmann equations (3.8) and (3.9) we arrive at the algebraic condition

$$\frac{\rho}{M^2_{\rm eff}}(\alpha+\beta r)^3(\alpha-\frac{\beta}{r}) + H_0^2(B_0 - r^2B_1) = 0\,. \tag{3.18}$$

5 Note that the Bianchi constraint gives two branches of solutions. The one we consider here is the so-called dynamical branch. See Refs. [179, 189] for the discussion of the second, algebraic branch.

The energy-momentum tensor for matter and radiation is covariantly conserved with respect to the effective metric, which means that the energy density ρ satisfies the continuity equation

$$\dot{\rho} + 3\frac{\dot{a}}{a}(\rho + p) = 0\,. \tag{3.19}$$

This motivates us to introduce $x \equiv \ln a$, the number of e-folds in terms of the effective scale factor a, as a time coordinate. In terms of x, we can recover the usual behaviour of the matter and radiation energy densities

$$\rho_{\rm M} = \rho_{\rm M}^{(0)} e^{-3x}\,, \qquad \rho_{\rm R} = \rho_{\rm R}^{(0)} e^{-4x}\,, \tag{3.20}$$

assuming that these two components are conserved separately. Here, $\rho_{\rm M}^{(0)}$ and $\rho_{\rm R}^{(0)}$ are the current values of the energy densities of matter and radiation, respectively.

It is easy to show that the coupling parameters α and β affect observables only though their ratio β/α, as we can assume $\alpha \neq 0$ without loss of generality[6] and then rescale $M_{\rm eff}^2$ by a factor of $1/\alpha^4$. Later in this chapter, when discussing the constraints, we will use this rescaling freedom and introduce a new parameter

$$\gamma \equiv \frac{\beta}{\alpha}\,, \tag{3.21}$$

which will play the role of the only extra parameter for doubly-coupled models compared to the singly-coupled ones. Identifying the effective Planck mass $M_{\rm eff}$ with the usual Planck mass $M_{\rm Pl}$, our doubly-coupled bimetric model now possesses six free parameters, β_n with $n = 0, ..., 4$, and γ. For now, however, let us keep both α and β explicit as it allows us to see

6 This is indeed the case because the singly-coupled bigravity theories with either of the metrics being coupled to matter are completely equivalent.

explicitly the duality properties of the background dynamics equations as well as the equations governing the propagation speed of the GWs.

Before we proceed with our studies of gravitational waves in the next sections, let us emphasise an important property of the cosmological evolution equations that we presented in this section. As can be seen easily at the level of the action, the theory is symmetric under the simultaneous interchanges $g_{\mu\nu} \leftrightarrow f_{\mu\nu}$, $\beta_n \to \beta_{4-n}$ and $\alpha \leftrightarrow \beta$ (or $\gamma \to 1/\gamma$), and therefore all the dynamical equations remain unchanged [179]. More concretely, let us consider two sets of parameters $\{\beta_0, \beta_1, \beta_2, \beta_3, \beta_4, \alpha, \beta\} = \{v_0, v_1, v_2, v_3, v_4, v_5, v_6\}$ and $\{\beta_0, \beta_1, \beta_2, \beta_3, \beta_4, \alpha, \beta\} = \{v_4, v_3, v_2, v_1, v_0, v_6, v_5\}$, where $v_{0,\dots,6}$ are some particular values of the parameters. It is easy to show that the solution of Eq. (3.18) for r with the first set of parameter values is identical to the solution for the quantity $\tilde{r} \equiv 1/r$ with the second set of parameter values. Now if we rewrite Eq. 3.14 in terms of $\tilde{r}$ (note that we do not make an actual interchange $r \to 1/r$, and we only rewrite the equations in terms of $\tilde{r}$) then for the two distinct sets of parameter values given above the two Friedmann equations are precisely the same. This, for example, implies that when scanning the single-parameter submodel with all the β_n parameters turned off except β_1 the space of all the cosmological solutions that we obtain is fully equivalent to the one for the submodel with only β_3 turned on (given that we leave α and β, or equivalently γ, free). This is a useful observation and will help us reduce the number of cases studied in the next sections.

3.3 THE SPEED OF GRAVITATIONAL WAVES

The spectrum of bimetric theories of gravity contains two gravitons, one massive and one massless, with five and two degrees of freedom, respectively. In order to study the properties of gravitational waves one needs to focus only on tensor modes, i.e. the helicity-2 modes of the gravitons. Massless and massive gravitons have two helicity-2 modes each. It is impor-

tant to note that in general the two metrics of the theory, $g_{\mu\nu}$ and $f_{\mu\nu}$, each contain a combination of massive and massless modes, and therefore the evolution equations for the g and f tensor modes do not represent directly the evolution of the tensor modes for massive and massless modes. Indeed, it is not possible in general to diagonalise the spectrum of spin-2 perturbations into mass eigenstates, and therefore the notion of mass does not make sense around arbitrary backgrounds [181]. One can specifically show [181] that mass eigenstates can be defined only around proportional metrics by computing the spectrum of linear perturbations and comparing their equations with those of linearised general relativity. Proportional metrics are therefore extremely interesting from this point of view, as the notion of spin-2 mass eigenstates does not exist for other types of backgrounds. As we mentioned in section 3.1, contrary to the theory of singly-coupled bigravity, the doubly-coupled theory admits proportional backgrounds (both in vacuum and in the presence of matter). It can be shown additionally that the effective metric of the theory, $g^{\text{eff}}_{\mu\nu}$, corresponds exactly to the massless mode around such backgrounds, while the massive mode is fully decoupled [181]. This immediately implies that the speed of GWs around proportional backgrounds measured by any detectors must be equal to the speed of light since the detectors only "see" the effective metric. Such solutions are therefore safe regarding the bounds from the GW observations. We will show later in this chapter that, in addition to the singly-coupled corner of the theory, proportional backgrounds are indeed the *only* solutions that survive the bounds from GWs.

As detailed in Appendix 3.6, the propagation equations for the g and f tensor modes h_g and h_f around the cosmological backgrounds are

$$h''_{g+/\times} + \left(\frac{N'}{N} - \frac{N'_g}{N_g} - \frac{a'}{a} + 3\frac{a'_g}{a_g}\right) h'_{g+/\times} - \frac{N_g^2}{N^2}\frac{a^2}{a_g^2}\nabla^2 h_{g+/\times} + \frac{N_g^2}{N^2}a^2 A(h_{f+/\times} - h_{g+/\times}) = 0\,, \tag{3.22}$$

$$h''_{f+/\times} + \left(\frac{N'}{N} - \frac{N'_f}{N_f} - \frac{a'}{a} + 3\frac{a'_f}{a_f}\right) h'_{f+/\times} - \frac{N_f^2}{N^2}\frac{a^2}{a_f^2}\nabla^2 h_{f+/\times} + \frac{N_f^2}{N^2}a^2 B(h_{g+/\times} - h_{f+/\times}) = 0\,. \tag{3.23}$$

Here, the prime denotes a derivative with respect to the conformal time corresponding to the effective metric, η_{eff}, which is defined through

$$\mathrm{d}\eta_{\text{eff}}^2 = \mathrm{d}t^2 N^2/a^2. \tag{3.24}$$

With this time coordinate the background effective metric reads

$$\mathrm{d}s_{\text{eff}}^2 = a^2(-\mathrm{d}\eta_{\text{eff}}^2 + \mathrm{d}x^2)\,. \tag{3.25}$$

First note that we have written the equations in terms of the time coordinate corresponding to the effective metric and not $g_{\mu\nu}$ or $f_{\mu\nu}$, because the effective metric is the one that couples to matter and therefore plays the role of the physical spacetime metric, used for measuring distances and time intervals. In addition, we chose to work with the conformal time because in this coordinate light rays travel as in a Minkowski spacetime, making η_{eff} a particularly useful time coordinate for identifying the propagation speeds of the gravitational waves.

We can now read off from Eqs. (3.22) and (3.23) the propagation speeds c_g and c_f for the gravitational waves h_g and h_f, respectively, as[7]

$$c_g^2 = \frac{N_g^2}{N^2}(\alpha + \beta r)^2 \,, \tag{3.26}$$

$$c_f^2 = \frac{N_f^2}{N^2}(\alpha \frac{1}{r} + \beta)^2 \,. \tag{3.27}$$

The ratio of the two speeds is a coordinate-independent quantity and is given by

$$\frac{c_f}{c_g} = b \equiv \frac{1}{r}\frac{N_f}{N_g} = \frac{1}{r}\frac{\dot{a}_f}{\dot{a}_g} \,. \tag{3.28}$$

As we will see, the quantity b will play a crucial role in the rest of the discussions in this chapter.

One should note again that in doubly-coupled bigravity one measures neither h_g nor h_f separately. The tensor modes measured by gravitational wave detectors are the ones corresponding to the effective metric $g^{\rm eff}_{\mu\nu}$. These observable modes can be written in terms of $h^{(g)}_{ij}$ and $h^{(f)}_{ij}$, the tensor modes of the g and f metrics respectively, as

$$\delta g^{(\rm eff)}_{ij} = a\left(\alpha h^{(g)}_{ij} + \beta h^{(f)}_{ij}\right) \,, \tag{3.29}$$

where

7 Note that since we are interested in bigravity solutions with the interaction scale $m \sim H_0$ in order to explain cosmic acceleration, the effects of the graviton mass on the speed of the gravitational waves are several orders of magnitude smaller than the sensitivity of current GW detectors. We therefore fully ignore the direct contributions from the mass terms to the speed.

$$h_{11}^{(I)} = a_I h_{I+}\,, \tag{3.30}$$
$$h_{12}^{(I)} = a_I h_{I\times} = h_{21}^{(I)}\,, \tag{3.31}$$
$$h_{22}^{(I)} = -a_I h_{I+}\,, \tag{3.32}$$

with $I \in \{g, f\}$ (see Appendix 3.6 for details).

The recent measurements of the GWs from neutron star mergers have imposed incredibly tight constraints on the speed of gravitons. The relative difference between the speed of GWs and that of light must be smaller than $\sim 10^{-15}$, which is practically zero. Let us therefore assume that the speed of GWs is exactly the same as the speed of light, and study its implications.

The mentioned bound on the speed of GWs tells us that at least one of the quantities c_g and c_f should be unity (note that $c = 1$ in our units). The reason for this is that at least one of the g or f graviton modes should have traveled with the speed of light when arriving at the detector. Keeping this in mind let us first assume that

- we are in a truly doubly-coupled regime (i.e. $\alpha \neq 0$ and $\beta \neq 0$),
- r is a finite and nonzero quantity,
- N_f and N_g are finite and nonzero.

Let us further set $N = 1$ and write the two speeds c_g and c_f as

$$c_g^2 = \frac{(\alpha + \beta r)^2}{(\alpha + br\beta)^2}\,, \tag{3.33}$$
$$c_f^2 = \frac{(\alpha \frac{1}{r} + \beta)^2}{(\alpha \frac{1}{br} + \beta)^2}\,. \tag{3.34}$$

Now it is clear that, first of all, when $b = 1$, both c_g and c_f become unity. Moreover, when either c_g or c_f is unity, we will necessarily have $b = 1$. This then tells us very strongly that in the case of finite and nonzero N_f, N_g and r, and under the assumption of $\alpha \neq 0$ and $\beta \neq 0$, $b = 1$ is the necessary and sufficient condition for compatibility with the GW experiments.

Let us now discuss the validity of the assumptions that we made above. From the Friedmann equation (3.14) we see that both infinite and zero values of r lead to singularity in the observable Hubble function H unless either α or β is zero, i.e. the theory is singly-coupled. This means that for physical solutions in the doubly-coupled regime r is necessarily finite and nonzero. Additionally, if $N_f = 0$ while N_g is finite and nonzero, we see that $c_f^2 = 0$ while $c_g^2 = (1 + \gamma r)^2$,[8] which is not equal to unity unless we are in the singly-coupled regime of $\beta = 0$. In exactly the same way the case of $N_g = 0$ while simultaneously N_f being finite and nonzero is excluded. In principle one should also consider the cases with one of the lapse functions $N_{g,f}$ going to infinity while their ratio is fixed[9]. Note however that such cases will not only produce unphysical propagation speeds in both g and f sectors, but they will also remove the second-order time-derivatives in the tensor propagation equations, hence rendering the initial data from the past lost at one particular instant in time (when the divergence happens). Based on these considerations we can conclude that the cases with $b = 0$ or $b \to \infty$ are excluded.

Finally, as it is expected, in the singly-coupled case (say, $\beta = 0$ and $\alpha = 1$), we have $N_g = 1$ and $c_g^2 = 1$, which is the only observationally important speed in this limit. It is very important to note that in such a singly-coupled limit $r \to 0$ or $r \to \infty$ are not necessarily dangerous since the potentially singular terms containing $\frac{1}{r}$ (as well as the terms containing r, which are dangerous when $r \to \infty$) are multiplied by both α and β and therefore vanish in the either case of $\alpha = 0$ or $\beta = 0$. Putting all these

8 Here we have used the expression for the effective lapse function $1 = \alpha N_g + \beta N_f$

9 Otherwise, obviously, they cannot satisfy the gauge fixing condition $N = 1$.

discussions together we arrive at an important statement: the propagation of gravitational waves in doubly-coupled bigravity is viable *if and only if* $b = 1$ or we are in a singly-coupled regime.

It is important to note that the current bounds on the speed of GWs have been placed through the observations at very low redshifts ($z \approx 0$), i.e. at almost the present time. This means that, strictly speaking, the viability conditions we discussed above are required to hold only at $z \approx 0$, including the condition $b = 1$. Let us for now assume that the constraint on the speed of GWs is valid not only in the present epoch but it applies also to the earlier epochs of the universe, i.e. we assume $b = 1$ at all times. Later on, when we discuss our numerical analysis, we will show a rather vigorous feature of the theory that imposing $b|_{z\approx 0} = 1$ will force b to be unity at all redshifts.

Imposing $b(z) = 1$ at all times tells us that the two background metrics $g_{\mu\nu}$ and $f_{\mu\nu}$ should be proportional. This can easily be seen by setting $b(z) = 1$ in Eq. (3.28) and noting that $r = a_f/a_g$, resulting in

$$\frac{a_f(z)}{a_g(z)} = C = \frac{N_f(z)}{N_g(z)}\,, \tag{3.35}$$

with C being some (constant) proportionality factor. In order to understand under which circumstances these proportional solutions exist, let us consider the early-time and late-time asymptotic limits of Eq. (3.18). By taking the future asymptotic limit, with $\rho \to 0$, we obtain

$$\beta_3 r_\infty^4 + (3\beta_2 - \beta_4) r_\infty^3 + 3(\beta_1 - \beta_3) r_\infty^2 + (\beta_0 - 3\beta_2) r_\infty - \beta_1 = 0 \tag{3.36}$$

for the value of r in the far future, r_∞. Note that r_∞ being a solution of this time-independent equation means that it is a constant. This in turn means that the two metrics are necessarily proportional in the far-future limit. Additionally, the early-universe limit of Eq. (3.18) fixes the value of r

to either γ or $-\gamma$. The latter does not give viable cosmologies [179], and therefore $r \to r_{-\infty} = \gamma$ is the only viable early-time limit. Restricting to the solutions for which r does not exhibit any singular behaviour [179], one can show that r should *monotonically* evolve between $r = r_{-\infty}$ and $r = r_{\infty}$ over the history. The monotonicity of r implies that when the two limiting values $r_{-\infty}$ and r_{∞} coincide, i.e. when $r_{\infty} = \gamma$, we have constant r over the entire history of the universe and hence the background metrics are proportional in that case.

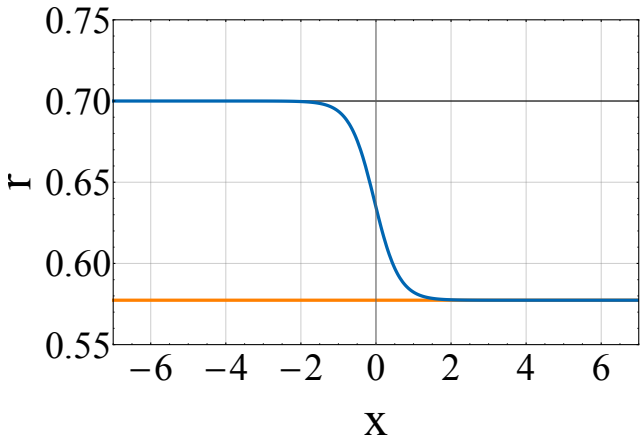

Figure 3.1: Behaviour of r, the ratio of the scale factors of the two metrics, as a function of the number of e-folds x, with $x = 0$ corresponding to the present time. The evolution of r has been shown with blue and orange curves for two different values of γ, both for a single-interaction-parameter model with only β_1 being turned on. The blue curve corresponds to a case where γ does not satisfy the special tuning condition for proportional metrics. The curve exhibits two constant-r epochs of $r_{-\infty} = \gamma$ and $r_{\infty} = 1/\sqrt{3}$, with the latter being the solution of Eq. (3.36) regardless of the value of β_1. The orange curve corresponds to a case where γ is chosen such that it is the solution of Eq. (3.36), i.e. $\gamma = r_{\infty} = 1/\sqrt{3}$.

Based on the discussions above, we can now formulate the necessary and sufficient conditions for the two background metrics to be proportional:

1. Background solutions are proportional **iff** r is given by $r = \gamma$ at all times, where $\gamma \equiv \beta/\alpha$. Note that one does not need to check whether this condition holds at all times; as we argued above, because of the monotonicity of r, having $r = \gamma$ even at one instant in time, other than the asymptotic past, is sufficient for the condition to be satisfied at all times.

2. Equivalently, the background solutions are proportional **iff** the parameters of the model solve the algebraic equation

$$\beta_3\gamma^4+(3\beta_2-\beta_4)\gamma^3+3(\beta_1-\beta_3)\gamma^2+(\beta_0-3\beta_2)\gamma-\beta_1=0\,. \quad (3.37)$$

We demonstrate these conditions in Fig. 3.1 by plotting the dependence of r on the number of e-folds x, with the present time given by $x = 0$, for a single-interaction-parameter scenario where only β_1 is turned on while $\beta_{0,2,3,4} = 0$. The blue curve corresponds to a case where γ does not satisfy the special tuning condition for proportional metrics. The curve exhibits two constant-r epochs. The far-past epoch corresponds to $r = \gamma$ (the horizontal, thin, black line), while the far-future limit is given by the solution of Eq. (3.36) for which $r_\infty = 1/\sqrt{3}$ regardless of the value of β_1. The orange curve corresponds to a case where γ is chosen such that it is the solution of Eq. (3.36), i.e. $\gamma = r_\infty = 1/\sqrt{3}$. The value of β_1 is not relevant for the arguments here because in this case the asymptotic value r_∞ is independent of the value of β_1 (the value of $r_{-\infty}$ is always independent of the values of β_n parameters). In order to illustrate our arguments, we have chosen two different values of β_1 for producing the two curves (blue and orange). As expected, they agree in the far-future limit, even though the values of β_1 are different for the two curves.

As we will see in the next section, bigravity models for which only one of the $\beta_{0,1,2,3,4}$ parameters is turned on are particularly interesting. For those

cases the proportional background solutions correspond to the following values of the parameter γ:

1. β_0 or β_4 only: $\gamma = r_\infty = 0$,
2. β_1 only: $\gamma = r_\infty = \frac{1}{\sqrt{3}}$,
3. β_2 only: $\gamma = r_\infty = 1$,
4. β_3 only: $\gamma = r_\infty = \sqrt{3}$.

Note that γ and therefore r_∞ in these cases are independent of the value of the corresponding β_n parameter. Note also that, as we discussed in the previous section, the single-parameter models with only β_1 or β_3 turned on are identical, as long as $r \leftrightarrow 1/r$ (or equivalently $\gamma \leftrightarrow 1/\gamma$), justifying the values $1/\sqrt{3}$ and $\sqrt{3}$ for r_∞ in these models. In addition, it is interesting to notice that for the β_0 and β_4 only models, proportional backgrounds do not exist, as in those cases γ is forced to be vanishing, and therefore the theory becomes singly-coupled.

All these cases of proportional background metrics with only one of the $\beta_{1,2,3}$ parameters being nonzero can be verified easily by applying the Bianchi constraint $H_g = rH_f$ to the Friedmann equations (3.8) and (3.9), obtaining

$$3H_g^2 = \frac{1}{M_{\rm eff}^2}\rho(1+\gamma r)^3 + H_0^2(\beta_0 + 3\beta_1 r + 3\beta_2 r^2 + \beta_3 r^3)\,, \tag{3.38}$$

$$3H_g^2 = \frac{\gamma}{M_{\rm eff}^2}\rho\frac{(1+\gamma r)^3}{r} + H_0^2(\frac{\beta_1}{r} + 3\beta_2 + 3\beta_3 r + \beta_4 r^2)\,. \tag{3.39}$$

In general, we have two dynamical variables a_g and a_f, which are determined by the two independent, dynamical equations (3.38) and (3.39). Now, if the two metrics are proportional, this means that a_g and a_f are also proportional, and r is a constant. We will then have effectively only one

dynamical variable, a_g or a_f, and the two dynamical equations (3.38) and (3.39) must be identical. This means that the right-hand sides of the two equations should be identically the same. Now, setting all the parameters β_n to zero, except for either of β_1, β_2, or β_3, we immediately arrive at the values for r_∞ and γ presented above for these three cases.

Now turning back to the condition for the speed of the gravitational waves to be identical to the speed of light, we argued that what is strictly needed is to have $b|_{z\approx 0} \approx 1$, as the speed of GWs has been measured only at the present epoch $z \approx 0$. If, additionally, the parameters of the model giving $b|_{z=0} = 1$ satisfy the algebraic equation (3.37) then they lead to proportional background solutions and $b = 1$ condition is satisfied at all times, implying necessarily that $c_g = c_f = 1$ at all times. The question of whether a set of parameters giving $b|_{z=0} = 1$ (hence $c_g|_{z=0} = c_f|_{z=0} = 1$) while not satisfying Eq. (3.37) can happen in our doubly-coupled bigravity models cannot be answered based on our analytical arguments here, and needs a numerical scanning of the parameter space. In principle it could be possible that the two background metrics would not be proportional whilst b would become unity at the present epoch simply as a coincidence for a specific combination of the parameters. We will however demonstrate later that for all the models that we study in this paper the cosmologically viable solutions with $b|_{z=0} = 1$ also satisfy Eq. (3.37), implying $b = 1$ at all times, and therefore the proportionality of the background metrics.

3.4 MCMC SCANS AND OBSERVATIONAL CONSTRAINTS

In this section we present the results of a set of MCMC scans of the parameter space of doubly-coupled bigravity when different sets of parameters are allowed to vary while the rest are fixed to zero. We should first emphasise that we do not intend here to perform a detailed parameter estimation of the model using cosmological observations. This has been done in Ref. [179] using the geometrical constraints on cosmic histories at the background

level.[10] We are rather interested in studying the impact of the constraints from the measurements of gravitational waves and the bounds on their speed on the cosmologically viable regions of the parameter space. We first perform MCMC scans of the models using similar cosmological datasets as those used in Ref. [179]. The geometrical constraints that we consider are a combination of the observed angular scales of the cosmic microwave background anisotropies [130], the supernovae redshift-luminosity relation [158], the measurements of the baryon acoustic oscillations (BAO) [159–163], and the local measurement of the Hubble constant H_0 [164]. Our scans provide a set of points in the parameter space of the models all of which are in good agreement with cosmological observations. We have checked that our results are in perfect agreement with the results of Ref. [179] for the cases studied in that paper. We then explore the implications of imposing the GW constraints on the points, and investigate whether and how strongly the cosmologically viable regions are affected by the GW observations.

Our full bigravity model contains seven free parameters, as far as our MCMC scans are concerned. These include the five β_n parameters for the interaction terms, the ratio of the couplings of the two metrics to matter γ, and the present value of the matter density parameter $\Omega_{\rm M}^0$, defined as

$$\Omega_{\rm M}^0 \equiv \frac{\rho_{\rm M}^0}{3M_{\rm eff}^2 H_0^2} \,. \tag{3.40}$$

Note that one should not necessarily expect to obtain a value for $\Omega_{\rm M}^0$ similar to the best-fit one in the standard model of cosmology, ΛCDM, for a bigravity model that fits the data well, even for proportional backgrounds where the interaction terms contribute with a Λ-like constant to the Friedmann equation. The reason, as explained in Ref. [179] in detail, is the extra factor

10 Note, however, that the MCMC scans presented in Ref. [179] include only single-β_n models, while in the current paper we consider also the cosmological constraints on two-parameter models.

appearing in the matter density term of the Friedmann equation. We will see below that indeed in some cases the viable points in the parameter space give values for $\Omega_{\rm M}^0$ that are significantly smaller than the ΛCDM value of ~ 0.3.

For each point in the parameter space of the theory we also output the corresponding values of r, b, c_g and c_f, all evaluated at the present time. These will allow us to check which parts of the parameter space agree with the observational constraint $c_g \approx 1$ (or $c_f \approx 1$), and to verify explicitly the conditions on b and r. We will particularly use the quantity $(c_g^2 - 1)(c_f^2 - 1)$ as a measure of how fit a point is to the observational constraints on the speed of GWs.

We perform our MCMC scans for various submodels, namely the single-parameter[11] models of β_0, β_1, and β_2 (with other β_n being set to zero in each case), and the two-parameter models of $\beta_0\beta_1$, $\beta_0\beta_2$, $\beta_1\beta_2$, and $\beta_1\beta_3$. One should note that, as we discussed before, the single-parameter models of β_3 and β_4 are identical to the β_1 and β_0 models, respectively, because of the duality properties of the theory. In addition, for the same reason, each one of the other two-parameter models is equivalent to one of the two-parameter models considered here, and their phenomenologies are therefore already captured. Our objective in this chapter is not to perform a detailed and extensive statistical analysis of the entire parameter space of doubly-coupled bigravity, and we are mainly interested in a qualitative understanding of the implications of the GW observations for the viability of the theory, which can very well be captured in the studies of single-parameter and two-parameter cases. We therefore do not discuss three- or higher-parameter models. As we will see, although the constraints are quite strong for most of these cases, the parameter space in some models still allows viable cosmologies, and clearly, by increasing the number of free parameters one expects to enlarge the number of possibilities for finding

11 This is only a terminological convention here, and strictly speaking, our single-parameter models have two free parameters, as γ is always a free parameter of the models.

viable scenarios within the model. We leave a detailed statistical analysis of the full model for future work.

3.4.1 *One-parameter models*

• **β_0 model**: Let us first emphasise that, contrary to singly-coupled bigravity, in the doubly-coupled theory the parameters β_0 and β_4 are no longer the explicit cosmological constants corresponding to the two metrics $g_{\mu\nu}$ and $f_{\mu\nu}$. The reason is that matter couples to the effective metric $g^{\rm eff}_{\mu\nu}$, which is a combination of $g_{\mu\nu}$ and $f_{\mu\nu}$. This can be seen explicitly by looking at the effective Friedmann equation (3.14) and comparing it with Eqs. (3.8) and (3.9). In addition, in the singly-coupled theory, where matter couples to, say, $g_{\mu\nu}$, β_0 behaves as the matter vacuum energy in the action of the theory, as it appears in the interaction terms as $\beta_0\sqrt{-g}$ (note that $e_0 = 1$). In the doubly-coupled theory, however, all the interaction parameters β_n directly receive contributions from quantum matter loops, and the definition of vacuum energy is more subtle than in the singly-coupled theory. It is therefore interesting to study a single-parameter, doubly-coupled model with only β_0 turned on, while all the other parameters β_n are set to zero — for the singly-coupled case this will be nothing but ΛCDM. The cosmology of this β_0 model in doubly-coupled bigravity has been studied in Ref. [179]. As a cross check of our results with the latter paper we show the $\gamma - \Omega^0_{\rm M}$ posterior in Fig. 3.2, which is in a good agreement with the corresponding result of Ref. [179]. Note that $\gamma = 0$ corresponds to the singly-coupled scenario, which reduces to ΛCDM for this β_0-only model.

Fig. 3.3 demonstrates the interdependence of r, b, the quantity $(c_g^2 - 1)(c_f^2 - 1)$ (capturing the deviations of the g and f gravitational wave speeds from the speed of light), and γ. Note that c_g, c_f, b, and r are all computed at $z = 0$.

Let us concentrate on the right panel of Fig. 3.3, where the present value of $(c_g^2 - 1)(c_f^2 - 1)$ has been depicted versus γ. This plot shows that in

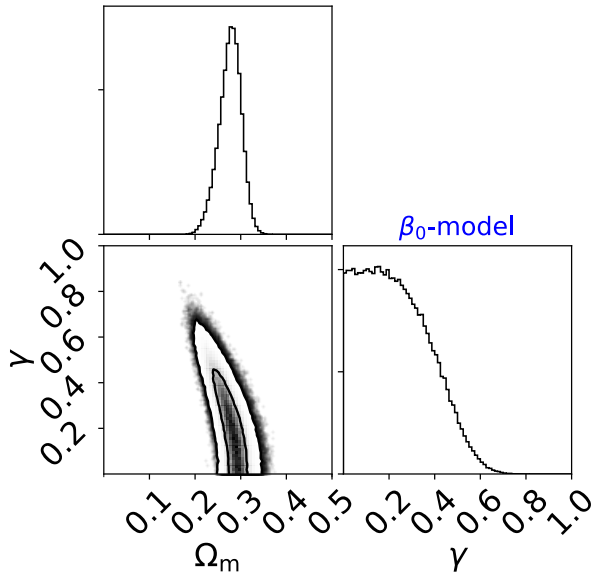

Figure 3.2: The plot shows the cosmologically viable samples in the $\gamma - \Omega_M^0$ parameter plane of the doubly-coupled β_0 model, where all the interaction parameters β_n are set to zero except for β_0, which is allowed to vary. The contours show the 68% and the 95% CLs.

order for the model to be cosmologically viable and simultaneously predict gravitational waves with the speed equal to the speed of light (i.e. for at least one of the two quantities c_g and c_f to be unity), γ is required to be zero, which in turn implies that the model needs to be singly-coupled. In this case r is forced to be vanishing, although r is no longer a meaningful quantity as there is no interaction between $g_{\mu\nu}$ and $f_{\mu\nu}$, and $f_{\mu\nu}$ completely decouples from the theory. This all tells us that β_0-model satisfies the cosmological and gravitational-wave constraints only in its singly-coupled limit, which is equivalent to ΛCDM. We do not see any cases of proportional metrics in this model, as such cases should also give GWs consistent with observations. Let us take a closer look at this and understand why such a situation does not happen in β_0-model by looking again at the condition for

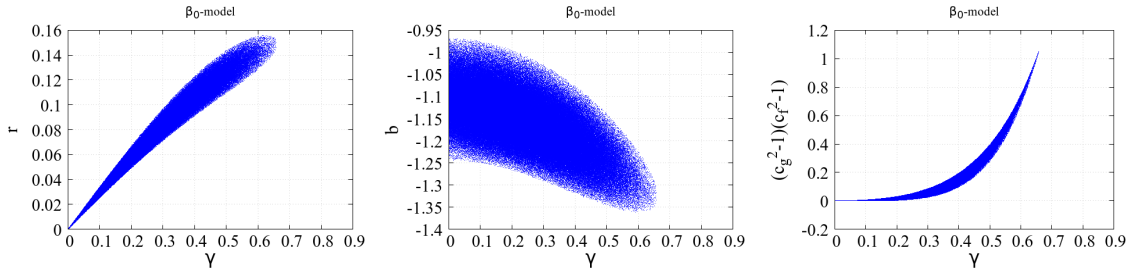

Figure 3.3: MCMC samples showing all the cosmologically viable points in the parameter space of the doubly-coupled β_0 model. The plots particularly demonstrate the interdependence of r (the ratio of the scale factors of the two metrics $g_{\mu\nu}$ and $f_{\mu\nu}$), $b \equiv \frac{1}{r}\frac{N_f}{N_g}$, the quantity $(c_g^2-1)(c_f^2-1)$ (capturing the deviations of the g and f gravitational wave speeds from the speed of light), and $\gamma \equiv \frac{\beta}{\alpha}$. Note that c_g, c_f, b, and r are all computed at $z = 0$. In this β_0 model, the only part of the parameter space that is left after imposing $c_g = 1$ or $c_g = 1$ is the singly-coupled submodel characterised by $\gamma = 0$.

proportional background metrics. As we argued in the previous section, for proportional backgrounds γ must satisfy Eq. (3.37), while $r_\infty = \gamma$. Setting all β_n parameters to zero except for β_0, we arrive at $\gamma = r_\infty = 0$. First of all, this is exactly what we see in the left panel of Fig. 3.3 for r and γ. Additionally, we are back to the condition $\gamma = 0$ that corresponds to a single coupling. This means that β_0-model does not admit any sets of (nontrivial) proportional backgrounds, unless we consider $f_{\mu\nu}$ to be proportional to $g_{\mu\nu}$ with a vanishing proportionality factor. The fact that this is a peculiar case can also be seen by looking at the middle panel of Fig. 3.2, which shows b versus γ. b is always negative, which means that the condition for proportional backgrounds, $b = 1$, can never be satisfied.

• **β_1 model**: Here we turn on only the β_1 parameter and set to zero all the other interaction parameters $\beta_{0,2,3,4}$. Similarly to the β_0 case, in Fig. 3.4 we show the $\gamma - \Omega_M^0$ posterior, again, in agreement with the corresponding result of Ref. [179].

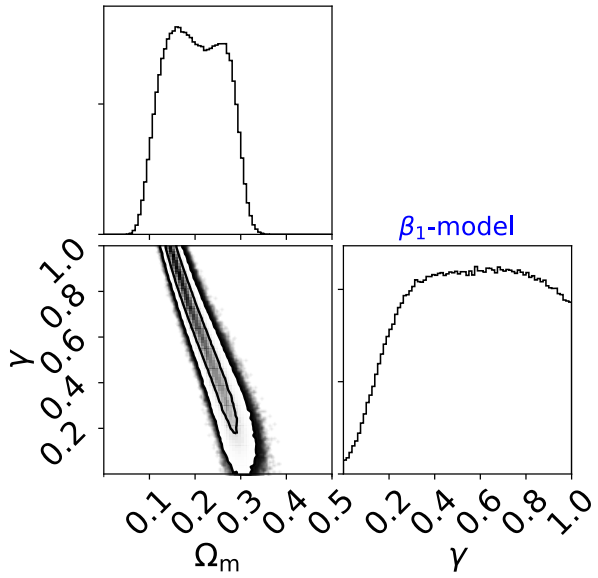

Figure 3.4: The same as in Fig. 3.2, but for the β_1 model.

Additionally, in Fig. 3.5 we demonstrate the interdependences of r, b, the quantity $(c_g^2-1)(c_f^2-1)$, and γ. From our discussions in the previous section, we expect this submodel to give the speed of gravity waves equal to the speed of light for the cases with $r_\infty = \gamma = 1/\sqrt{3}$, where the background metrics are proportional, as well as for the singly-coupled corners with $\gamma = 0$. The right panel of Fig. 3.5 presents the dependence of $(c_g^2-1)(c_f^2-1)|_{z=0}$ on the value of γ as a result of our numerical scans. We first notice that no viable combinations of the parameters provide c_g and c_f both larger or smaller than the speed of light, as $(c_g^2-1)(c_f^2-1)$ is always negative or zero. The plot also shows two points with $(c_g^2-1)(c_f^2-1)=0$, one of which being the obvious limit of single coupling with $\gamma = 0$, and the other one, as expected, corresponding to the case of proportional backgrounds with $\gamma = 1/\sqrt{3}$, depicted by the vertical, red line. This becomes more clear by looking at the left and the middle panels of Fig. 3.5, showing r

and b versus γ. The red lines in the plots show that indeed $\gamma = 1/\sqrt{3}$ corresponds to $r = 1/\sqrt{3}$ and $b = 1$, as expected. Also note that b is always positive for all the cosmologically viable points in the parameter space of this model. Although most of the original, cosmologically viable points are now excluded and the model is highly constrained, our results show that there still remain some freedom in choosing β_1 for the fixed $\gamma = 1/\sqrt{3}$. It is also interesting to note that the preferred values of $\Omega_{\rm M}^0$ are smaller than the ΛCDM value of ~ 0.3. In summary, as expected, the viable points in the parameter space of the model correspond to the scenarios which do not represent the full dynamics of the doubly-coupled model. One remaining region is the singly-coupled limit, and the other one corresponds to the cases where the background metrics are proportional, and we again effectively have only one dynamical metric at work. In this latter case, the model is effectively equivalent to ΛCDM, at the level of the background (and linear perturbations [181]).

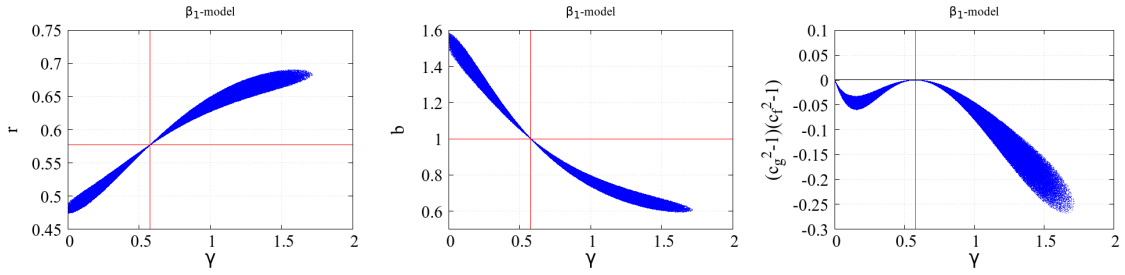

Figure 3.5: The same as in Fig. 3.3, but for the doubly-coupled β_1 model where all the interaction parameters β_n are set to zero except for β_1. In this case, the only parts of the parameter space that are left after imposing $(c_g^2 - 1)(c_f^2 - 1) = 0$ are the singly-coupled submodel characterised by $\gamma = 0$, and the solutions with the two background metrics being proportional, with $\gamma = 1/\sqrt{3}$, illustrated by the red lines in the plots.

• **β_2 model**: Fig. 3.6 shows the $\gamma - \Omega_{\rm M}^0$ posterior for the β_2 model. Fig. 3.7 additionally demonstrates the viable samples for the β_2 model in $r - \gamma$, $b - \gamma$, and $(c_g^2 - 1)(c_f^2 - 1) - \gamma$ planes. All the panels clearly show

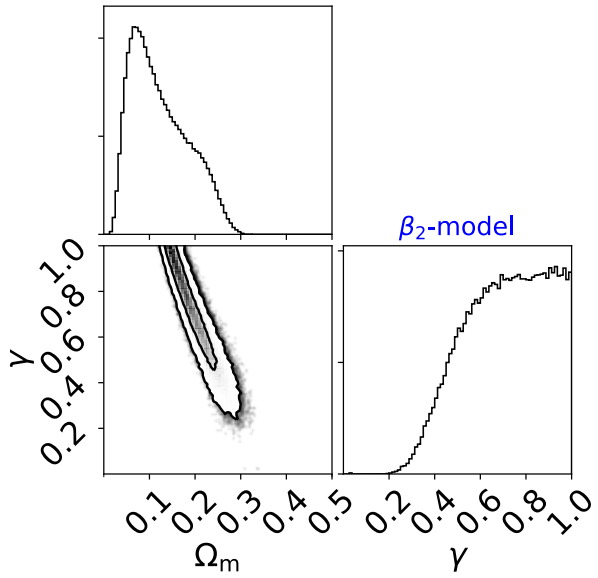

Figure 3.6: The same as in Fig. 3.2, but for the β_2 model.

that the singly-coupled subset of the parameter space (with $\gamma = 0$) is not viable cosmologically as there are no points with $\gamma = 0$ that fit the data. This is in agreement with the results of Ref. [206]. The model, however, provides excellent fits to the data for $\gamma \gtrsim 0.3$. Looking now at the right panel of Fig. 3.7, we see that the only points in the parameter space that are consistent with $(c_g^2 - 1)(c_f^2 - 1) = 0$ today, i.e. with the bounds from the GW observations, are the ones for which $\gamma = 1$, meaning that the metrics are proportional. These points correspond to $b = 1$ (see the middle panel). This is in agreement with our findings in the previous section for the β_2 model, with $r_\infty = \gamma = 1$ for proportional metrics. For all the other cosmologically viable points the tensor modes of one of the two metrics $g_{\mu\nu}$ and $f_{\mu\nu}$ travel faster and the other ones travel slower than light.

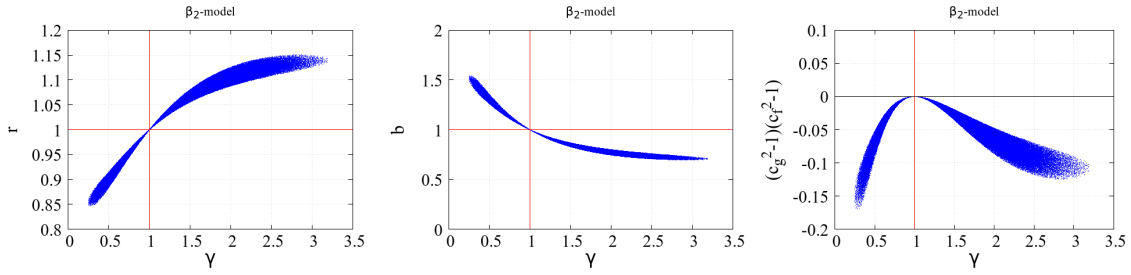

Figure 3.7: The same as in Figs. 3.3 and 3.5, but for the doubly-coupled β_2 model where all interaction parameters β_n are set to zero except for β_2. In this case, the only part of the parameter space consistent with $(c_g^2 - 1)(c_f^2 - 1) = 0$ is the one corresponding to the two background metrics being proportional, with $\gamma = 1$.

3.4.2 *Two-parameter models*

Let us now turn on two of the interaction parameters β_n and let them vary. As we argued earlier, many of these submodels are physically equivalent because of the symmetry of the theory. We therefore study four representative cases of $\beta_0\beta_1$, $\beta_0\beta_2$, $\beta_1\beta_2$, and $\beta_1\beta_3$ models. Note that even though for example the model with only β_1 turned on is identical to the model with only β_3 turned on, when the two parameters are both nonzero the resulting two-parameter model can in general be very different from the single-parameter ones, with generally richer phenomenologies. The reason is that the two parameters can take two different values, making the model different from the cases with only one of the parameters left free.

The results of our MCMC explorations for these models are presented in Fig. 3.8, where r computed at the present time is given in terms of the coupling ratio γ. The colour code shows the values of $\log_{10}|(c_g^2 - 1)(c_f^2 - 1)|$.

• **$\beta_1\beta_2$ and $\beta_1\beta_3$ models**: Looking at the two upper panels of Fig. 3.8 for these models, we observe an interesting feature. The points in the parameter space of both models for which $|(c_g^2 - 1)(c_f^2 - 1)|$ is small, seem to be residing on a diagonal line. All the other points are excluded by gravitational

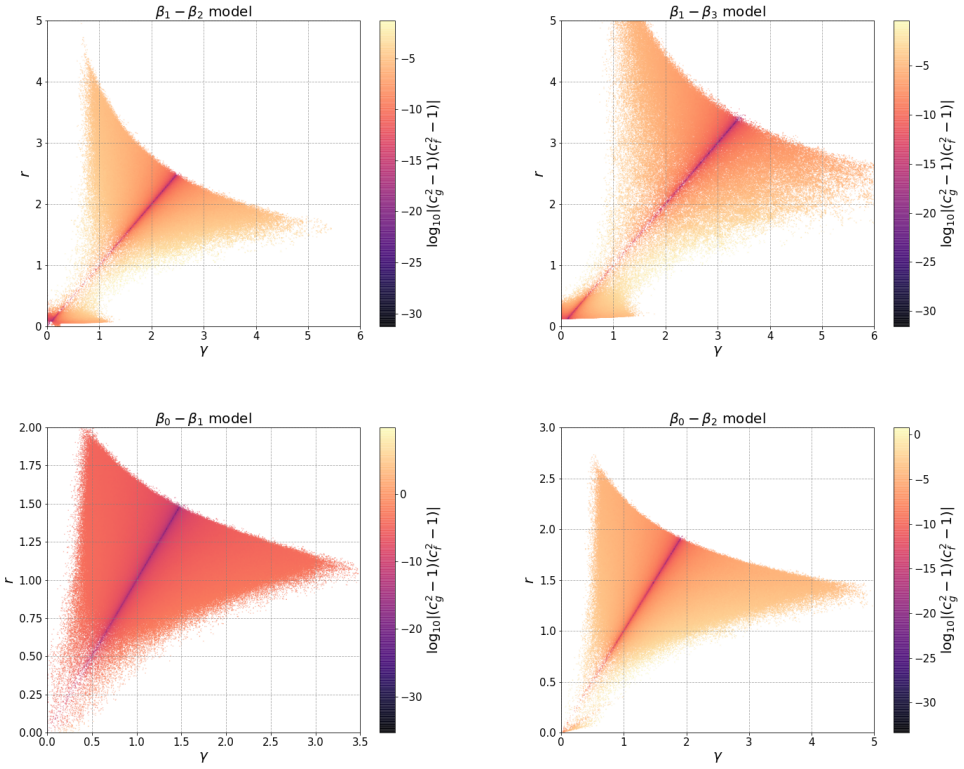

Figure 3.8: Results of the MCMC explorations for the two-parameter models $\beta_0\beta_1$, $\beta_0\beta_2$, $\beta_1\beta_2$ and $\beta_1\beta_3$. All the cosmologically viable points are shown in the $r-\gamma$ plane, and the colour in each panel shows the values of $\log_{10}|(c_g^2-1)(c_f^2-1)|$ as a measure for how fit the points are to the bounds on the speed of gravitational waves. Here, r and $\log_{10}|(c_g^2-1)(c_f^2-1)|$ are all computed at $z=0$.

waves, although they give good fits to the cosmological observations. Let us try to understand this favoured, thin region. We argued in the previous section that if r becomes equal to γ, even at one point over the history (in addition to the far in the past), the two background metrics of the model should be proportional at all times. This means that in particular if a point in the parameter space requires $r = \gamma$ at the present time, that point should correspond to proportional metrics. Now looking at the plots of r versus γ for both $\beta_1\beta_2$ and $\beta_1\beta_3$ models, we see that the very thin, line-like part of the favoured region is indeed the $r = \gamma$ line. This therefore shows that one main region with $(c_g^2 - 1)(c_f^2 - 1) \approx 0$ corresponds in fact to the cases with proportional backgrounds. The other tiny region with $(c_g^2 - 1)(c_f^2 - 1)$ being very small is the one in the vicinity of $\gamma = 0$. The plots are therefore consistent with our analytical arguments in the previous section that only singly-coupled submodels or the ones with the two background metrics being proportional are consistent with the speed of gravitational waves being the same as the speed of light. The observations of gravitational waves therefore highly constrain these two bigravity models as it was the case also for the single-parameter models. Note that the upper cuts in the plots are the result of the finite ranges which we have chosen in our MCMC scans for the β_n parameters. We have checked that by increasing these ranges the cuts on the plots systematically move upwards, but the main features do not change — the thin, favoured regions only extend to larger γ and r.

• **$\beta_0\beta_1$ and $\beta_0\beta_2$ models**: Let us now investigate the two $\beta_0\beta_1$ and $\beta_0\beta_2$ models, by studying the two lower panels of Fig. 3.8. Overall, the same features as in the previous models of $\beta_1\beta_2$ and $\beta_1\beta_3$ can be seen here, especially that proportional backgrounds survive the bounds on the speed of gravitational waves. This can be seen again as a thin $r = \gamma$ line. There is however an interesting difference in these two models compared to the previous ones.

The parameters β_1 and β_2 being zero in each case while γ is also set to zero corresponds to ΛCDM, with β_0 playing the role of the cosmological

constant. We may therefore expect a large concentration of cosmologically viable points in the $\gamma \approx 0$ region. Even though this region does exist, as is better visible for the $\beta_0\beta_1$ model, the majority of the viable points seem to be clustering around large γ, especially for the $\beta_0\beta_2$ model. In order to understand this, let us look at Figs. 3.2 and 3.6 for the single-parameter, β_0 and β_2 models. It is clear from these figures that the models act in opposite ways. While the β_0 model favours small γ, β_2-model does not admit γ smaller than ~ 0.3. Although we may expect the entire range of γ to be covered by turning on both of the parameters, our numerical investigations show that the points in the parameter space of the $\beta_0\beta_2$ model fit the cosmological observations better when β_0 is not zero and γ is large. That is why the density of the points in the figures is higher at large γ, where the model deviates significantly from the singly-coupled scenario. The same holds for the $\beta_0\beta_1$ model, although in that case the singly-coupled submodel is less disfavoured. This can be understood by looking at Fig. 3.4 for the single-parameter, β_1 model, where the plots show that small γ are cosmologically viable, contrary to the β_2 model.

3.4.3 *Further remarks*

Before we end the discussions of our numerical investigation, let us present the results of our MCMC scans for all the two-parameter models of $\beta_1\beta_2$, $\beta_1\beta_3$, $\beta_0\beta_1$, and $\beta_0\beta_2$, as well as the single-parameter models of β_1 and β_2, now in terms of the speed of the gravitational waves corresponding to the two metrics of the theory, $g_{\mu\nu}$ and $f_{\mu\nu}$. These have been shown in Fig. 3.9. In order to see how far each cosmologically viable point in the parameter space is from the proportional backgrounds, we colour-code the points by the value of $|b-1|$. All the quantities c_g, c_f, and b have been computed at the present time, i.e. at $z = 0$.

First of all, the plots confirm our analytical arguments in the previous section that having $c_g = 1$ ($c_f = 1$) automatically implies $c_f = 1$ ($c_g = 1$),

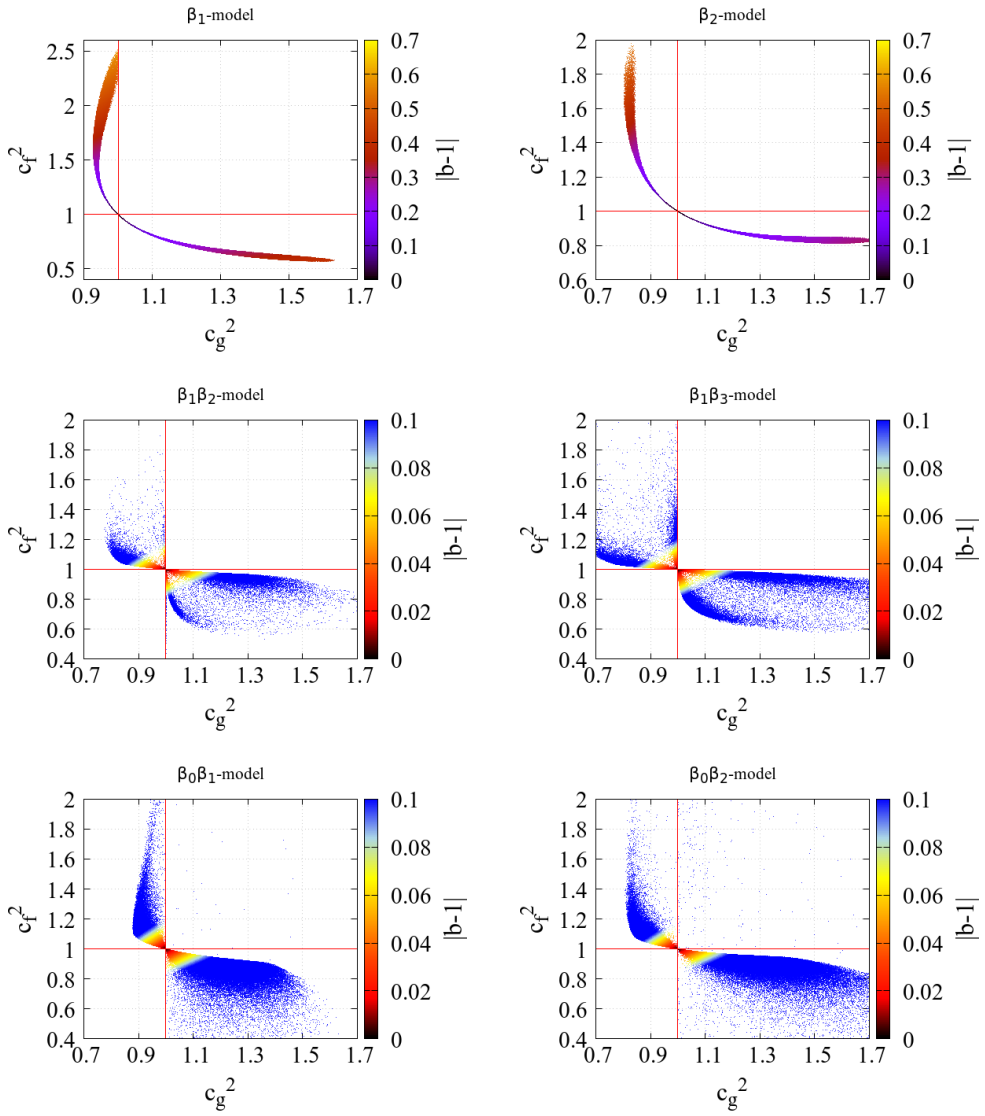

Figure 3.9: MCMC samples showing the values of the speed of gravitational waves for the tensor modes corresponding to the two metrics $g_{\mu\nu}$ and $f_{\mu\nu}$ for the two-parameter models of $\beta_1\beta_2$, $\beta_1\beta_3$, $\beta_0\beta_1$, and $\beta_0\beta_2$, as well as the single-parameter β_1 and β_2 models. The colour shows the value of $|b-1|$ at each point in the parameter space, as a measure of the deviation from proportional backgrounds (with $b = 1$). The red, vertical and horizontal lines show $c_g = 1$ and $c_f = 1$, respectively. Again, all the quantities have been computed at the present time ($z = 0$).

unless the theory is singly-coupled. In addition, the plots also show that $c_f = c_g = 1$ is equivalent to $b = 1$, i.e. it corresponds to proportional backgrounds, as expected. These can clearly be seen in all the panels. Let us first focus on the single-parameter cases of β_1 and β_2, i.e. the first two upper panels of Fig. 3.9. The intersections of the $c_g = 1$ and $c_f = 1$ lines in both models correspond to the proportional backgrounds, as $b = 1$ at those points. In addition, for the β_1 model we see that there are points for which $c_g^2 = 1$ while c_f^2 takes larger values (~ 2.3). This is fully consistent with our previous discussions that the β_1 model admits cosmologically viable singly-coupled solutions — these are the points with $c_g = 1$ and therefore consistent with the GW observations. The β_2 model, on the other hand, does not allow singly-coupled models consistent with cosmological observations, and we therefore do not see any points in the β_2 panel of Fig. 3.9 with $c_g = 1$ and $c_f \neq 1$. Note that in our analysis where we work with γ instead of α and β, the singly-coupled models are captured only by $g_{\mu\nu}$ being the physical metric, as we fix α to unity and therefore $\gamma = \beta$. That is why we do not see any points with $c_f = 1$ and $c_g \neq 1$ for the β_1 model. Let us now focus on the two-parameter models. As we discussed above, the $\beta_0\beta_1$ and $\beta_0\beta_2$ models do not favour singly-coupled solutions, and that is why we do not see many points in the corresponding panels of Fig. 3.9 with $c_g = 1$ and $c_f \neq 1$. Out of the two other two-parameter models of $\beta_1\beta_2$ and $\beta_1\beta_3$, we see that in the latter case there is a concentration of cosmologically favoured samples along the vertical line of $c_g^2 = 1$ even with $c_f^2 \neq 1$ in the $\beta_1\beta_2$ and $\beta_1\beta_3$ panels of Fig. 3.9. This is again consistent with our findings above that singly-coupled bigravity is not disfavoured in the $\beta_1\beta_3$ model.

3.5 CONCLUSIONS

In this chapter we have extensively studied the implications of the recently detected gravitational waves from a neutron star merger and their elec-

tromagnetic counterpart on the viability of the doubly-coupled theory of bimetric gravity. As a result we have identified the regions of the parameter space that are consistent with both cosmological observations and gravitational wave measurements. We have been interested in models that provide an alternative explanation for the late-time acceleration of the Universe, and therefore require an interaction (or mass) scale of the order of the present value of the Hubble parameter (i.e. $m \sim H_0$). Our studies have been based on both an analytical investigation of cosmic evolution and propagation of tensor modes in the theory, as well as a numerical exploration of the parameter space of the models using MCMC inference. We have demonstrated that the only regions of the parameter space that survive both the cosmological and gravitational wave constraints are those with the two background metrics being proportional or the singly-coupled submodels. Our findings therefore demonstrate that the theory is strongly constrained by the bounds on the speed of gravity waves if it is considered as the mechanism behind cosmic acceleration.

The cases with proportional backgrounds are particularly interesting for various reasons [181]. First of all, the background evolution of the Universe as well as linear perturbations mimic those of the ΛCDM model, and the model is therefore consistent with all the existing cosmological observations. This also means that the model does not suffer from any ghost or gradient instabilities, which are the typical drawbacks of singly-coupled cosmological scenarios, in the (visible) sector where the cosmological perturbations are coupled to matter. The model is however expected to deviate from general relativity, and therefore ΛCDM, at the nonlinear level and in the early Universe such as the radiation era, where a vector instability in the (hidden) sector decoupled from matter would have to be cured by an as yet unknown UV completion. The expected nonlinear deviations from general relativity in the late Universe open up an interesting route for further tests of the theory using the observations of structure formation and evolution at nonlinear scales. In addition, graviton mass eigenstates can be diagonalised only

around the proportional backgrounds, and therefore the notion of spin-2 mass makes sense only in those cases — singly-coupled bigravity does not admit proportional metrics in the presence of matter. Moreover, the effective metric of the doubly-coupled theory, which is the one that couples to matter, corresponds to the massless modes at the linear level, while the massive modes are fully decoupled; the massive and massless modes however mix at the nonlinear level.

We therefore conclude that the recent, tight constraints on the speed of gravitational waves leave us with a highly constrained corner of bigravity which is theoretically healthy at low energies[12] and observationally viable. It remains to be seen whether the model will also fit the cosmological observations at the nonlinear level, or will be ruled out; we leave the investigation of this interesting question for future work.

3.6 APPENDIX: TENSOR MODES

Here we present the detailed derivation of tensor perturbations and their propagation equations in doubly-coupled bimetric gravity. We present the calculations in the metric formalism at the level of the equations of motion, as well as at the action level, both in metric and vierbein formalisms.

Derivation from equations of motion. — Here our starting point is the full (modified) Einstein equations for the two metrics $g_{\mu\nu}$ and $f_{\mu\nu}$, which are given by (see Ref. [181] for details)

12 These models are valid below the cut-off scale Λ_3 and are therefore well suited for a description of the late-time Universe.

$$(\mathbb{X}^{-1})^{(\mu}{}_{\alpha} G_g^{\nu)\alpha} + m^2 \sum_{n=0}^{3} (-1)^n \beta_n g^{\alpha\beta} (\mathbb{X}^{-1})^{(\mu}{}_{\alpha} Y^{\beta)}_{(n)\nu} =$$
$$= \frac{\alpha}{M_{\rm eff}^2} \sqrt{\frac{\det g_{\rm eff}}{\det g}} \left(\alpha (\mathbb{X}^{-1})^{(\mu}{}_{\alpha} T^{\nu)\alpha} + \beta T^{\mu\nu} \right) , \tag{3.41}$$

and

$$\mathbb{X}^{(\mu}{}_{\alpha} G_f^{\nu)\alpha} + m^2 \sum_{n=0}^{3} (-1)^n \beta_{4-n} f^{\alpha\beta} \mathbb{X}^{(\mu}{}_{\alpha} \hat{Y}^{\nu)}_{(n)\beta} =$$
$$= \frac{\beta}{M_{\rm eff}^2} \sqrt{\frac{\det g_{\rm eff}}{\det f}} \left(\alpha T^{\mu\nu} + \beta \mathbb{X}^{(\mu}{}_{\alpha} T^{\nu)\alpha} \right) , \tag{3.42}$$

where $G_g^{\mu\nu}$ and $G_f^{\mu\nu}$ are the Einstein tensors for $g_{\mu\nu}$ and $f_{\mu\nu}$, respectively, $T^{\mu\nu}$ is the stress-energy tensor corresponding to the effective metric $g^{\rm eff}_{\mu\nu}$, and the square-root matrices $\mathbb{X}$ and $\mathbb{X}^{-1}$ are defined through

$$\mathbb{X}^{\mu}{}_{\alpha} \mathbb{X}^{\alpha}{}_{\nu} \equiv g^{\mu\beta} f_{\beta\nu} , \tag{3.43}$$
$$(\mathbb{X}^{-1})^{\mu}{}_{\alpha} (\mathbb{X}^{-1})^{\alpha}{}_{\nu} \equiv f^{\mu\beta} g_{\beta\nu} . \tag{3.44}$$

Now, the linear metric perturbations for g and f tensor modes $h_{g+/\times}$ and $h_{f+/\times}$ can be written as

$$\begin{aligned} {\rm d}s_g^2 = -N_g^2 {\rm d}t^2 &+ a_g^2 [(1+h_{g+}){\rm d}x^2 + (1-h_{g+}){\rm d}y^2 \\ &+ {\rm d}z^2 + 2h_{g\times} dx dy] , \end{aligned} \tag{3.45}$$
$$\begin{aligned} {\rm d}s_f^2 = -N_f^2 {\rm d}t^2 &+ a_f^2 [(1+h_{f+}){\rm d}x^2 + (1-h_{f+}){\rm d}y^2 \\ &+ {\rm d}z^2 + 2h_{f\times} {\rm d}x {\rm d}y] . \end{aligned} \tag{3.46}$$

Plugging these into Eqs. (3.43) and (3.44) we find

$$\mathbb{X}^{\alpha}{}_{\beta}=\begin{pmatrix} \frac{N_f}{N_g} & 0 & 0 & 0 \\ 0 & \frac{a_f}{a_g}+\frac{a_f}{a_g}\frac{(h_{f+}-h_{g+})}{2} & \frac{a_f}{a_g}\frac{(h_{f\times}-h_{g\times})}{2} & 0 \\ 0 & \frac{a_f}{a_g}\frac{(h_{f\times}-h_{g\times})}{2} & \frac{a_f}{a_g}+\frac{a_f}{a_g}\frac{(h_{f+}-h_{g+})}{2} & 0 \\ 0 & 0 & 0 & \frac{a_f}{a_g} \end{pmatrix}, \tag{3.47}$$

and

$$(\mathbb{X}^{-1})^{\alpha}{}_{\beta}=\begin{pmatrix} \frac{N_g}{N_f} & 0 & 0 & 0 \\ 0 & \frac{a_g}{a_f}-\frac{a_g}{a_f}\frac{(h_{f+}-h_{g+})}{2} & \frac{a_g}{a_f}\frac{(h_{g\times}-h_{f\times})}{2} & 0 \\ 0 & \frac{a_g}{a_f}\frac{(h_{g\times}-h_{f\times})}{2} & \frac{a_g}{a_f}-\frac{a_g}{a_f}\frac{(h_{f+}-h_{g+})}{2} & 0 \\ 0 & 0 & 0 & \frac{a_g}{a_f} \end{pmatrix}, \tag{3.48}$$

for the square-root matrices at the linear order.

Having these expressions for $\mathbb{X}$ and $\mathbb{X}^{-1}$, the nonvanishing parts of the tensor sector of the effective metric can be shown to be

$$\delta g^{\rm eff}_{11}=-\delta g^{\rm eff}_{22}\equiv a^2 h_{{\rm eff}+}=a\left(\alpha a_g h_{g+}+\beta a_f h_{f+}\right), \tag{3.49}$$

$$\delta g^{\rm eff}_{12}=\delta g^{\rm eff}_{21}\equiv a^2 h_{{\rm eff}\times}=a\left(\alpha a_g h_{g\times}+\beta a_f h_{f\times}\right). \tag{3.50}$$

By using Eqs. (3.47) and (3.48) in the field equations we recover Friedmann equations at the background level, while at the linear order we obtain the propagation equations for the tensor modes $h_{g+/\times}$ and $h_{f+/\times}$,

$$\begin{aligned}
\frac{1}{N_g^2}\ddot{h}_{g+/\times} &+ (3\frac{H_g}{N_g} - \frac{\dot{N}_g}{N_g^3})\dot{h}_{g+/\times} - \frac{1}{a_g^2}\nabla^2 h_{g+/\times} \\
&+ A(h_{f+/\times} - h_{g+/\times}) = 0\,, \qquad (3.51)\\
\frac{1}{N_f^2}\ddot{h}_{f+/\times} &+ (3\frac{H_f}{N_f} - \frac{\dot{N}_f}{N_f^3})\dot{h}_{f+/\times} - \frac{1}{a_f^2}\nabla^2 h_{f+/\times} \\
&+ B(h_{g+/\times} - h_{f+/\times}) = 0\,, \qquad (3.52)
\end{aligned}$$

where

$$\begin{aligned}
A &\equiv r\frac{1}{M_{\rm eff}^2}\left(\alpha\beta p(\alpha+\beta r)\left(\alpha + \frac{\beta N_f}{N_g}\right)\right. \\
&- \left. m^2 M_{\rm eff}^2\left(\beta_1 + \frac{N_f\left(\beta_2 + \beta_3 r\right)}{N_g} + \beta_2 r\right)\right)\,, \qquad (3.53)\\
B &\equiv \frac{1}{r}\frac{1}{M_{\rm eff}^2}\left(\alpha\beta p(\beta + \alpha\frac{1}{r})\left(\beta + \frac{\alpha N_g}{N_f}\right)\right. \\
&- \left. m^2 M_{\rm eff}^2\left(\beta_3 + \frac{N_g\left(\beta_2 + \beta_1\frac{1}{r}\right)}{N_f} + \beta_2\frac{1}{r}\right)\right)\,, \qquad (3.54)
\end{aligned}$$

with p here being the pressure of the matter sector.

It should be noted that these two propagation equations can be written in a form that manifestly shows the symmetry of the interaction terms (i.e. the symmetry of the mass matrix). This can be seen by rewriting the propagation equations as

$$\frac{d}{dt}\left(\frac{a_g^3}{N_g}\dot{h}_{g+/\times}\right) - a_g^3 N_g \frac{1}{a_g^2}\nabla^2 h_{g+/\times} + a_g^3 N_g A(h_{f+/\times} - h_{g+/\times}) = 0\,, \tag{3.55}$$

$$\frac{d}{dt}\left(\frac{a_f^3}{N_f}\dot{h}_{f+/\times}\right) - a_f^3 N_f \frac{1}{a_f^2}\nabla^2 h_{f+/\times} + a_g^3 N_g A(h_{g+/\times} - h_{f+/\times}) = 0\,, \tag{3.56}$$

where now the same factor of $a_g^3 N_g A$ appears in front of $h_{f+/\times}$ in the first equation and in front of $h_{g+/\times}$ in the second equation.

Derivation of the quadratic action. — In order to facilitate the comparison with the results of Refs. [192, 193] let us also present the calculation of the graviton mass matrix at the level of the action. In this analysis we ignore the matter sector, i.e. we study a fully dark energy dominated epoch.

First of all, by varying the background part of the action with respect to the lapses and scale factors we recover the background equations of motion

$$3H_g^2 = m^2 B_0\,, \qquad 3H_f^2 = m^2 B_1\,, \tag{3.57}$$

$$\ddot{a}_g = \frac{1}{2}m^2 a_g N_g^2 \left(B_0 + (\beta_1 + 2\beta_2 r + \beta_3 r^2)\left(\frac{N_f}{N_g} - r\right)\right) + a_g H_g \dot{N}_g - \frac{1}{2}a_g H_g^2 N_g^2\,, \tag{3.58}$$

$$\ddot{a}_f = \frac{1}{2}m^2 a_f N_f^2 \left(B_1 + (\beta_3 + 2\frac{\beta_2}{r} + \frac{\beta_1}{r^2})\left(\frac{N_g}{N_f} - \frac{1}{r}\right)\right) + a_f H_f \dot{N}_f - \frac{1}{2}a_f H_f^2 N_f^2\,. \tag{3.59}$$

Our objective here is to obtain the mass terms of the gravitational waves. In principle, the calculation of the quadratic action is straightforward, but

the subtle point here is that besides the potential terms of bigravity, also the two Einstein-Hilbert terms contribute with additional terms quadratic in $h_{g+/\times}$ and $h_{f+/\times}$. Let us exemplify this by looking at the kinetic term of the g-sector. First of all, there is a contribution from the volume factor, which reads as

$$S^{(2)} \supset -\frac{M_{\rm eff}^2}{2}\int \mathrm{d}^4x \left(-\frac{N_g a_g^3}{2}(h_{g\times}^2 + h_{g+}^2)\right)\bar{R}_g\,, \tag{3.60}$$

where $\bar{R}_g$ is the background part of the Ricci scalar, which is given by

$$\bar{R}_g = 6\frac{a_g N_g \ddot{a}_g - a_g \dot{a}_g \dot{N}_g + N_g \dot{N}_g^2}{a_g^2 N_g^3}\,. \tag{3.61}$$

Additional contributions come from some of the terms in the perturbed part of the Ricci scalar, namely from

$$\begin{aligned} S^{(2)} \supset -\frac{M_{\rm eff}^2}{2}\int \mathrm{d}^4x [f(t)(h_{g+}\dot{h}_{g+} &+ h_{g\times}\dot{h}_{g\times}) + \\ F(t)(h_{g+}\ddot{h}_{g+} &+ h_{g\times}\ddot{h}_{g\times})]\,, \end{aligned} \tag{3.62}$$

where

$$f(t) = \frac{a_g}{N_g^2}\left(2a_g^2\dot{N}_g - 8a_g N_g \dot{a}_g\right),\; F(t) = -2\frac{a_g^3}{N_g}\,. \tag{3.63}$$

The corresponding contributions to the mass matrix are given by

$$S^{(2)} \supset -\frac{M_{\rm eff}^2}{2}\int \mathrm{d}^4x \frac{\ddot{F}(t) - \dot{f}(t)}{2}(h_{g+}^2 + h_{g\times}^2)\,. \tag{3.64}$$

Note that we needed to divide by a factor of 2 in the last expression, because in the original terms only the variations with respect to the fields under the time derivatives could contribute to the mass terms in the equations of motion.

These contributions should be added to the contributions from the potential terms. In order to find the latter we also need the second-order piece of the $\mathbb{X}^{\mu}{}_{\nu}$ matrix, the nonvanishing components of which are found to be

$$\delta^{(2)}\mathbb{X}^{1}{}_{1} = \delta^{(2)}\mathbb{X}^{2}{}_{2} = -r\sum_{\star=\times,+}\frac{h_{f\star}^{2}-3h_{g\star}^{2}+2h_{f\star}h_{g\star}}{8}\,, \tag{3.65}$$

$$\delta^{(2)}\mathbb{X}^{1}{}_{2} = \delta^{(2)}\mathbb{X}^{2}{}_{1} = -r\frac{h_{f\times}h_{g+}-h_{g\times}h_{f+}}{2}\,. \tag{3.66}$$

Combining all the potential terms and dropping an overall factor of $1/2$ from the action we obtain the graviton mass terms

$$S^{(2)} \supset M_{\rm eff}^{2}\int \mathrm{d}^{4}x\frac{1}{2}\sum_{\star=\times,+}\mathbb{M}^{IJ}h_{I\star}h_{J\star}\,, \tag{3.67}$$

where the mass matrix is found to be

$$\begin{aligned}\mathbb{M}^{gg} &= \mathbb{M}^{ff} = -\mathbb{M}^{gf} = -\mathbb{M}^{fg}\\ &= m^{2}a_{g}^{3}N_{g}r\left(\beta_{1}+\beta_{2}(\frac{N_{f}}{N_{g}}+r)+\beta_{3}\frac{N_{f}}{N_{g}}r\right).\end{aligned} \tag{3.68}$$

Note particularly that we have recovered the same interaction terms as in Eqs. (3.55) and (3.56).

In Refs. [192, 193] the interaction sector has been written in terms of the constrained metric vierbeins as

$$
\begin{aligned}
S_{\text{interaction}} &= m^2 M_{\text{eff}}^2 \sum_{IJKL} m^{IJKL} \times \\
&\times \int d^4x \epsilon_{abcd} \epsilon^{\mu\nu\rho\sigma} e^a_{I\mu} e^b_{J\nu} e^c_{K\rho} e^d_{L\sigma} \,, \qquad (3.69)
\end{aligned}
$$

where the tetrad fields (or vierbeins) are defined through

$$
g^I_{\mu\nu} = \eta_{ab} e^a_{I\mu} e^b_{I\nu} \,. \qquad (3.70)
$$

Here I labels the two metrics, $I = \{g, f\}$, μ and ν are the covariant indices, and a and b are the indices in the local Lorentz frame. The interaction matrix m^{IJKL} is fully symmetric and its components in terms of the $\beta_{0,\ldots,4}$ parameters are given by

$$
m^{gggg} = \frac{\beta_0}{24} \,, \quad m^{fggg} = \frac{\beta_1}{24} \,, \qquad (3.71)
$$

$$
m^{ffgg} = \frac{\beta_2}{24} \,, \quad m^{fffg} = \frac{\beta_3}{24} \,, \quad m^{ffff} = \frac{\beta_4}{24} \,, \qquad (3.72)
$$

with the other components being trivially related to the ones above due to the total symmetry of the m^{IJKL} matrix.

In order to derive the mass sector of the quadratic action in the vierbein formalism we first derive the tensor perturbations of the vierbeins by linearising Eq. (3.70). As a result, for the $e^a_{I\mu}$ matrix we have

$$
e_I = \begin{pmatrix}
N_I & 0 & 0 & 0 \\
0 & a_I(1 + \frac{1}{2} h_{I+}) & \frac{a_I}{2} h_{I\times} & 0 \\
0 & \frac{a_I}{2} h_{I\times} & a_I(1 - \frac{1}{2} h_{I+}) & 0 \\
0 & 0 & 0 & a_I
\end{pmatrix} . \qquad (3.73)
$$

The total mass matrix is built up from two different parts of the action as before.

The first (diagonal) contribution comes from the Einstein-Hilbert terms in the action, and is given by

$$S^{(2)}_{\text{masses, EH}} = -\frac{M^2_{\text{eff}}}{2}\int \mathrm{d}^4x \sum_{\star=\times,+} \delta m^2_{gg} h^g_\star h^g_\star + (g \to f)\,, \tag{3.74}$$

where we have found that

$$\delta m^2_{gg} = -\frac{N_g a_g^3}{4}\bar{R}_g - \frac{\ddot{F}(t) - \dot{f}(t)}{4}\,, \tag{3.75}$$

$$\delta m^2_{ff} = \delta m^2_{gg}(g \to f)\,. \tag{3.76}$$

Here $F(t)$ and $f(t)$ are the same functions as in Eq. (3.63).

The second part comes from the expansion of the potential term (3.69) to second order in the gravitons. Direct calculation gives

$$S^{(2)}_{\text{masses, pot}} = \frac{1}{4}m^2 M^2_{\text{eff}}\int \mathrm{d}^4x \sum_{\star=\times,+} \hat{m}^2_{IJ} h^I_\star h^J_\star\,, \tag{3.77}$$

where

$$\hat{m}^2_{gg} = N_g a_g^3\left(\beta_2 r\frac{N_f}{N_g} + \beta_1 r + \beta_1\frac{N_f}{N_g} + \beta_0\right), \tag{3.78}$$

$$\hat{m}^2_{ff} = N_f a_f^3\left(\beta_3\frac{1}{r} + \beta_2\frac{1}{r}\frac{N_g}{N_f} + \beta_4 + \beta_3\frac{N_g}{N_f}\right), \tag{3.79}$$

$$\hat{m}^2_{fg} = \hat{m}^2_{gf} = N_g a_g^3 r\left(\beta_2\frac{N_f}{N_g} + \beta_3 r\frac{N_f}{N_g} + \beta_1 + \beta_2 r\right). \tag{3.80}$$

Adding the two sectors, making use of the background equations of motion (3.57), (3.58), and (3.59), and dropping an overall factor of $1/2$ from the

action, we retrieve the action (3.67) with the mass matrix given exactly by (3.68).

The massless and massive modes. — The dynamics of the two gravitons can be better understood by switching to the canonically normalised basis

$$h_{I\star} = D_I \bar{h}_{I\star}\,, \tag{3.81}$$

where $\star = +/\times$ and we have defined

$$D_I \equiv \left(\frac{N_I}{a_I^3}\right)^{1/2}\,. \tag{3.82}$$

In this new basis the mass matrix reads

$$\overline{\mathbb{M}} = \mathcal{M}^2 \begin{pmatrix} D_g^2 & -D_g D_f \\ -D_g D_f & D_f^2 \end{pmatrix}\,, \tag{3.83}$$

where $\mathcal{M}^2 = \mathbb{M}^{gg}$. In this basis the graviton equations read

$$\ddot{\bar{h}}_{I\star} - c_I^2 \frac{N^2}{a^2}\nabla^2 \bar{h}_{I\star} + \overline{\mathbb{M}}^{IJ}\bar{h}_{J\star} - D_I \frac{\mathrm{d}^2}{\mathrm{d}t^2}\left(\frac{1}{D_I}\right)\bar{h}_{I\star} = 0\,, \tag{3.84}$$

where we have identified the speeds of the waves in the effective conformal time (for which photons have a normalised speed $c_\gamma = 1$):

$$c_I = \frac{aN_I}{a_I N}. \tag{3.85}$$

It is easy to see that this mass matrix always has a massless and a massive eigenmodes given by

$$\overline{V}_0 = \begin{pmatrix} 1 \\ D_g/D_f \end{pmatrix}\,,\ \overline{V}_m = \begin{pmatrix} 1 \\ -D_f/D_g \end{pmatrix}\,, \tag{3.86}$$

with eigen-mass-square being

$$M^2a^2 = \mathcal{M}^2(D_g^2 + D_f^2)\,, \tag{3.87}$$

where the factor of a^2 has been included to comply with the usual definition for the mass of graviton in FLRW space-times. In the case of proportional metrics, when $r = \gamma$, the above mass-eigenvectors reduce to

$$\overline{V}_0 = \begin{pmatrix} 1 \\ \gamma \end{pmatrix},\ \overline{V}_m = \begin{pmatrix} 1 \\ -\gamma^{-1} \end{pmatrix}, \tag{3.88}$$

which guarantees that one can diagonalise the system of dynamical equations (3.84) by simply adding linear combinations of the two propagation equations with constant coefficients.

Now, one can see that the canonically normalised massless eigenmode is associated to the effective graviton modes. Indeed, first of all, from Eqs. (3.49) and (3.50) we see that $h_{\rm eff} = \alpha D(\bar{h}_g + \gamma\bar{h}_f)$, with $D \equiv \sqrt{N/a^3}$. The canonically normalised version of this field is the massless mode $\bar{h}_0 \equiv \bar{h}_g + \gamma\bar{h}_f$. The massive mode, on the other hand, corresponds to the difference $\bar{h}_m = \bar{h}_g - \bar{h}_f/\gamma$.

Combining the equations of motion in (3.84) appropriately, we obtain

$$\ddot{\bar{h}}_{0\star} - \nabla^2\bar{h}_{0\star} - \frac{\ddot{a}}{a}\bar{h}_{0\star} = 0\,, \tag{3.89}$$

$$\ddot{\bar{h}}_{m\star} - \nabla^2\bar{h}_{m\star} + (M^2a^2 - \frac{\ddot{a}}{a})\bar{h}_{m\star} = 0\,. \tag{3.90}$$

Here we have used the fact that for the proportional backgrounds we have $D_I = a_I^{-1}$ if we pick the lapses as $N_I = a_I$. Moreover, recalling that

$$a_g = \frac{\alpha}{\alpha^2+\beta^2}a\,,\quad a_f = \frac{\beta}{\alpha^2+\beta^2}a\,, \tag{3.91}$$

we see that $D_I \mathrm{d}^2 \left(D_I^{-1} \right) / \mathrm{d}t^2 = \ddot{a}/a$. The first of these dynamical equations is the propagation equation of gravitons in general relativity, with the gravitons being massless but receiving a "pseudo"-mass of the form $-\ddot{a}/a$. The second one is the propagation equation for a massive graviton of mass M. Notice that for both modes the speed of propagation is one, and that (3.91) implies that the light cones for gravitons and photons coincide.

4

MIMETIC MASSIVE COSMOLOGY

In this chapter we study the first cosmological implications of a novel massive gravity theory, recently proposed by Chamseddine and Mukhanov, known as the *mimetic theory of massive gravity*. This is a theory of ghost-free massive gravity, which additionally contains a so-called *mimetic dark matter* component. In an echo of other modified gravity theories, there are self-accelerating solutions which contain a ghost instability. In the ghost-free region of parameter space, the effect of the graviton mass on the cosmic expansion history amounts to an effective negative cosmological constant, a radiation component, and a negative curvature term. This allows us to place constraints on the model parameters—particularly the graviton mass—by insisting that the effective radiation and curvature terms be within observational bounds. The late-time acceleration must be accounted for by a separate positive cosmological constant or other dark energy sector. We impose further constraints at the level of perturbations by demanding linear stability. We comment on the possibility of distinguishing this theory from ΛCDM with current and future large-scale structure surveys.

This chapter is based on: A. Solomon, V. Vardanyan, Y. Akrami,
Massive mimetic cosmology,
Phys. Lett. B **794** (2019) 135, arXiv:1902.08533.

4.1 INTRODUCTION

Chamseddine and Mukhanov have recently proposed [207, 208] a novel ghost-free theory of massive gravity in which one of the four Stückelberg scalars is constrained in the same way as in the mimetic theory of dark matter [209], spontaneously breaking Lorentz invariance. In this chapter, we study the immediate implications of this mimetic massive gravity for cosmological theory and observation.

From a field-theoretic perspective, general relativity is the unique theory (in four spacetime dimensions) of a massless spin-2 particle, or graviton. It is therefore natural to ask whether it is possible to endow the graviton with a non-zero mass, and what sort of theoretical structures would result [36]. A closely related line of inquiry asks whether it is possible for two or more gravitons to interact [210]. Most nonlinear realizations of such theories suffer from the so-called Boulware-Deser ghost instability [195]. As we have discussed earlier, the past decade has seen the construction of models which avoid this instability, allowing for the construction of ghost-free theories of massive gravity [37, 38, 40, 43–45, 211] and bimetric and multimetric gravity [44, 46, 47]. We refer the reader to the reviews [48, 49] on massive gravity and [51, 52] on bimetric gravity. The theory of mimetic massive gravity proposed in [207, 208] takes a new and alternative path to a ghost-free nonlinear theory of massive gravity.

A generic theory of massive gravity propagates six degrees of freedom, which should be thought of as the five helicity states of a massive graviton plus an additional, ghostly scalar. The easiest way to understand the degrees-of-freedom counting is to observe that a graviton mass breaks diffeomorphism invariance. This is a gauge symmetry and so can be restored by the addition of four Stückelberg scalars Φ^A, which propagate in addition to the two (now potentially massive) tensor modes of general relativity.

As an illustration, consider a Lorentz-invariant theory of massive gravity. In order to construct non-trivial, non-derivative interactions for the metric,

one requires a second "reference" metric. The simplest choice for this metric is that of flat space, $\eta_{\mu\nu}$, but the addition of this prior geometry breaks diffeomorphism invariance; for instance, there are preferred coordinate systems in which $\eta_{\mu\nu} = \text{diag}(-1, 1, 1, 1)$. But diffeomorphism invariance is simply a redundancy in description, and can be restored by the addition of redundant variables, i.e., replacing $\eta_{\mu\nu} \to \eta_{AB}\partial_\mu\Phi^A\partial_\nu\Phi^B$, where $\eta_{AB} = \text{diag}(-1, 1, 1, 1)$ and the four fields Φ^A transform as spacetime scalars. One can always, by means of a diffeomorphism, choose the unitary gauge in which $\Phi^A = x^A$, and we recover the original description of the theory in terms of a symmetry-breaking reference metric. Generic interaction terms for the graviton, e.g., generic functions of $g^{\mu\alpha}\eta_{AB}\partial_\alpha\Phi^A\partial_\nu\Phi^B$, will lead to dynamics for each of these four scalars, in addition to the two modes of general relativity, for a total of six degrees of freedom.

At the linear level, i.e., linearizing the metric about flat space in unitary gauge, $g_{\mu\nu} = \eta_{\mu\nu} + h_{\mu\nu}$ and $\Phi^A = x^A$, we find that one of the six degrees of freedom leads to a ghost instability unless we specifically arrange the mass term into the Fierz-Pauli form, $\mathcal{L}_{\text{mass}} \sim h_{\mu\nu}^2 - h^2$, in which case the dynamics of the ghostly mode take the form of a total derivative. Continuing this procedure at higher orders in perturbation theory—i.e., continually packaging ghostly operators into total derivative structures—leads uniquely to the non-linear massive gravity theory of de Rham, Gabadadze, and Tolley (dRGT) [37, 38].

The recent proposal of Chamseddine and Mukhanov takes a novel alternative approach to eliminating the dangerous ghostly mode [207, 208]. Noticing that the ghost can be associated to the Φ^0 Stückelberg mode, they propose imposing the constraint $g^{\mu\nu}\partial_\mu\Phi^0\partial_\nu\Phi^0 = -1$. This is motivated by a similar construction known as mimetic gravity [209], in which the constrained scalar winds up behaving like dark matter.[1] Mimetic massive gravity takes this constrained scalar to be one of the Stückelberg modes

1 For an earlier construction in which a constrained scalar mimics dark matter and dark energy, see [212].

of a massive graviton, eliminating the ghost. They propose the following action, designed to ensure stability at the linear level (notice that the mass term is not of the Fierz-Pauli form),

$$S = \int \mathrm{d}^4x\sqrt{-g}\left[\frac{M_{\rm pl}^2}{2}R + \frac{m^2M_{\rm pl}^2}{8}\left(\frac{1}{2}\bar{h}^2 - \bar{h}_{AB}^2\right) + \lambda(X+1)\right] + S_{\rm matter}, \quad (4.1)$$

with $X \equiv g^{\mu\nu}\partial_\mu\Phi^0\partial_\nu\Phi^0$, and

$$\bar{h}^{AB} \equiv g^{\mu\nu}\partial_\mu\Phi^A\partial_\nu\Phi^B - \eta^{AB}. \quad (4.2)$$

Internal indices (given by capital Roman letters) are raised and lowered with the Minkowski metric. The field equations are[2]

$$G_{\mu\nu} = \frac{1}{M_{\rm pl}^2}T_{\mu\nu} - \frac{2\lambda}{M_{\rm pl}^2}\partial_\mu\Phi^0\partial_\nu\Phi^0 + \frac{m^2}{2}\left(\bar{h}_{AB} - \frac{1}{2}\bar{h}\eta_{AB}\right)\left(\partial_\mu\Phi^A\partial_\nu\Phi^B - \frac{1}{4}\bar{h}^{AB}g_{\mu\nu}\right), \quad (4.3)$$

$$0 = \nabla_\mu\left[\frac{2\lambda}{M_{\rm pl}^2}\partial^\mu\Phi^0\delta_A^0 - \frac{m^2}{2}\left(\bar{h}_{AB} - \frac{1}{2}\bar{h}\eta_{AB}\right)\partial^\mu\Phi^B\right], \quad (4.4)$$

$$X = -1. \quad (4.5)$$

The last of these aligns $\dot{\Phi}^0$ with the lapse of $g_{\mu\nu}$. An upshot of this construction is that the constrained mode behaves as a pressureless fluid, i.e., this theory provides a natural (mimetic) dark matter candidate [207, 208].[3]

2 Note the sign differences between the right-hand side of the Einstein equations and the corresponding equation in [207], which is due to the mostly positive metric convention we employ.

3 One should note that the phenomenology of mimetic dark matter is still in the early stages of development compared to traditional particle dark matter models such as weakly interacting massive particles (WIMPs) or axions, and it is premature to consider mimetic gravity as a serious alternative to those models. For example, since the mimetic dark matter

We end this section by making a connection with the existing literature on Lorentz-violating massive gravity and demonstrating the absence of certain well-known features of Lorentz-invariant massive gravity, namely the van Dam-Veltman-Zakharov (vDVZ) discontinuity [214, 215] and the Higuchi bound [216]. The vDVZ discontinuity refers to the failure of linearized Lorentz-invariant massive gravity to reduce to general relativity in the massless limit; this requires nonlinear effects in order to restore general relativity in the Newtonian limit [58, 59]. The Higuchi bound is a stability bound for massive gravity on de Sitter space, placing a lower bound on the graviton mass, $m^2 \geq 2H^2$, with H the Hubble rate. It is well-known that breaking Lorentz invariance changes both of these conclusions dramatically [217, 218].

At the level of linear perturbations around flat space, the general SO(3)-invariant mass term in unitary gauge ($\Phi^A = x^A$) can be written as [217]

$$\mathcal{L}_{\text{mass}} = \frac{1}{8} M_{\text{pl}}^2 \left(m_0^2 h_{00}^2 + 2m_1^2 h_{0i}^2 - m_2^2 h_{ij}^2 + m_3^2 h_{ii}^2 - 2m_4^2 h_{00} h_{ii} \right). \tag{4.6}$$

The linearized mass term in (4.1) in unitary gauge is (treating λ as first-order)

$$\mathcal{L}_{\text{mass}} = \frac{m^2 M_{\text{pl}}^2}{8} \left(-\frac{1}{2} h_{00}^2 + 2h_{0i}^2 - h_{ij}^2 + \frac{1}{2} h_{ii}^2 - h_{00} h_{ii} \right) + \lambda h_{00}. \tag{4.7}$$

---

only interacts gravitationally with the Standard Model, we do not expect to have a thermal production mechanism, in contrast to many traditional dark matter scenarios such as WIMPs. Indeed, when the theory is shift-symmetric in Φ^0, the energy density of this component is set entirely by an integration constant and so is determined by initial conditions. It may also be necessary to tune the parameters of the model in order to obtain the right values of the dark matter density over the entire cosmic history, and higher-derivative effective field theory corrections play an important role [213]. We refer the reader to, e.g., [213] for discussions of the constraints that early-universe considerations place on the properties and evolution of mimetic dark matter throughout cosmic history.

The λ equation of motion sets $h_{00} = 0$, which we can impose in the action[4] to find

$$m_0^2 = m_4^2 = 0, \quad m_1^2 = m_2^2 = 2m_3^2 = 1. \tag{4.8}$$

This allows us to easily make contact with the existing literature on Lorentz-violating massive gravity. The analysis of [217] shows that for these m_i parameters, the Newtonian limit is the usual one, while the vDVZ discontinuity is absent. The analogue of the Higuchi bound in Lorentz-violating massive gravity was derived in [218], and for our values of the m_i parameters, it reduces simply to $H^2 > 0$, which is trivially satisfied.

4.2 FLAT-SPACE PERTURBATIONS

In this section, we briefly review the behavior of perturbations about flat space in mimetic massive gravity, as discussed in [207, 208]. This will place stability conditions on the theory which will be relevant when we move to cosmological solutions.

The equations of motion (4.3)–(4.5) in vacuum are solved by[5]

$$g_{\mu\nu} = \eta_{\mu\nu}, \qquad \Phi^A = x^A, \qquad \lambda = 0. \tag{4.9}$$

4 This is justified because, on shell, the h_{00} equation of motion simply sets the value of λ, while h_{00} drops out of the h_{ij} equations of motion. The dynamics are therefore equivalent.

5 This is the only solution that is manifestly invariant under rotations, i.e., with $g_{\mu\nu} = \mathrm{diag}(-1, 1, 1, 1)$ and $\Phi^A = \left\{\varphi(t), \beta x^i\right\}$. *A priori* it may be possible to have flat solutions with inhomogeneous Stückelbergs Φ^A, or equivalently solutions with $\Phi^A = x^A$ and $g_{\mu\nu} = \eta_{\mu\nu}$ with $\eta_{\mu\nu}$ written in a nonstandard coordinate system, but we do not consider these here.

We expand the action (4.1) to quadratic order around the Minkowski solution, focusing on scalar modes,

$$g_{00} = -(1+2\phi), \tag{4.10}$$
$$g_{0i} = \partial_i B, \tag{4.11}$$
$$g_{ij} = (1-2\psi)\delta_{ij} + 2\partial_i\partial_j E, \tag{4.12}$$
$$\Phi^A = x^A + \left\{\pi^0, \partial^i\pi\right\}, \tag{4.13}$$
$$\lambda = \delta\lambda. \tag{4.14}$$

Three of these fields—ϕ, B, and $\delta\lambda$—are auxiliary, as they appear without time derivatives in the action, and so can be integrated out using their equations of motion. Note that the auxiliary structure is precisely the same as in general relativity, since the mass term and Lagrange multiplier do not introduce any derivatives of the metric.

We can use diffeomorphism invariance to remove a further two modes. When gauge fixing at the level of the action, one must take care to only eliminate variables whose equations of motion are contained in the equations of motion of the remaining variables, otherwise we will lose information after picking a gauge. Following the procedure of [219], we see that we can safely take π^0 and one of (E, π) to vanish. Picking unitary gauge, $\pi^0 = \pi = 0$, we obtain the flat-space quadratic action (in Fourier space),

$$\delta_2 S = \int \mathrm{d}t M_{\rm pl}^2 \left(-\dot{\vec{\mathcal{X}}}^{\rm T}\mathbb{K}\dot{\vec{\mathcal{X}}} + \vec{\mathcal{X}}^{\rm T}\left(k^2\mathbb{G} + m^2\mathbb{M}\right)\vec{\mathcal{X}}\right), \tag{4.15}$$

where $\vec{\mathcal{X}} \equiv (\psi, k^2 E)$ and the matrices $\mathbb{K}$, $\mathbb{G}$, and $\mathbb{M}$ are given by

$$\mathbb{K} = \begin{pmatrix} 3 + \frac{4k^2}{m^2} & 1 \\ 1 & 0 \end{pmatrix}, \tag{4.16}$$

$$\mathbb{G} = \begin{pmatrix} 1 & 0 \\ 0 & 0 \end{pmatrix}, \tag{4.17}$$

$$\mathbb{M} = \frac{1}{4} \begin{pmatrix} 3 & 1 \\ 1 & -1 \end{pmatrix}. \tag{4.18}$$

As described in [208], this system can be diagonalized by replacing ψ with the Lagrange multiplier $\delta\lambda$, which we had previously integrated out using

$$\delta\lambda = \frac{M_{\rm pl}^2}{4} \left[(4k^2 + 3m^2)\psi + k^2 m^2 E \right], \tag{4.19}$$

to find

$$\delta_2 S = \int \mathrm{d}t \frac{1}{4k^2 + 3m^2} \left[k^4 m^2 M_{\rm pl}^2 \left(\dot{E}^2 - (k^2 + m^2) E^2 \right) - \frac{1}{M_{\rm pl}^2} \left(\frac{16}{m^2} \dot{\delta\lambda}^2 - 4\delta\lambda^2 \right) \right]. \tag{4.20}$$

If we take $m^2 > 0$, we can canonically normalize,

$$\delta\lambda_{\rm c} \equiv \frac{4}{m M_{\rm pl} \sqrt{2k^2 + \frac{3}{2}m^2}} \delta\lambda, \tag{4.21}$$

$$E_{\rm c} \equiv \frac{m M_{\rm pl} k^2}{\sqrt{2k^2 + \frac{3}{2}m^2}} E, \tag{4.22}$$

to obtain the final action,

$$\delta_2 S = \int \mathrm{d}t \left[\frac{1}{2}\dot{E}_\mathrm{c}^2 - \frac{1}{2}(k^2 + m^2)E_\mathrm{c}^2 - \frac{1}{2}\dot{\delta\lambda}_\mathrm{c}^2 + \frac{1}{8}m^2\delta\lambda_\mathrm{c}^2 \right]. \tag{4.23}$$

The only dynamical degree of freedom here is E_c, which is healthy and has mass m. The field $\delta\lambda_\mathrm{c}$ has the wrong sign on both its kinetic and mass terms, but does not propagate due to the absence of a gradient term; its equation of motion,

$$\ddot{\delta\lambda}_\mathrm{c} + \frac{m^2}{4}\delta\lambda_\mathrm{c} = 0, \tag{4.24}$$

leads to a dispersion relation $\omega^2 = m^2/4$ and is solved simply by [208]

$$\delta\lambda_\mathrm{c} = C(\vec{x}) \sin\left(\frac{mt}{2}\right) + D(\vec{x}) \cos\left(\frac{mt}{2}\right), \tag{4.25}$$

where C and D are space-dependent constants of integration. The authors of [208] identify this mode with the mimetic dark matter.[6]

When we discuss cosmology in the next section, we will find ourselves tempted by the possibility of taking $m^2 < 0$. *A priori* this is merely a parameter choice, but the flat-space analysis shows why this would be a poor decision. By looking at the action (4.20), we see that, for negative m^2, the overall sign in front of the action flips depending on whether $k^2 > 3|m^2|/4$ or $k^2 < 3|m^2|/4$, a sign of pathological behavior. In particular, for scales $k^2 > 3|m^2|/4$, upon canonically normalizing we find the action (4.23) with an overall minus sign, so that the dynamical mode E_c is a ghost.

6 See [208] for an argument for why this mode is not a ghost, despite having an overall wrong-sign action. In principle, one might worry that when quantizing or considering nonlinearities, a coupling will be induced between $\delta\lambda_\mathrm{c}$ and other fields which will lead to an Ostrogradski instability. On the other hand, due to the lack of a gradient term this mode is not a propagating degree of freedom in the usual sense. We will remain agnostic about this question and limit ourselves to considerations of classical, linear stability, which this system clearly satisfies for $m^2 > 0$. See, e.g., [220, 221] for detailed discussions of classical and quantum properties of modes lacking a gradient term.

4.3 COSMOLOGICAL SOLUTIONS

In this section we investigate the FLRW cosmological solutions of mimetic massive gravity. Consider the homogeneous and isotropic ansatz

$$g_{\mu\nu} = \mathrm{diag}(-1, a(t)^2\delta_{ij}), \tag{4.26}$$

$$\Phi^A = \left\{\varphi(t), \beta x^i\right\}. \tag{4.27}$$

In principle one could allow β to depend on time, but this breaks homogeneity and isotropy as it induces $\vec{x}$-dependent terms in the stress-energy tensor of the Stückelberg fields. Note that on-shell, the Lagrange multiplier enforces $\varphi = t$ (up to a constant). We will include a general matter sector with density ρ and pressure p. We will find this sector needs to contain a cosmological constant, much like in general relativity, but does not need to include dark matter, as this role can be played by the mimetic dark matter (which is an exactly pressureless perfect fluid).

The Einstein and scalar equations of motion are

$$3H^2 = \frac{\rho}{M_{\mathrm{pl}}^2} - \frac{2\lambda}{M_{\mathrm{pl}}^2} - \frac{3m^2}{16}\left(\frac{\beta^4}{a^4} - 6\frac{\beta^2}{a^2} + 5\right), \tag{4.28}$$

$$2\dot{H} + 3H^2 = -\frac{p}{M_{\mathrm{pl}}^2} - \frac{m^2}{16}\left(3 - \frac{\beta^4}{a^4} - 2\frac{\beta^2}{a^2}\right), \tag{4.29}$$

$$0 = \frac{\mathrm{d}}{\mathrm{d}t}\left\{a^3\left[\frac{3m^2}{4}\left(1 - \frac{\beta^2}{a^2}\right) + \frac{2\lambda}{M_{\mathrm{pl}}^2}\right]\right\}. \tag{4.30}$$

We can solve for λ by integrating the Φ^0 equation of motion (4.30), finding

$$-\frac{2\lambda}{M_{\mathrm{pl}}^2} = \frac{\mathcal{C}}{a^3} + \frac{3m^2}{4}\left(1 - \frac{\beta^2}{a^2}\right), \tag{4.31}$$

where $\mathcal{C}$ is an integration constant. Plugging this into the Friedmann equation (4.28), we obtain

$$3H^2 = \frac{\rho}{M_{\rm pl}^2} + \frac{\mathcal{C}}{a^3} - \frac{3m^2}{16}\left(1 - \frac{\beta^2}{a^2}\right)^2 . \tag{4.32}$$

Note that the contribution from λ exactly cancels out that from the last term of the Einstein equation (4.3), so the very simple form for $\rho_\varphi \equiv -3m^2M_{\rm pl}^2(1-\beta^2/a^2)^2/16$ is entirely due to the term proportional to $g_{\mu\nu}$ in the stress tensor. The integration constant provides a dust-like contribution to the Friedmann equation, which is to be expected as this is a theory of mimetic dark matter.

We can get a better sense of the physical picture by expanding out the Friedmann equation and absorbing the mimetic dark matter $\mathcal{C}$ into ρ, finding

$$3H^2 = \frac{\rho}{M_{\rm pl}^2} - \frac{3m^2}{16}\left(\frac{\beta^4}{a^4} - \frac{2\beta^2}{a^2} + 1\right) . \tag{4.33}$$

For $m^2 > 0$ ($m^2 < 0$), we see that the mass term generates an effective negative (positive) cosmological constant, an effective negative (positive) curvature, and an effective radiation component with negative (positive) energy density. Note that these add on to any cosmological constant, radiation, and curvature already present cosmologically; for example, while we have assumed a flat cosmology as our ansatz, observational bounds on spatial curvature will constrain the sum of any pre-existing curvature and the curvature-like term generated by the graviton mass.

Note that for $m^2 < 0$ we have late-time acceleration, with $\Lambda_{\rm eff} = 3|m^2|/16$. However, as discussed in the previous section, we need $m^2 > 0$ in order to avoid a ghost around flat space. This is reminiscent of the situation in the Dvali-Gabadadze-Porrati (DGP) model [222], where one branch of solutions has self-accelerating cosmological expansion [223, 224] but is plagued by a

ghost [225, 226], while the other branch is healthy but cannot account for cosmic acceleration.

Let us assume that the energy density ρ in (4.33) contains dust (including the mimetic dark matter), radiation, and dark energy components. Then, in terms of the density parameters,

$$\Omega_{i,0} = \frac{\rho_{i,0}}{3M_{\rm pl}^2 H_0^2}, \tag{4.34}$$

the components of the Friedmann equation which are modified by mimetic massive gravity are

$$\Omega_{\Lambda,0} = \bar{\Omega}_{\Lambda,0} - \frac{m^2}{16H_0^2} \tag{4.35}$$

$$\Omega_{K,0} = \frac{m^2}{8H_0^2}\beta^2, \tag{4.36}$$

$$\Omega_{\rm r,0} = \bar{\Omega}_{\rm r,0} - \frac{m^2}{16H_0^2}\beta^4, \tag{4.37}$$

where $\bar{\Omega}_{\Lambda,0}$ and $\bar{\Omega}_{\rm r,0}$ are the densities associated to dark energy and Standard Model radiation. Using observational bounds on the curvature and radiation densities, we can place constraints on the model parameters m^2 and β. We will not consider any bounds coming from the presence of the effective cosmological constant, even though it contributes a negative and potentially large (if $m^2 \gg H_0$) amount to $\Omega_{\Lambda,0}$. Particle physics also predicts a large (and potentially negative) vacuum energy, and since we are not worrying about that, it seems inconsistent to worry about the contribution from mimetic massive gravity. One might expect that whatever solves the former problem will also solve the latter.[7]

7 See [227] for a proposed solution to the cosmological constant problem in the context of Lorentz-violating massive gravity, which is closely related to mimetic massive gravity.

We will use observational constraints on $\Omega_{K,0}$ and $\Omega_{\mathrm{r},0}$ to bound our two free parameters, m^2 and β. *Planck* 2018 constrains $\Omega_{K,0} = 0.0007 \pm 0.0019$, which we parametrize as $|\Omega_{K,0}| < \delta_K$, with $\delta_K \sim 0.003$ [8]. We will take this to be a constraint on the contribution from mimetic massive gravity alone,

$$\frac{m^2}{8H_0^2}\beta^2 < \delta_K. \tag{4.38}$$

We remind the reader that what we are really bounding is the sum of the mimetic massive gravity contribution and any "bare" curvature, but unless there is significant tuning between these two, we can simply take this as a constraint on the mimetic massive gravity piece alone.

To bound the mimetic contribution to the radiation density, we will use constraints from big bang nucleosynthesis (BBN). At the time of BBN, radiation dominates. The exact value of the Hubble rate at the time of nucleosynthesis, which depends on the radiation density, determines the freeze-out abundance of neutrons and therefore the primordial abundance of helium-4, which is subject to tight observational bounds. The constraints are conveniently phrased in terms of the "speed-up factor" $\zeta \equiv H/\bar{H}$, where H and $\bar{H}$ are the Hubble rate and its expected value, respectively, at the time of BBN. The difference between the observed and predicted helium-4 abundance, $|\Delta Y_P|$, is related to the speed-up factor by [228]

$$\Delta Y_P = 0.08(\zeta^2 - 1). \tag{4.39}$$

Current observational bounds imply [229]

$$|\Delta Y_P| \lesssim 0.01. \tag{4.40}$$

Comparing the Friedmann equation (4.33) with and without the mimetic radiation contribution, and focusing on radiation domination, we find

$$\zeta^2 - 1 = -\frac{m^2\beta^4}{16\bar{\Omega}_{\mathrm{r},0}H_0^2}, \tag{4.41}$$

where the value for the present-day radiation density associated to photons and neutrinos, $\bar{\Omega}_{\mathrm{r},0} \sim 10^{-4}$, is determined entirely by the CMB temperature and the effective number of neutrino species and is therefore not dependent on our modification of gravity.[8] Combining this with (4.40) we arrive at the constraint

$$\frac{m^2}{16H_0^2}\beta^4 < \delta_{\mathrm{r}}, \tag{4.42}$$

where

$$\delta_{\mathrm{r}} \equiv \frac{\max(|\Delta Y_P|)\bar{\Omega}_{\mathrm{r},0}}{0.08} \approx \mathcal{O}(10^{-5}). \tag{4.43}$$

We can rewrite our constraints (4.38) and (4.42) as inequalities for m/H_0 and β alone in two different régimes,

$$\frac{m}{H_0} < \begin{cases} \frac{\sqrt{8\delta_K}}{\beta}, & \beta < \sqrt{\frac{2\delta_{\mathrm{r}}}{\delta_K}} \\ \frac{4\sqrt{\delta_{\mathrm{r}}}}{\beta^2}, & \beta > \sqrt{\frac{2\delta_{\mathrm{r}}}{\delta_K}}. \end{cases} \tag{4.44}$$

These are plotted in 4.1.

Finally, we note that the strong-coupling scale for this theory is of order $\Lambda_2 = \sqrt{mM_{\mathrm{pl}}}$ [208]. If m is of order the present-day Hubble scale, $m \sim 10^{-33}$ eV, then the strong coupling scale is $\Lambda_2 \sim$ meV, i.e., the theory breaks down slightly below the millimeter scale. As we see from (4.44), for sufficiently small β, m could potentially be much larger than H_0, leading to a correspondingly larger strong-coupling scale.

4.4 COSMOLOGICAL PERTURBATIONS

As we have seen, at the background level, cosmological solutions in mimetic massive gravity do not differ appreciably from ΛCDM. We therefore proceed to study cosmological perturbations around the FLRW background.

8 See [230] for a measurement of the CMB temperature.

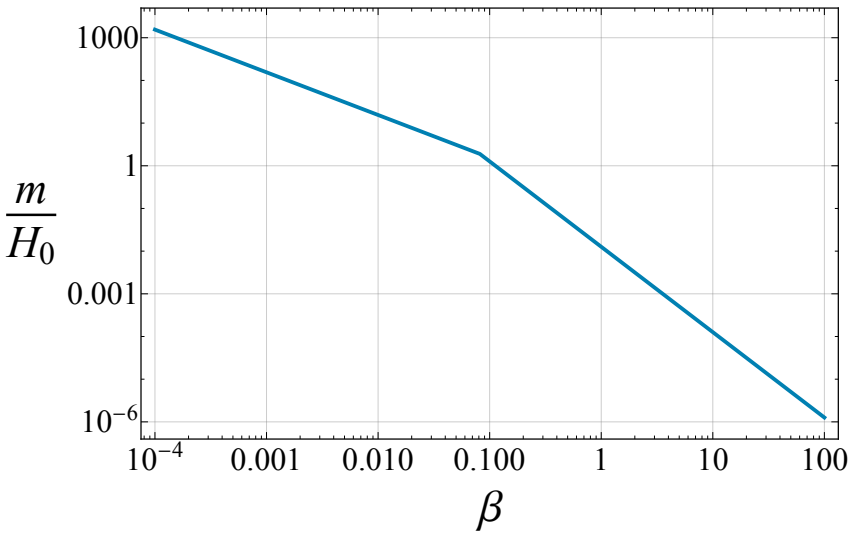

Figure 4.1: Upper limits on m/H_0 and β for $(\delta_K, \delta_r) = (0.003, 10^{-5})$.

This will tell us how cosmological large-scale structure (LSS) evolves in this theory in comparison to ΛCDM. Since mimetic massive gravity differs from general relativity, we would expect modifications to the gravitational Poisson equation and the slip relation, which could in principle allow for observational tests of this alternative model against ΛCDM and distinguish the two using the current and future LSS surveys. However, as we will see, stability of cosmological perturbations and the bounds (4.44) place strong constraints on the model which suggest that this theory should be observationally indistinguishable from GR in the linear regime.

4.4.1 *Stability bound*

We begin by studying the stability of cosmological perturbations using the second-order action formalism. Since, as discussed in 4.3, this theory does not possess ghost-free self-accelerating solutions, we include a cosmological constant, although it will not affect any of the results in this section. Since

the theory already contains a pressureless fluid, namely the mimetic dark matter, we need not introduce an additional matter field. Our analysis is therefore valid for all times after matter-radiation equality.

We define the linearized metric, Stückelberg fields, and Lagrange multiplier as

$$\begin{aligned} \mathrm{d}s^2 &= -(1+2\phi)\mathrm{d}t^2 + 2a\partial_i B \mathrm{d}t\mathrm{d}x^i \\ &\quad + a^2\left[(1-2\psi)\delta_{ij} + 2\partial_i\partial_j E\right]\mathrm{d}x^i\mathrm{d}x^j, \qquad (4.45) \\ \Phi^0 &= t + \pi^0, \qquad (4.46) \\ \Phi^i &= \beta\left(x^i + \partial^i\pi\right), \qquad (4.47) \\ \lambda &= \bar{\lambda} + \delta\lambda, \qquad (4.48) \end{aligned}$$

where we are restricting ourselves to scalar perturbations, and $\bar{\lambda}$ is the background value given in (4.31). The calculation of the quadratic action proceeds analogously to the flat-space case discussed in section 4.2. Expanding the action (4.1) (with a cosmological constant) to quadratic order in perturbations, we find that the variables ϕ, B, and $\delta\lambda$ are auxiliary—that is, they appear without time derivatives—and can therefore be integrated out using their equations of motion. To safely fix a gauge at the level of the action, we again follow the procedure of [219], finding that we can eliminate one each of (ψ,π^0) and (E,π). We will choose to work in unitary gauge, $\pi^0 = \pi = 0$, so that $\Phi^A = (t, \beta x^i)$ is unperturbed. The final action, in Fourier space and after integrations by parts, is

$$\delta_2 S = \int \mathrm{d}t M_{\mathrm{pl}}^2 a^3 \left(-\dot{\vec{\mathcal{X}}}^{\mathrm{T}}\mathbb{K}\dot{\vec{\mathcal{X}}} + \vec{\mathcal{X}}^{\mathrm{T}}\left(\frac{k^2}{a^2}\mathbb{G} + m^2\mathbb{M}\right)\vec{\mathcal{X}}\right), \qquad (4.49)$$

where $\vec{\mathcal{X}} \equiv (\psi, k^2 E)$ and the matrices $\mathbb{K}$, $\mathbb{G}$, and $\mathbb{M}$ are given by

$$\mathbb{K} = \begin{pmatrix} 3 - \frac{8a^2}{\beta^2 - 3a^2}\frac{k^2}{m^2\beta^2} & 1 \\ 1 & 0 \end{pmatrix} \tag{4.50}$$

$$\mathbb{G} = \begin{pmatrix} 1 & 0 \\ 0 & 0 \end{pmatrix} \tag{4.51}$$

$$\mathbb{M} = \frac{1}{8}\frac{\beta^2}{a^2}\left(1 + \frac{\beta^2}{a^2}\right)\begin{pmatrix} 3 & 1 \\ 1 & -1 \end{pmatrix} \tag{4.52}$$

Since we are interested in the implications of mimetic massive gravity for the growth and properties of large-scale structure in the late Universe, let us focus on subhorizon scales (i.e., $k^2 \gg a^2H^2$) and assume the quasi-static (QS) approximation. In order to use this approximation, we first need to ensure that fluctuations in this regime are stable. Ignoring time variation in $a(t)$, which will be subdominant in the limit $k^2 \gg a^2H^2$, and assuming solutions of the form $\vec{\mathcal{X}} = \vec{\mathcal{X}}_0 e^{i\omega t}$, the equations of motion following from the action (4.49) are

$$\left(-\omega^2\mathbb{K} + \frac{k^2}{a^2}\mathbb{G} + m^2\mathbb{M}\right)\vec{\mathcal{X}} = 0. \tag{4.53}$$

We can then derive stability conditions from the dispersion relations, obtained by solving

$$\begin{aligned} 0 &= \det\left(-\omega^2\mathbb{K} + \frac{k^2}{a^2}\mathbb{G} + m^2\mathbb{M}\right) \\ &= \frac{\omega^4}{a^2+\beta^2} - \frac{\omega^2 k^2}{a^2(3a^2-\beta^2)} - \frac{5\omega^2 m^2\beta^2}{8a^4} + \frac{k^2 m^2\beta^2}{8a^6} + \frac{m^4\beta^4(a^2+\beta^2)}{16a^8} \end{aligned} \tag{4.54}$$

for ω^2.

The dispersion relations arising from (4.54) are complicated, but simplify significantly in the limit $k \gg aH$ when we take into account the constraints (4.44) on m/H_0, which we obtained by requiring that the radiation and curvature densities generated by the mass term not exceed observational bounds. Consider replacing m and β in (4.54) with the following two parameters,[9]

$$\epsilon_1 \equiv \left(\frac{m\beta}{k}\right)^2, \qquad \epsilon_2 \equiv \left(\frac{m\beta^2}{ka}\right)^2. \tag{4.55}$$

We proceed to show that the bounds (4.44) imply that each of these is much smaller than unity on subhorizon scales for all times after matter-radiation equality.

For both ϵ_1 and ϵ_2 we can put upper bounds on the numerators and lower bounds on the denominators. Let us start with the numerators. For ϵ_1, multiply each side of (4.44) by β. We see there is a strict upper bound on the combination $m\beta$,

$$m\beta \leq \sqrt{8\delta_K} H_0 \approx 0.15 H_0 \tag{4.56}$$

where we have taken $\delta_K \sim 0.003$ as a representative value. We can similarly find a bound on the numerator of ϵ_2 by multiplying both sides of (4.44) by β^2, finding

$$m\beta^2 \leq 4\sqrt{\delta_r} H_0 \approx 10^{-2} H_0 \tag{4.57}$$

for $\delta_r \sim 10^{-5}$.

Now we move on to the denominators. The subhorizon limit is given by $k \gg aH$. For the sake of argument let us be conservative and assume that k is only slightly subhorizon, $k/a \approx \mathcal{O}(1)H$.[10] At any given time

9 To do this replacement, first replace $m \to \sqrt{\epsilon_1}\beta/k$, and then replace any remaining factors of β with $\beta \to \sqrt{\epsilon_2/\epsilon_1}a$.

10 Of course, the deeper in the subhorizon regime k is, the smaller ϵ_1 and ϵ_2 become.

from matter-radiation equality to the present, where we can trust our analysis, the Hubble rate H is related to its present-day value H_0 by $H = H_0\sqrt{\Omega_{\Lambda,0} + \Omega_{\mathrm{m},0}a^{-3}}$. Putting this together with the bounds we have derived on $m\beta$ and $m\beta^2$, we find

$$\epsilon_1 \lesssim \frac{0.02}{\Omega_{\Lambda,0}a^2 + \Omega_{\mathrm{m},0}a^{-1}} \ll 1, \tag{4.58}$$

$$\epsilon_2 \lesssim \frac{10^{-4}}{\Omega_{\Lambda,0}a^4 + \Omega_{\mathrm{m},0}a} \ll 1 \text{ for } z \lesssim 3000. \tag{4.59}$$

Note that while the upper bound on ϵ_1 is always much smaller than unity for $0 < a \leq 1$, the upper bound on ϵ_2 in fact grows as a^{-1} at early times. However, it grows slowly and has a factor of 10^{-4} to compete with, so that $\max(\epsilon_2)$ does not reach unity until $z \sim 3000$, right around matter-radiation equality. Therefore in principle there might be a handful of modes—right around the horizon scale and at the earliest moments of matter domination—for which terms going as ϵ_2 affect the subhorizon dispersion relation, *if* $m\beta^2$ takes the largest value allowed by the constraints. We will continue to take $\epsilon_2 \ll 1$, with the understanding that if this particular situation is realized, then at those very early times we are only considering modes with $k \gtrsim 10aH$, for which ϵ_2 is certainly smaller than unity.

Dropping terms subdominant in ϵ_1 and ϵ_2, the dispersion relation (4.54) becomes

$$0 \approx \frac{\omega^4}{a^2 + \beta^2} - \frac{\omega^2 k^2}{a^2(3a^2 - \beta^2)} + \frac{k^2 m^2 \beta^2}{8a^6}. \tag{4.60}$$

Solving for ω^2, and again dropping terms subleading in $\epsilon_1 = (m\beta/k)^2$, we find the dispersion relations for our two modes,

$$\omega^2 \approx \frac{k^2}{a^2}\frac{a^2 + \beta^2}{3a^2 - \beta^2}, \tag{4.61}$$

$$\omega^2 \approx \frac{m^2\beta^2}{8a^2}\left(3 - \frac{\beta^2}{a^2}\right). \tag{4.62}$$

Each of these implies the same stability condition,

$$\frac{\beta^2}{a^2} < 3. \tag{4.63}$$

This tells us that no matter what the value of β is, our cosmological solutions are *unstable* at sufficiently high redshifts,

$$z > \sqrt{3}\beta^{-1} - 1. \tag{4.64}$$

This early time instability can however be safely pushed back to unobservably early times by taking the parameter β to be sufficiently small.[11] Because we are assuming matter and dark energy domination, we can trust our stability condition as far back as matter-radiation equality at $z_{\rm eq} \approx 3400$. Demanding stability from $z_{\rm eq}$ onward, we find a constraint on β,[12]

$$\beta \lesssim 5 \times 10^{-4}. \tag{4.65}$$

4.4.2 *Cosmological tensor mass*

Another possible cosmological bound on the parameters m and β comes from constraints on the graviton mass. The tightest bounds currently come from LIGO, $m_{\rm T} \leq 7.7 \times 10^{-23}$ eV [231].[13] To compute the mass of tensor

11 This is similar to massive bimetric gravity, which possesses an early-time instability that can be rendered safe in the limit where the ratio of the two Planck masses becomes small [53].

12 It is plausible that the result (4.63) holds, at least on an order-of-magnitude basis, through radiation domination as well (see, again, the example of bigravity [53]). In this case, we should demand that the instability be pushed back to before big bang nucleosynthesis, with $z_{\rm BBN} \approx 3 \times 10^8$, which would imply a stronger constraint of $\beta \lesssim 10^{-8}$. We do not have much observational handle on the presumably radiation-dominated era before BBN, and therefore should not demand that the instability be absent then; indeed, a mild enough instability might have interesting consequences, such as the formation of primordial black holes.

13 See [232] for a helpful summary of bounds on the graviton mass from a variety of experiments and observations.

fluctuations on a cosmological background, we linearize the Einstein equation (4.3) around $g_{\mu\nu} = \bar{g}_{\mu\nu} + h_{\mu\nu}$, with $\bar{g}_{\mu\nu} = \mathrm{diag}(-1, a^2\delta_{ij})$, $h_{00} = 0$, and h_{ij} transverse and traceless, i.e., $h_{ii} = \partial_i h_{ij} = 0$. The Einstein equation is

$$\ddot{h}_{ij} + 3H\dot{h}_{ij} - \frac{\nabla^2}{a^2}h_{ij} + m_{\mathrm{T}}^2 h_{ij} = 0 \tag{4.66}$$

with the tensor mass given by

$$m_{\mathrm{T}}^2 \equiv \frac{m^2}{2}\frac{\beta^2}{a^2}\left(1 + \frac{\beta^2}{a^2}\right) \tag{4.67}$$

The structure of the Einstein equation is such that m_{T}^2/m^2 has to be a (quadratic) polynomial in β^2/a^2. What is non-trivial is that the degree-zero term in that polynomial cancels out, i.e., the expression for m_{T}^2/m^2 starts at order β^2/a^2. This means that gravitational waves propagating over cosmological distances (at low redshift, i.e., $a \sim \mathcal{O}(1)$) do not depend on m alone; instead they involve the combinations $m\beta$ and $m\beta^2$ which, as we have seen, are strongly constrained by the cosmological background. In particular, recalling that $m^2\beta^2 \lesssim 10^{-2}H_0^2$ and $m^2\beta^4 \lesssim 10^{-4}H_0^2$, we see that m_{T} at the present era is at most of order $10^{-1}H_0 \sim 10^{-34}$ eV, far below the LIGO bounds. Moreover, our stability condition (4.65) has no bearing on m_{T}. No matter how tiny β is, the constraints (4.44) place a constant upper bound on $m\beta$, so that the smaller β is, the larger m is allowed to be, leaving $m_{\mathrm{T}} \approx m\beta/(\sqrt{2}a)$ fixed. It is interesting to note that, without demanding that this model provide cosmic acceleration, the tensor mass is nevertheless forced to be smaller than the Hubble scale. Finally, we note that around a flat background, the tensor mass is simply m, so local tests of gravity might be able to place constraints on m that are not possible with gravitational waves that propagate over cosmological distances.

4.4.3 *Quasistatic limit*

Finally, let us comment on the testability of mimetic massive gravity using near-future LSS surveys. We will find it convenient to work in Newtonian gauge, $B = E = 0$. Linearizing the Einstein equations (4.3), and leaving in a generic stress-energy tensor $T_{\mu\nu}$ for completeness, we obtain

$$6H^2\phi - \frac{2}{a^2}\partial^i\partial_i\psi + 6H\dot{\psi} = \frac{1}{M_{\rm pl}^2}\delta T_0^0 + 2\frac{\delta\lambda}{M_{\rm pl}^2} - \frac{m^2}{4}\frac{\beta^2}{a^2}\mathcal{Q}_1\left(3\psi + \partial^i\partial_i\pi\right), \tag{4.68}$$

$$-2\partial_i\left(\dot{\psi} + H\phi\right) = \frac{\delta T_i^0}{M_{\rm pl}^2} + \frac{2\bar{\lambda}}{M_{\rm pl}^2}\partial_i\pi^0 + \frac{m^2}{4}\mathcal{Q}_1\left(\partial_i\pi^0 - \beta^2\partial_i\dot{\pi}\right), \tag{4.69}$$

$$6\left[\ddot{\psi} + 3H\dot{\psi} + H\dot{\phi} + (3H^2 + 2\dot{H})\phi\right] + \frac{2}{a^2}\partial^i\partial_i\left(\phi - \psi\right) = \frac{1}{M_{\rm pl}^2}\delta T_i^i - \frac{m^2}{4}\frac{\beta^2}{a^2}\mathcal{Q}_2\left(3\psi + \partial^i\partial_i\pi\right), \tag{4.70}$$

$$\frac{1}{a^2}\partial^i\partial_j\left(\psi - \phi\right) = \frac{1}{M_{\rm pl}^2}\delta T_j^i + \frac{m^2}{2}\frac{\beta^2}{a^2}\mathcal{Q}_2\partial^i\partial_j\pi, \quad i \neq j, \tag{4.71}$$

where $\mathcal{Q}_1 \equiv \left(3 - \frac{\beta^2}{a^2}\right)$ and $\mathcal{Q}_2 \equiv \left(1 + \frac{\beta^2}{a^2}\right)$.

Moving to Fourier space, specializing to a pressureless fluid without anisotropic stress, and taking the quasistatic limit, $\ddot{X} \sim H\dot{X} \sim H^2X \ll k^2X$ for any perturbation X, Eqs. (4.68), (4.70) and (4.71) become

$$\frac{2k^2}{a^2}\psi = \frac{1}{M_{\rm pl}^2}\left(2\delta\lambda - \bar{\rho}\delta\right) - \frac{m^2}{4}\frac{\beta^2}{a^2}\mathcal{Q}_1\left(3\psi - k^2\pi\right), \tag{4.72}$$

$$\frac{2k^2}{a^2}\left(\phi - \psi\right) = \frac{m^2}{4}\frac{\beta^2}{a^2}\mathcal{Q}_2\left(3\psi - k^2\pi\right), \tag{4.73}$$

$$\frac{1}{a^2}\left(\phi - \psi\right) = -\frac{m^2}{2}\frac{\beta^2}{a^2}\mathcal{Q}_2\pi, \tag{4.74}$$

where $\bar{\rho}$ and δ are the background density and overdensity of the dust component. Note that these are degenerate with the mimetic dark matter, as expected.

Combining these equations, we obtain the modified Poisson equation and the slip relation,

$$-k^2\psi = 4\pi G\mu(a,k)a^2(\delta\rho - 2\delta\lambda), \tag{4.75}$$

$$\psi = \eta(a,k)\phi, \tag{4.76}$$

where the modified-gravity parameters μ and η are given by

$$\mu(a,k) = \frac{1}{1+\frac{1}{2}\frac{m^2\beta^2}{k^2}\left(3-\frac{\beta^2}{a^2}\right)}, \tag{4.77}$$

$$\eta(a,k) = \frac{1}{1+\frac{1}{2}\frac{m^2\beta^2}{k^2}\left(1+\frac{\beta^2}{a^2}\right)}. \tag{4.78}$$

These parametrize observable deviations from general relativity, in which $\mu = \eta = 1$.

The constraints we have already derived on m and β preclude μ and η from deviating from unity at a level accessible to near-future observations. The stability constraint (4.63) requires the terms in parentheses to be $\mathcal{O}(1)$, while the background constraint (4.56) sets $m^2\beta^2 \lesssim 0.02H_0^2$, so that

$$\mu - 1 \sim \eta - 1 \sim \mathcal{O}\left(\frac{m^2\beta^2}{k^2}\right) \lesssim 10^{-2}\left(\frac{H_0}{k}\right)^2. \tag{4.79}$$

It is therefore highly unlikely that cosmological observations will be able to test this model against ΛCDM in the linear and subhorizon regime.

4.5 CONCLUSIONS

In this chapter we have studied the first cosmological implications of the recently-proposed theory of mimetic massive gravity. We find that the

theory is unable to self-accelerate without introducing a ghost. Its effects on Friedmann-Lemaître-Robertson-Walker cosmological backgrounds are to introduce effective radiation, curvature, and cosmological constant terms, as well as a dust-like mimetic dark matter component. We place constraints (4.44) on the theory parameters by demanding that the effective radiation and curvature terms be within observational bounds. In the ghost-free region of parameter space, $m^2 > 0$, the effective cosmological constant is negative-definite, so a separate dark energy sector, which we take to be a positive cosmological constant, is required to explain the late-time acceleration of the Universe.

We further studied the behavior of cosmological perturbations in the subhorizon, quasistatic limit. The model generically suffers from an instability at early times. However, since our analysis only included a pressureless dust component (in addition to a cosmological constant), the calculation can only be trusted as far back as matter-radiation equality. This allowed us to place a further constraint on the theory parameters by insisting that the instability be absent throughout matter domination. With these constraints, the deviations from ΛCDM in the linear, subhorizon regime are likely too small to be observable.

Not surprisingly, since this is a theory of massive gravity, it predicts massive tensor modes. We have calculated the tensor mass around cosmological backgrounds and found that, taking into account the constraints imposed by the cosmological background, this mass must be at least an order of magnitude below the Hubble scale, far outside the currently-available constraints on the graviton mass. Unlike other theories of massive gravity, in which the graviton mass is comparable to the Hubble scale in order to provide late-time acceleration, this bound on the graviton mass is solely due to the requirement that the effective radiation and curvature terms in the Friedmann equation not be too large.

What are the remaining prospects for cosmological tests of mimetic massive gravity? We emphasize that our analysis does not apply in two

important regimes: horizon-size scales and nonlinear scales. One or both of these may possess signatures which could be used to distinguish mimetic massive gravity from ΛCDM, or otherwise to rule out additional regions of parameter space. One expects that nonlinear scales will require N-body simulations, while at horizon-size scales we cannot apply the quasistatic approximation and would need to solve the perturbation equations numerically, as in other theories of modified gravity [233]. For the latter, we note that the mass scales appearing in the action (4.49) for cosmological perturbations are not simply m, which can be arbitrarily large (in the limit of small β), but rather $m\beta$ and $m\beta^2$, which we have shown must both be at least an order of magnitude smaller than the Hubble scale. It therefore might be difficult for this theory to produce effects at horizon scales that are larger than cosmic variance. Note that scales $k \sim m\beta$ and $k \sim m\beta^2$ are super-horizon and therefore not observable.

Acknowledgments We are grateful to Marco Crisostomi, Sergei Dubovsky, Riccardo Penco, Jeremy Sakstein, and Filippo Vernizzi for helpful discussions. We thank the referee for useful comments on the draft.

Part III

SCREENING MECHANISMS IN MODIFIED GRAVITY

5

SPLASHBACK RADIUS IN SYMMETRON GRAVITY

In this final chapter we have studied the effects of screening mechanisms in modified gravity on the dynamics of the spherical collapse of dark matter. In particular, we investigate the splashback scale in *symmetron modified gravity*. The splashback radius $r_{\rm sp}$ has been identified in cosmological N-body simulations as an important scale associated with gravitational collapse and the phase-space distribution of recently accreted material. We employ a semi-analytical approach, namely the self-similar spherical collapse framework, to study the spherical collapse of dark matter haloes in symmetron gravity. We provide, for the first time, insights into how the phenomenology of splashback is affected by modified gravity. The symmetron is a scalar-tensor theory which exhibits a screening mechanism whereby higher-density regions are screened from the effects of a fifth force. In this model, we find that, as over-densities grow over cosmic time, the inner region becomes heavily screened. In particular, we identify a sector of the parameter space for which material currently sitting at the splashback radius $r_{\rm sp}$, during its collapse has followed the formation of this screened region. As a result, we find that for this part of the parameter space the splashback radius is maximally affected by the symmetron force and we predict changes in $r_{\rm sp}$ up to around 10% compared to its General Relativity value. Because this margin is within the precision of present splashback experiments, we expect this feature to soon provide constraints for Symmetron gravity on

previously unexplored scales.

This chapter is based on: O. Contigiani, V. Vardanyan, A. Silvestri, *Splashback radius in symmetron gravity*, Phys. Rev. D **99** (2019) 064030 , arXiv:1812.05568.

5.1 INTRODUCTION

Gravity, one of the fundamental forces of nature, plays a crucial role in inferring our model of the cosmos as well as all the precision constraints placed on fundamental physics through cosmology. The theory of General Relativity (GR) introduced by Einstein a century ago [7], provided a coherent theoretical framework within which to study all gravitational phenomena. While it is arguably one of the most successful theories of modern physics, having passed a host of empirical phenomena, there remain regimes of curvature and scale where GR has yet to be accurately tested. Its theoretical and phenomenological limitations are being fully explored, with an endeavour which is carried out at virtually all energy scales, ranging from the ultraviolet properties of the theory, down to energy scale of H_0, associated to the present-day expansion rate of the Universe [1].

Upcoming large scale structure (LSS) surveys will provide unprecedented constraints on gravity on cosmological scales, allowing to discriminate among many theories alternative to GR. The phenomenology of theories of modified gravity (MG) on linear cosmological scales is fairly well understood, and it is commonly characterized in terms of modifications in the relation between matter density contrast and, respectively, the lensing and Newtonian potential [234–236]. On the other hand, it is well known that non-linear mechanisms in MG theories "screen away" the effects of additional degrees of freedom in high-density regions. This ensures that any fifth force is suppressed and MG reduces to GR in regions where it has been tested with remarkable accuracy [55].

A natural regime of interest is the intermediate range, between the screened and unscreened regimes, e.g. the regions of space at the boundaries of dark matter haloes. To this extent, a feature that is gaining prominence is the so-called *splashback*, which corresponds to an observable steepening of dark matter halo density profile close to the boundary [237]. Locally, the position of this steepening contains interesting information about the

clustering of dark matter shells and it can be understood as the dividing radius of single-stream and multistream sectors of the dark matter phase space. This feature has already been noticed in the self-similar spherical collapse framework developed and studied in [238, 239], and generalized to 3D collapse in [240]. Self-similarity, however, is fully operational in a universe without a characteristic scale, such as the Einstein-de Sitter (EdS) universe with $\Omega_m = 1$. Even though realistic applications of the same principle to ΛCDM universe are possible [241], in this chapter we will focus on the collapse in EdS scenario and will leave more realistic scenarios for future work.

The profiles of the largest dark matter haloes in the Universe, where galaxy clusters reside, can be mapped by measuring the deformation of background sources [242, 243]. This technique, known as lensing, has been used to measure the splashback feature around clusters [244, 245]. It should be noted however that the most stringent constraints are obtained using the distribution of subhaloes traced by the cluster galaxy members [246–249]. In this case, the interpretation is nevertheless not straightforward and an accurate comparison with N-body ΛCDM simulations is required.

In this chapter we consider the splashback radius in MG scenarios, investigating the microscopic effects of alternative theories of gravity on the dark matter shells accreting into the halo. Since we aim at gaining insight on the physical details, we do not resort to numerical simulations, but rather employ a semi-analytical method based on the framework of self-similar spherical collapse of [238]. We focus on the class of theories of gravity that display the Symmetron screening mechanism [250]. While we present an overview of the Symmetron gravity in the main text, let us mention here that our analysis can be easily extended to other types of screening mechanisms, e.g. to Chameleon screening exhibited by $f(R)$ models [251, 252], where the density dependence is explicitly in the scalar field mass, rather than the field couplings.

We have organized our presentation as follows. In section 5.2 we have presented the basics of the standard spherical collapse framework. In section 5.3 have brought necessary details about the self-similar solutions and have presented the relevant equations of motion for the collapsing shells. We have additionally obtained the self-similar density profile used later in the chapter. In section 5.3 we discuss the basics of Symmetron gravity and present the relvant equation. In section 5.5 we present our numerical methods and demonstrate the effect of the Symmetron force on the phase space of the dark matter halo and the shift in the splashback radius. Finally, we discuss the implications of our findings and suggest potential further studies in section 5.6.

5.2 SPHERICAL COLLAPSE

In the introduction of this thesis we have presented the basics of the cosmological perturbation theory in the *linear* regime. This framework already predicts the overall large scale structure of the universe. However, the gravitational interactions force the small overdensities to decouple from the Hubble expansion and form higher density structures, known as dark matter halos. Here the density contrast (our small perturbation variable in the linear perturbation theory) is not in the perturbative regime anymore. Much of the progress in understanding these structures has been achieved through numerical simulations. Interestingly, it is now acknowledged that dark matter halos have quite universal properties. They are phenomenologically very rich structures and are supposed to be sensitive to the various aspects of the cosmological model, and, particularly, to the underlying theory of gravity. Given our overall motivation in this thesis, namely exploring various observables in the universe which can be used to constrain the fundamental properties of the cosmological theories, it would have been rather unfair to dismiss the possibility of exploiting the collapsed non-linear structure in the universe for our purposes.

With this motivation in mind, let us try to understand the basic properties of the collapse in a simple approximation of spherical symmetry. Let us start with a discussion in Einstein-de-Sitter universe, which is a flat model with $\Omega_{\rm m} = 1$. Consider a small tophat overdensity of mass $M(t_{\rm in})$ at some high redshift $z_{\rm in}$. The outer shells of matter evolve following their equations of motion

$$\ddot{r} = -\frac{G_{\rm N} M(r; t_{\rm i})}{r^2}, \tag{5.1}$$

where the left-hand side is the Newtonian force $F_N(r)$ proportional to Newton's gravitational constant $G_{\rm N}$.

It is useful to define the density contrast as $\delta \equiv (ar_0/r)^3 - 1$, where r_0 is the initial radius of the considered shell. Inverting this and plugging in Eq. (5.1) we will obtain a differential equation for δ, which will be useful for obtaining the linear solution. However, the point of considering the spherical collapse is to explore the situations where the density contrast is not very small and is governed by the non-linear dynamics of the collapse. For that purpose it is more convenient to work directly with Eq. (5.1), which can be easily integrated once to yield

$$\dot{r}^2 = 2\frac{G_{\rm N} M(r; t_{\rm i})}{r} - \mathcal{C}. \tag{5.2}$$

Here $\mathcal{C}$ is a positive integration constant given by $\mathcal{C} = 8\pi G_{\rm N} \bar{\rho}_{\rm in} r_{\rm in}^2 \Delta_{\rm in}/3$, with the index "in" denoting the quantities at the initial time $t_{\rm in}$, and Δ being the fractional mass contrast (compared to the homogeneous background) within the shell, at the given time.

We can present the solution of this equation in a parametric form as $r = G_{\rm N} M(1 - \cos\theta)/\mathcal{C}$ and $t = G_{\rm N} M(\theta - \sin\theta)/\mathcal{C}^{3/2}$, with θ being an angle in the range $[0, 2\pi]$. The radius of the shell reaches its maximum when $\theta = \pi$, and is known as the "turn-around radius". For our case of Einstein-de-Sitter universe we obtain

$$\delta_{\rm total} = \frac{9}{2}\frac{(\theta - \sin\theta)^2}{(1 - \cos\theta)^3}. \tag{5.3}$$

Additionally, in the linear regime we have

$$\delta_{\rm lin} = \frac{3}{5}\left(\frac{3}{4}(\theta - \sin\theta)\right)^{2/3}. \tag{5.4}$$

At the turn-around, $\delta_{\rm total} = (3\pi/4)^2 \approx 4.6$ and $\delta_{\rm lin} \approx 1.063$. Additionally, when $\theta = 2\pi$, the full density contrast becomes singular, while the linear one is $\delta_{\rm lin} \approx 1.686$. Of course, for a realistic collapse the shells will virialize at some point, and the collapse will not be singular. We will not go to all these complications here, but let us just note that as the velocities of the shells are the smallest at their turn-around, they are supposed to spend most of the evolution near the turn-around radius. It is therefore a reasonable first approximation to assume that the mass enclosed within the radius at a fixed fraction of the turnaround scale is the same as the initial mass enclosed within that shell. This is what is assumed in the seminal paper Ref. [253]. Particularly, let as assume that the initial overdensity scales with radius as $\delta_{\rm in} \sim r_{\rm in}^{-3\epsilon} \sim M^{-\epsilon}$ (the case of the top-hat overdensity considered above is given by $\epsilon = 0$). The given shell is at turn-around at the epoch given by $t_{\rm ta} \sim \delta_{\rm in}^{3/2}$ (this follows from the parametric solutions found above). Therefore the mass growth of the halo scales as $M \sim t^{2/3\epsilon} \sim a^{1/\epsilon}$.

If we could work out how the turn-around radius depends on the mass enclosed in it, i.e. finding the functional form of $r_{\rm ta}(M)$, we could deduce the shape of the density profile. This is possible to do by comparing the total energies at the initial time and at turnaround. The result is that $r_{\rm ta} \approx r_{\rm in}/\delta_{\rm in} \sim r_{\rm in}^{1+3\epsilon} \sim M^{(3\epsilon+1)/3}$. From here we then immediately obtain the mass profile as $M(r) \sim r^{3/(3\epsilon+1)}$ and the density profile as

$$\rho(r) \sim r^{-\frac{9\epsilon}{3\epsilon+1}}. \tag{5.5}$$

The crucial assumption here was the conservation of mass within a particular spherical shell. This is assumption is known to fail - the shells cross each other and the mass within them is dynamically changing during

the collapse. To take into account the shell crossing phenomenon one needs to either rely on more advanced analytical modelling, or on numerical simulations. We are going to discuss an elegant approach in the next section, where we will be able to gain important insights on the collapse phenomenon with shell-crossing.

5.3 SELF-SIMILAR SPHERICAL COLLAPSE

Here we are going to discuss the self-similar solutions in the problem of spherical collapse. In this context, the idea of self-similarity was introduced for the first time in [238], where it was shown that around EdS backgrounds, where the scale factor scales as a power-law of cosmic time, $a(t) \propto t^{2/3}$, the spherical collapse equations admit self-similar and self-consistent solutions. The basic idea is that when written in an appropriately rescaled coordinates, the trajectories of different dark matter shells can be shown to be identical. For our spherically symmetric problem our aim will be to rewrite all the observable quantities as

$$q(r,t) = Q(t)\mathcal{Q}(r(t)/R(t)), \tag{5.6}$$

where the functions $Q(t)$ and $R(t)$ should be power-laws on t (see e.g. Ref. [254]).

The material surrounding a scale-free perturbation initially coupled to the Hubble flow eventually reaches turn-around and collapses onto a central overdensity. We denote by $R(t)$ and $M(r,t)$ the position of the turn-around radius at a time t and the mass contained within the radius r, respectively. The mass within the turn-around radius can be written as a function of scale factor as:

$$M(R,t) \propto a(t)^s, \tag{5.7}$$

where the parameter $s \equiv 1/\epsilon$ is referred to as the *accretion rate*. In this model, $M(R,t)$ and $R(t)$ are related to each other through

$$\frac{4\pi}{3}R(t)^3\rho_b(t) = \left(\frac{4}{3\pi}\right)^2 M(R,t), \tag{5.8}$$

where $\rho_b(t)$ is the EdS background density at time t. This additionally implies that the position R as a function of time also depends on s:

$$R(t) \propto a(t)^{1+s/3}. \tag{5.9}$$

Notice that s and the mass of the present-day perturbation are the only free parameters of this model. In this work, we choose a fixed value of $s = 1.5$ for the accretion rate, known to be representative for the low-redshift Universe in numerical simulations [237, 255].

While before the turn-around the mass within a shell is manifestly constant, afterwards this is not true. Indeed, as multiple shells start orbiting the halo, their trajectories start intersecting. This phenomenon is known as shell-crossing and it is the principal reason why integrating Eq. (5.1) is not straightforward.

If we label each shell of material by its turn-around time t_* and radius r_*, such that $R(t_*) = r_*$, the trajectory for each shell is found to be independent of these quantities when self-similarity is satisfied. This can be verified by rewriting the equation of motion for the given shell in terms of the rescaled variables

$$\lambda = \frac{r}{r_*}, \quad \tau = \frac{t}{t_*}; \tag{5.10}$$

and by enforcing the mass profile $M(r)$ to be of the form:

$$M(r,t) = M(R,t)\mathcal{M}(r/R). \tag{5.11}$$

Notice that, from Eq. (5.9) it follows that the rescaling of the local turn-around radius $\Lambda = \frac{R(t)}{r_*}$ can be also written as a function of τ alone:

$$\Lambda(\tau) = \tau^{2/3+2s/9}. \tag{5.12}$$

The system is then evolved through the following self-similarity equations for $\lambda(\tau)$ and $\mathcal{M}(\lambda/\Lambda)$:

$$\frac{d^2\lambda}{d\tau^2} = -\frac{\pi^2}{8}\frac{\tau^{2s/3}}{\lambda^2}\mathcal{M}\left(\frac{\lambda}{\Lambda(\tau)}\right), \tag{5.13}$$

$$\mathcal{M}(y) = \frac{2s}{3}\int_1^\infty \frac{d\tau}{\tau^{1+2s/3}}\mathcal{H}\left(y - \frac{\lambda(\tau)}{\Lambda(\tau)}\right), \tag{5.14}$$

where $\mathcal{H}$ is the Heaviside step function. The turn-around initial conditions for $\lambda(\tau)$ are $\lambda(\tau = 1) = 1$, $d\lambda/d\tau(\tau = 1) = 0$. Notice that because these two equations are coupled to each other, they should be solved jointly to obtain self-consistent solutions for the orbits and the mass profile. This is done by starting from an initial guess for $\mathcal{M}(y)$ and then evaluating numerically the trajectories $\lambda(\tau)$ using Eq. (5.13). The corresponding $\mathcal{M}(y)$, evaluated using Eq. (5.14), is then taken as an initial guess for the next iteration. This is repeated until convergence is reached and a final result for $M(r,t)$ is obtained. The corresponding density profile is then simply

$$\rho(r,t) = \frac{1}{4\pi r^2}\frac{dM}{dr}(r,t). \tag{5.15}$$

Notice in particular that its time-dependence is completely described by $\rho_b(t)$ and $R(t)$.

In Fig. 5.1 we show the trajectories of the rescaled shells for different values of ϵ, obtained through the integration of Eq. (5.13).

This figure particularly demonstrates the fact that as time passes the shells get buried deeper and deeper into the halo and their oscillation amplitudes decay with time. Note particularly that as expected qualitatively, this decay is more pronounced for larger values of the accretion rate.

Given the time evolution of the shells, it is now useful to look at the corresponding phase space snapshots of all the shells. In Fig. 5.2 we have

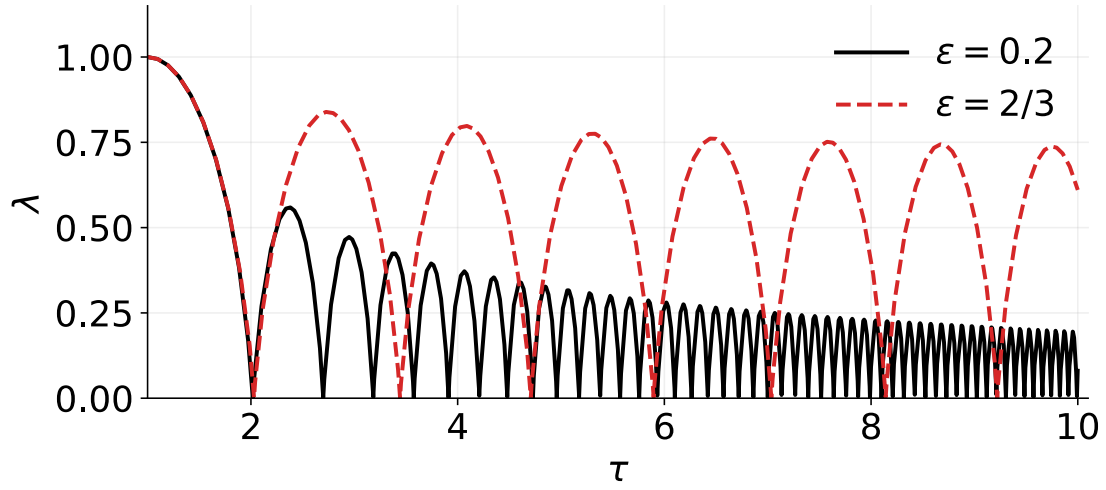

Figure 5.1: The evolution of the shell positions in the rescaled coordinates. We present the evolution for two values of accretion rate s.

computed the present-day phase-space positions of the shells for the same two values of the accretion rate as in Fig. 5.1. The colorbar indicates the redshift when the given shell has been at turnaround. It is particularly noteworthy that the radius separating the multi-stream/single-stream region (two dashed, vertical lines in both of the panels), also referred to as the splashback radius $r_{\rm sp}$ of the halo, is smaller in the case of the larger accretion rate. The corresponding values in the units of present-day turn-around radius are $r_{\rm sp}^{\epsilon=0.2}/R(t_0) = 0.12$ and $r_{\rm sp}^{\epsilon=2/3}/R(t_0) = 0.31$.

Finally, as mentioned above, an important outcome of this analysis is the matter density profile of the halo, which we present in Fig. 5.3. Note particularly the presence of the non-physical sharp caustic peak, which in a more realistic scenario would have been smoothed out by additional physical phenomena, such as matter inhomogeneities and non-radial orbits of the shells, not considered here.

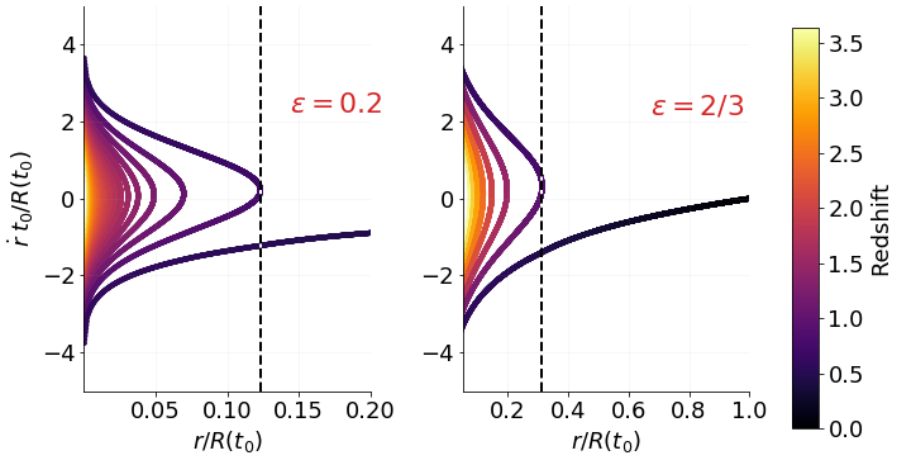

Figure 5.2: The snapshots of the shell phase spaces for the same values of the accretion rates as in Fig. 5.1. The snapshots are taken at the present time. The colorbar indicates the redshift when the given shell has been at turnaround. It is particularly noteworthy that the radius separating the multi-stream/single-stream region (two dashed, vertical lines in both of the panels), also referred to as the splashback radius $r_{\rm sp}$ of the halo, is smaller in the case of the larger accretion rate. The corresponding values in the units of present-day turn-around radius are $r_{\rm sp}^{\epsilon=0.2}/R(t_0) = 0.12$ and $r_{\rm sp}^{\epsilon=2/3}/R(t_0) = 0.31$.

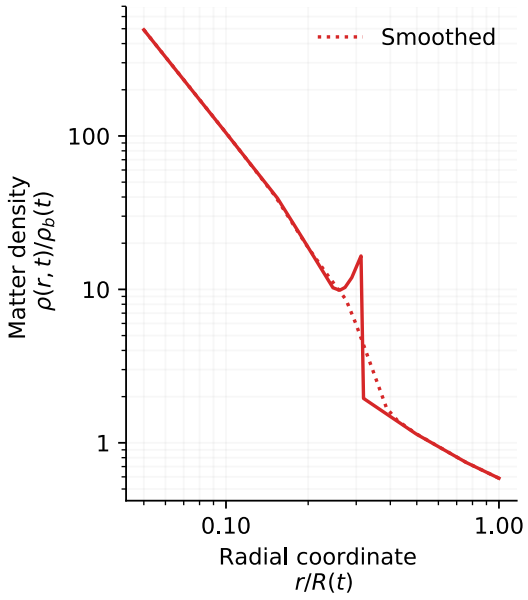

Figure 5.3: Prescription for the spherical halo density profile. The red dotted line is a smoothed version of the self-consistent profile which removes the non-physical sharp caustic.

It can be useful to note that the framework considered here can be applied in other configurations. Particularly, it can be applied to other 1-dimensional configurations, such as planar and cylindrical collapse. Additionally, in Ref. [240] the problem of tri-axial self-similar collapse is considered. For the sake of interest let us present the results for the case of self-similar planar collapse. The correspodning equation of motion in this case is (see [238])

$$\frac{d^2\lambda}{d\tau^2} = \frac{4}{9}\frac{\lambda}{\tau^2} - \frac{4}{3}\tau^{2s/3-4/3}\mathcal{M}\left(\frac{\lambda}{\Lambda(\tau)}\right), \tag{5.16}$$

with

$$\Lambda(\tau) = \tau^{2/3+2s/3}. \tag{5.17}$$

Fig. 5.4 demonstrates the shell trajectory for the case of $\epsilon = 0.6$. Note the qualitative difference compared to the spherical trajectories.

Analogously to the spherical case, in Fig. 5.5 we present the corresponding phase space snapshot of the shells for the same value of the accretion rate as in Fig. 5.4. Here z is the relevant coordinate, i.e. the distance from the plane of symmetry. The distance from the plane of symmetry separating the multi-streaming region from the single-streaming one is given by two dashed, vertical lines. The corresponding values in the units of present-day turn-around distance are $z_{\rm sp}^{\epsilon=0.2}/Z(t_0) = 0.08$.

5.4 SYMMETRON GRAVITY

In this section, we provide a brief overview of Symmetron gravity and introduce the framework needed to study its effects on spherical collapse.

We consider a scalar-tensor theory of the form

$$S = S_\varphi + S_M\left(\tilde{g}_{\mu\nu}, \Psi\right), \tag{5.18}$$

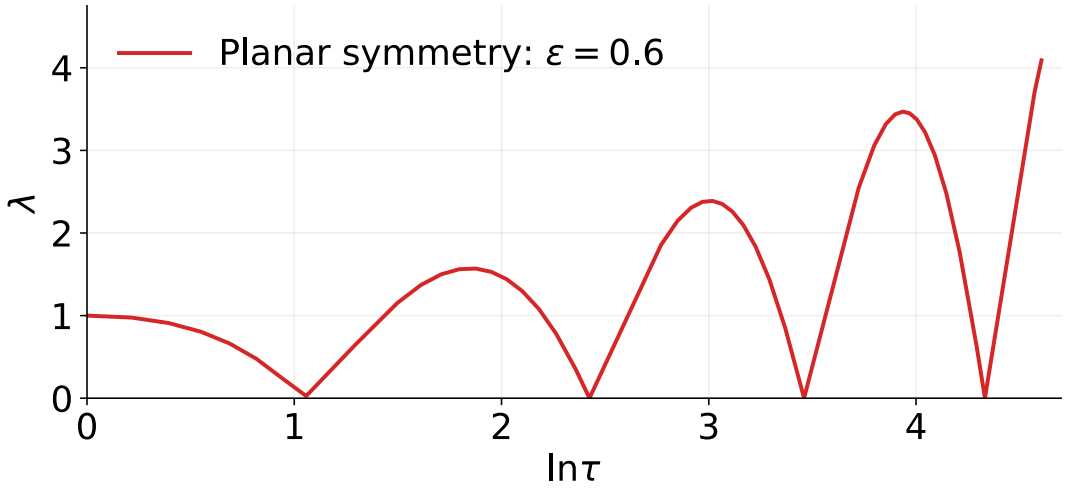

Figure 5.4: The evolution of the shell positions in the rescaled coordinates in the case of planar collapse.

with

$$S_\varphi = \int \sqrt{-g}\, d^4x \left[\frac{M_{\rm Pl}^2}{2} R - \frac{1}{2}\nabla^\mu\varphi\nabla_\mu\varphi - V(\varphi) \right], \tag{5.19}$$

$M_{\rm Pl}$ being the Planck mass, and $S_{\rm M}$ the action for the matter fields. The scalar field φ couples to the Einstein frame metric $g_{\mu\nu}$ with Ricci scalar R, while matter fields (collectively represented by Ψ) couple to the Jordan frame metric $\tilde{g}_{\mu\nu}$. The two metrics are assumed to be related by the transformation

$$\tilde{g}_{\mu\nu} = A^2(\varphi) g_{\mu\nu}. \tag{5.20}$$

Notice that such model is fully specified by the functions $A(\varphi)$ and $V(\varphi)$. Varying the action with respect to φ gives us the equation of motion:

$$\Box\varphi = V_{,\varphi} - A^3(\varphi)A_{,\varphi}(\varphi)\rho \equiv \tilde{V}_{,\varphi}(\varphi), \tag{5.21}$$

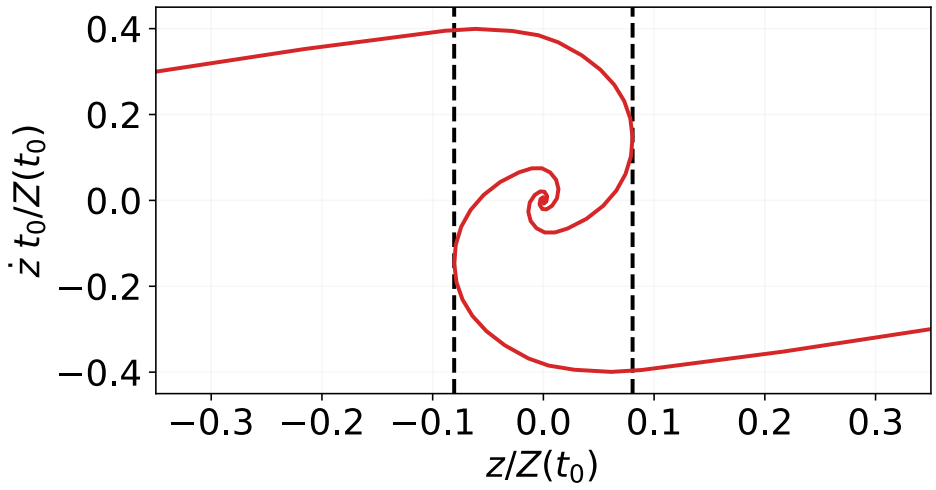

Figure 5.5: The phase space snapshot of the shells for the same value of the accretion rate as in Fig. 5.4. The snapshot is taken at the present time. The distance from the plane of symmetry separating the multi-streaming region from the single-streaming one is given by two dashed, vertical lines. The corresponding values in the units of present-day turn-around distance are $z_{\rm sp}^{\epsilon=0.2}/Z(t_0) = \pm 0.08$.

where ρ is the trace of the matter stress-energy tensor, equal to the local matter density, and $\tilde{V}(\varphi)$ is an effective potential. The fifth force per unit mass exerted by the field φ and experienced by a matter test particle can then be written as:

$$F_\varphi = -\nabla \log A(\varphi). \tag{5.22}$$

In this chapter we will focus on a realization of such a theory, namely the Symmetron model specified by the functions:

$$V(\varphi) = -\frac{1}{2}\mu\varphi^2 + \frac{1}{4}\lambda\varphi^4, \tag{5.23}$$

$$A(\varphi) = 1 + \frac{1}{2}\frac{\varphi^2}{M^2}, \tag{5.24}$$

and effective potential:

$$\tilde{V}(\varphi) = \frac{1}{2}\left(\frac{\rho}{M^2} - \mu^2\right)\varphi^2 + \frac{1}{4}\lambda\varphi^4. \tag{5.25}$$

In this parametrization, the Symmetron naturally assumes the form of an Effective Field Theory with $\varphi \to -\varphi$ symmetry.

In high-density regions, where the condition

$$\rho > \rho_{ssb} \equiv M^2\mu^2 \tag{5.26}$$

is satisfied, the effective potential $\tilde{V}(\varphi)$ has only one minimum in $\varphi = 0$ and the field is driven towards it, resulting in a null fifth force. In other words, high-density regions are screened. In low-density environments, on the other hand, the minimum is not located at zero. For example, for $\rho = 0$ the vacuum expectation value is given by $\varphi_0 = \mu/\sqrt{\lambda}$.

The fifth force can be constrained by local tests of gravity; to see in detail how local limits translate into bounds on the mass scale M and the Mexican

hat parameters μ, λ we refer the reader to [250], for a general overview, and to the introduction of [256], for a more recent analysis.

In an EdS background, the average matter density as a function of redshift z is

$$\rho_b = \frac{1}{6\pi G t^2} \propto (1+z)^3. \tag{5.27}$$

As the Universe expands, the Symmetron can undergo spontaneous symmetry breaking (SSB) when $\rho_b(z_{\rm ssb}) = \rho_{\rm ssb}$. For more details about the cosmological evolution of the Symmetron field and the allowed expansion histories, we refer the reader to [57, 257]. Let us stress however that we are not interested in the possibility of using the field φ to drive the late-time expansion of the Universe, but we are only interested in the additional fifth force and its effects on spherical collapse.

In this paper we will work in terms of the dimensionless field $\chi = \varphi/\varphi_0$ and Symmetron parameters composed by the average matter density at symmetry breaking ρ_{ssb}, the vacuum Compton wavelength

$$\lambda_0 = \frac{1}{\sqrt{2}\mu}, \tag{5.28}$$

and the dimensionless coupling

$$\beta = \frac{\varphi_0 M_{\rm Pl}}{M^2}. \tag{5.29}$$

Using these parameters, the fifth force sourced by the Symmetron field can be written as:

$$F_\varphi = -16\pi G \beta^2 \lambda_0^2 \rho_{ssb}\, \chi \nabla\chi. \tag{5.30}$$

5.5 SPHERICAL COLLAPSE WITH THE SYMMETRON

Having introduced the Symmetron, let us now go back to the original goal of this chapter, i.e. study spherical collapse in Symmetron gravity with a particular focus on splashback.

The splashback radius is commonly defined as the point where the density profile $\rho(r)$ is at its steepest. While this steepening is noteworthy because it can be detected as a departure from an equilibrium profile, this definition is clearly not suited for our study, where we assume a predefined density profile. Fortunately, the splashback radius is also known to be connected to the apocenter of recently accreted material and the location of the latest caustic visible in the density profile. Here we study the effects of the Symmetron force on splashback by using this latter definition.

Our simulation is based on a system of equations that includes the spherical collapse equations, as discussed in Sec. 5.3, coupled to the equation for the Symmetron field profile, discussed in Sec. 5.4. We start by presenting our numerical method to compute both the Symmetron field profile and the additional fifth force for the assumed density profile. We then proceed to integrate the shell equation to predict the fractional change in the splashback position in the presence of the Symmetron force.

5.5.1 *Field profile*

Assuming the temporal evolution of the field to be very fast compared to the other time-scales of the problem, i.e. the Hubble timescale and that of the clustering of matter, the dimensionless field profile $\chi(r)$ sourced by a density profile $\rho(r,t)$ satisfies the following equation:

$$\frac{d^2\chi}{dr^2} + \frac{2}{r}\frac{d\chi}{dr} = \frac{1}{2\lambda_0^2}\left[\left(\frac{\rho(r,t)}{\rho_{ssb}} - 1\right)\chi + \chi^3\right] . \tag{5.31}$$

This quasi-static approximation is common in the literature [258–260] and has been tested in the context of N-body simulations [261, 262]. In order to provide a rough, order of magnitude justification for this assumption, let us just mention that the timescale associated with the field dynamics in vacuum is given by $\sim \lambda_0/c$. It is clear that in order for the Symmetron field to be relevant for the dynamics of the spherical collapse, this λ_0 should be

of the same order of magnitude as the scale of the cluster itself. The latter, of course, is several orders of magnitude smaller than c/H_0.

The *static* Symmetron equation of motion (5.31) is a non-linear elliptical boundary value problem, for which we set the standard boundary conditions of vanishing spatial gradient of the field at $r = 0$ and $r \to \infty$. We use a one-dimensional version of the Newton-Gauss-Seidel relaxation method for the numerical integration of the equation. This is a standard method used for obtaining the scalar field profiles in N-body simulations with modifications of gravity mentioned above.

In practice, we discretize our $1D$ static Symmetron equation of motion on a regular grid of size h and use a second order discretization scheme for all the derivatives.[1] The resulting equation takes the form

$$\mathcal{L}[\chi_{i+1}, \chi_{i-1}; \chi_i] = 0, \tag{5.32}$$

where

$$\mathcal{L}[\chi_{i+1}, \chi_{i-1}; \chi_i] \equiv \mathcal{D}_{\rm K}[\chi_{i+1}, \chi_{i-1}; \chi_i] - \mathcal{D}_{\rm P}[\chi_i, \rho_i] \tag{5.33}$$

contains the discretization of the Laplace operator

$$\mathcal{D}_{\rm K} \equiv \frac{\chi_{i+1} + \chi_{i-1} - 2\chi_i}{h^2} + \frac{2}{r_i}\frac{\chi_{i+1} - \chi_{i-1}}{2h} \tag{5.34}$$

and the effective potential:

$$\mathcal{D}_{\rm P} = \frac{1}{\lambda_0^2}\left(\left(\frac{\rho_i}{\rho_{\rm ssb}} - 1\right)\chi_i + \chi_i^3\right). \tag{5.35}$$

The basic idea of the relaxation methods is to find a field profile from this equation which is closer to the real solution than a randomly chosen

1 We have tested some outputs of our integrator against the results of version where higher order discretization schemes are employed. For our particular problem we did not encounter significant differences in performance of the integrator and performed the main analysis with the version which employs the second order scheme.

initial guess. This step is iterated over multiple (improved) guesses labelled $\chi_n(i)$ until convergence is reached.

At a given step we define an improved (new) field profile:

$$\chi^{\rm new}(i) = \chi_n(i) - \left.\frac{\mathcal{L}(\chi(i))}{\partial\mathcal{L}(\chi(i))/\partial\chi(i)}\right|_{\chi(i)=\chi_n(i)}. \tag{5.36}$$

Then we use a part of this *new* χ as the field profile for our next relaxation iteration:

$$\chi_{n+1}(i) = \omega\chi^{\rm new} + (1-\omega)\chi_n, \tag{5.37}$$

where $0 < \omega \leqslant 1$ is a weight parameter with, in principle, a problem-dependent optimal value.

We employ two intuitive convergence diagnostics, where at each step we terminate the iteration if a certain parameter is within a predefined threshold. The first parameter is the residual function:

$$\mathcal{R}_1 \equiv \sqrt{\sum_i \mathcal{L}[\chi(i+1), \chi(i-1); \chi(i)]^2}, \tag{5.38}$$

and the second one is the all-mesh average of the fractional change in the field profile.

$$\mathcal{R}_2 \equiv \sqrt{\sum_i (\chi^{\rm new}(i) - \chi^{\rm old}(i))^2}. \tag{5.39}$$

To validate our integrator and convergence thresholds we compare the numerical solution to a known analytic solution. Below we present two different configurations.

For the first example let's first note that we can always plug a non-zero field profile in Eq. (5.31) and reconstruct a unique density profile which serves as a source for the mentioned field profile. As an example, we can choose a particular $\chi \sim \tanh(r)$ field profile. The gray line in the left panel

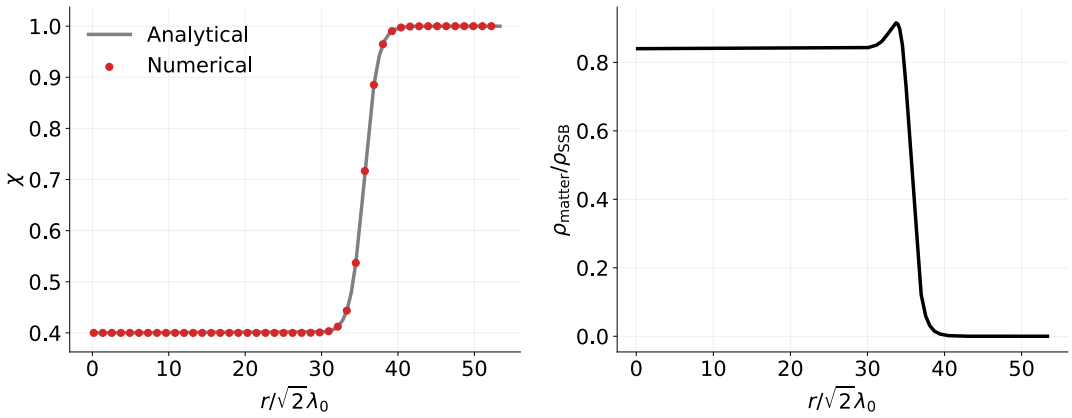

Figure 5.6: The gray line in the left panel is a chosen, non-zero field profile. The right panel demonstrates the corresponding reconstruction obtained by plugging the gray line from the left panel into Eq. (5.31). The red dots in the left panel are the result of the numerical integration using the density profile from the right panel as an input source.

of Fig. 5.6 is the chosen field profile. Thr right panel of the same figure demonstrates the corresponding reconstruction obtained by plugging the gray line from the left panel into Eq. (5.31). The red dots in the left panel are the result of the numerical integration using the density profile from the right panel as an input source. As one can see, the numerical integration successfully matches the expected analytical field configuration.

As our second example we consider the configuration of two parallel plates with infinitely high density, separated by a vacuum gap. Let the coordinate perpendicular to the plates be z with the gap width being Δz and the plate surfaces being placed at $-\Delta z/2$ and $+\Delta z/2$. The field equation of motion in this setup is given by

$$\frac{d^2\chi}{d\hat{z}^2} = \frac{1}{2\lambda_0^2}\left[(\tilde{\rho}(\hat{z}) - 1)\,\chi + \chi^3\right] , \tag{5.40}$$

where we have additionally defined $\hat{z} \equiv \sqrt{2} z \lambda_0$ and $\tilde{\rho}(\hat{z}) \equiv \rho(\hat{z})/M^2\mu^2$. We can integrate this equation once in a z-interval where the density is constant. Choosing two subsequent intervals being $(0, \Delta\hat{z}/2)$ and $(\Delta\hat{z}/2, \infty)$ we can show that the value of the field on the plate surface χ_s is zero up to negligible corrections of order of the ratio of the vacuum matter density to the plate density. Then, choosing an interval $(0, \hat{z})$ with $\hat{z} < \Delta\hat{z}/2$ we obtain

$$\hat{z} = \frac{1}{\sqrt{1 - \frac{\chi_g^2}{2}}} \left[F\left(\pi/2, \sqrt{\frac{\chi_g^2}{2 - \chi_g^2}}\right) - F\left(\sin^{-1}\frac{\chi}{\chi_g}, \sqrt{\frac{\chi_g^2}{2 - \chi_g^2}}\right) \right], \quad (5.41)$$

where F is the elliptic integral of the first kind, and χ_g is the field value in the middle of the gap. Fixing $\hat{z}$ to $\Delta\hat{z}/2$ and setting $\chi = 0$ we can numerically solve for χ_g. Having the latter we will then have χ as a function of $\hat{z}$ in the gap (written in terms of the Jacobi elliptic function).

We solve the Symmetron equation of motion Eq. (5.40) in the gap subject to boundary conditions $\chi(-\Delta\hat{z}/2) = 0 = \chi(+\Delta\hat{z}/2)$. In Fig. 5.7 we compare this with the numerical solution of Eq. (5.41).

For both of the considered examples the solver has been demonstrated to be able to converge to the correct solution with sub-percent level accuracy. The convergence has been checked to be robust against several numerical details, such as the grid resolution.

When solving for the density profile plotted in Fig. 5.3, we numerically evaluate the equation of motion in the range $[0, 2]$ for $r/R(t)$, where the density profile for $r \geq R(t)$ is assumed to be constant. We make sure that the arbitrary choice of the upper limit has no effect on our results by testing larger values.

5.5.2 *Splashback*

Once the Symmetron field profiles are found as a function of time, the present-day phase-space distribution of recently accreted material can be

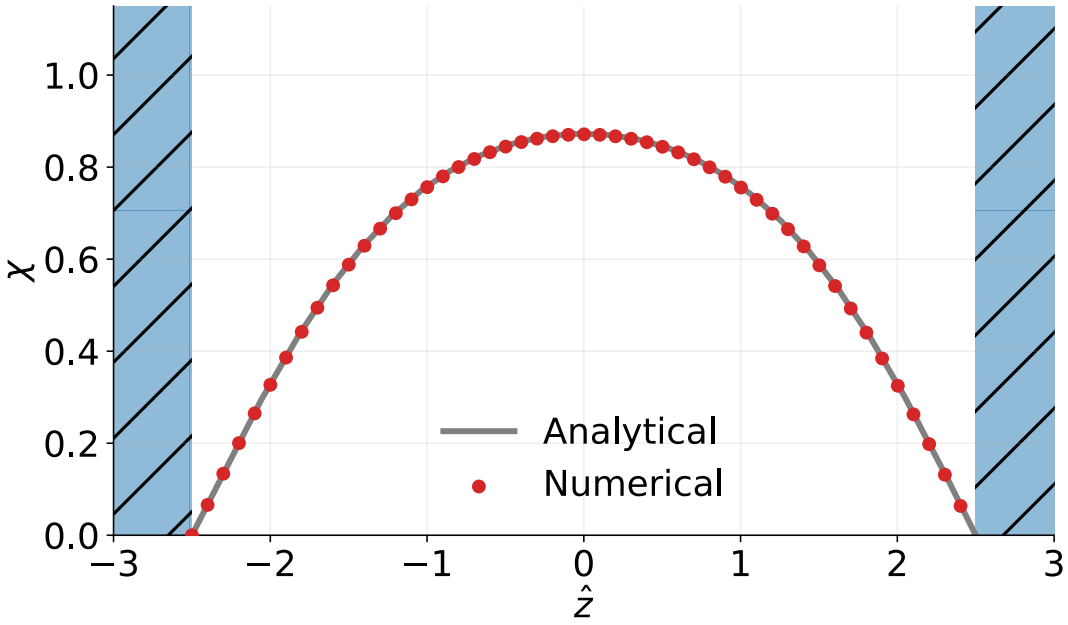

Figure 5.7: The field profile in the vacuum region between two infinitely dense parallel plates. The gray line is obtained by numerically solving Eq. (5.41). The red dots are the numerical solutions of the Symmetron equation of motion Eq. (5.40).

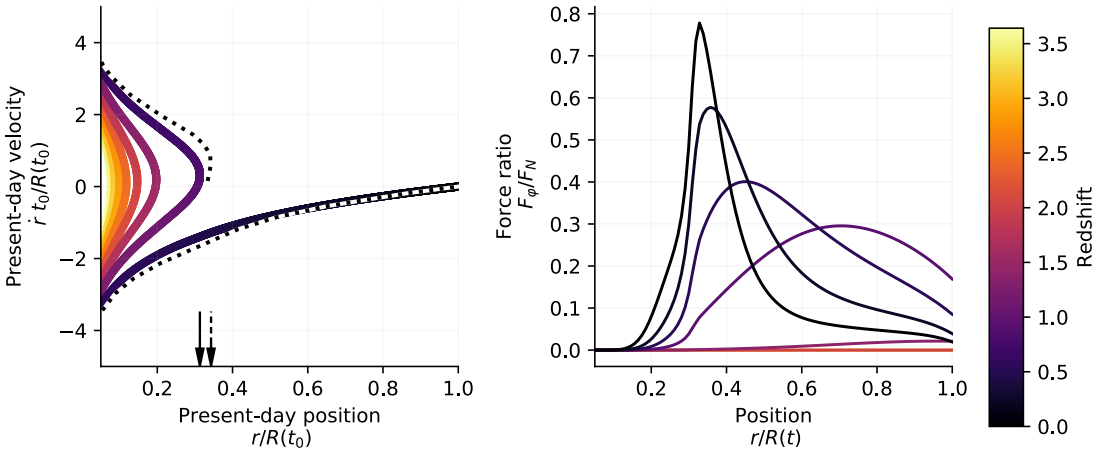

Figure 5.8: Effects of the Symmetron force on the splashback location for $\beta = 3, z_{\rm ssb} = 2$ and $\lambda_0/R(t_0) = 0.05$. On *the left panel* we show the phase-space distribution of shells around a spherically symmetric halo, where the shells are color-coded by their turn-around redshift. The dotted line shows how this distribution is affected by the presence of the Symmetron force. The arrows on the bottom point to the inferred splashback radius in the two cases. On *the right panel* we display the ratio between the Symmetron and the Newtonian force profiles, $\frac{F_S}{F_N}$, for different instants in time. At high redshifts, when the innermost material is accreted, the Symmetron force is ten times smaller than its peak value today.

obtained by integrating numerically the equation of motion (5.1) with added fifth force (5.30) for different collapse times.

We find that after imposing self-similarity, the collapse equations can be written only as a function of three dimensionless Symmetron parameters: the redshift of symmetry breaking $z_{\rm ssb}$, the dimensionless coupling β, and the ratio $\lambda_0/R(t_0)$ between the vacuum Compton wavelength λ_0 and the present-day turn-around radius $R(t_0)$. An important combination of these parameters is

$$f = (1+z_{\rm ssb})^3\beta^2\frac{\lambda_0^2}{R^2(t_0)}, \tag{5.42}$$

which explicitly sets the strength of the Symmetron force according to Eq. (5.30).

From our testing, we found that values $\lambda_0/R(t_0) \in [0.02, 0.1]$ offer non-trivial cases. For $\lambda_0 \sim R(t_0)$ we always obtain *thin-shell*-like solutions, while for $\lambda_0 \ll R(t_0)$ the field is heavy and simply relaxes onto the minimum of the potential $\tilde{V}(\chi)$ in Eq. (5.25).

In Fig. 5.8 we illustrate our method and show how the Symmetron force modifies the phase-space configuration of the latest accreted orbits (left panel). We find that the splashback position is significantly affected for parameter values $f \sim 1$, $z_{\rm ssb} \sim 2$ and $\lambda_0/R(t_0) \sim 0.1$. These values imply $M \lesssim 10^{-3}M_{\rm Pl}$, which is in agreement with local tests of gravity [250].

From the same figure (right panel), it is clear that the innermost regions of the overdensity are screened from the effects of the fifth force at all times and this becomes relevant in the outer regions only for $z \ll z_{\rm ssb}$. Past this point, the force profile slowly transitions from a *thick-shell* to a *thin-shell* like behaviour, where the force gets progressively concentrated around the surface of the screened region [263]. Due to the sudden drop in density associated with splashback, this surface is delimited by the splashback radius.

A systematic exploration of the Symmetron effects on this feature as a function of all parameters is presented in Fig. 5.9, which represents our main result. A clear trend with $z_{\rm ssb}$ is visible. Notice that the fractional change on the splashback position has an optimal peak as a function of $z_{\rm ssb}$ that is independent of f. If we call $z_{\rm sp}$ the accretion redshift of the shell currently sitting at the splashback position after its first pericenter, i.e. the *splashback shell*, we see that the effect is maximized when $z_{\rm sp} \simeq z_{\rm ssb}$. This is easily explained by studying the profile of the fifth force over time. For $z_{\rm sp} \gg z_{\rm ssb}$, the selected shell collapses when the Symmetron is in its symmetric phase and the material spends the rest of its trajectory in a screened region, away from the effects of the fifth-force; for $z_{\rm sp} \ll z_{\rm ssb}$, the thin shell has had time to form before $z_{\rm sp}$ and the shell feels the effects of the fifth force only during a small fraction of its trajectory. Between these two limiting cases there is an efficient $z_{\rm ssb}$ for which the splashback shell has time to follow the formation of the thin shell and it is optimally positioned near the peak of the force profile for most of its trajectory. In our figure, we show how this peak still has a dependence on λ_0, introduced by the presence of this factor on the Symmetron equation of motion (5.31).

To conclude this section, we point out that the smoothness of the density profile as plotted in Fig. 5.3 has little impact on our results and no impact on the trends discussed above. Differences between the two prescriptions exist only for $\lambda_0 \ll R(t_0)$, when the field profile becomes susceptible to the small-scale features of the profile. However, since we expect the sharp caustic to be smoothed by gravitational instabilities, for the main results we chose not to use the discontinuous profile and assumed instead its smoothed version. Notice also that considering such high-resolution scenarios would introduce additional caveats (e.g. the presence of sub-structure) that are not the focus of this chapter.

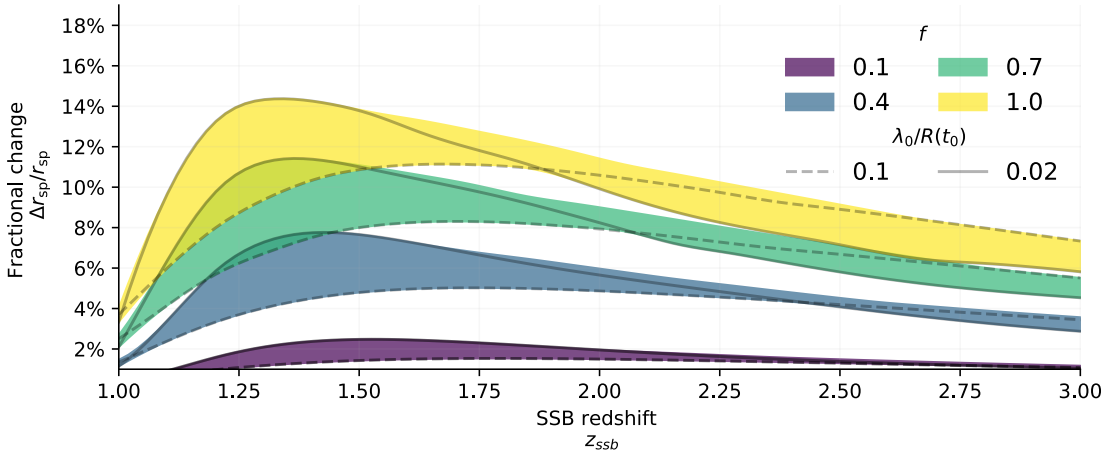

Figure 5.9: Percentage change in the splashback position in Symmetron gravity as a function of Symmetron parameters: the dimensionless force strength f and the SSB redshift $z_{\rm ssb}$. The spread of the different curves is given by variations of the third parameter, the vacuum Compton wavelength of the field λ_0. We emphasize in particular the cases $\lambda_0/R(t_0) = 0.1$ (dashed line) and $\lambda_0/R(t_0) = 0.02$ (solid line), where $R(t_0)$ is the present-day turn-around radius.

5.6 DISCUSSION AND CONCLUSION

In this chapter, we have explored how Symmetron gravity affects the splashback feature at the edges of cosmological haloes. In our approach, we assume a self-similar mass distribution motivated by spherical collapse in an EdS Universe, where the shape of the spherically symmetric matter distribution is assumed to be only a function of $r/R(t)$. This allows us to easily solve for the corresponding Symmetron fifth force and estimate its effects on the splashback feature by studying the changed phase-space distribution of recently accreted shells.

The main limitation of our study is the lack of a fully consistent framework where the density profile, the turn-around physics and the phase-space distribution are solved for in conjunction with the newly introduced Symmetron equation of motion. As an example, we would expect a consistent framework to take into account the back-reaction of the scalar field on the density profile.

While deriving self-consistent solutions is outside the scope of this paper and more suited to N-body simulation studies, we find it useful to discuss the impact of our assumptions on the results. Changes to the turn-around physics are commonly studied through the use of different approximations, like a scale-dependent Newton's constant [264–268]. In our case, if we maintain the assumptions of self-similarity and power-law accretion in Eq. (5.7), the main change to our formalism will come in the form of upgrading the numerical constant appearing in Eq. (5.8) to a function of the perturbation scale and cosmic time.

Previous works have estimated these corrections to be of the order of a few percentage points at $z \simeq 0$; see [263] for results in Symmetron gravity and [268] for similar results in $f(R)$ theory. In particular, we expect our assumption to first break at a redshift z such that the condition $F_\varphi(r) \sim F_N(r)$ is satisfied at the turnaround radius $r = R(t)$. In our analysis, however, we have seen that the effects on splashback are maximized when the collapse

redshift of the splashback shell $z_{\rm sp}$ is equivalent to this transition redshift. After this point, the splashback shell is confined in the inner region and we expect its trajectory to be unaffected by the turn-around physics. Therefore, we consider our results around the peak of Fig. 5.9 to be robust against this assumption. For the same reason, however, we expect to lose predictability for higher values of $z_{\rm ssb}$, since the initial condition of the splashback shell will differ from what we have assumed.

Notice that the argument presented above also implies that our results can be extended to a standard ΛCDM scenario. The present-day splashback shell is expected to have collapsed in the matter-dominated era and to have followed a trajectory mostly unaffected by the late-time expansion, especially for low values of the accretion rate s like the one considered here [241].

Effects of modified gravity on the structure of dark matter halos are usually presented in the form of changes in the small-scale power spectra [258, 260, 269, 270] and two-point correlation functions [271] or the whole phase-space distribution [272, 273]. In this analysis, we focused instead on a particular scale, the splashback radius, and showed that up to a 10% change can be induced (Fig. 5.9). It should be pointed out that [274] was the first work to explore how modified gravity affects the splashback position. We stress, however, that our work differs from theirs in three major aspects. First, here we focus on Symmetron gravity which displays a different screening mechanism from the chameleon or k-mouflage explored in [274] . Second, while their results based on N-body simulations represent more realistic predictions, they do not allow for a simple exploration of the theory parameter space. Third, with our semi-analytical approach, we are able to gain insight by obtaining quantitative results as a function of multiple theory parameters and provide an explanation for the visible trends. All this said, it also should be mentioned that the quantitative estimation of the modelling uncertainties will still resort on N-body simulations. This is

an interesting aspect and we leave its systematic investigation to a future work.

Observationally, splashback can be measured predominantly around galaxy clusters, for which the present-day turn-around radius $R(t_0)$ is of the order of a few Mpc. Our results, therefore, imply that this feature can be used to constrain fifth forces with vacuum Compton wavelength λ_0 just below the Mpc scale. Because the measurements of splashback in the galaxy distributions around clusters have already achieved a precision below the size of our predicted effect [246–249], we expect to soon be able to constrain not only the Symmetron, but other fifth force models on similar scales.

Note in particular that, while other works have explored the possibility of constraining Symmetron gravity on Mpc scales [275, 276], the range considered here for λ_0 is unconstrained for this model. Thus we expect a measurement based on splashback to naturally complement other results based on laboratory experiments [277, 278], stellar and compact astrophysical objects [279, 280] or galactic disks and stellar clusters [256, 281, 282].

As the physics of splashback matures into a new cosmological observable, we expect it to play a powerful role in testing modifications of gravity, complementary to already established techniques such as those for large scale structure.

Acknowledgments We thank Bhuvnesh Jain and Masahiro Takada for helpful discussions.

BIBLIOGRAPHY

[1] Adam G. Riess et al. "Observational evidence from supernovae for an accelerating universe and a cosmological constant." In: *Astron. J.* 116 (1998), pp. 1009–1038. DOI: 10.1086/300499. arXiv: astro-ph/9805201 [astro-ph].

[2] S. Perlmutter et al. "Measurements of Omega and Lambda from 42 high redshift supernovae." In: *Astrophys. J.* 517 (1999), pp. 565–586. DOI: 10.1086/307221. arXiv: astro-ph/9812133 [astro-ph].

[3] Jerome Martin. "Everything You Always Wanted To Know About The Cosmological Constant Problem (But Were Afraid To Ask)." In: *Comptes Rendus Physique* 13 (2012), pp. 566–665. DOI: 10.1016/j.crhy.2012.04.008. arXiv: 1205.3365 [astro-ph.CO].

[4] A. Friedman. "Über die Krümmung des Raumes." In: *Zeitschrift für Physik* 10.1 (1922), pp. 377–386. ISSN: 0044-3328. DOI: 10.1007/BF01332580. URL: https://doi.org/10.1007/BF01332580.

[5] A. Friedmann. "Über die Möglichkeit einer Welt mit konstanter negativer Krümmung des Raumes." In: *Zeitschrift für Physik* 21.1 (1924), pp. 326–332. ISSN: 0044-3328. DOI: 10.1007/BF01328280. URL: https://doi.org/10.1007/BF01328280.

[6] M. Livio. "Lost in translation: Mystery of the missing text solved." In: 479 (Nov. 2011), pp. 171–173. DOI: 10.1038/479171a.

[7] Albert Einstein. "The Foundation of the General Theory of Relativity." In: *Annalen Phys.* 49.7 (1916), pp. 769–822. DOI: 10.1002/andp.200590044,10.1002/andp.19163540702.

[8] N. Aghanim et al. "Planck 2018 results. VI. Cosmological parameters." In: (2018). arXiv: 1807.06209 [astro-ph.CO].

[9] L. Amendola and S. Tsujikawa. *Dark Energy: Theory and Observations*. 2010.

[10] S. Dodelson. *Modern cosmology*. 2003.

[11] C. Wetterich. "Cosmology and the Fate of Dilatation Symmetry." In: *Nucl. Phys.* B302 (1988), pp. 668–696. DOI: 10.1016/0550-3213(88)90193-9. arXiv: 1711.03844 [hep-th].

[12] Bharat Ratra and P. J. E. Peebles. "Cosmological consequences of a rolling homogeneous scalar field." In: *Phys. Rev. D* 37 (12 1988), pp. 3406–3427. DOI: 10.1103/PhysRevD.37.3406. URL: https://link.aps.org/doi/10.1103/PhysRevD.37.3406.

[13] Georges Obied, Hirosi Ooguri, Lev Spodyneiko, and Cumrun Vafa. "De Sitter Space and the Swampland." In: (2018). arXiv: 1806.08362 [hep-th].

[14] Andrei D. Linde. "The Inflationary Universe." In: *Rept. Prog. Phys.* 47 (1984), pp. 925–986. DOI: 10.1088/0034-4885/47/8/002.

[15] A. D. Sakharov. "Cosmological Transitions With a Change in Metric Signature." In: *Sov. Phys. JETP* 60 (1984). [Sov. Phys. Usp.34,409(1991)], pp. 214–218.

[16] Raphael Bousso and Joseph Polchinski. "Quantization of four form fluxes and dynamical neutralization of the cosmological constant." In: *JHEP* 06 (2000), p. 006. DOI: 10.1088/1126-6708/2000/06/006. arXiv: hep-th/0004134 [hep-th].

[17] Shamit Kachru, Renata Kallosh, Andrei D. Linde, and Sandip P. Trivedi. "De Sitter vacua in string theory." In: *Phys. Rev.* D68 (2003), p. 046005. DOI: 10.1103/PhysRevD.68.046005. arXiv: hep-th/0301240 [hep-th].

[18] Michael R. Douglas. "The Statistics of string / M theory vacua." In: *JHEP* 05 (2003), p. 046. DOI: 10.1088/1126-6708/2003/05/046. arXiv: hep-th/0303194 [hep-th].

[19] Leonard Susskind. "The Anthropic landscape of string theory." In: (2003). arXiv: hep-th/0302219 [hep-th].

[20] Andrei Linde. "A brief history of the multiverse." In: *Rept. Prog. Phys.* 80.2 (2017), p. 022001. DOI: 10.1088/1361-6633/aa50e4. arXiv: 1512.01203 [hep-th].

[21] Eran Palti. "The Swampland: Introduction and Review." In: 2019. arXiv: 1903.06239 [hep-th].

[22] Yashar Akrami, Renata Kallosh, Andrei Linde, and Valeri Vardanyan. "The Landscape, the Swampland and the Era of Precision Cosmology." In: *Fortsch. Phys.* 67.1-2 (2019), p. 1800075. DOI: 10.1002/prop.201800075. arXiv: 1808.09440 [hep-th].

[23] Edmund J. Copeland, M. Sami, and Shinji Tsujikawa. "Dynamics of dark energy." In: *Int. J. Mod. Phys.* D15 (2006), pp. 1753–1936. DOI: 10.1142/S021827180600942X. arXiv: hep-th/0603057 [hep-th].

[24] Austin Joyce, Bhuvnesh Jain, Justin Khoury, and Mark Trodden. "Beyond the Cosmological Standard Model." In: *Phys. Rept.* 568 (2015), pp. 1–98. DOI: 10.1016/j.physrep.2014.12.002. arXiv: 1407.0059 [astro-ph.CO].

[25] Sean M. Carroll, Mark Hoffman, and Mark Trodden. "Can the dark energy equation - of - state parameter w be less than -1?" In: *Phys. Rev.* D68 (2003), p. 023509. DOI: 10.1103/PhysRevD.68.023509. arXiv: astro-ph/0301273 [astro-ph].

[26] James M. Cline, Sangyong Jeon, and Guy D. Moore. "The Phantom menaced: Constraints on low-energy effective ghosts." In: *Phys. Rev.* D70 (2004), p. 043543. DOI: 10.1103/PhysRevD.70.043543. arXiv: hep-ph/0311312 [hep-ph].

[27] M. Ostrogradsky. In: *Mem. Ac. St. Petersbourg* 6 (1850), p. 385.

[28] Richard P. Woodard. "Avoiding dark energy with 1/r modifications of gravity." In: *Lect. Notes Phys.* 720 (2007), pp. 403–433. DOI: 10.1007/978-3-540-71013-4_14. arXiv: astro-ph/0601672 [astro-ph].

[29] Gregory Walter Horndeski. "Second-order scalar-tensor field equations in a four-dimensional space." In: *Int. J. Theor. Phys.* 10 (1974), pp. 363–384. DOI: 10.1007/BF01807638.

[30] C. Deffayet, S. Deser, and G. Esposito-Farese. "Generalized Galileons: All scalar models whose curved background extensions maintain second-order field equations and stress-tensors." In: *Phys. Rev.* D80 (2009), p. 064015. DOI: 10.1103/PhysRevD.80.064015. arXiv: 0906.1967 [gr-qc].

[31] C. Brans and R. H. Dicke. "Mach's Principle and a Relativistic Theory of Gravitation." In: *Phys. Rev.* 124 (3 1961), pp. 925–935. DOI: 10.1103/PhysRev.124.925. URL: https://link.aps.org/doi/10.1103/PhysRev.124.925.

[32] Antonio De Felice, Tsutomu Kobayashi, and Shinji Tsujikawa. "Effective gravitational couplings for cosmological perturbations in the most general scalar-tensor theories with second-order field equations." In: *Phys. Lett.* B706 (2011), pp. 123–133. DOI: 10.1016/j.physletb.2011.11.028. arXiv: 1108.4242 [gr-qc].

[33] B. P. Abbott et al. "GW170817: Observation of Gravitational Waves from a Binary Neutron Star Inspiral." In: *Phys. Rev. Lett.* 119.16 (2017), p. 161101. DOI: 10.1103/PhysRevLett.119.161101. arXiv: 1710.05832 [gr-qc].

[34] A. Goldstein et al. "An Ordinary Short Gamma-Ray Burst with Extraordinary Implications: Fermi-GBM Detection of GRB 170817A."

In: *Astrophys. J.* 848.2 (2017), p. L14. DOI: 10.3847/2041-8213/aa8f41. arXiv: 1710.05446 [astro-ph.HE].

[35] Jose María Ezquiaga and Miguel Zumalacárregui. "Dark Energy in light of Multi-Messenger Gravitational-Wave astronomy." In: *Front. Astron. Space Sci.* 5 (2018), p. 44. DOI: 10.3389/fspas.2018.00044. arXiv: 1807.09241 [astro-ph.CO].

[36] M. Fierz and W. Pauli. "On relativistic wave equations for particles of arbitrary spin in an electromagnetic field." In: *Proc.Roy.Soc.Lond.* A173 (1939), pp. 211–232. DOI: 10.1098/rspa.1939.0140.

[37] Claudia de Rham and Gregory Gabadadze. "Generalization of the Fierz-Pauli Action." In: *Phys.Rev.* D82 (2010), p. 044020. DOI: 10.1103/PhysRevD.82.044020. arXiv: 1007.0443 [hep-th].

[38] Claudia de Rham, Gregory Gabadadze, and Andrew J. Tolley. "Resummation of Massive Gravity." In: *Phys.Rev.Lett.* 106 (2011), p. 231101. DOI: 10.1103/PhysRevLett.106.231101. arXiv: 1011.1232 [hep-th].

[39] S.F. Hassan and Rachel A. Rosen. "On Non-Linear Actions for Massive Gravity." In: *JHEP* 1107 (2011), p. 009. DOI: 10.1007/JHEP07(2011)009. arXiv: 1103.6055 [hep-th].

[40] S.F. Hassan and Rachel A. Rosen. "Resolving the Ghost Problem in non-Linear Massive Gravity." In: *Phys.Rev.Lett.* 108 (2012), p. 041101. DOI: 10.1103/PhysRevLett.108.041101. arXiv: 1106.3344 [hep-th].

[41] Claudia de Rham, Gregory Gabadadze, and Andrew J. Tolley. "Ghost free Massive Gravity in the Stückelberg language." In: *Phys.Lett.* B711 (2012), pp. 190–195. DOI: 10.1016/j.physletb.2012.03.081. arXiv: 1107.3820 [hep-th].

[42] Claudia de Rham, Gregory Gabadadze, and Andrew J. Tolley. "Helicity Decomposition of Ghost-free Massive Gravity." In: *JHEP* 1111 (2011), p. 093. DOI: 10.1007/JHEP11(2011)093. arXiv: 1108.4521 [hep-th].

[43] S.F. Hassan, Rachel A. Rosen, and Angnis Schmidt-May. "Ghost-free Massive Gravity with a General Reference Metric." In: *JHEP* 1202 (2012), p. 026. DOI: 10.1007/JHEP02(2012)026. arXiv: 1109.3230 [hep-th].

[44] S.F. Hassan and Rachel A. Rosen. "Confirmation of the Secondary Constraint and Absence of Ghost in Massive Gravity and Bimetric Gravity." In: *JHEP* 1204 (2012), p. 123. DOI: 10.1007/JHEP04(2012)123. arXiv: 1111.2070 [hep-th].

[45] S.F. Hassan, Angnis Schmidt-May, and Mikael von Strauss. "Proof of Consistency of Nonlinear Massive Gravity in the Stückelberg Formulation." In: *Phys.Lett.* B715 (2012), pp. 335–339. DOI: 10.1016/j.physletb.2012.07.018. arXiv: 1203.5283 [hep-th].

[46] Kurt Hinterbichler and Rachel A. Rosen. "Interacting Spin-2 Fields." In: *JHEP* 1207 (2012), p. 047. DOI: 10.1007/JHEP07(2012)047. arXiv: 1203.5783 [hep-th].

[47] S.F. Hassan and Rachel A. Rosen. "Bimetric Gravity from Ghost-free Massive Gravity." In: *JHEP* 1202 (2012), p. 126. DOI: 10.1007/JHEP02(2012)126. arXiv: 1109.3515 [hep-th].

[48] Claudia de Rham. "Massive Gravity." In: *Living Rev.Rel.* 17 (2014), p. 7. DOI: 10.12942/lrr-2014-7. arXiv: 1401.4173 [hep-th].

[49] Kurt Hinterbichler. "Theoretical Aspects of Massive Gravity." In: *Rev.Mod.Phys.* 84 (2012), pp. 671–710. DOI: 10.1103/RevModPhys.84.671. arXiv: 1105.3735 [hep-th].

[50] Kurt Hinterbichler. "Cosmology of Massive Gravity and its Extensions." In: *51st Rencontres de Moriond on Cosmology La Thuile*. 2017. arXiv: 1701.02873 [astro-ph.CO]. URL: http://inspirehep.net/record/1508592/files/arXiv:1701.02873.pdf.

[51] Angnis Schmidt-May and Mikael von Strauss. "Recent developments in bimetric theory." In: *J. Phys.* A49.18 (2016), p. 183001. DOI: 10.1088/1751-8113/49/18/183001. arXiv: 1512.00021 [hep-th].

[52] Adam Ross Solomon. "Cosmology Beyond Einstein." PhD thesis. Cham: Cambridge U., 2015. DOI: 10.1007/978-3-319-46621-7. arXiv: 1508.06859 [gr-qc]. URL: http://www.springer.com/gp/book/9783319466200.

[53] Yashar Akrami, S. F. Hassan, Frank Könnig, Angnis Schmidt-May, and Adam R. Solomon. "Bimetric gravity is cosmologically viable." In: *Phys. Lett.* B748 (2015), pp. 37–44. DOI: 10.1016/j.physletb.2015.06.062. arXiv: 1503.07521 [gr-qc].

[54] E. Mortsell and J. Enander. "Scalar instabilities in bimetric gravity: The Vainshtein mechanism and structure formation." In: *JCAP* 1510.10 (2015), p. 044. DOI: 10.1088/1475-7516/2015/10/044. arXiv: 1506.04977 [astro-ph.CO].

[55] C. M. Will. *Theory and experiment in gravitational physics*. 1993. ISBN: 9780521439732.

[56] Justin Khoury and Amanda Weltman. "Chameleon cosmology." In: *Phys. Rev.* D69 (2004), p. 044026. DOI: 10.1103/PhysRevD.69.044026. arXiv: astro-ph/0309411 [astro-ph].

[57] Kurt Hinterbichler, Justin Khoury, Aaron Levy, and Andrew Matas. "Symmetron Cosmology." In: *Phys. Rev.* D84 (2011), p. 103521. DOI: 10.1103/PhysRevD.84.103521. arXiv: 1107.2112 [astro-ph.CO].

[58] A.I. Vainshtein. "To the problem of nonvanishing gravitation mass." In: *Phys.Lett.* B39 (1972), pp. 393–394. DOI: 10.1016/0370-2693(72)90147-5.

[59] Eugeny Babichev and Cédric Deffayet. "An introduction to the Vainshtein mechanism." In: *Class.Quant.Grav.* 30 (2013), p. 184001. DOI: 10.1088/0264-9381/30/18/184001. arXiv: 1304.7240 [gr-qc].

[60] Y. Akrami et al. "Planck 2018 results. X. Constraints on inflation." In: (2018). arXiv: 1807.06211 [astro-ph.CO].

[61] E. Komatsu et al. "Seven-Year Wilkinson Microwave Anisotropy Probe (WMAP) Observations: Cosmological Interpretation." In: *Astrophys. J. Suppl.* 192 (2011), p. 18. DOI: 10.1088/0067-0049/192/2/18. arXiv: 1001.4538 [astro-ph.CO].

[62] Urbano Franca and Rogerio Rosenfeld. "Fine tuning in quintessence models with exponential potentials." In: *JHEP* 10 (2002), p. 015. DOI: 10.1088/1126-6708/2002/10/015. arXiv: astro-ph/0206194 [astro-ph].

[63] Renata Kallosh, Andrei D. Linde, Sergey Prokushkin, and Marina Shmakova. "Supergravity, dark energy and the fate of the universe." In: *Phys. Rev.* D66 (2002), p. 123503. DOI: 10.1103/PhysRevD.66.123503. arXiv: hep-th/0208156 [hep-th].

[64] Yashar Akrami, Renata Kallosh, Andrei Linde, and Valeri Vardanyan. "Dark energy, α-attractors, and large-scale structure surveys." In: *JCAP* 1806.06 (2018), p. 041. DOI: 10.1088/1475-7516/2018/06/041. arXiv: 1712.09693 [hep-th].

[65] Yashar Akrami, Philippe Brax, Anne-Christine Davis, and Valeri Vardanyan. "Neutron star merger GW170817 strongly constrains doubly coupled bigravity." In: *Phys. Rev.* D97.12 (2018), p. 124010. DOI: 10.1103/PhysRevD.97.124010. arXiv: 1803.09726 [astro-ph.CO].

[66] Adam R. Solomon, Valeri Vardanyan, and Yashar Akrami. "Massive mimetic cosmology." In: *Phys. Lett.* B794 (2019), pp. 135–142. DOI: 10.1016/j.physletb.2019.05.045. arXiv: 1902.08533 [astro-ph.CO].

[67] Omar Contigiani, Valeri Vardanyan, and Alessandra Silvestri. "Splashback radius in symmetron gravity." In: *Phys. Rev.* D99.6 (2019), p. 064030. DOI: 10.1103/PhysRevD.99.064030. arXiv: 1812.05568 [astro-ph.CO].

[68] S. Bellucci, A. A. Saharian, D. H. Simonyan, and V. V. Vardanyan. "Fermionic currents in topologically nontrivial braneworlds." In: *Phys. Rev.* D98.8 (2018), p. 085020. DOI: 10.1103/PhysRevD.98.085020. arXiv: 1808.01577 [hep-th].

[69] S. Bellucci, A. A. Saharian, and V. Vardanyan. "Fermionic currents in AdS spacetime with compact dimensions." In: *Phys. Rev.* D96.6 (2017), p. 065025. DOI: 10.1103/PhysRevD.96.065025. arXiv: 1707.08878 [hep-th].

[70] Valeri Vardanyan, Yashar Akrami, Luca Amendola, and Alessandra Silvestri. "On nonlocally interacting metrics, and a simple proposal for cosmic acceleration." In: *JCAP* 1803.03 (2018), p. 048. DOI: 10.1088/1475-7516/2018/03/048. arXiv: 1702.08908 [gr-qc].

[71] S. Bellucci, A. A. Saharian, and V. Vardanyan. "Hadamard function and the vacuum currents in braneworlds with compact dimensions: Two-brane geometry." In: *Phys. Rev.* D93.8 (2016), p. 084011. DOI: 10.1103/PhysRevD.93.084011. arXiv: 1512.06569 [hep-th].

[72] S. Bellucci, A. A. Saharian, and V. Vardanyan. "Vacuum currents in braneworlds on AdS bulk with compact dimensions." In: *JHEP* 11 (2015), p. 092. DOI: 10.1007/JHEP11(2015)092. arXiv: 1508.07255 [hep-th].

[73] Valeri Vardanyan and Luca Amendola. "How can we tell whether dark energy is composed of multiple fields?" In: *Phys. Rev.* D92.2 (2015), p. 024009. DOI: 10.1103/PhysRevD.92.024009. arXiv: 1502.05922 [gr-qc].

[74] E. R. Bezerra de Mello, A. A. Saharian, and V. Vardanyan. "Induced vacuum currents in anti-de Sitter space with toral dimensions." In: *Phys. Lett.* B741 (2015), pp. 155–162. DOI: 10.1016/j.physletb.2014.12.036. arXiv: 1410.2860 [hep-th].

[75] Valeri Vardanyan, Daniel Weedman, and Lusine Sargsyan. "Seeking the Epoch of Maximum Luminosity for Dusty Quasars." In: *Astrophys. J.* 790 (2014), p. 88. DOI: 10.1088/0004-637X/790/2/88. arXiv: 1406.2002 [astro-ph.GA].

[76] Renata Kallosh and Andrei Linde. "Universality Class in Conformal Inflation." In: *JCAP* 1307 (2013), p. 002. DOI: 10.1088/1475-7516/2013/07/002. arXiv: 1306.5220 [hep-th].

[77] Sergio Ferrara, Renata Kallosh, Andrei Linde, and Massimo Porrati. "Minimal Supergravity Models of Inflation." In: *Phys. Rev.* D88.8 (2013), p. 085038. DOI: 10.1103/PhysRevD.88.085038. arXiv: 1307.7696 [hep-th].

[78] Renata Kallosh, Andrei Linde, and Diederik Roest. "Superconformal Inflationary α-Attractors." In: *JHEP* 11 (2013), p. 198. DOI: 10.1007/JHEP11(2013)198. arXiv: 1311.0472 [hep-th].

[79] Sergio Cecotti and Renata Kallosh. "Cosmological Attractor Models and Higher Curvature Supergravity." In: *JHEP* 05 (2014), p. 114. DOI: 10.1007/JHEP05(2014)114. arXiv: 1403.2932 [hep-th].

[80] Mario Galante, Renata Kallosh, Andrei Linde, and Diederik Roest. "Unity of Cosmological Inflation Attractors." In: *Phys. Rev. Lett.* 114.14 (2015), p. 141302. DOI: 10.1103/PhysRevLett.114.141302. arXiv: 1412.3797 [hep-th].

[81] Renata Kallosh and Andrei Linde. "Escher in the Sky." In: *Comptes Rendus Physique* 16 (2015), pp. 914–927. DOI: 10.1016/j.crhy.2015.07.004. arXiv: 1503.06785 [hep-th].

[82] P. A. R. Ade et al. "Planck 2015 results. XX. Constraints on inflation." In: *Astron. Astrophys.* 594 (2016), A20. DOI: 10.1051/0004-6361/201525898. arXiv: 1502.02114 [astro-ph.CO].

[83] Eric V. Linder. "Dark Energy from α-Attractors." In: *Phys. Rev.* D91.12 (2015), p. 123012. DOI: 10.1103/PhysRevD.91.123012. arXiv: 1505.00815 [astro-ph.CO].

[84] Konstantinos Dimopoulos and Charlotte Owen. "Quintessential Inflation with α-attractors." In: *JCAP* 1706.06 (2017), p. 027. DOI: 10.1088/1475-7516/2017/06/027. arXiv: 1703.00305 [gr-qc].

[85] Swagat S. Mishra, Varun Sahni, and Yuri Shtanov. "Sourcing Dark Matter and Dark Energy from α-attractors." In: *JCAP* 1706.06 (2017), p. 045. DOI: 10.1088/1475-7516/2017/06/045. arXiv: 1703.03295 [gr-qc].

[86] Satadru Bag, Swagat S. Mishra, and Varun Sahni. "New tracker models of dark energy." In: (2017). arXiv: 1709.09193 [gr-qc].

[87] Carsten van de Bruck, Konstantinos Dimopoulos, Chris Longden, and Charlotte Owen. "Gauss-Bonnet-coupled Quintessential Inflation." In: (2017). arXiv: 1707.06839 [astro-ph.CO].

[88] Konstantinos Dimopoulos and Charlotte Owen. "Instant Preheating in Quintessential Inflation with α-Attractors." In: (2017). arXiv: 1712.01760 [astro-ph.CO].

[89] P. J. E. Peebles and A. Vilenkin. "Quintessential inflation." In: *Phys. Rev.* D59 (1999), p. 063505. DOI: 10.1103/PhysRevD.59.063505. arXiv: astro-ph/9810509 [astro-ph].

[90] John Joseph M. Carrasco, Renata Kallosh, and Andrei Linde. "Cosmological Attractors and Initial Conditions for Inflation." In: *Phys. Rev.* D92.6 (2015), p. 063519. DOI: 10.1103/PhysRevD.92.063519. arXiv: 1506.00936 [hep-th].

[91] Andrei D. Linde. "Inflation and Quantum Cosmology." In: *in: Three Hundred Years of Gravitation, Cambridge U. Press, 1987* (Print-86-0888, July 1, 1986), pp. 604–630.

[92] Yoshiki Ueno and Kazuhiro Yamamoto. "Constraints on α-attractor inflation and reheating." In: *Phys. Rev.* D93.8 (2016), p. 083524. DOI: 10.1103/PhysRevD.93.083524. arXiv: 1602.07427 [astro-ph.CO].

[93] Mehdi Eshaghi, Moslem Zarei, Nematollah Riazi, and Ahmad Kiasatpour. "CMB and reheating constraints to α-attractor inflationary models." In: *Phys. Rev.* D93.12 (2016), p. 123517. DOI: 10.1103/PhysRevD.93.123517. arXiv: 1602.07914 [astro-ph.CO].

[94] Renata Kallosh, Andrei Linde, Diederik Roest, and Yusuke Yamada. "$\overline{D3}$ induced geometric inflation." In: *JHEP* 07 (2017), p. 057. DOI: 10.1007/JHEP07(2017)057. arXiv: 1705.09247 [hep-th].

[95] C. L. Bennett et al. "Nine-Year Wilkinson Microwave Anisotropy Probe (WMAP) Observations: Final Maps and Results." In: *Astrophys. J. Suppl.* 208 (2013), p. 20. DOI: 10.1088/0067-0049/208/2/20. arXiv: 1212.5225 [astro-ph.CO].

[96] R. Adam et al. "Planck 2015 results. I. Overview of products and scientific results." In: *Astron. Astrophys.* 594 (2016), A1. DOI: 10.1051/0004-6361/201527101. arXiv: 1502.01582 [astro-ph.CO].

[97] Sigurd Naess et al. "The Atacama Cosmology Telescope: CMB Polarization at $200 < \ell < 9000$." In: *JCAP* 1410.10 (2014), p. 007. DOI: 10.1088/1475-7516/2014/10/007. arXiv: 1405.5524 [astro-ph.CO].

[98] R. Keisler et al. "Measurements of Sub-degree B-mode Polarization in the Cosmic Microwave Background from 100 Square Degrees of SPTpol Data." In: *Astrophys. J.* 807.2 (2015), p. 151. DOI: 10.1088/0004-637X/807/2/151. arXiv: 1503.02315 [astro-ph.CO].

[99] S. W. Henderson et al. "Advanced ACTPol Cryogenic Detector Arrays and Readout." In: *J. Low. Temp. Phys.* 184.3-4 (2016), pp. 772–779. DOI: 10.1007/s10909-016-1575-z. arXiv: 1510.02809 [astro-ph.IM].

[100] B. A. Benson et al. "SPT-3G: A Next-Generation Cosmic Microwave Background Polarization Experiment on the South Pole Telescope." In: *Proc. SPIE Int. Soc. Opt. Eng.* 9153 (2014), 91531P. DOI: 10.1117/12.2057305. arXiv: 1407.2973 [astro-ph.IM].

[101] Maximilian H. Abitbol et al. "CMB-S4 Technology Book, First Edition." In: (2017). arXiv: 1706.02464 [astro-ph.IM].

[102] T. Matsumura et al. "LiteBIRD: Mission Overview and Focal Plane Layout." In: *J. Low. Temp. Phys.* 184.3-4 (2016), pp. 824–831. DOI: 10.1007/s10909-016-1542-8.

[103] T. Matsumura et al. "Mission design of LiteBIRD." In: (2013). [J. Low. Temp. Phys.176,733(2014)]. DOI: 10.1007/s10909-013-0996-1. arXiv: 1311.2847 [astro-ph.IM].

[104] Catherine Heymans et al. "CFHTLenS: The Canada-France-Hawaii Telescope Lensing Survey." In: *Mon. Not. Roy. Astron. Soc.* 427 (2012), p. 146. DOI: 10.1111/j.1365-2966.2012.21952.x. arXiv: 1210.0032 [astro-ph.CO].

[105] Liping Fu et al. "CFHTLenS: Cosmological constraints from a combination of cosmic shear two-point and three-point correlations." In: *Mon. Not. Roy. Astron. Soc.* 441 (2014), pp. 2725–2743. DOI: 10.1093/mnras/stu754. arXiv: 1404.5469 [astro-ph.CO].

[106] H. Hildebrandt et al. "KiDS-450: Cosmological parameter constraints from tomographic weak gravitational lensing." In: *Mon. Not. Roy. Astron. Soc.* 465 (2017), p. 1454. DOI: 10.1093/mnras/stw2805. arXiv: 1606.05338 [astro-ph.CO].

[107] F. Koehlinger et al. "KiDS-450: The tomographic weak lensing power spectrum and constraints on cosmological parameters." In: *Mon. Not. Roy. Astron. Soc.* 471 (2017), p. 4412. DOI: 10.1093/mnras/stx1820. arXiv: 1706.02892 [astro-ph.CO].

[108] Kyle S. Dawson et al. "The SDSS-IV extended Baryon Oscillation Spectroscopic Survey: Overview and Early Data." In: *Astron. J.* 151 (2016), p. 44. DOI: 10.3847/0004-6256/151/2/44. arXiv: 1508.04473 [astro-ph.CO].

[109] T. Abbott et al. "Cosmology from cosmic shear with Dark Energy Survey Science Verification data." In: *Phys. Rev.* D94.2 (2016), p. 022001. DOI: 10.1103/PhysRevD.94.022001. arXiv: 1507.05552 [astro-ph.CO].

[110] M. A. Troxel et al. "Dark Energy Survey Year 1 Results: Cosmological Constraints from Cosmic Shear." In: (2017). arXiv: 1708.01538 [astro-ph.CO].

[111] T. M. C. Abbott et al. "Dark Energy Survey Year 1 Results: Cosmological Constraints from Galaxy Clustering and Weak Lensing." In: (2017). arXiv: 1708.01530 [astro-ph.CO].

[112] Amir Aghamousa et al. "The DESI Experiment Part I: Science,Targeting, and Survey Design." In: (2016). arXiv: 1611.00036 [astro-ph.IM].

[113] Amir Aghamousa et al. "The DESI Experiment Part II: Instrument Design." In: (2016). arXiv: 1611.00037 [astro-ph.IM].

[114] Paul A. Abell et al. "LSST Science Book, Version 2.0." In: (2009). arXiv: 0912.0201 [astro-ph.IM].

[115] Phil Marshall et al. "Science-Driven Optimization of the LSST Observing Strategy." In: (2017). DOI: 10.5281/zenodo.842713. arXiv: 1708.04058 [astro-ph.IM].

[116] Philip Bull, Pedro G. Ferreira, Prina Patel, and Mario G. Santos. "Late-time cosmology with 21cm intensity mapping experiments." In: *Astrophys. J.* 803.1 (2015), p. 21. DOI: 10.1088/0004-637X/803/1/21. arXiv: 1405.1452 [astro-ph.CO].

[117] Matt J. Jarvis, David Bacon, Chris Blake, Michael L. Brown, Sam N. Lindsay, Alvise Raccanelli, Mario Santos, and Dominik Schwarz. "Cosmology with SKA Radio Continuum Surveys." In: (2015). arXiv: 1501.03825 [astro-ph.CO].

[118] David Bacon et al. "Synergy between the Large Synoptic Survey Telescope and the Square Kilometre Array." In: *PoS* AASKA14 (2015), p. 145. arXiv: 1501.03977 [astro-ph.CO].

[119] Thomas D. Kitching, David Bacon, Michael L. Brown, Philip Bull, Jason D. McEwen, Masamune Oguri, Roberto Scaramella, Keitaro Takahashi, Kinwah Wu, and Daisuke Yamauchi. "Euclid & SKA Synergies." In: (2015). arXiv: 1501.03978 [astro-ph.CO].

[120] S. Yahya, P. Bull, M. G. Santos, M. Silva, R. Maartens, P. Okouma, and B. Bassett. "Cosmological performance of SKA HI galaxy surveys." In: *Mon. Not. Roy. Astron. Soc.* 450.3 (2015), pp. 2251–2260. DOI: 10.1093/mnras/stv695. arXiv: 1412.4700 [astro-ph.CO].

[121] Mario G. Santos et al. "Cosmology with a SKA HI intensity mapping survey." In: (2015). arXiv: 1501.03989 [astro-ph.CO].

[122] R. Laureijs et al. "Euclid Definition Study Report." In: (2011). arXiv: 1110.3193 [astro-ph.CO].

[123] Luca Amendola et al. "Cosmology and Fundamental Physics with the Euclid Satellite." In: (2016). arXiv: 1606.00180 [astro-ph.CO].

[124] D. Spergel et al. "Wide-Field InfrarRed Survey Telescope-Astrophysics Focused Telescope Assets WFIRST-AFTA 2015 Report." In: (2015). arXiv: 1503.03757 [astro-ph.IM].

[125] R. Hounsell et al. "Simulations of the WFIRST Supernova Survey and Forecasts of Cosmological Constraints." In: (2017). arXiv: 1702.01747 [astro-ph.IM].

[126] Sergio Ferrara and Renata Kallosh. "Seven-disk manifold, α-attractors, and B modes." In: *Phys. Rev.* D94.12 (2016), p. 126015. DOI: 10.1103/PhysRevD.94.126015. arXiv: 1610.04163 [hep-th].

[127] Renata Kallosh, Andrei Linde, Timm Wrase, and Yusuke Yamada. "Maximal Supersymmetry and B-Mode Targets." In: *JHEP* 04 (2017), p. 144. DOI: 10.1007/JHEP04(2017)144. arXiv: 1704.04829 [hep-th].

[128] Andrei D. Linde. "Chaotic Inflation." In: *Phys. Lett.* B129 (1983), pp. 177–181. DOI: 10.1016/0370-2693(83)90837-7.

[129] Renata Kallosh and Andrei Linde. "Planck, LHC, and α-attractors." In: *Phys. Rev.* D91 (2015), p. 083528. DOI: 10.1103/PhysRevD.91.083528. arXiv: 1502.07733 [astro-ph.CO].

[130] P. A. R. Ade et al. "Planck 2015 results. XIII. Cosmological parameters." In: *Astron. Astrophys.* 594 (2016), A13. DOI: 10.1051/0004-6361/201525830. arXiv: 1502.01589 [astro-ph.CO].

[131] N. Aghanim et al. "Planck intermediate results. LI. Features in the cosmic microwave background temperature power spectrum and shifts in cosmological parameters." In: *Astron. Astrophys.* 607 (2017), A95. DOI: 10.1051/0004-6361/201629504. arXiv: 1608.02487 [astro-ph.CO].

[132] Evan McDonough and Marco Scalisi. "Inflation from Nilpotent Kähler Corrections." In: *JCAP* 1611.11 (2016), p. 028. DOI: 10.1088/1475-7516/2016/11/028. arXiv: 1609.00364 [hep-th].

[133] Matthew Dodelson, Xi Dong, Eva Silverstein, and Gonzalo Torroba. "New solutions with accelerated expansion in string theory." In: *JHEP* 12 (2014), p. 050. DOI: 10.1007/JHEP12(2014)050. arXiv: 1310.5297 [hep-th].

[134] Jerome Martin, Christophe Ringeval, and Vincent Vennin. "Encyclopedia Inflationaris." In: *Phys. Dark Univ.* 5-6 (2014), pp. 75–235. DOI: 10.1016/j.dark.2014.01.003. arXiv: 1303.3787 [astro-ph.CO].

[135] Renata Kallosh and Andrei D. Linde. "Dark energy and the fate of the universe." In: *JCAP* 0302 (2003), p. 002. DOI: 10.1088/1475-7516/2003/02/002. arXiv: astro-ph/0301087 [astro-ph].

[136] John Joseph M. Carrasco, Renata Kallosh, Andrei Linde, and Diederik Roest. "Hyperbolic geometry of cosmological attractors." In: *Phys. Rev.* D92.4 (2015), p. 041301. DOI: 10.1103/PhysRevD.92.041301. arXiv: 1504.05557 [hep-th].

[137] Renata Kallosh and Andrei Linde. "Cosmological Attractors and Asymptotic Freedom of the Inflaton Field." In: *JCAP* 1606.06 (2016), p. 047. DOI: 10.1088/1475-7516/2016/06/047. arXiv: 1604.00444 [hep-th].

[138] M. Cicoli, C. P. Burgess, and F. Quevedo. "Fibre Inflation: Observable Gravity Waves from IIB String Compactifications." In: *JCAP* 0903 (2009), p. 013. DOI: 10.1088/1475-7516/2009/03/013. arXiv: 0808.0691 [hep-th].

[139] Renata Kallosh, Andrei Linde, Diederik Roest, Alexander Westphal, and Yusuke Yamada. "Fibre Inflation and α-attractors." In: (2017). arXiv: 1707.05830 [hep-th].

[140] Renata Kallosh, Andrei Linde, and Timm Wrase. "Coupling the Inflationary Sector to Matter." In: *JHEP* 04 (2016), p. 027. DOI: 10.1007/JHEP04(2016)027. arXiv: 1602.07818 [hep-th].

[141] Philippe Brax, Carsten van de Bruck, Jerome Martin, and Anne-Christine Davis. "Decoupling Dark Energy from Matter." In: *JCAP* 0909 (2009), p. 032. DOI: 10.1088/1475-7516/2009/09/032. arXiv: 0904.3471 [hep-th].

[142] Daniel Baumann. *The Physics of Inflation: A Course for Graduate Students in Particle Physics and Cosmology*. http://www.damtp.cam.ac.uk/user/db275/TEACHING/INFLATION/Lectures.pdf.

[143] Daniel Baumann. "Inflation." In: *Physics of the large and the small, TASI 09, proceedings of the Theoretical Advanced Study Institute in Elementary Particle Physics, Boulder, Colorado, USA, 1-26 June 2009*. 2011, pp. 523–686. DOI: 10.1142/9789814327183_0010. arXiv: 0907.5424 [hep-th]. URL: https://inspirehep.net/record/827549/files/arXiv:0907.5424.pdf.

[144] David H. Lyth and Antonio Riotto. "Particle physics models of inflation and the cosmological density perturbation." In: *Phys. Rept.* 314 (1999), pp. 1–146. DOI: 10.1016/S0370-1573(98)00128-8. arXiv: hep-ph/9807278 [hep-ph].

[145] M. Chevallier and D. Polarski. "Accelerating Universes with Scaling Dark Matter." In: *International Journal of Modern Physics D* 10 (2001), pp. 213–223. DOI: 10.1142/S0218271801000822. eprint: gr-qc/0009008.

[146] E. V. Linder. "Exploring the Expansion History of the Universe." In: *Physical Review Letters* 90.9, 091301 (Mar. 2003), p. 091301. DOI: 10.1103/PhysRevLett.90.091301. eprint: astro-ph/0208512.

[147] L. H. Ford. "Gravitational Particle Creation and Inflation." In: *Phys. Rev.* D35 (1987), p. 2955. DOI: 10.1103/PhysRevD.35.2955.

[148] E. J. Chun, S. Scopel, and I. Zaballa. "Gravitational reheating in quintessential inflation." In: *JCAP* 0907 (2009), p. 022. DOI: 10.1088/1475-7516/2009/07/022. arXiv: 0904.0675 [hep-ph].

[149] Ya. B. Zeldovich and A.A. Starobinsky. "Particle Production and Vacuum Polarization in an Anisotropic Gravitational Field." In: *JETP* 34 (1972), p. 1159.

[150] Ya. B. Zeldovich and A.A. Starobinsky. "Rate of particle production in gravitational fields." In: *JETP Lett.* 26 (1977), p. 252.

[151] Alexei A. Starobinsky. "A New Type of Isotropic Cosmological Models Without Singularity." In: *Phys. Lett.* 91B (1980), pp. 99–102. DOI: 10.1016/0370-2693(80)90670-X.

[152] Gary N. Felder, Lev Kofman, and Andrei D. Linde. "Instant preheating." In: *Phys. Rev.* D59 (1999), p. 123523. DOI: 10.1103/PhysRevD.59.123523. arXiv: hep-ph/9812289 [hep-ph].

[153] Gary N. Felder, Lev Kofman, and Andrei D. Linde. "Inflation and preheating in NO models." In: *Phys. Rev.* D60 (1999), p. 103505. DOI: 10.1103/PhysRevD.60.103505. arXiv: hep-ph/9903350 [hep-ph].

[154] Lev Kofman, Andrei D. Linde, Xiao Liu, Alexander Maloney, Liam McAllister, and Eva Silverstein. "Beauty is attractive: Moduli trapping at enhanced symmetry points." In: *JHEP* 05 (2004), p. 030. DOI: 10.1088/1126-6708/2004/05/030. arXiv: hep-th/0403001 [hep-th].

[155] Andrei D. Linde. "Particle physics and inflationary cosmology." In: *Contemp. Concepts Phys.* 5 (1990), pp. 1–362. arXiv: hep-th/0503203 [hep-th].

[156] Daniel Green, Bart Horn, Leonardo Senatore, and Eva Silverstein. "Trapped Inflation." In: *Phys. Rev.* D80 (2009), p. 063533. DOI: 10.1103/PhysRevD.80.063533. arXiv: 0902.1006 [hep-th].

[157] Anshuman Maharana and Ivonne Zavala. "Post-inflationary Scalar Tensor Cosmology and Inflationary Parameters." In: (2017). arXiv: 1712.07071 [hep-ph].

[158] M. Betoule et al. "Improved cosmological constraints from a joint analysis of the SDSS-II and SNLS supernova samples." In: *Astron. Astrophys.* 568 (2014), A22. DOI: 10.1051/0004-6361/201423413. arXiv: 1401.4064 [astro-ph.CO].

[159] Florian Beutler, Chris Blake, Matthew Colless, D. Heath Jones, Lister Staveley-Smith, Lachlan Campbell, Quentin Parker, Will Saunders, and Fred Watson. "The 6dF Galaxy Survey: Baryon Acoustic Oscillations and the Local Hubble Constant." In: *Mon. Not. Roy. Astron. Soc.* 416 (2011), pp. 3017–3032. DOI: 10.1111/j.1365-2966.2011.19250.x. arXiv: 1106.3366 [astro-ph.CO].

[160] Chris Blake et al. "The WiggleZ Dark Energy Survey: mapping the distance-redshift relation with baryon acoustic oscillations." In: *Mon. Not. Roy. Astron. Soc.* 418 (2011), pp. 1707–1724. DOI: 10.1111/j.1365-2966.2011.19592.x. arXiv: 1108.2635 [astro-ph.CO].

[161] Lauren Anderson et al. "The clustering of galaxies in the SDSS-III Baryon Oscillation Spectroscopic Survey: Baryon Acoustic Oscillations in the Data Release 9 Spectroscopic Galaxy Sample." In: *Mon. Not. Roy. Astron. Soc.* 427.4 (2013), pp. 3435–3467. DOI: 10.1111/j.1365-2966.2012.22066.x. arXiv: 1203.6594 [astro-ph.CO].

[162] Lauren Anderson et al. "The clustering of galaxies in the SDSS-III Baryon Oscillation Spectroscopic Survey: baryon acoustic oscillations in the Data Releases 10 and 11 Galaxy samples." In: *Mon. Not. Roy. Astron. Soc.* 441.1 (2014), pp. 24–62. DOI: 10.1093/mnras/stu523. arXiv: 1312.4877 [astro-ph.CO].

[163] Ashley J. Ross, Lado Samushia, Cullan Howlett, Will J. Percival, Angela Burden, and Marc Manera. "The clustering of the SDSS DR7 main Galaxy sample - I. A 4 per cent distance measure at $z = 0.15$." In: *Mon. Not. Roy. Astron. Soc.* 449.1 (2015), pp. 835–847. DOI: 10.1093/mnras/stv154. arXiv: 1409.3242 [astro-ph.CO].

[164] Adam G. Riess et al. "A 2.4% Determination of the Local Value of the Hubble Constant." In: *Astrophys. J.* 826.1 (2016), p. 56. DOI: 10.3847/0004-637X/826/1/56. arXiv: 1604.01424 [astro-ph.CO].

[165] C. Wetterich. "Cosmology and the Fate of Dilatation Symmetry." In: *Nucl. Phys.* B302 (1988), pp. 668–696. DOI: 10.1016/0550-3213(88)90193-9.

[166] Bharat Ratra and P. J. E. Peebles. "Cosmological Consequences of a Rolling Homogeneous Scalar Field." In: *Phys. Rev.* D37 (1988), p. 3406. DOI: 10.1103/PhysRevD.37.3406.

[167] Renata Kallosh, Jan Kratochvil, Andrei D. Linde, Eric V. Linder, and Marina Shmakova. "Observational bounds on cosmic doomsday." In: *JCAP* 0310 (2003), p. 015. DOI: 10.1088/1475-7516/2003/10/015. arXiv: astro-ph/0307185 [astro-ph].

[168] J. Garriga and A. Vilenkin. "Testable anthropic predictions for dark energy." In: *Phys. Rev.* D67 (2003), p. 043503. DOI: 10.1103/PhysRevD.67.043503. arXiv: astro-ph/0210358 [astro-ph].

[169] Renata Kallosh and Andrei D. Linde. "M theory, cosmological constant and anthropic principle." In: *Phys. Rev.* D67 (2003), p. 023510. DOI: 10.1103/PhysRevD.67.023510. arXiv: hep-th/0208157 [hep-th].

[170] Jaume Garriga, Andrei D. Linde, and Alexander Vilenkin. "Dark energy equation of state and anthropic selection." In: *Phys. Rev.* D69 (2004), p. 063521. DOI: 10.1103/PhysRevD.69.063521. arXiv: hep-th/0310034 [hep-th].

[171] Andrei Linde. "On the problem of initial conditions for inflation." In: *Black Holes, Gravitational Waves and Spacetime Singularities Rome, Italy, May 9-12, 2017*. 2017. arXiv: 1710.04278 [hep-th]. URL: http://inspirehep.net/record/1630432/files/arXiv:1710.04278.pdf.

[172] Yashar Akrami, Tomi S. Koivisto, David F. Mota, and Marit Sandstad. "Bimetric gravity doubly coupled to matter: theory and cosmological implications." In: *JCAP* 1310 (2013), p. 046. DOI: 10.1088/1475-7516/2013/10/046. arXiv: 1306.0004 [hep-th].

[173] Yashar Akrami, Tomi S. Koivisto, and Adam R. Solomon. "The nature of spacetime in bigravity: two metrics or none?" In: *Gen.Rel.Grav.* 47 (2014), p. 1838. DOI: 10.1007/s10714-014-1838-4. arXiv: 1404.0006 [gr-qc].

[174] S.F. Hassan, Angnis Schmidt-May, and Mikael von Strauss. "On Consistent Theories of Massive Spin-2 Fields Coupled to Gravity." In: *JHEP* 1305 (2013), p. 086. DOI: 10.1007/JHEP05(2013)086. arXiv: 1208.1515 [hep-th].

[175] Nicola Tamanini, Emmanuel N. Saridakis, and Tomi S. Koivisto. "The Cosmology of Interacting Spin-2 Fields." In: *JCAP* 1402 (2014), p. 015. DOI: 10.1088/1475-7516/2014/02/015. arXiv: 1307.5984 [hep-th].

[176] Yasuho Yamashita, Antonio De Felice, and Takahiro Tanaka. "Appearance of Boulware-Deser ghost in bigravity with doubly coupled matter." In: *Int.J.Mod.Phys.* D23 (2014), p. 3003. DOI: 10.1142/S0218271814430032. arXiv: 1408.0487 [hep-th].

[177] Claudia de Rham, Lavinia Heisenberg, and Raquel H. Ribeiro. "On couplings to matter in massive (bi-)gravity." In: *Class.Quant.Grav.* 32.3 (2015), p. 035022. DOI: 10.1088/0264-9381/32/3/035022. arXiv: 1408.1678 [hep-th].

[178] S.F. Hassan, Mikica Kocic, and Angnis Schmidt-May. "Absence of ghost in a new bimetric-matter coupling." In: (2014). arXiv: 1409.1909 [hep-th].

[179] Jonas Enander, Adam R. Solomon, Yashar Akrami, and Edvard Mortsell. "Cosmic expansion histories in massive bigravity with symmetric matter coupling." In: *JCAP* 01 (2015), p. 006. DOI: 10.1088/1475-7516/2015/01/006. arXiv: 1409.2860 [astro-ph.CO].

[180] Adam R. Solomon, Jonas Enander, Yashar Akrami, Tomi S. Koivisto, Frank Könnig, et al. "Cosmological viability of massive gravity with generalized matter coupling." In: *JCAP* 1504 (2015), p. 027. DOI: 10.1088/1475-7516/2015/04/027. arXiv: 1409.8300 [astro-ph.CO].

[181] Angnis Schmidt-May. "Mass eigenstates in bimetric theory with matter coupling." In: *JCAP* 1501.01 (2015), p. 039. DOI: 10.1088/1475-7516/2015/01/039. arXiv: 1409.3146 [gr-qc].

[182] Claudia de Rham, Lavinia Heisenberg, and Raquel H. Ribeiro. "Ghosts & Matter Couplings in Massive (bi-&multi-)Gravity." In: *Phys.Rev.* D90 (2014), p. 124042. DOI: 10.1103/PhysRevD.90.124042. arXiv: 1409.3834 [hep-th].

[183] A. Emir Gümrükçüoğlu, Lavinia Heisenberg, and Shinji Mukohyama. "Cosmological perturbations in massive gravity with doubly coupled matter." In: *JCAP* 1502 (2015), p. 022. DOI: 10.1088/1475-7516/2015/02/022. arXiv: 1409.7260 [hep-th].

[184] Lavinia Heisenberg. "Quantum corrections in massive bigravity and new effective composite metrics." In: *Class.Quant.Grav.* 32.10 (2015), p. 105011. DOI: 10.1088/0264-9381/32/10/105011. arXiv: 1410.4239 [hep-th].

[185] A. Emir Gümrükçüoğlu, Lavinia Heisenberg, Shinji Mukohyama, and Norihiro Tanahashi. "Cosmology in bimetric theory with an effective composite coupling to matter." In: *JCAP* 1504.04 (2015), p. 008. DOI: 10.1088/1475-7516/2015/04/008. arXiv: 1501.02790 [hep-th].

[186] Kurt Hinterbichler and Rachel A. Rosen. "Note on ghost-free matter couplings in massive gravity and multigravity." In: *Phys. Rev.* D92.2 (2015), p. 024030. DOI: 10.1103/PhysRevD.92.024030. arXiv: 1503.06796 [hep-th].

[187] Lavinia Heisenberg. "More on effective composite metrics." In: *Phys. Rev.* D92 (2015), p. 023525. DOI: 10.1103/PhysRevD.92.023525. arXiv: 1505.02966 [hep-th].

[188] Lavinia Heisenberg. "Non-minimal derivative couplings of the composite metric." In: *JCAP* 1511.11 (2015), p. 005. DOI: 10.1088/1475-7516/2015/11/005. arXiv: 1506.00580 [hep-th].

[189] Macarena Lagos and Johannes Noller. "New massive bigravity cosmologies with double matter coupling." In: *JCAP* 1601.01 (2016), p. 023. DOI: 10.1088/1475-7516/2016/01/023. arXiv: 1508.05864 [gr-qc].

[190] Scott Melville and Johannes Noller. "Generalised matter couplings in massive bigravity." In: *JHEP* 01 (2016), p. 094. DOI: 10.1007/JHEP01(2016)094. arXiv: 1511.01485 [hep-th].

[191] Lavinia Heisenberg and Alexandre Refregier. "Cosmology in massive gravity with effective composite metric." In: *JCAP* 1609.09 (2016), p. 020. DOI: 10.1088/1475-7516/2016/09/020. arXiv: 1604.07306 [gr-qc].

[192] Philippe Brax, Anne-Christine Davis, and Johannes Noller. "Dark Energy and Doubly Coupled Bigravity." In: *Class. Quant. Grav.* 34.9 (2017), p. 095014. DOI: 10.1088/1361-6382/aa6856. arXiv: 1606.05590 [gr-qc].

[193] Philippe Brax, Anne-Christine Davis, and Johannes Noller. "Gravitational Waves in Doubly Coupled Bigravity." In: *Phys. Rev.* D96.2 (2017), p. 023518. DOI: 10.1103/PhysRevD.96.023518. arXiv: 1703.08016 [gr-qc].

[194] Philippe Brax, Sebastian Cespedes, and Anne-Christine Davis. "Signatures of graviton masses on the CMB." In: (2017). arXiv: 1710.09818 [astro-ph.CO].

[195] D.G. Boulware and Stanley Deser. "Can gravitation have a finite range?" In: *Phys.Rev.* D6 (1972), pp. 3368–3382. DOI: 10.1103/PhysRevD.6.3368.

[196] Denis Comelli, Marco Crisostomi, Kazuya Koyama, Luigi Pilo, and Gianmassimo Tasinato. "Cosmology of bigravity with doubly coupled matter." In: *JCAP* 1504 (2015), p. 026. DOI: 10.1088/1475-7516/2015/04/026. arXiv: 1501.00864 [hep-th].

[197] Antonio De Felice, Takashi Nakamura, and Takahiro Tanaka. "Possible existence of viable models of bi-gravity with detectable graviton oscillations by gravitational wave detectors." In: *PTEP* 2014 (2014), 043E01. DOI: 10.1093/ptep/ptu024. arXiv: 1304.3920 [gr-qc].

[198] Ippocratis D. Saltas, Ignacy Sawicki, Luca Amendola, and Martin Kunz. "Anisotropic Stress as a Signature of Nonstandard Propagation of Gravitational Waves." In: *Phys. Rev. Lett.* 113.19 (2014), p. 191101. DOI: 10.1103/PhysRevLett.113.191101. arXiv: 1406.7139 [astro-ph.CO].

[199] Giulia Cusin, Ruth Durrer, Pietro Guarato, and Mariele Motta. "Gravitational waves in bigravity cosmology." In: *JCAP* 1505.05 (2015), p. 030. DOI: 10.1088/1475-7516/2015/05/030. arXiv: 1412.5979 [astro-ph.CO].

[200] Tatsuya Narikawa, Koh Ueno, Hideyuki Tagoshi, Takahiro Tanaka, Nobuyuki Kanda, and Takashi Nakamura. "Detectability of bigravity with graviton oscillations using gravitational wave observations." In: *Phys. Rev.* D91 (2015), p. 062007. DOI: 10.1103/PhysRevD.91.062007. arXiv: 1412.8074 [gr-qc].

[201] Luca Amendola, Frank Könnig, Matteo Martinelli, Valeria Pettorino, and Miguel Zumalacarregui. "Surfing gravitational waves: can bigravity survive growing tensor modes?" In: *JCAP* 1505 (2015), p. 052. DOI: 10.1088/1475-7516/2015/05/052. arXiv: 1503.02490 [astro-ph.CO].

[202] Matthew Johnson and Alexandra Terrana. "Tensor Modes in Bigravity: Primordial to Present." In: *Phys. Rev.* D92.4 (2015), p. 044001. DOI: 10.1103/PhysRevD.92.044001. arXiv: 1503.05560 [astro-ph.CO].

[203] Kevin Max, Moritz Platscher, and Juri Smirnov. "Gravitational Wave Oscillations in Bigravity." In: *Phys. Rev. Lett.* 119.11 (2017), p. 111101. DOI: 10.1103/PhysRevLett.119.111101. arXiv: 1703.07785 [gr-qc].

[204] Atsushi Nishizawa. "Generalized framework for testing gravity with gravitational-wave propagation. I. Formulation." In: (2017). arXiv: 1710.04825 [gr-qc].

[205] Kevin Max, Moritz Platscher, and Juri Smirnov. "Decoherence of Gravitational Wave Oscillations in Bigravity." In: (2017). arXiv: 1712.06601 [gr-qc].

[206] Yashar Akrami, Tomi S. Koivisto, and Marit Sandstad. "Cosmological constraints on ghost-free bigravity: background dynamics and late-time acceleration." In: *Proceedings, 13th Marcel Grossmann Meeting (MG13)*. 2015, pp. 1252–1254. DOI: 10.1142/9789814623995_0138. arXiv: 1302.5268 [astro-ph.CO]. URL: https://inspirehep.net/record/1220533/files/arXiv:1302.5268.pdf.

[207] Ali H. Chamseddine and Viatcheslav Mukhanov. "Ghost Free Mimetic Massive Gravity." In: *JHEP* 06 (2018), p. 060. DOI: 10.1007/JHEP06(2018)060. arXiv: 1805.06283 [hep-th].

[208] Ali H. Chamseddine and Viatcheslav Mukhanov. "Mimetic Massive Gravity: Beyond Linear Approximation." In: *JHEP* 06 (2018), p. 062. DOI: 10.1007/JHEP06(2018)062. arXiv: 1805.06598 [hep-th].

[209] Ali H. Chamseddine and Viatcheslav Mukhanov. "Mimetic Dark Matter." In: *JHEP* 11 (2013), p. 135. DOI: 10.1007/JHEP11(2013)135. arXiv: 1308.5410 [astro-ph.CO].

[210] C.J. Isham, Abdus Salam, and J.A. Strathdee. "F-dominance of gravity." In: *Phys.Rev.* D3 (1971), pp. 867–873. DOI: 10.1103/PhysRevD.3.867.

[211] Paolo Creminelli, Alberto Nicolis, Michele Papucci, and Enrico Trincherini. "Ghosts in massive gravity." In: *JHEP* 0509 (2005), p. 003. DOI: 10.1088/1126-6708/2005/09/003. arXiv: hep-th/0505147 [hep-th].

[212] Eugene A. Lim, Ignacy Sawicki, and Alexander Vikman. "Dust of Dark Energy." In: *JCAP* 1005 (2010), p. 012. DOI: 10.1088/1475-7516/2010/05/012. arXiv: 1003.5751 [astro-ph.CO].

[213] Leila Mirzagholi and Alexander Vikman. "Imperfect Dark Matter." In: *JCAP* 1506 (2015), p. 028. DOI: 10.1088/1475-7516/2015/06/028. arXiv: 1412.7136 [gr-qc].

[214] H. van Dam and M. J. G. Veltman. "Massive and massless Yang-Mills and gravitational fields." In: *Nucl. Phys.* B22 (1970), pp. 397–411. DOI: 10.1016/0550-3213(70)90416-5.

[215] V. I. Zakharov. "Linearized gravitation theory and the graviton mass." In: *JETP Lett.* 12 (1970). [Pisma Zh. Eksp. Teor. Fiz.12,447(1970)], p. 312.

[216] Atsushi Higuchi. "Forbidden Mass Range for Spin-2 Field Theory in De Sitter Space-time." In: *Nucl.Phys.* B282 (1987), p. 397. DOI: 10.1016/0550-3213(87)90691-2.

[217] S. L. Dubovsky. "Phases of massive gravity." In: *JHEP* 10 (2004), p. 076. DOI: 10.1088/1126-6708/2004/10/076. arXiv: hep-th/0409124 [hep-th].

[218] D. Blas, D. Comelli, F. Nesti, and L. Pilo. "Lorentz Breaking Massive Gravity in Curved Space." In: *Phys. Rev.* D80 (2009), p. 044025. DOI: 10.1103/PhysRevD.80.044025. arXiv: 0905.1699 [hep-th].

[219] Macarena Lagos, Máximo Bañados, Pedro G. Ferreira, and Sebastián García-Sáenz. "Noether Identities and Gauge-Fixing the Action for Cosmological Perturbations." In: *Phys. Rev.* D89 (2014), p. 024034. DOI: 10.1103/PhysRevD.89.024034. arXiv: 1311.3828 [gr-qc].

[220] S. Dubovsky, T. Gregoire, A. Nicolis, and R. Rattazzi. "Null energy condition and superluminal propagation." In: *JHEP* 03 (2006), p. 025. DOI: 10.1088/1126-6708/2006/03/025. arXiv: hep-th/0512260 [hep-th].

[221] Solomon Endlich, Alberto Nicolis, Riccardo Rattazzi, and Junpu Wang. "The Quantum mechanics of perfect fluids." In: *JHEP* 04 (2011), p. 102. DOI: 10.1007/JHEP04(2011)102. arXiv: 1011.6396 [hep-th].

[222] G. R. Dvali, Gregory Gabadadze, and Massimo Porrati. "4-D gravity on a brane in 5-D Minkowski space." In: *Phys. Lett.* B485 (2000), pp. 208–214. DOI: 10.1016/S0370-2693(00)00669-9. arXiv: hep-th/0005016 [hep-th].

[223] Cedric Deffayet. "Cosmology on a brane in Minkowski bulk." In: *Phys. Lett.* B502 (2001), pp. 199–208. DOI: 10.1016/S0370-2693(01)00160-5. arXiv: hep-th/0010186 [hep-th].

[224] Cedric Deffayet, G. R. Dvali, and Gregory Gabadadze. "Accelerated universe from gravity leaking to extra dimensions." In: *Phys. Rev.* D65 (2002), p. 044023. DOI: 10.1103/PhysRevD.65.044023. arXiv: astro-ph/0105068 [astro-ph].

[225] Dmitry Gorbunov, Kazuya Koyama, and Sergei Sibiryakov. "More on ghosts in DGP model." In: *Phys. Rev.* D73 (2006), p. 044016. DOI: 10.1103/PhysRevD.73.044016. arXiv: hep-th/0512097 [hep-th].

[226] Christos Charmousis, Ruth Gregory, Nemanja Kaloper, and Antonio Padilla. "DGP Specteroscopy." In: *JHEP* 10 (2006), p. 066. DOI: 10.1088/1126-6708/2006/10/066. arXiv: hep-th/0604086 [hep-th].

[227] Justin Khoury, Jeremy Sakstein, and Adam R. Solomon. "Superfluids and the Cosmological Constant Problem." In: *JCAP* 1808.08 (2018), p. 024. DOI: 10.1088/1475-7516/2018/08/024. arXiv: 1805.05937 [hep-th].

[228] Xue-lei Chen, Robert J. Scherrer, and Gary Steigman. "Extended quintessence and the primordial helium abundance." In: *Phys. Rev.* D63 (2001), p. 123504. DOI: 10.1103/PhysRevD.63.123504. arXiv: astro-ph/0011531 [astro-ph].

[229] Richard H. Cyburt, Brian D. Fields, Keith A. Olive, and Tsung-Han Yeh. "Big Bang Nucleosynthesis: 2015." In: *Rev. Mod. Phys.* 88 (2016), p. 015004. DOI: 10.1103/RevModPhys.88.015004. arXiv: 1505.01076 [astro-ph.CO].

[230] D. J. Fixsen. "The Temperature of the Cosmic Microwave Background." In: 707 (2009), pp. 916–920. DOI: 10.1088/0004-637X/707/2/916. arXiv: 0911.1955 [astro-ph.CO].

[231] Benjamin P. Abbott et al. "GW170104: Observation of a 50-Solar-Mass Binary Black Hole Coalescence at Redshift 0.2." In: *Phys. Rev. Lett.* 118.22 (2017). [Erratum: Phys. Rev. Lett.121,no.12,129901(2018)], p. 221101. DOI: 10.1103/PhysRevLett.118.221101, 10.1103/PhysRevLett.121.129901. arXiv: 1706.01812 [gr-qc].

[232] Claudia de Rham, J. Tate Deskins, Andrew J. Tolley, and Shuang-Yong Zhou. "Graviton Mass Bounds." In: *Rev. Mod. Phys.* 89.2 (2017), p. 025004. DOI: 10.1103/RevModPhys.89.025004. arXiv: 1606.08462 [astro-ph.CO].

[233] Jonas Enander, Yashar Akrami, Edvard Mörtsell, Malin Renneby, and Adam R. Solomon. "Integrated Sachs-Wolfe effect in massive bigravity." In: *Phys.Rev.* D91 (2015), p. 084046. DOI: 10.1103/PhysRevD.91.084046. arXiv: 1501.02140 [astro-ph.CO].

[234] Gong-Bo Zhao, Tommaso Giannantonio, Levon Pogosian, Alessandra Silvestri, David J. Bacon, Kazuya Koyama, Robert C. Nichol, and Yong-Seon Song. "Probing modifications of General Relativity using current cosmological observations." In: *Phys. Rev.* D81 (2010), p. 103510. DOI: 10.1103/PhysRevD.81.103510. arXiv: 1003.0001 [astro-ph.CO].

[235] P. A. R. Ade et al. "Planck 2015 results. XIV. Dark energy and modified gravity." In: *Astron. Astrophys.* 594 (2016), A14. DOI: 10.1051/0004-6361/201525814. arXiv: 1502.01590 [astro-ph.CO].

[236] Levon Pogosian and Alessandra Silvestri. "What can cosmology tell us about gravity? Constraining Horndeski gravity with Σ and μ." In: *Phys. Rev.* D94.10 (2016), p. 104014. DOI: 10.1103/PhysRevD.94.104014. arXiv: 1606.05339 [astro-ph.CO].

[237] Benedikt Diemer and Andrey V. Kravtsov. "Dependence of the outer density profiles of halos on their mass accretion rate." In: *Astrophys. J.* 789 (2014), p. 1. DOI: 10.1088/0004-637X/789/1/1. arXiv: 1401.1216 [astro-ph.CO].

[238] J. A. Fillmore and P. Goldreich. "Self-similar gravitational collapse in an expanding universe." In: 281 (1984), pp. 1–8. DOI: 10.1086/162070.

[239] E. Bertschinger. "Self - similar secondary infall and accretion in an Einstein-de Sitter universe." In: *Astrophys. J. Suppl.* 58 (1985), p. 39. DOI: 10.1086/191028.

[240] Yoram Lithwick and Neal Dalal. "Self-Similar Solutions of Triaxial Dark Matter Halos." In: *Astrophys. J.* 734 (2011), p. 100. DOI: 10.1088/0004-637X/734/2/100. arXiv: 1010.3723 [astro-ph.CO].

[241] Xun Shi. "The outer profile of dark matter haloes: an analytical approach." In: *Mon. Not. Roy. Astron. Soc.* 459.4 (2016), pp. 3711–3720. DOI: 10.1093/mnras/stw925. arXiv: 1603.01742 [astro-ph.CO].

[242] Nick Kaiser and Gordon Squires. "Mapping the dark matter with weak gravitational lensing." In: *Astrophys. J.* 404 (1993), pp. 441–450. DOI: 10.1086/172297.

[243] Keiichi Umetsu, Tom Broadhurst, Adi Zitrin, Elinor Medezinski, Dan Coe, and Marc Postman. "A Precise Cluster Mass Profile Averaged from the Highest-Quality Lensing Data." In: *Astrophys. J.* 738 (2011), p. 41. DOI: 10.1088/0004-637X/738/1/41. arXiv: 1105.0444 [astro-ph.CO].

[244] Keiichi Umetsu and Benedikt Diemer. "Lensing Constraints on the Mass Profile Shape and the Splashback Radius of Galaxy Clusters." In: *Astrophys. J.* 836.2 (2017), p. 231. DOI: 10.3847/1538-4357/aa5c90. arXiv: 1611.09366 [astro-ph.CO].

[245] O. Contigiani, H. Hoekstra, and Y. M. Bahé. "Weak lensing constraints on splashback around massive clusters." In: (2018). arXiv: 1809.10045 [astro-ph.CO].

[246] Surhud More et al. "Detection of the Splashback Radius and Halo Assembly bias of Massive Galaxy Clusters." In: *Astrophys. J.* 825.1 (2016), p. 39. DOI: 10.3847/0004-637X/825/1/39. arXiv: 1601.06063 [astro-ph.CO].

[247] Eric Baxter, Chihway Chang, Bhuvnesh Jain, Susmita Adhikari, Neal Dalal, Andrey Kravtsov, Surhud More, Eduardo Rozo, Eli Rykoff, and Ravi K. Sheth. "The Halo Boundary of Galaxy Clusters in the SDSS." In: *Astrophys. J.* 841.1 (2017), p. 18. DOI: 10.3847/1538-4357/aa6ff0. arXiv: 1702.01722 [astro-ph.CO].

[248] Chihway Chang et al. "The Splashback Feature around DES Galaxy Clusters: Galaxy Density and Weak Lensing Profiles." In: *Astrophys. J.* 864.1 (2018), p. 83. DOI: 10.3847/1538-4357/aad5e7. arXiv: 1710.06808 [astro-ph.CO].

[249] T. Shin et al. "Measurement of the Splashback Feature around SZ-selected Galaxy Clusters with DES, SPT and ACT." In: (2018). arXiv: 1811.06081 [astro-ph.CO].

[250] Kurt Hinterbichler and Justin Khoury. "Symmetron Fields: Screening Long-Range Forces Through Local Symmetry Restoration." In: *Phys. Rev. Lett.* 104 (2010), p. 231301. DOI: 10.1103/PhysRevLett.104.231301. arXiv: 1001.4525 [hep-th].

[251] Salvatore Capozziello, Sante Carloni, and Antonio Troisi. "Quintessence without scalar fields." In: *Recent Res. Dev. Astron. Astrophys.* 1 (2003), p. 625. arXiv: astro-ph/0303041 [astro-ph].

[252] Sean M. Carroll, Vikram Duvvuri, Mark Trodden, and Michael S. Turner. "Is cosmic speed - up due to new gravitational physics?" In: *Phys. Rev.* D70 (2004), p. 043528. DOI: 10.1103/PhysRevD.70.043528. arXiv: astro-ph/0306438 [astro-ph].

[253] J. E. Gunn and J. R. Gott III. "On the Infall of Matter Into Clusters of Galaxies and Some Effects on Their Evolution." In: 176 (Aug. 1972), p. 1. DOI: 10.1086/151605.

[254] H. Mo, F. C. van den Bosch, and S. White. *Galaxy Formation and Evolution*. May 2010.

[255] Camila A. Correa, J. Stuart B. Wyithe, Joop Schaye, and Alan R. Duffy. "The accretion history of dark matter haloes – II. The connections with the mass power spectrum and the density profile." In: *Mon. Not. Roy. Astron. Soc.* 450.2 (2015), pp. 1521–1537. DOI: 10.1093/mnras/stv697. arXiv: 1501.04382 [astro-ph.CO].

[256] Ciaran A.J. O'Hare and Clare Burrage. "Stellar kinematics from the symmetron fifth force in the Milky Way dxisk." In: *Phys. Rev.* D98.6 (2018), p. 064019. DOI: 10.1103/PhysRevD.98.064019. arXiv: 1805.05226 [astro-ph.CO].

[257] K. Bamba, R. Gannouji, M. Kamijo, S. Nojiri, and M. Sami. "Spontaneous symmetry breaking in cosmos: The hybrid symmetron as a dark energy switching device." In: *JCAP* 1307 (2013), p. 017. DOI: 10.1088/1475-7516/2013/07/017. arXiv: 1211.2289 [hep-th].

[258] Anne-Christine Davis, Baojiu Li, David F. Mota, and Hans A. Winther. "Structure Formation in the Symmetron Model." In: *Astrophys. J.* 748 (2012), p. 61. DOI: 10.1088/0004-637X/748/1/61. arXiv: 1108.3081 [astro-ph.CO].

[259] Joseph Clampitt, Bhuvnesh Jain, and Justin Khoury. "Halo Scale Predictions of Symmetron Modified Gravity." In: *JCAP* 1201 (2012), p. 030. DOI: 10.1088/1475-7516/2012/01/030. arXiv: 1110.2177 [astro-ph.CO].

[260] Philippe Brax, Anne-Christine Davis, Baojiu Li, Hans A. Winther, and Gong-Bo Zhao. "Systematic Simulations of Modified Gravity: Symmetron and Dilaton Models." In: *JCAP* 1210 (2012), p. 002. DOI: 10.1088/1475-7516/2012/10/002. arXiv: 1206.3568 [astro-ph.CO].

[261] Claudio Llinares and David F. Mota. "Cosmological simulations of screened modified gravity out of the static approximation: effects on matter distribution." In: *Phys. Rev.* D89.8 (2014), p. 084023. DOI: 10.1103/PhysRevD.89.084023. arXiv: 1312.6016 [astro-ph.CO].

[262] Johannes Noller, Francesca von Braun-Bates, and Pedro G. Ferreira. "Relativistic scalar fields and the quasistatic approximation in theories of modified gravity." In: *Phys. Rev.* D89.2 (2014), p. 023521. DOI: 10.1103/PhysRevD.89.023521. arXiv: 1310.3266 [astro-ph.CO].

[263] Laura Taddei, Riccardo Catena, and Massimo Pietroni. "Spherical collapse and halo mass function in the symmetron model." In: *Phys. Rev.* D89.2 (2014), p. 023523. DOI: 10.1103/PhysRevD.89.023523. arXiv: 1310.6175 [astro-ph.CO].

[264] Bjoern Malte Schaefer and Kazuya Koyama. "Spherical collapse in modified gravity with the Birkhoff-theorem." In: *Mon. Not. Roy. Astron. Soc.* 385 (2008), pp. 411–422. DOI: 10.1111/j.1365-2966.2008.12841.x. arXiv: 0711.3129 [astro-ph].

[265] Ph. Brax, R. Rosenfeld, and D. A. Steer. "Spherical Collapse in Chameleon Models." In: *JCAP* 1008 (2010), p. 033. DOI: 10.1088/1475-7516/2010/08/033. arXiv: 1005.2051 [astro-ph.CO].

[266] Bin Hu, Xue-Wen Liu, and Rong-Gen Cai. "CHAM: a fast algorithm of modelling non-linear matter power spectrum in the sCreened HAlo Model." In: *Mon. Not. Roy. Astron. Soc.* 476.1 (2018), pp. L65–L68. DOI: 10.1093/mnrasl/sly032. arXiv: 1712.09017 [astro-ph.CO].

[267] Shin'ichi Nojiri, Sergei D. Odintsov, and Valerio Faraoni. "Effects of modified gravity on the turnaround radius in cosmology." In: *Phys. Rev.* D98.2 (2018), p. 024005. DOI: 10.1103/PhysRevD.98.024005. arXiv: 1806.01966 [gr-qc].

[268] Rafael C. C. Lopes, Rodrigo Voivodic, Luis Raul Abramo, and Laerte Sodré Jr. "Turnaround radius in $f(R)$ model." In: *JCAP* 1809.09 (2018), p. 010. DOI: 10.1088/1475-7516/2018/09/010. arXiv: 1805.09918 [astro-ph.CO].

[269] Weiguang Cui, Pengjie Zhang, and Xiaohu Yang. "Nonlinearities in modified gravity cosmology I: signatures of modified gravity in the nonlinear matter power spectrum." In: *Phys. Rev.* D81 (2010), p. 103528. DOI: 10.1103/PhysRevD.81.103528. arXiv: 1001.5184 [astro-ph.CO].

[270] Baojiu Li, Wojciech A. Hellwing, Kazuya Koyama, Gong-Bo Zhao, Elise Jennings, and Carlton M. Baugh. "The nonlinear matter and velocity power spectra in f(R) gravity." In: *Mon. Not. Roy. Astron. Soc.* 428 (2013), pp. 743–755. DOI: 10.1093/mnras/sts072. arXiv: 1206.4317 [astro-ph.CO].

[271] Lucas Lombriser, Fabian Schmidt, Tobias Baldauf, Rachel Mandelbaum, Uros Seljak, and Robert E. Smith. "Cluster Density Profiles as a Test of Modified Gravity." In: *Phys. Rev.* D85 (2012), p. 102001. DOI: 10.1103/PhysRevD.85.102001. arXiv: 1111.2020 [astro-ph.CO].

[272] Tsz Yan Lam, Takahiro Nishimichi, Fabian Schmidt, and Masahiro Takada. "Testing Gravity with the Stacked Phase Space around Galaxy Clusters." In: *Phys. Rev. Lett.* 109 (2012), p. 051301. DOI: 10.1103/PhysRevLett.109.051301. arXiv: 1202.4501 [astro-ph.CO].

[273] Ying Zu, D. H. Weinberg, Elise Jennings, Baojiu Li, and Mark Wyman. "Galaxy Infall Kinematics as a Test of Modified Gravity." In: *Mon. Not. Roy. Astron. Soc.* 445.2 (2014), pp. 1885–1897. DOI: 10.1093/mnras/stu1739. arXiv: 1310.6768 [astro-ph.CO].

[274] Susmita Adhikari, Jeremy Sakstein, Bhuvnesh Jain, Neal Dalal, and Baojiu Li. "Splashback in galaxy clusters as a probe of cosmic expansion and gravity." In: *JCAP* 1811.11 (2018), p. 033. DOI: 10.1088/1475-7516/2018/11/033. arXiv: 1806.04302 [astro-ph.CO].

[275] Amir Hammami and David F. Mota. "Probing modified gravity via the mass-temperature relation of galaxy clusters." In: *Astron. Astrophys.* 598 (2017), A132. DOI: 10.1051/0004-6361/201629003. arXiv: 1603.08662 [astro-ph.CO].

[276] Max Gronke, David F. Mota, and Hans A. Winther. "Universal predictions of screened modified gravity on cluster scales." In: *Astron. Astrophys.* 583 (2015), A123. DOI: 10.1051/0004-6361/201526611. arXiv: 1505.07129 [astro-ph.CO].

[277] Clare Burrage, Andrew Kuribayashi-Coleman, James Stevenson, and Ben Thrussell. "Constraining symmetron fields with atom interferometry." In: *JCAP* 1612 (2016), p. 041. DOI: 10.1088/1475-7516/2016/12/041. arXiv: 1609.09275 [astro-ph.CO].

[278] Philippe Brax, Anne-Christine Davis, Benjamin Elder, and Leong Khim Wong. "Constraining screened fifth forces with the electron magnetic moment." In: *Phys. Rev.* D97.8 (2018), p. 084050. DOI: 10.1103/PhysRevD.97.084050. arXiv: 1802.05545 [hep-ph].

[279] Bhuvnesh Jain, Vinu Vikram, and Jeremy Sakstein. "Astrophysical Tests of Modified Gravity: Constraints from Distance Indicators in the Nearby Universe." In: *Astrophys. J.* 779 (2013), p. 39. DOI: 10.1088/0004-637X/779/1/39. arXiv: 1204.6044 [astro-ph.CO].

[280] Philippe Brax, Anne-Christine Davis, and Jeremy Sakstein. "Pulsar Constraints on Screened Modified Gravity." In: *Class. Quant. Grav.* 31 (2014), p. 225001. DOI: 10.1088/0264-9381/31/22/225001. arXiv: 1301.5587 [gr-qc].

[281] Claudio Llinares. "Testing modified gravity with globular clusters: the case of NGC 2419." In: *Mon. Not. Roy. Astron. Soc.* 476.1 (2018), pp. L29–L33. DOI: 10.1093/mnrasl/sly021. arXiv: 1802.02001 [astro-ph.CO].

[282] Harry Desmond, Pedro G. Ferreira, Guilhem Lavaux, and Jens Jasche. "The Fifth Force in the Local Cosmic Web." In: (2018). DOI: 10.1093/mnrasl/sly221. arXiv: 1802.07206 [astro-ph.CO].

SUMMARY

In the last several decades our understanding of cosmology has evolved enormously. We now have a phenomenologically self-consistent model, known as the *Cosmological Standard Model* or ΛCDM, which is able to fit the huge amount of observational data with only a few free parameters. Modern cosmological research is now largely driven by the studies exploring the possible extensions of, and alternatives to, this standard picture. This is motivated, first of all, by a few theoretical puzzles in the Cosmological Standard Model. Indeed, while we can effectively describe the observational data, we are still lacking a consistent theoretical picture of the so-called dark sector, namely *dark energy*, which drives the present-day *cosmic acceleration*, and *dark matter*, which is responsible for the *Large Scale Structure* formation of the universe.

However, even if we dismiss these important puzzles, considering them to be too complicated to be tackled with our current knowledge, the study of alternative cosmological models is important given the fact that the quality of cosmological data is progressively evolving forward. This will give us a chance to test many of our current theoretical ideas and to find new directions to move forward. An informative example is the study of gravity. Cosmological observations are able to teach us a lot about the underlying theory of gravity and we might be able to find deviations from the General Theory of Relativity at cosmological scales. Therefore, while being largely motivated as an explanation of cosmic acceleration, such investigations of alternative gravity theories at cosmological scales can also be considered independently from the problem of cosmic acceleration.

With this big picture in mind, the topic of the present thesis is the investigation of phenomena beyond the cosmological standard model in various regimes of interest. Below we briefly summarize the content of the dissertation.

- Chapter 1 sets the stage for the entire thesis. In this chapter we introduce the main concepts of modern cosmology. We present a very short review of cosmological perturbation theory and discuss the essential observations. We also give short introductions to the topics of dynamical dark energy/quintessence, modifications of gravity and screening mechanisms.

- Chapter 2 is dedicated to a study of a new class of inflationary models known as cosmological *α-attractors*. We promote these models towards a unified framework describing both inflation and dark energy. We construct and study several phenomenologically rich models which are compatible with current observations. In the simplest models, with vanishing cosmological constant Λ, one has the tensor to scalar ratio $r = \frac{12\alpha}{N^2}$, with N being the number of e-folds till the end of inflation, and the asymptotic equation of state of dark energy $w = -1 + \frac{2}{9\alpha}$. For example, for a theoretically interesting model given by $\alpha = 7/3$ one finds $r \sim 10^{-2}$ and the asymptotic equation of state is $w \sim -0.9$. Future observations, including large-scale structure surveys as well as Cosmic Microwave Background B-mode polarization experiments will test these, as well as more general models presented here. We also discuss the gravitational reheating in models of quintessential inflation and argue that its investigation may be interesting from the point of view of inflationary cosmology. Such models require a much greater number of *e*-folds, and therefore predict a spectral index n_s that can exceed the value in more conventional models of inflationary α-attractors by about 0.006. This suggests a way to distinguish the conventional inflationary models from the models of quintessential

inflation, even if the latter predict $w = -1$. This chapter is based on Ref. [64].

- The topic of Chapter 3 is the theory of massive bigravity, where one has two dynamical tensor degrees of freedom. We consider an interesting extension where both of the metrics are coupled to the matter sector, which is known as the *doubly-coupled bigravity*. The main aim of this chapter is the study of gravitational-wave propagation in this theory. We demonstrate that the bounds on the speed of gravitational waves imposed by the recent detection of gravitational waves emitted by a pair of merging neutron stars and their electromagnetic counterpart, events GW170817 and GRB170817A, strongly limit the viable solution space of the doubly-coupled models. We have shown that these bounds either force the two metrics to be proportional at the background level or the models to become singly-coupled (i.e. only one of the metrics to be coupled to the matter sector). The mentioned proportional background solutions are particularly interesting. Indeed, it is shown that they provide stable cosmological solutions with phenomenologies equivalent to that of ΛCDM at the background level and at the level of linear perturbations. The nonlinearities, on the other hand, are expected to show deviations from ΛCDM. This chapter is based on Ref. [65].

- In Chapter 4 we study the first cosmological implications of a novel massive gravity theory, recently proposed by Chamseddine and Mukhanov, known as the *mimetic theory of massive gravity*. This is a theory of ghost-free massive gravity, which additionally contains a so-called *mimetic dark matter* component. In an echo of other modified gravity theories, there are self-accelerating solutions which contain a ghost instability. In the ghost-free region of parameter space, the effect of the graviton mass on the cosmic expansion history amounts to an effective negative cosmological constant, a radiation component, and

a negative curvature term. This allows us to place constraints on the model parameters—particularly the graviton mass—by insisting that the effective radiation and curvature terms be within observational bounds. The late-time acceleration must be accounted for by a separate positive cosmological constant or other dark energy sector. We impose further constraints at the level of perturbations by demanding linear stability. We comment on the possibility of distinguishing this theory from ΛCDM with current and future large-scale structure surveys. This chapter is based on Ref. [66].

- The final Chapter 5 is dedicated to the study of the effects of screening mechanisms in modified gravity on the dynamics of the spherical collapse of dark matter. In particular, we investigate the splashback scale in *symmetron modified gravity.* The splashback radius $r_{\rm sp}$ has been identified in cosmological N-body simulations as an important scale associated with gravitational collapse and the phase-space distribution of recently accreted material. We employ a semi-analytical approach, namely the self-similar spherical collapse framework, to study the spherical collapse of dark matter haloes in symmetron gravity. We provide, for the first time, insights into how the phenomenology of splashback is affected by modified gravity. The symmetron is a scalar-tensor theory which exhibits a screening mechanism whereby higher-density regions are screened from the effects of a fifth force. In this model, we find that, as over-densities grow over cosmic time, the inner region becomes heavily screened. In particular, we identify a sector of the parameter space for which material currently sitting at the splashback radius $r_{\rm sp}$, during its collapse has followed the formation of this screened region. As a result, we find that for this part of the parameter space the splashback radius is maximally affected by the symmetron force and we predict changes in $r_{\rm sp}$ up to around 10% compared to its General Relativity value. Because this margin

is within the precision of present splashback experiments, we expect this feature to soon provide constraints for symmetron gravity on previously unexplored scales. This chapter is based on Ref. [67].

SAMENVATTING

In de laatste decennia is ons begrip van de kosmologie sterk toegenomen. Wij hebben tegenwoordig een fenomenologisch intrinsiek consistent model, bekend als het "Cosmological Standard Model" of "ΛCDM", dat erin slaagt de enorme hoeveelheid waarnemingen te interpreteren met slechts een paar vrije parameters. Hedendaags kosmologisch onderzoek is voornamelijk gericht op de studie naar de mogelijke uitbreiding van of alternatieven voor dit standaardmodel. Dit wordt in eerste instantie gemotiveerd door enkele theoretische problemen in het Kosmologisch Standaard Model. Hoewel we inderdaad de waarnemingen effectief kunnen beschrijven, ontbreekt nog steeds een consistent theoretisch beeld van de zogenaamde donkere sector, d.w.z. de donkere energie die de huidige kosmische versnelling aandrijft en de donkere materie die verantwoordelijk is voor de vorming van de grote-schaalstructuur van het universum.

Zelfs als we deze belangrijke problemen negeren, met de veronderstelling dat ze te ingewikkeld zijn om met onze huidige kennis aangepakt te worden, is de studie van alternatieve kosmologische modellen belangrijk gezien het feit dat de kwaliteit van kosmologische gegevens voortdurend beter wordt. Deze ontwikkeling geeft ons een kans om veel van onze huidige theoretische ideeën te testen en nieuwe richtingen te vinden om naartoe te werken. Een informatief voorbeeld is de studie van de zwaartekracht. Kosmologische waarnemingen kunnen ons veel leren over de onderliggende theorie van de zwaartekracht, en mogelijkerwijs kunnen we op kosmologische schalen afwijkingen vinden van de algemene relativiteitstheorie. Daarom is dergelijk onderzoek van alternatieve zwaartekrachttheorieën, hoewel grotendeels

gemotiveerd met het oog op een verklaring voor kosmische versnelling, ook onafhankelijk van dit vraagstuk van belang.

Het onderwerp van dit proefschrift is, met dit bredere beeld in het achterhoofd, het onderzoek van fenomenen voorbij het kosmologische standaardmodel in verschillende interessante richtingen. Hieronder geven we een korte samenvatting van de inhoud van het proefschrift.

- Hoofdstuk 1 biedt een inleiding op het proefschrift. In dit hoofdstuk zullen we de belangrijkste concepten van de moderne kosmologie introduceren. We presenteren een beknopt overzicht van de kosmologische storingstheorie en bespreken de essentiële waarnemingen. We geven ook korte inleidingen op de onderwerpen van dynamische donkere energie/kwintessens, modificaties van zwaartekracht en afschermingsmechanismen.

- Hoofdstuk 2 is gewijd aan de bestudering van een nieuwe klasse van inflatoire modellen bekend als kosmologische *α-attractoren*. We brengen deze modellen naar voren als een gemeenschappelijk kader voor de beschrijving van zowel inflatie als donkere energie. Wij construeren en bestuderen een aantal fenomenologisch rijke modellen die compatibel zijn met de huidige waarnemingen. In de eenvoudigste modellen, met een kosmologische constante Λ naar nul, heeft men de *tensor-to-scalar ratio* $r = \frac{12\alpha}{N^2}$, waarbij N het aantal e-foldings is tot het einde van de inflatie, en de asymptotische toestandsvergelijking van donkere energie $w = -1 + \frac{2}{9\alpha}$. Bijvoorbeeld, voor een theoretisch interessant model gegeven door $\alpha = 7/3$ vindt men $r \sim 10^{-2}$ en de asymptotische toestandsvergelijking is $w \sim -0.9$. Toekomstige waarnemingen, inclusief zowel opnamen van de grote-schaalstructuur als experimenten betreffende de B-mode polarisatie van de kosmische achtergrondstraling, zullen deze testen, evenals meer algemene modellen die hier worden gepresenteerd. Wij bespreken ook de gravitationele verhitting in modellen van kwintessentiële inflatie en stellen

dat het onderzoek daarvan interessant kan zijn vanuit het oogpunt van inflatoire kosmologie. Dergelijke modellen vereisen een veel groter aantal e-foldings en voorspellen daarom een spectraalindex n_s die de waarde in meer conventionele modellen van inflatoire α-attractoren kan overtreffen met ongeveer 0.006. Dit suggereert een manier om de modellen van kwintessentiële inflatie te onderscheiden van de conventionele inflatoire modellen, zelfs als de eerstgenoemde $w = -1$ voorspelt. Dit hoofdstuk is gebaseerd op Ref. [64].

- Het onderwerp van hoofdstuk 3 is de theorie van "massive bigravity" waar twee dynamische tensorvrijheidsgraden aanwezig zijn. We beschouwen een interessante uitbreiding waarbij beide metrieken gekoppeld zijn aan de materie-sector die bekend staat als "doubly-coupled bigravity". Het voornaamste doel van dit hoofdstuk is de bestudering van de voortplanting van zwaartekrachtsgolven in deze theorie. We tonen aan dat de snelheidsgrenzen van de zwaartekrachtsgolven opgelegd door de recente detectie van zwaartekrachtsgolven uitgestraald door een tweetal samenvoegende neutronensterren en hun elektromagnetische tegenhanger, gebeurtenissen GW170817 en GRB170817A, de mogelijke oplossingsruimte van de dubbelgekoppelde modellen aanzienlijk verkleinen. We hebben laten zien dat deze snelheidsgrenzen ofwel de twee metrieken dwingen evenredig te zijn op het achtergrondniveau ofwel de modellen om enkelvoudig gekoppeld te worden (d.w.z. alleen één van de metrieken is gekoppeld aan de materie-sector). Ook is aangetoond dat de genoemde proportionele oplossingen stabiele kosmologieën bieden die fenomenologisch gelijk zijn aan de oplossing van ΛCDM op het niveau van de achtergrond en het niveau van lineaire verstoringen. Aan de andere kant zullen de niet-lineariteiten naar verwachting afwijkingen van ΛCDM vertonen. Dit hoofdstuk is gebaseerd op Ref. [65].

- In hoofdstuk 4 bestuderen we de eerste kosmologische implicaties van een nieuwe zwaartekrachttheorie, recent voorgesteld door Chamseddine en Mukhanov, bekend als de "mimetic theory of massive gravity". Dit is een theorie van "ghost"-vrije massieve zwaartekracht, die bovendien een zogenaamde mimetische donkere materie component bevat. Net als in andere gemodificeerde zwaartekrachttheorieën zijn er zelfversnellende oplossingen die een "ghost"-instabiliteit bevatten. In het "ghost"-vrije gebied van de parameterruimte komt het effect van de gravitonmassa op de geschiedenis van de kosmische expansie overeen met een effectieve negatieve kosmologische constante, een stralingscomponent, en een negatieve krommingsterm. Hiermee kunnen we grenzen opleggen aan de modelparameters, met name de gravitonmassa, door te eisen dat de effectieve stralings- en kromtetermen binnen waarnemingsgrenzen liggen. De kosmische versnelling moet worden verklaard door een afzonderlijke positieve kosmologische constante of een andere donkere energiesector. Door lineaire stabiliteit te eisen leggen we op het niveau van verstoringen verdere beperkingen op. Met het oog op huidige en toekomstige opnamen van de grote-schaalstructuur bespreken we ook de mogelijkheid om deze theorie te onderscheiden van ΛCDM. Dit hoofdstuk is gebaseerd op Ref. [66].

- Hoofdstuk 5, het laatste, is gewijd aan de studie van de effecten van afschermingsmechanismen in gemodificeerde zwaartekrachttheorie en op de dynamiek van de sferische instorting van donkere materie. We onderzoeken in het bijzonder de zogenoemde "splashback scale" in "symmetron modified gravity". De "splashback"-straal $r_{\rm sp}$ is in kosmologische N-body simulaties vastgesteld als een belangrijke schaal geassocieerd met zwaartekrachtinstorting en de faseruimteverdeling van recent samengetrokken materie (accretie). We maken gebruik van een semi-analytische benadering, namelijk het kader van de zelfgeli-

jkvormige sferische instorting, om de sferische instorting van donkere materiehalo's in symmetrongravitatie te bestuderen. Wij bieden voor het eerst inzicht in hoe de fenomenologie van "splashback" wordt beïnvloed door gemodificeerde zwaartekracht. De symmetron is een scalar-tensor theorie die een afschermingsmechanisme vertoont waarbij gebieden met hogere dichtheid worden afgeschermd van de effecten van een vijfde kracht. In dit model vinden we dat als overdichtheden groeien in de kosmische tijd, het binnengebied zwaar afgeschermd wordt. In het bijzonder identificeren we een sector van de parameterruimte waarvoor materie die momenteel op de "splashback"-straal zit tijdens de instorting de vorming van dit afgeschermde gebied gevolgd heeft. Daarbij hebben wij ontdekt dat voor dit deel van de parameterruimte de "splashback"-straal maximaal beïnvloed is door de symmetronkracht, en we voorspellen veranderingen in $r_{\rm sp}$ tot ongeveer 10% in vergelijking met zijn algemene relativiteitswaarde. Aangezien deze marge binnen de precisie van huidige "splashback"-experimenten valt, verwachten we dat deze straal binnenkort randvoorwaarden zal bieden voor symmetrongravitatie op voorheen onontgonnen schalen. Dit hoofdstuk is gebaseerd op Ref. [67].

LIST OF PUBLICATIONS

- A. Solomon, V. Vardanyan, Y. Akrami
"Massive mimetic cosmology",
Phys. Lett. B **794** (2019) 135, arXiv:1902.08533 [Chapter 4].

- O. Contigiani, V. Vardanyan, A. Silvestri
"The splashback radius in symmetron gravity",
Phys. Rev. D **99** (2019) 064030, arXiv:1812.05568 [Chapter 5].

- Y. Akrami, R. Kallosh, A. Linde, V. Vardanyan
"The landscape, the swampland and the era of precision cosmology",
Fortsch. Phys. **67** (2018) 1800075, arXiv:1808.09440.

- S. Bellucci, A. A. Saharian, D. Simonyan, V. Vardanyan
"Fermionic currents in topologically nontrivial braneworlds",
Phys. Rev. D **98** (2018) 085020, arXiv:1808.01577.

- Y. Akrami, Ph. Brax, A.-C. Davis, V. Vardanyan
"Neutron star merger GW170817 strongly constrains doubly-coupled bigravity",
Phys. Rev. D **97** (2018) 124010, arXiv:1803.09726 [Chapter 3].

- Y. Akrami, R. Kallosh, A. Linde, V. Vardanyan
"Dark energy, α-attractors, and large-scale structure surveys",
JCAP **1806** (2018) 041, arXiv:1712.09693 [Chapter 2].

- S. Bellucci, A. A. Saharian, V. Vardanyan
"Fermionic currents in AdS spacetime with compact dimensions",
Phys. Rev. D **96** (2017) 065025, arXiv:1707.08878.

- V. Vardanyan, Y. Akrami, L. Amendola, A. Silvestri
  "On nonlocally interacting metrics, and a simple proposal for cosmic acceleration",
  JCAP **1803** (2018) 048, arXiv:1702.08908.

- S. Bellucci, A. A. Saharian, V. Vardanyan
  "Hadamard function and the vacuum currents in braneworlds with compact dimensions: Two-branes geometry",
  Phys. Rev. D **93** (2016) 084011, arXiv:1512.06569.

- S. Bellucci, A. A. Saharian, V. Vardanyan
  "Vacuum currents in braneworlds on AdS bulk with compact dimensions",
  JHEP **11** (2015) 092, arXiv:1508.07255.

- V. Vardanyan, L. Amendola
  "How can we tell whether dark energy is composed of multiple fields?",
  Phys. Rev. D **92** (2015) 024009, arXiv:1502.05922.

- E. R. Bezerra de Mello, A. A. Saharian, V. Vardanyan
  "Induced vacuum currents in anti-de Sitter space with toral dimensions",
  Phys. Lett. B **741** (2015) 155, arXiv:1410.2860.

- V. Vardanyan, D. Weedman, L. Sargsyan
  "Seeking the Epoch of Maximum Luminosity for Dusty Quasars",
  The Astrophysical Journal, **790** (2014) 88, arXiv:1406.2002.
  [has been highlighted in Nature: Nature 514, 43-44 (02 October 2014), doi:10.1038/514043a].

CURRICULUM VITAE

I was born in November 1992 in Yerevan, Armenia. I am a graduate of Yerevan PhysMath school, where my interest in physics and astrophysics was ignited, primarily, via participation in national- and international-level physics and astronomy Olympiads.

From 2009 to 2013 I studied physics at the Faculty of Physics at Yerevan State University, alongside of which I have done research at the Yerevan Physics Institute and at the Byurakan Astrophysical Observatory.

From 2013 to 2015 I have been a DAAD-funded master student at the Faculty of Physics and Astronomy of the Ruprecht-Karls University in Heidelberg, Germany. I did my MSc research at the Institute of Theoretical Physics of the same university.

From 2015 onwards, I am a De Sitter cosmology PhD student at the Lorentz Institute for Theoretical Physics and at the Sterrewacht Leiden, University of Leiden. During the four years of the PhD research I have assisted in teaching numerous theoretical physics courses at both the MSc and BSc levels. Additionally, I have co-organized the De Sitter Cosmology Journal Club meetings and the Gravitational Wave meetings, both organized jointly by the Lorentz Institute and Leiden Observatory.

After my PhD I will be a postdoctoral researcher at the Kavli Institute for Mathematics and Physics of the Universe in Tokyo, Japan.

ACKNOWLEDGEMENTS

- First and foremost, I would like to express my deepest gratitude towards my supervisors Ana Achúcarro and Alessandra Silvestri. I am indebted to them for their trust and the opportunity to pursue my own research ideas with considerable independence. You have created an amazing cosmological atmosphere at the Lorentz Institute, and I am very proud for being a small part of that.

- I would like to thank my two mentors at the Leiden Observatory, Henk Hoekstra and Koen Kuijken, for all the advise and support provided throughout these years. I have truly enjoyed all the interactions with your amazing Weak Lensing group. I am indebted to you for (perhaps unknowingly) re-igniting my interest in astrophysics and observational aspects of cosmology.

- During my research career I have been very fortunate to be attached to a large cloud of amazing collaborators. I am particularly very thankful to Luca Amendola, Yashar Akrami, Stefano Bellucci, E. Bezerra de Mello, Philippe Brax, Anne-Christine Davis, Guadalupe Cañas Herrera, Omar Contigiani, Benjamin Elder, Renata Kallosh, Andrei Linde, Aram Saharian, Hayk Sargsyan, Lusine Sargsyan, David Simonyan, Adam Solomon and Daniel Weedman for all the exciting work that we have done together. Each one of you have strongly contributed in forging my current understanding of physics. I am looking forward to starting new projects with you.

- PhD years would have been rather dull without all the fellow cosmologists in Leiden. Special thanks go to all the past and present

members of the "Leiden Cosmology Gang". All the Postdocs, fellow PhD candidates and the master students in our group have been an amazing company in and outside the work.

- During my years in The Netherlands I have never encountered any administrative burden. This is largely due to the professional staff in the administrative sector of the university, to whom I express my gratitude. Particularly, I would like to thank the super-efficient secretaries of the Lorentz Institute.

- I would like to thank my friends outside the cosmological circle. Particular acknowledgements go to Hrach, Satenik, Tsovinar, Hayk and Lilith. Thank you for all the amazing dinner gatherings accompanied with charming discussions on linguistics, amazing movie events, and your friendship overall. Special thanks are due to Tsovinar for her help with realizing the cover-art idea of this thesis, as well as her help with the translation of the Summary into Dutch.

- I am very thankful to my wife Nvard for being such an amazing partner in life. Your dedication and support during my PhD years have been truly astounding. On the multiple occasions when I have stayed at the Institute till very late in the evening, you have never expressed a tiny bit of a complaint; this is the right moment to thank you for all of that. This thesis is as much yours, as it is my own. I am also very grateful to the other members of my family, particularly, my sister Anna, brothers Vahagn and Sedrak, mother Hranush and my late father Vanik for all their love.